

YUKON EXPLORATION & GEOLOGY 2014





YUKON
EXPLORATION
& GEOLOGY

2014

Edited by

K.E. MacFarlane, M.G. Nordling and
P.J. Sack

Yukon Geological Survey

Energy, Mines and Resources

Government of Yukon

Published under the authority of the Department of Energy, Mines and Resources, Government of Yukon <http://www.emr.gov.yk.ca>.

Printed in Whitehorse, Yukon, 2015.

Publié avec l'autorisation du Ministère de l'Énergie, des Mines et des Ressources du gouvernement du Yukon, <http://www.emr.gov.yk.ca>.

Imprimé à Whitehorse (Yukon) en 2015.

©Department of Energy, Mines and Resources, Government of Yukon

ISSN 1718-8326 (on-line version)

This, and other Yukon Geological Survey publications, may be obtained from:

Yukon Geological Survey

102-300 Main Street

Box 2703 (K-102)

Whitehorse, Yukon, Canada Y1A 2C6

phone (867) 667-3201, e-mail geology@gov.yk.ca

Visit the Yukon Geological Survey website at www.geology.gov.yk.ca.

In referring to this publication, please use the following citation:

Yukon Exploration and Geology 2014. K.E. MacFarlane, M.G. Nordling and P.J. Sack (eds.), 2015. Yukon Geological Survey, 165 p.

Papers can be downloaded from the Yukon Geological Survey website.

Front cover photograph: Looking south at Profile Mountain and the junction of the Kaskawulsh, Dusty and Alsek rivers. Photo by David Moynihan.

Inside cover photograph: Yukon Geological Survey staff - (*back row, left to right*) Charlie Roots, Matt Hutchison, David Moynihan, Jeff Bond, Johann Slam, Derek Torgerson and Patrick Sack; (*middle row, left to right*) Tiffani Fraser, Monica Nordling, Karen MacFarlane, Olwyn Bruce, Panya Lipovsky, Steve Israel, Kristen Kennedy and Robert Deklerk; (*kneeling*) Rosie Cobbett (and Sawyer) and Midori Kirby. Missing from photo: Carolyn Relf, Don Murphy, Maurice Colpron, Sue Roy, Lara Lewis, Syd Van Loon, Sarah Laxton, Bailey Staffen and Brett Elliot.

PREFACE

Yukon Exploration and Geology (YEG) and the Yukon Exploration and Geology Overview continue to be the main publications of the Yukon Geological Survey (Energy, Mines and Resources, Government of Yukon). Individual YEG papers, with colour images, are available in digital format only and can be downloaded from our website. The YEG Overview is available in a digital format; this year the limited print run is available in colour.

YEG 2014 contains up-to-date information on mining and mineral exploration activity, studies by industry and results of recent geological field studies. Information in this volume comes from prospectors, exploration and government geologists, mining companies and students who are willing to contribute to public geoscience for the benefit of the scientific community, general public and mineral and petroleum industries of Yukon. Their efforts are appreciated.

Monica Nordling has once again joined me in the merriment of YEG season and co-edited this volume. Thank you Monica for trying to keep me sane – and more importantly thank you for the mug with the helpful editing tips. Thanks also to my various Yukon Geological Survey colleagues for submissions and valuable assistance in reviewing manuscripts prior to them being submitted. Your expertise makes my job easier.

We welcome any input or suggestions that you may have to improve future YEG publications. Please contact me at (867) 667-8519, or by e-mail at karen.macfarlane@gov.yk.ca.


Karen MacFarlane

IN MEMORIAM



BOB CATHRO

Most of Bob's career was spent in northern Canada. Bob graduated from the UBC Geological Engineering program in 1959, and subsequently worked as a mine geologist at the Eldorado uranium mine (NWT), Verna uranium mine (Sask.), Giant Yellowknife gold mine (NWT), and the United Keno Hill silver mines (Yukon). In 1966, he and fellow geological engineer Al Archer founded the consulting firm Archer, Cathro & Associates Ltd. The firm has specialized in Yukon mining exploration since then and remains as one of the top Yukon explorers after nearly 50 years. During Bob's tenure as partner the firm made several discoveries or significant advancements of important Yukon mineral deposits. These include Casino (copper-gold-molybdenum), Wolverine and Marg (copper-

lead-zinc-silver-gold), Mactung (tungsten), Carmacks Copper (copper-gold), Wellgreen (nickel-copper-platinum) and Division Mountain (coal). Bob remained a partner in "AC" until his retirement in 1989.

Bob played a leading role in the 1972 creation and annual updates to Archer Cathro's Northern Cordillera Mineral Inventory. Through the 1970s and 1980s the Inventory was the most comprehensive file on mineral exploration history and property data in Canada. It was sold to the Yukon government in 1990 to become the foundation for the current Yukon MINFILE database.

Bob served on the editorial boards of the CIM Special Volumes 15 (1976) and 45 (1995) on Porphyry Deposits of the Canadian Cordillera and GAC Publication #2 (2000) on VMS Deposits of Latin America. His passion for research and science history flourished in retirement when he authored nearly 50 articles on the evolution of economic geology (CIM Magazine) and edited a series on the Great Mining Camps of Canada (Geoscience Canada).

Bob always believed strongly in giving back to his industry. He served as a Director, Vice-President (1978-81), President (1982-1983) and Past-President (1984-1985) of the BC and Yukon Chamber of Mines (now AMEBC). The present Mineral Exploration RoundUp conference had its roots in 1982 as a conversation on a ferry between Chamber Managing Director Jack Patterson, President Bob Cathro and soon-to-become Vice-President Nick Carter.

Over his career, Bob received several awards including the A.O. Dufresne Exploration Achievement Award in 1991 from the Canadian Institute of Mining, Metallurgy and Petroleum (CIM), for "outstanding contribution to mineral exploration in B.C. and Yukon, and for his commitment to the north". In 1999 Bob and Al Archer were co-winners of the H.H. "Spud" Huestis Award for excellence in prospecting and mineral exploration, awarded by (now) AMEBC. In 2002, Archer Cathro was inducted to the Yukon Prospectors' Association Honour Roll, reflecting their exploration successes over the years. The Geological Association of Canada presented Bob with its Distinguished Service Award in 2003.

Bob Cathro, the pioneering western Canadian mineral exploration geologist, mining industry leader, and amateur historian, died at age 79 at his home in Chemainus, BC on August 26, 2014. A friend and mentor to many in the industry, he will be greatly missed.

IN MEMORIAM



Bob Thompson describes to Lew Green (gray jacket) a geological re-interpretation in the Southern Ogilvie Mountains. Photo courtesy of Charlie Roots, 1986.

LEWIS GREEN

Dr. Lewis Green, geologist and writer of mining and surveying history, died November 11, 2014. He was 93. Lew contributed to information about and appreciation of Yukon through his field mapping, geological and mining reports, and with two of his books.

Son of an influential BC and federal politician, Lew began at McGill, but his student life was interrupted by World War II. With the Black Watch (Royal Highland Regiment) he took part in the liberation of Holland. Upon return, he graduated in geology at UBC and, along with three class-mates, proceeded to have a distinguished career with the Geological Survey of Canada. From 1954 through '57 he mapped north and west of Keno Hill, one of the last field parties to use pack-horses. By 1957 the GSC had begun using helicopters to deploy geologists on mountain traverses, and at that point Lew was engaged in reconnaissance in the Nahanni, Pelly and Glenlyon ranges.

During the extraordinary summer of 1961, with close cooperation of pilot Pat Callison and Klondike Helicopters of Whitehorse, Lew Green undertook "GSC Operation Ogilvie" to geologically map the mountains from Keno westward to the Alaska border. The late Jim Roddick and Doug Craig were part of that project, which resulted in three maps and a memoir¹, each impressive for its thoroughness, detail and pioneering resolution of stratigraphy.

Lew was appointed Resident Geologist in Whitehorse from 1962 to 1966, where he advised prospectors and companies, and produced both annual and occasional reports on the mineral industry of Yukon. With his wife Kathy and five children, he moved to Vancouver in 1966 to become a consulting geologist and investigate history of the early 20th century.

Two of his books (*The Gold Hustlers* and *The Boundary Hunters*) are significant for their thorough research and insights to events in Yukon. They are based upon records that are now difficult to access and not well covered in other references:

The Gold Hustlers (Alaska Northwest Co., 1977; 3rd printing, 1985) describes the second phase of placer mining in the Klondike district. It details the granting of mining concessions and competition between the companies of ANC Treadgold and those of Joseph Boyle, as well as the financing and construction of dredges, power plants, and the 'Yukon Ditch' (diverting water from the headwaters of the Tombstone and Little Twelvemile rivers). Lew interviewed old-timers, tracked down documents of the protracted court cases and settlements, and worked through records of the companies, to write a lucid account.

¹Green, L.H., 1972. *Geology of Nash Creek, Larsen Creek, and Dawson map areas, Yukon Territory. Geological Survey of Canada, Memoir 364, 157 p., and 3 maps at 1:250000 scale.*

The Boundary Hunters (UBC Press, 1982) relates the adventures and methods of marking the Alaskan boundary from Dixon entrance, through the Coast Mountains, the Wrangell-St. Elias ranges, and northward to the Arctic Ocean between 1906 and 1913. It was a joint Canadian-American geodetic survey in exceedingly rough topography, facing river and glacier hazards and rugged weather, with little mechanized equipment and no communication with the outside world. Through good planning, dedication and perhaps smiling fortune, more than 50 field parties sustained few accidents although their many adventures make a good read for those passionate about fieldwork.

His third book, ***The Great Years: Gold Mining in the Bridge River Valley*** (Tricouni Press, 2000) describes the Pioneer-Bralorne mines which were the top producer of lode gold in BC during the 20th century. They are about 180 km northeast of Vancouver. During the depression this valley was one of the few bright spots in the BC economy. Green's book is like having the mine manager show you around: it is replete with assays and stock market fluctuations, but also describes the community life.

Lew had many interests and loved to travel. He was a keen observer: inquisitive and humble, and enthusiastic of the efforts by the next generations of geologists. He was a friend to many within the GSC and exploration community. Kathy, his partner since UBC days, was strong support for his activities and pushed him to finish the books. The couple always spoke wistfully of their years in Yukon. In the 1960s Lew knew the geology of Yukon better than anyone, and remembered it vividly until near the end.



The helicopter at the end of the traverse. Photo by L.H. Green, 1960, from the GSC photo archives.



TABLE OF CONTENTS

Geology of the Takhanne River (NTS 115A/2) and Kluhini River (115A/7) map areas, southwest Yukon E. Bordet, S. Israel and D. Moynihan	1
Using terrestrial cosmogenic nuclides to constrain timing of penultimate ice advance in the Ogilvie Mountains, Yukon L. Brown, B. Ward, J.D. Bond and J. Gosse	17
Advances in the mineralization styles and petrogenesis of the Coffee gold deposit, Yukon E. Buitenhuis, L. Boyce and C. Finnigan	29
Stratigraphy, geochemistry and source rock potential of the Boundary Creek Formation, North Slope, Yukon and a description of its burning shale locality T.A. Fraser and L. Reinhardt	45
Palaeoenvironment, palaeohydrography and chemostratigraphic zonation of the Canol Formation, Richardson Mountains, north Yukon M.P. Hutchison and T.A. Fraser	73
The Bear Creek assemblage: A latest Triassic volcano-sedimentary succession in southwest Yukon S. Israel, M. Colpron, J. Cubley, D. Moynihan, D.C. Murphy and C. Relf	99
Summary of Yukon Geological Survey permafrost monitoring network results, 2008-2013 P.S. Lipovsky	113
Preliminary detrital zircon geochronology of the Neruokpuk Formation in the Barn Mountains, Yukon W.C. McClelland, M. Colpron, K. Piepjohn, W. von Gosen, W. Ward and J.V. Strauss	123
Soft sediment textures in clasts in Wernecke Breccia: Reconstruction of an eroded late Paleoproterozoic succession in northern Yukon J. Verbaas, D.J. Thorkelson, H.D. Gibson, D.D. Marshall and D. Milidragovic	145
Fault tectonics in the Rapid depression of the Yukon North Slope (Canadian Arctic) - Summary of preliminary results W. Von Gosen, K. Piepjohn, D.C. Murphy, C. Brandes, W.C. McClelland and M. Colpron	157

Geology of the Takhanne River (NTS 115A/2) and Kluhini River (115A/7) map areas, southwest Yukon

E. Bordet, S. Israel¹ and D. Moynihan
Yukon Geological Survey

Bordet, E., Israel, S. and Moynihan, D., 2015. Geology of the Takhanne River (NTS 115A/2) and Kluhini River (115A/7) map areas, southwest Yukon. *In: Yukon Exploration and Geology 2014*, K.E. MacFarlane, M.G. Nordling and P.J. Sack (eds.), Yukon Geological Survey, p. 1-16.

ABSTRACT

Bedrock mapping of the Takhanne River (NTS 115A/2) and Kluhini River (NTS 115A/7) map areas in southwest Yukon extends previous mapping of the Coast plutonic complex from the Haines Junction area south to the British Columbia border. The area is characterized by deformed and metamorphosed rocks of the Yukon-Tanana terrane and other Paleozoic to Mesozoic rocks that occur as roof pendants within the Paleocene Ruby Range plutonic suite. Yukon-Tanana rocks appear to be thrust over the Paleozoic to Mesozoic rocks to the west, possibly during Late Cretaceous shortening. Metamorphic mineral assemblages indicate a southwest decrease in metamorphic grade with rocks of the Yukon-Tanana terrane showing P-T conditions of 635-655°C and 6.3-7.9 kbar and rocks in the southernmost part of the study area exhibiting relatively low (~3.5-4 kbar) pressures related to intrusion of the Ruby Range suite. The regional stratigraphic relationships of the Paleozoic to Mesozoic rocks in the study area are not well constrained. They may be related to one of three regionally significant units: 1) the Jura-Cretaceous Dezadeash Formation; 2) the Triassic and older Bear Creek assemblage; or 3) the Kluane schist.

¹steve.israel@gov.yk.ca

INTRODUCTION

Bedrock mapping in southwest Yukon during the summer of 2014 covered areas southeast of Haines Junction, east and southeast of Dezadeash Lake, to the British Columbia border (NTS 115A/2 and 7; Figs. 1 and 2). Previous regional bedrock mapping of this area, between 1946 and 1950 by Kindle (1952), provided a broad geological framework for the relationships between Paleozoic to Cenozoic metamorphic and plutonic rocks. This report extends detailed 1:50 000-scale bedrock mapping initiated in 2011 to the north of the present study area (Israel *et al.*, 2011; Israel and Westberg, 2011; Israel and Westberg, 2012; Israel and Kim, 2014). More specifically, the current study continues 1:50 000-scale bedrock mapping initiated in the Granite Lake area to the north (Israel and Kim, 2013, 2014), and further investigates the nature and extent of lithostratigraphic successions defined in that region in an effort to clarify the genetic and structural relationships between Paleozoic metamorphic assemblages, and younger (Mesozoic to Cenozoic) overlap assemblages and intrusive rocks. The purpose of this project is to determine geologic relationships between the diverse lithotectonic elements and to increase understanding of the overall tectonic and metallogenic evolution of southwest Yukon.

Exposure in the area is excellent along high peaks and ridges and very poor in the wide bush-covered valleys. Access relies primarily on helicopter, although a number of bedrock outcrops are found along, and close to, the Haines Road, south of Dezadeash Lake (Fig. 1).

REGIONAL GEOLOGY

The bedrock geology of southwest Yukon is characterized by the juxtaposition of Neoproterozoic to Mesozoic terranes, parallel to the main northwest-trending Cordilleran structural grain. The terranes are from west to east: Alexander, Wrangellia, Yukon-Tanana and Stikinia (Fig. 1).

The Alexander terrane and Wrangellia, which together form the Insular terranes, were accreted to the western margin of the Intermontane terranes (Yukon-Tanana and Stikinia in southwest Yukon) during the Middle Jurassic or possibly earlier (McClelland *et al.*, 1992; van der Heyden, 1992; Nelson *et al.*, 2013). In southwest Yukon, the Insular terranes are juxtaposed against the Intermontane terranes along the Denali fault; a large, crustal-scale, dextral strike-slip fault with an offset of as much as 400 km that occurred during the latest Cretaceous (?) through the Cenozoic.

Two assemblages of metamorphosed sedimentary and volcanic rocks occur between the Insular and Intermontane terranes (Fig. 1). The Kluane schist, which structurally underlies the Yukon-Tanana terrane, is a sequence of quartz-biotite schist that is interpreted to represent one of several Jura-Cretaceous basins that formed at the boundary between the Intermontane and Insular terranes (Israel *et al.*, 2011; Nelson *et al.*, 2013). The Shakwak fault, an inferred structural feature of unknown kinematics, separates the Kluane schist from the Bear Creek assemblage to the southwest (Fig. 1). The Bear Creek assemblage is characterized by strongly deformed and metamorphosed intermediate to mafic volcanic flows and volcanoclastic rocks interlayered with meta-siltstone, mudstone and sandstone (Israel *et al.*, 2014). The age of the Bear Creek assemblage is Late Triassic and older but its relationships within the regional stratigraphic framework is not known.

The Jura-Cretaceous turbiditic deposits of the Dezadeash Formation overly Wrangellia, the Alexander terrane and rocks assigned to the Bear Creek assemblage (Fig. 1). The Dezadeash Formation is part of several Jura-Cretaceous basins that occur along the boundary of the Insular and Intermontane terranes, including the Nutzotin (in eastern Alaska) and Gravina basins (in southeast Alaska). In southwest Yukon, rocks of the Dezadeash Formation are strongly deformed by at least two phases of folding, and metamorphosed to lower greenschist facies (Eisbacher, 1976).

The Paleocene Ruby Range batholith intrudes across the structural boundary between the Kluane schist and Yukon-Tanana terrane. The Ruby Range suite occurs as a northwest-trending batholith of felsic to intermediate composition, extending to the southeast into northern British Columbia, and cut off by the Denali fault at its northwest end (Fig. 1). The base of the batholith is foliated, grading upward into massive, undeformed intrusive rock (Israel *et al.*, 2011). The Ruby Range batholith ranges from ~64 to ~57 Ma (Israel *et al.*, 2011; Israel and Westberg, 2012).

LITHOLOGY

The Ruby Range batholith intrudes Yukon-Tanana schist, gneiss and a poorly defined succession of Paleozoic to Mesozoic metasedimentary rocks. All of these rocks are separated from the Dezadeash Formation and rocks of Wrangellia by the Tatshenshini fault in Yukon and the Denali fault in northwestern British Columbia (Fig. 2).

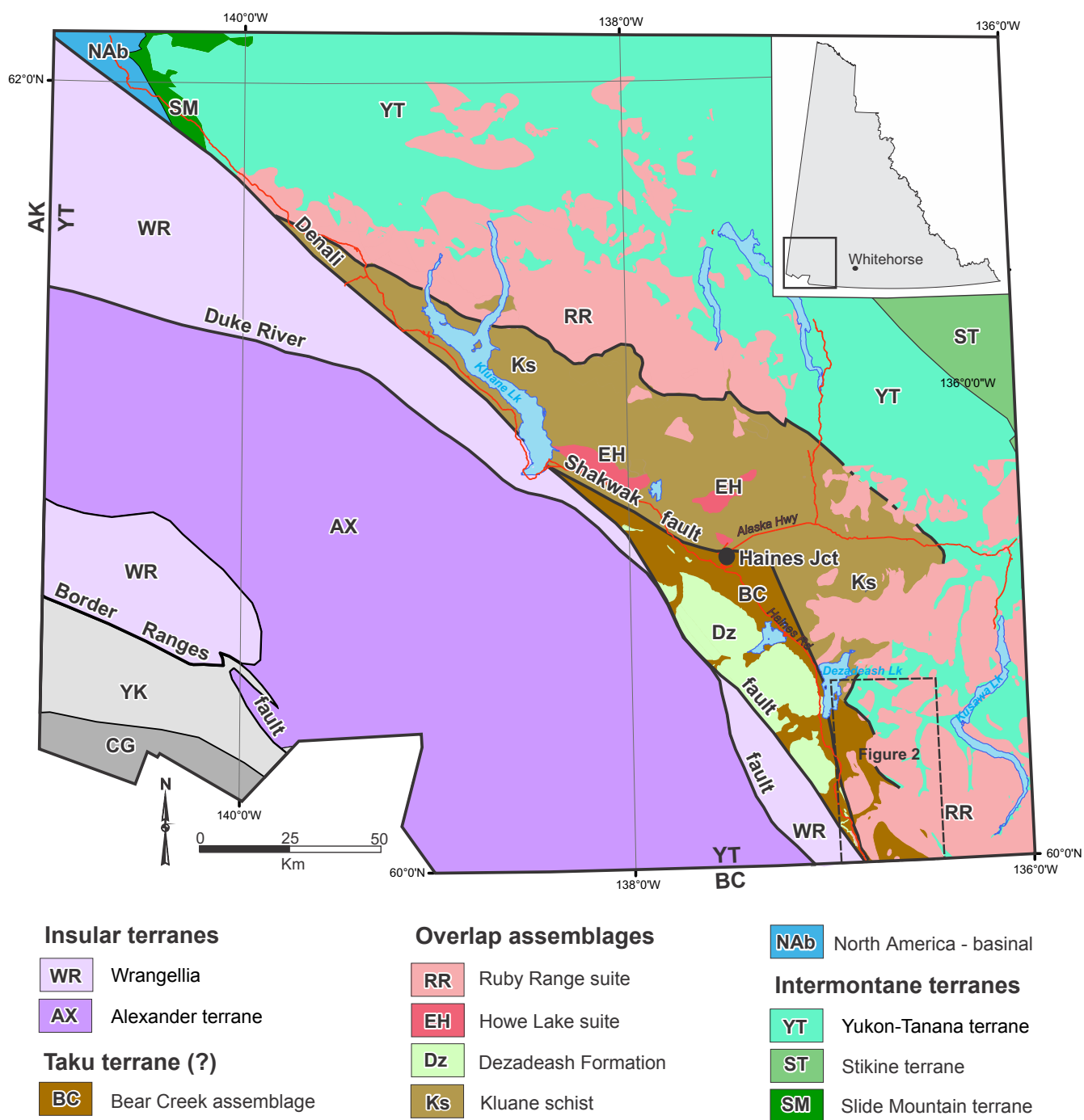
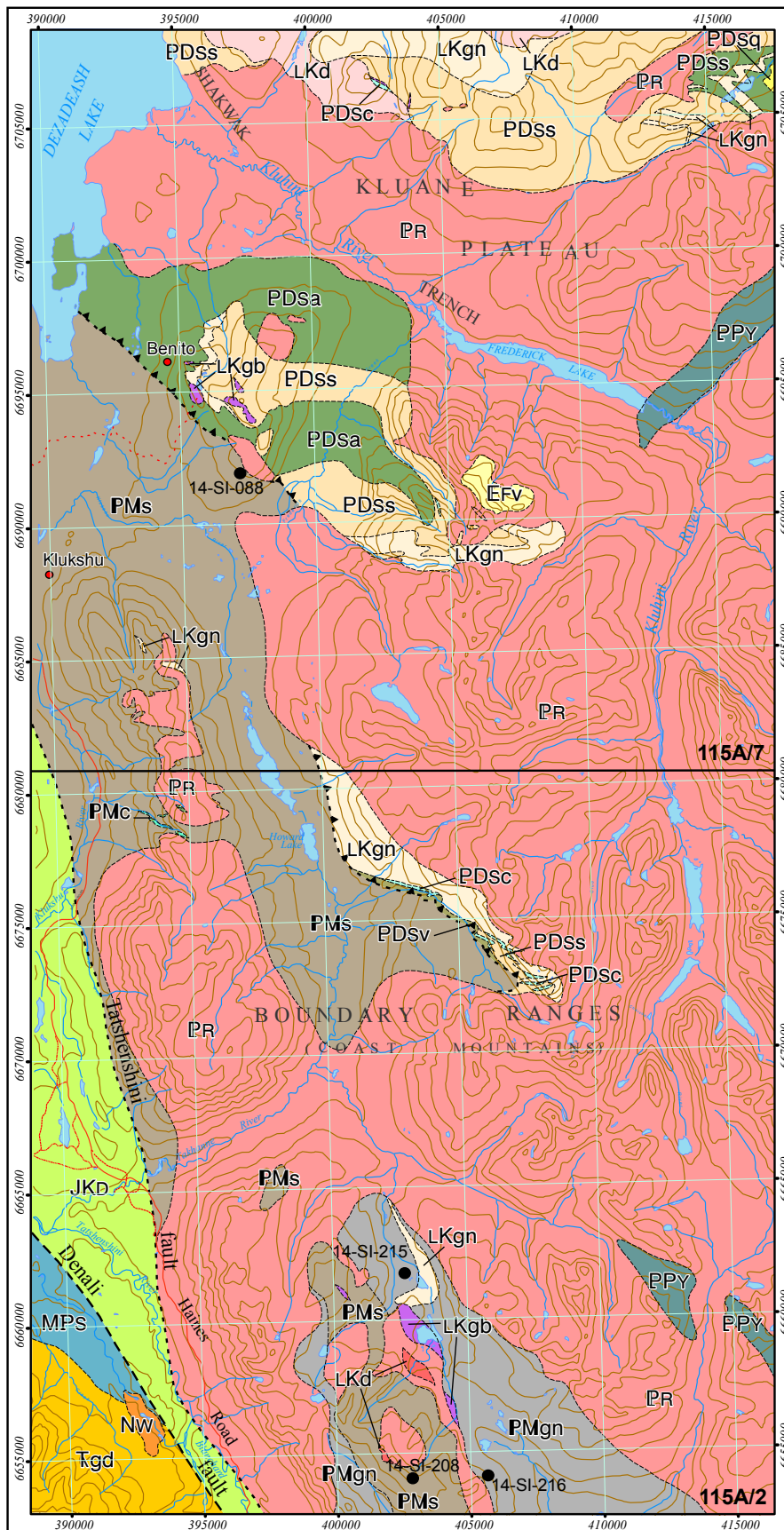


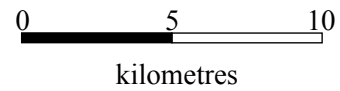
Figure 1. Terrane map of southwest Yukon (modified after Nelson et al., 2013). Inset map shows location with respect to the rest of Yukon. Location of the study area (Fig. 2) is shown by dashed line box. AK-Alaska, YT-Yukon Territory, BC-British Columbia.



SYMBOLS

- geologic contacts (defined, approximate)....
- fault (strike-slip, unknown).....
- thrust fault (inferred).....
- MINFILE Occurrence.....
- Haines Road.....
- Trail.....
- Rock sample location.....

5000 Metre Grid
 Universal Transverse
 Mercator Projection
 NAD 83 Zone 8



MINFILE		
Number	Name	Deposit Type
115A022	Klukshu	VMS
115A023	Benito	unknown

Figure 2. Preliminary bedrock geology map of the Takhanne River (NTS 115A/2) and Kluhini River (NTS 115A/7) map areas. Legend is on opposite page.

LEGEND

OVERLAP ASSEMBLAGES

NEOGENE

WRANGELL VOLCANIC ROCKS:

NW basaltic-andesitic, andesitic and dacitic lava flows; dacite and rhyolite domes; minor silicic pyroclastic deposits;

EOCENE (?)

FREDERICK LAKE VOLCANIC COMPLEX:

EFv coherent flow-banded andesitic to dacitic lavas and subvolcanic intrusions; silicic tuff and lapilli

PALEOCENE

RUBY RANGE BATHOLITH (ca. 64-57 Ma):

PR medium to coarse-grained, equigranular, light grey to white biotite +/- hornblende granodiorite; fine to coarse-grained, salt and pepper hornblende +/- biotite quartz diorite; biotite, muscovite K-feldspar pegmatite dikes; in part coeval with Rhyolite Creek volcanoplutonic complex

LATE CRETACEOUS (?)

LKgb coarse-grained, dark brown-black, hornblende +/- biotite, plagioclase, pyroxene, gabbro dikes and stocks

LKd fine to coarse-grained hornblende diorite to tonalite with abundant garnets; locally grading into garnet amphibolite

LKgn medium to coarse-grained, mylonitic to weakly deformed, biotite, quartz +/- garnet orthogneiss; dark grey weathered, dark and light grey banded fresh; commonly interlayered with biotite schist or amphibolite of Snowcap assemblage; inferred Late Cretaceous in age, but could be as old as Permian

LATE JURASSIC TO EARLY CRETACEOUS

DEZADEASH FORMATION:

JKD interbedded light to dark buff-grey lithic greywacke, sandstone, siltstone, thin dark grey shale, argillite and conglomerate; mass-flow conglomerate; rare light grey tuff

TRIASSIC

MOUNT BEATON BATHOLITH (ca. 217 Ma):

Tgd medium to coarse-grained, unfoliated, hornblende diorite to hornblende, biotite, quartz diorite; salt and pepper appearance; locally abundant dark grey fine-grained gabbro; may in part be equivalent to Early Cretaceous Kluane Ranges Suite

TAKU TERRANE (?)

PALEOZOIC TO MESOZOIC

PMc white to beige weathered limestone and marble; strongly deformed; light to dark grey bands found throughout; structurally and stratigraphically interleaved with PMs

PMs fine to medium-grained, garnet-biotite schist and metasedimentary rocks; brown to rusty weathered, dark grey fresh; layers variably richer in quartz or biotite

PMgn medium- to coarse-grained, orange weathered, dark grey to black, biotite-quartz-feldspar +/- kyanite-sillimanite paragneiss; fine-grained, banded grey to dark grey metasedimentary rocks

WRANGELLIA

MISSISSIPPIAN-CARBONIFEROUS

STATION CREEK FORMATION:

MPS basalt flows and breccia; volcanoclastic siltstone and sandstone; crystal tuff and chert

YUKON-TANANA TERRANE

PROTEROZOIC TO PERMIAN

PPY Undivided Yukon Tanana terrane rocks; intensely deformed schist, orthogneiss, and calc-silicates rocks; greenschist to amphibolite facies

PROTEROZOIC TO DEVONIAN

SNOWCAP ASSEMBLAGE:

PDSq medium-grained, sugary, massive to banded and strongly folded light grey weathered quartzite; felsic metavolcanic rocks and biotite psammitic schist

PDSv brown-rusty weathered, dark grey metavolcanic sandstone and conglomerate; dark grey-green garnet-biotite metabasalt; fine-grained dark grey metasedimentary rocks; interlayered with marble of the Snowcap assemblage

PDsc fine to medium-grained, grey-cream weathered, light grey to white marble occurring as lenses and thick layers (up to several metres wide) within schist, orthogneiss, metavolcanic or metasedimentary rocks; locally associated with ultramafic rock lenses; internally strongly deformed

PDSa medium-grained, dark and light grey banded amphibolite gneiss with abundant garnets; fine-grained dark green to black garnet amphibolite schist; fine- to medium-grained, rusty-brown weathered, dark green massive metabasalt

PDSs fine to medium-grained, light to dark grey and brown weathered biotite, muscovite, quartz, garnet schist; locally abundant aluminosilicates (sillimanite, +/- kyanite); locally migmatitic

YUKON-TANANA TERRANE (PPY)

The Yukon-Tanana terrane occurs as isolated remnants of a Neoproterozoic (?) to Paleozoic continental margin assemblage intruded by Mesozoic to Cenozoic intrusive rocks of the Ruby Range batholith. Yukon-Tanana rocks immediately north of the present study area are thrust over the Kluane schist (Israel *et al.*, 2011). Rocks assigned to the Yukon-Tanana terrane consist dominantly of schist, orthogneiss, and calc-silicates. Metamorphic mineral assemblages indicate that Yukon-Tanana rocks range

from upper greenschist to amphibolite facies. They are intensely deformed, with tight centimetre-scale microfolds indicating a dominant S to SSW vergence of larger-scale folds. Internally, mappable units are complexly deformed, showing evidence for multiple phases of deformation. Based mainly on lithologic composition and texture, rocks of the Yukon-Tanana terrane in southwest Yukon are interpreted to be part of the Neoproterozoic to Devonian Snowcap assemblage, the oldest part of the Yukon-Tanana terrane (Colpron *et al.*, 2006). The Snowcap assemblage in southwest Yukon comprises five main mappable units.

Snowcap Assemblage

Biotite-muscovite schist (PDSS)

The rocks considered to be the lowest structural level of the Yukon-Tanana terrane in the study area are characterized by a thick, extensive package of pale to dark brown-rusty weathered, fine to medium-grained, garnet-biotite-muscovite-quartz schist (Fig. 3a). The schist outcrops mainly in the northern and central part of the study area (Fig. 2). Thickness of this unit is not known as its lower contact is inferred to be a fault, and the upper contact with the overlying amphibolite is not exposed. The amount of biotite varies throughout the unit, sometimes dominating the rock with few other minerals other than quartz. Garnet, kyanite ± sillimanite are locally abundant. The texture and mineralogy of the schist sometimes makes it difficult to distinguish it from the granodiorite orthogneiss that intrudes into, and is structurally interleaved with it. The age of this unit is not known but it is likely pre-Carboniferous based upon its assignment to the Snowcap assemblage.

Metabasalt/Amphibolite (PDSa)

This unit comprises amphibolite schist to gneiss, and massive greenstone. It outcrops extensively in the central part of NTS 115A/7 where it is structurally interleaved and infolded with the underlying schist of unit PDSS (Fig. 2). The unit occurs mainly as dark grey to black, coarse to fine-grained amphibolite composed of hornblende, plagioclase, biotite and variable amounts of garnet (Fig. 3b). Amphibolite gneiss locally displays fine black and white banding where segregation of leucocratic feldspar and quartz layers occurs. Exposures of massive greenstone occur within the more typically gneissic rocks where locally the greenstone is rusty brown weathered, displaying what may be primary vesicles. Orthogneiss (likely LKgn) is commonly interlayered with amphibolite gneiss, as observed in the northeastern part of the map area (Fig. 2).

The protolith of the greenstone is likely a mafic volcanic rock, while the amphibolite gneiss could be mafic intrusions. The close spatial relationship between the greenstone and gneiss may suggest the gneiss is closely related to greenstone, possibly being subvolcanic intrusions. As with the underlying schist, the age of the amphibolite unit is not constrained but is likely pre-Carboniferous.

Quartzite (PDSq)

A unit of light grey to pinkish weathered quartzite interlayered with possible felsic metavolcanic rocks is exposed in the northeasternmost part of the study area (Fig. 2). The quartzite is typically thinly banded and displays a sugary texture. The light and dark bands within the quartzite are excellent at displaying the strongly folded nature of the unit (Fig. 3c). Exposure of this unit is not extensive within the mapped area, but where present the quartzite appears to be overlying the amphibolite unit. The thickness of the quartzite in the study area is unknown from present data but must be at least several tens of metres based upon outcrops visited during this study and previous years (Israel and Kim, 2013).

Metavolcanic/metavolcaniclastic rocks (PDSv)

A sequence of metavolcanic and metavolcaniclastic rocks is found spatially associated with the marble of unit PDSC (Fig. 3d). The lower contact of the metavolcanic unit is not exposed and it is difficult to determine its relationship with underlying units. PDSv comprises brown, rusty weathered, dark grey metavolcanic sandstone, conglomerate and dark grey-green garnet-biotite-metabasalt. It is distinct from other metabasalt/amphibolite (e.g., PDSa) assemblages based on lithology, texture, and stratigraphic associations. PDSv is found at the base of, and interlayered with, overlying marble (PDSC) in the central part of the study area, southeast of Howard Lake (Fig. 2). Thin, brown weathered quartzite bands are interlayered with the metavolcanic rocks near the marble. The thickness of this unit is about 20 m, but it is likely structurally thickened. The age of the unit is not known, it has been assigned to the Snowcap assemblage and therefore by definition likely pre-Carboniferous in age; however, it is possible the unit might be the lowest member of the Finlayson assemblage, a Devonian to Mississippian package of metavolcanic and metasedimentary rocks within the Yukon-Tanana terrane.

Marble (PDSC)

Marble is best preserved in the central part of the study area, where relatively continuous northeast dipping beds can be followed for hundreds of metres, interlayered with thicker sections of schist (PDSS), orthogneiss (LKgn), and metavolcanic rocks (PDSv). The marble is typically grey-cream weathered, pale to medium grey, thinly to thickly layered, and locally interbedded with 20 to 30 cm-thick dark brown-rusty weathered layers of quartzite (Fig. 3e). Interlayered with pure marble are coarser grained, more silica-rich layers suggestive of calcareous

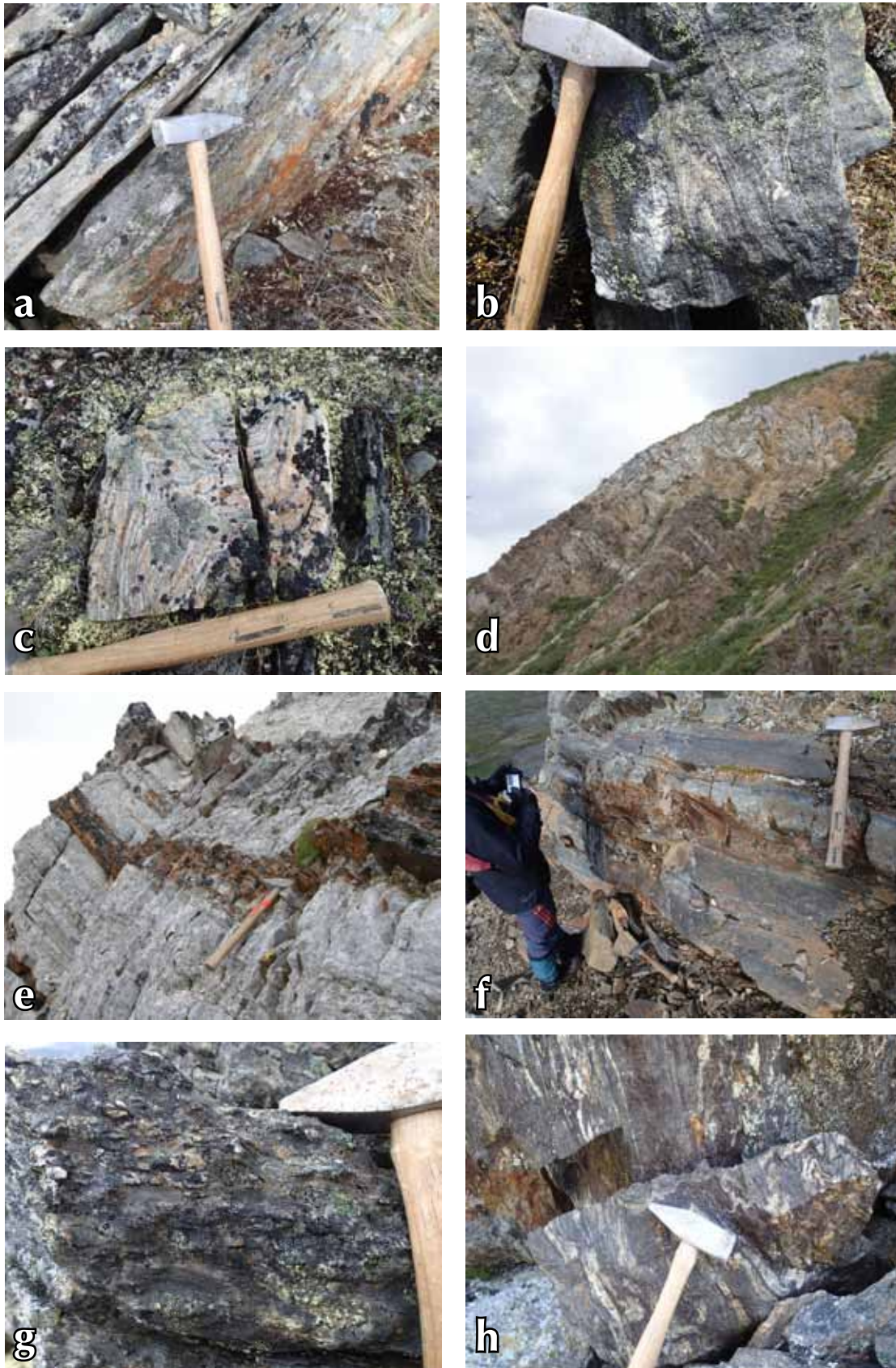


Figure 3. (a) Garnet-muscovite-biotite-quartz schist of the lower Snowcap assemblage, unit PDss; (b) strongly deformed amphibolite gneiss of unit PDsa; (c) banded, light grey to pinkish quartzite of unit PDsq; (d) interlayered volcanic, volcanoclastic, and carbonate rocks of the upper Snowcap assemblage, unit PDsv and PDsc; (e) marble with thin interbed of orange/brown weathered quartzite in the upper Snowcap assemblage; (f) primary bedding within Paleozoic to Mesozoic (PMs) metamorphosed siltstone/sandstone turbidites; (g) quartzite clasts within metaconglomerate of unit PMs; (h) paleozoic to Mesozoic migmatitic paragneiss of unit PMgn.

sandstone to calcareous mudstone protoliths. The thickness of individual marble sections can be up to 50 m; however field associations and successive interlayering of marble with metavolcaniclastic or metabasaltic rocks suggest the existence of a several hundred metres-thick composite sequence, likely resulting from structural thickening. Marble is internally strongly deformed, with tight, isoclinal folds and interference patterns indicating several phases of deformation.

PALEOZOIC TO MESOZOIC METAMORPHIC ROCKS

A package of metasedimentary and paragneissic rocks occupy much of the central part of the map area (Fig. 2). These rocks are different enough from those of the Yukon-Tanana terrane that they have been mapped as separate stratigraphic entities. They are interpreted to structurally underlie the Yukon-Tanana terrane; however their age and stratigraphic affinity remains unknown.

Metasedimentary rocks (PMs)

Garnet-biotite \pm staurolite \pm kyanite-bearing metasedimentary rocks cover a large portion of the western and southern part of the study area. They are dominantly composed of fine to medium-grained meta-sandstone, siltstone and mudstone (Fig. 3f). Primary stratigraphic layering is well-preserved, as are sedimentary structures such as graded beds and cross-bedding. Biotite-rich layers can take on a schistose appearance and a through going foliation is found in all rock types. Rare beds of meta-conglomerate are found within the metasedimentary succession, commonly several metres in thickness (Fig. 3g). Clasts within the meta-conglomerate are exclusively quartzite, between one and five centimetres in diameter. Together, the metasedimentary succession appears to represent a turbidite sequence. The thickness of the unit is not well-constrained but is probably at least several hundred metres. Locally preserved carbonate layers are found in the west-central part of the map area (unit **PMc**). These are discontinuous bands of white to beige marble up to several tens of metres thick. They are interleaved with metasedimentary rocks of **PMs** and often form large pods. The age of these rocks is unknown.

Paragneiss (PMgn)

A distinct succession of garnet-sillimanite \pm andalusite-bearing rocks is mapped in the southernmost part of the study area, and extends south of the Yukon-BC border.

The unit comprises orange weathered dark grey to black, biotite-quartz-feldspar paragneiss, as well as finer grained, banded grey to dark grey metasedimentary rocks containing variable amounts of biotite. Locally the rock is migmatitic with leucosomes parallel to and crosscutting foliation (Fig. 3h). The paragneiss appears to pass gradationally up into the overlying metasedimentary unit described above. Intrusive contacts exist between this succession and the undeformed to weakly foliated granodiorite and hornblende-diorite of the Ruby Range suite and Late Cretaceous gabbroic intrusions.

DEZADEASH FORMATION (JKD)

The Dezadeash Formation is composed of meta-sandstone, siltstone and mudstone, interpreted to be a thick turbidite succession (~3000 m; Eisbacher, 1976). Its age is constrained by Oxfordian to Valanginian fossil collections (Late Jurassic to Early Cretaceous; Eisbacher, 1976). The Dezadeash Formation extends east of the Denali fault from Haines Junction southward to northern British Columbia. It is exposed in the southwest corner of the map area where it is separated from the Yukon-Tanana terrane and other metamorphic rocks to the east by the Tatshenshini fault (Fig. 2; Lowey, 2000), an enigmatic structure with undefined kinematics and timing. To the west the Dezadeash Formation is juxtaposed to Paleozoic and Mesozoic rocks of Wrangellia across the Denali fault (Fig. 2). Near Million Dollar falls, rocks of the Dezadeash Formation are strongly deformed and metamorphosed and appear similar to rocks of **PMs** (Fig. 4a).

IGNEOUS ROCKS

Intrusive rocks occupy up to 80% of the map area (Fig. 2). The majority of these belong to the late to post-kinematic quartz-diorite, hornblende-diorite and granodiorite of the Paleocene Ruby Range batholith. Other intrusive phases, including strongly foliated to gneissic granodiorite, tonalite, diorite and gabbro, are likely Late Cretaceous and occur throughout the area. A volcanic complex of probable Eocene age (?) is reported for the first time south of Frederick Lake.

Late Cretaceous intrusive rocks (LKgn, LKgb, LKd)

Dark grey weathered, medium to coarse-grained, dark and light grey banded orthogneiss (**LKgn**) of granodioritic composition occurs throughout the map area (Figs. 2, 4b). The gneiss is often associated with unit **PDSSs**, but is also found interlayered with amphibolite and metabasalt (**PDSa**). Common minerals include plagioclase, biotite,

quartz, hornblende and variable amounts of garnet. The orthogneiss shows variable degrees of internal deformation, from mylonitic fabric to areas of more massive igneous textures. The age of the orthogneiss within the mapped area is not known, however similar rocks along strike to the north are Late Cretaceous (~75 Ma; J.L. Crowley, *pers. comm.*, 2014).

Medium to coarse-grained hornblende-biotite-garnet diorite to tonalite intrusions (LKd) are mapped in the southernmost and northernmost parts of the study area (Fig. 2). The bodies in the south appear to grade locally into garnet hornblendite and massive, hornblende ± biotite diorite. The unit overall is strongly foliated to massive. Garnet within the intrusions range in size from ~2 mm up to 2 cm (Fig. 4c). Similar garnet-bearing, foliated to massive, diorite to gabbro plutons were mapped in the Granite Lake area, just north of the present map area (Israel and Kim, 2013). One such body extends south into the north-central part of NTS 115A/07, where it intrudes schist of the Yukon-Tanana terrane and probable Late Cretaceous orthogneiss (Fig. 2). Rocks of unit LKd are intruded by granodiorite of the Ruby Range suite. The age of garnet-bearing diorite is not well constrained, but is likely Late Cretaceous, similar to unit LKgn.

Gabbroic dikes and larger intrusive bodies occur throughout the study area (LKgb). They intrude metamorphosed country rock and commonly have brown to black weathered surfaces and dark greyish green fresh surfaces (Fig. 4d). Most are coarse grained, dominantly composed of hornblende ± pyroxene and plagioclase. Secondary mineral phases include biotite, epidote and chlorite. All gabbro bodies observed are undeformed. The relationships between the gabbro and other intrusive rock types are not clear, except that they are intruded by undeformed granodiorite of the Ruby Range suite, likely making the gabbro Late Cretaceous in age.

Ruby Range Suite (PR)

The dominant intrusive phase in the study area belongs to the Ruby Range suite, comprising grey-beige-rusty weathered, white to grey, medium to coarsely crystalline, biotite-bearing granodiorite. It is generally undeformed, but locally grades into weakly to moderately foliated granodiorite. Composition of the Ruby Range suite changes somewhat towards the south, where hornblende-biotite-phyric quartz diorite to granodiorite dominates. Exposures here are white to pale grey, coarsely crystalline and contain plagioclase, hornblende and biotite, and varying amounts of quartz. Flattened, elongated xenoliths

of darker, biotite and hornblende-rich rock are commonly aligned parallel to foliation (Fig. 4e). Several pegmatite dikes commonly crosscut other igneous phases of the Ruby Range batholith. They are very coarse grained, and contain quartz, plagioclase, K-feldspar, biotite and muscovite. Pegmatite dikes range from 20-30 cm to several metres-wide and are likely the last phases of Ruby Range-related magmatism.

The Ruby Range suite intrudes all other rocks types in the field area except the volcanics discussed below. Ages for the Ruby Range suite north of the present study area are Paleocene and range from 61 Ma to 55 Ma (Israel and Westberg, 2012).

Frederick Lake volcanic complex (EFv)

Volcanic rocks covering an area of approximately 2 km by 2 km south of Frederick Lake (Fig. 2) are not identified on previous maps (Kindle, 1952). They comprise a range of coherent and fragmental volcanic units of intermediate to felsic compositions. Dacitic to andesitic breccia and flow-banded layers composed of plagioclase and quartz phenocrysts in a light to dark grey fine-grained, aphanitic groundmass are either volcanic flows or subvolcanic intrusions (Fig. 4f). Orange weathered, pale grey-green, very fine grained rhyodacite represents the most felsic coherent phase and contains minor pyrite. Finally, flow-banded rhyolitic ash tuff, crystal lapilli tuff and breccia were mapped. These coherent flows and subvolcanic intrusions, as well as volcanoclastic facies (breccia, tuff and lapilli), are interpreted as part of a large volcanic complex. Only the southern and western contacts of this complex are defined where volcanic rocks overlie undeformed granodiorite of the Ruby Range batholith. Several U/Pb samples were collected to assess age relationship with the surrounding intrusive rocks, but it is inferred from field relationships that the volcanic rocks may be Paleocene in age.

STRUCTURE AND METAMORPHISM

The dominant foliation within the schist and gneiss strikes northwest and dips moderately to steeply towards the northeast. This foliation is folded by tight to isoclinal, upright to overturned folds (Fig. 5a) that generally trend northwest and southeast. These folds are deformed by a later phase of tight folds that plunge towards the northeast. Northwest-trending folds may be related to an inferred thrust fault that places rocks of the Yukon-Tanana terrane over unit **PMs** in the central part of NTS 115A/7 (Fig. 2).

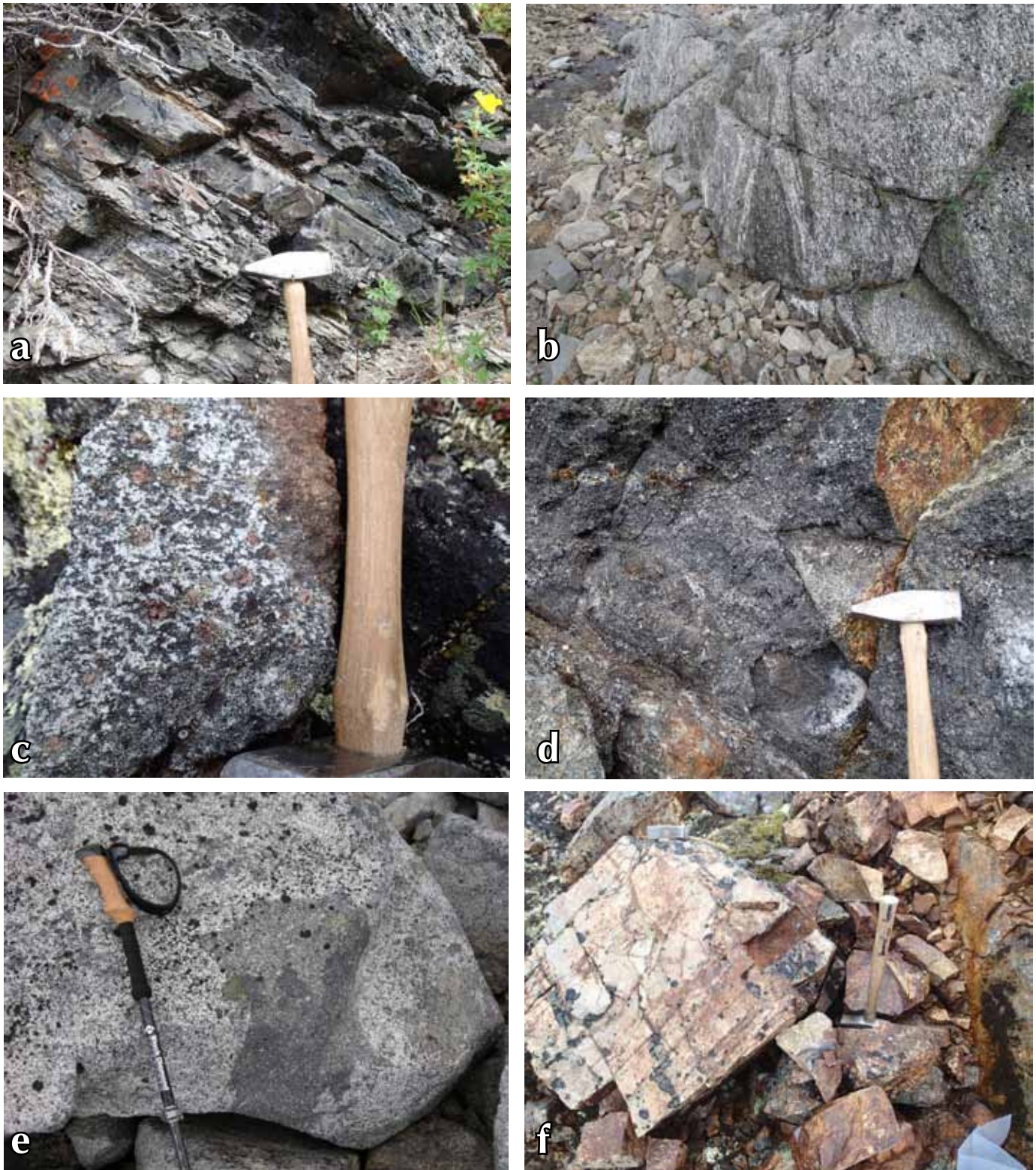


Figure 4. (a) Strongly deformed and metamorphosed Jura-Cretaceous turbidites of the Dezadeash Formation near Million Dollar falls; (b) isoclinally folded Late Cretaceous orthogneiss; (c) garnet-rich hornblende diorite found in the southern part of the study area; (d) dark grey to orange weathered, hornblende \pm pyroxene gabbro of probable Late Cretaceous age; (e) large mafic xenolith within quartz diorite of the Paleocene Ruby Range suite; (f) slightly flow banded, beige to brown weathered rhyodacite of the Frederick Lake volcanic complex.

Folds near this fault have sheared upper limbs suggesting tops towards the southwest motion (Fig. 5b). Moderately northeast-dipping shear zones found throughout the area outline high-strain areas that underwent at least some apparent dextral translation (Fig. 5c). True kinematics of these shear zones is not well constrained as no good lineation was observed at these localities. The timing of motion across these shear zones is unknown.

Metamorphic grade in the area generally decreases from northeast to southwest. Kyanite and garnet are abundant within Yukon-Tanana schist in the northern part of the map area (Fig. 5d). Metapelitic rocks in the footwall of the thrust fault separating the Yukon-Tanana terrane from unit **PMS** contain garnet, kyanite, staurolite as well as biotite, muscovite and quartz (Fig. 6a; Sample 14-SI-088 on Fig. 2). This mineral assemblage indicates middle amphibolite facies metamorphism and intermediate pressure conditions. A preliminary phase diagram for this rock indicates stability of the mineral assemblage Ky-St-Grt-Bt-Ms-Ilm over the P-T interval of 635-650°C and 6.3-6.7 kbars (Fig. 7). Staurolite and kyanite are generally aligned with main through going fabric (defined by biotite and muscovite) with some curved inclusion trails observed within staurolite suggesting a pre to syn-porphyroblast development of the foliation (Fig. 6a,b).

In contrast rocks found farther south and southwest exhibit metamorphic assemblages indicative of much lower pressures. The metasedimentary rocks of unit **PMS** in the far south of the map area have the mineral assemblage biotite, cordierite, plagioclase, quartz, staurolite, sillimanite and minor phases including graphite (Fig. 5e; Sample 14-SI-208 on Fig. 2). Staurolite is wrapped by the main foliation and partially replaced by relatively inclusion-free cordierite (Fig. 6c). Cordierite also forms single porphyroblasts that grow across the main foliation. A sample of the paragneiss found northeast and topographically lower than 14-SI-208 has the mineral assemblage biotite, quartz, plagioclase, cordierite, sillimanite, muscovite and minor phases (Sample 14-SI-215 on Fig. 2). The rock has prominent ellipsoidal white nodules that are typically 2-7 mm in length, are flattened and define a lineation. They are composed of cordierite, which encases sillimanite (Fig. 6d). The sillimanite-cordierite nodules may represent the location of pseudomorphed porphyroblasts, possibly of staurolite (?). The strained nature of the cordierite suggests it experienced some deformation, possibly syn-intrusive. A final sample of the paragneiss from the southernmost part

of the map area has a similar mineral assemblage to the previous two samples but has abundant andalusite (Fig. 5f). Porphyroblasts of andalusite and lesser staurolite are partially replaced by cordierite, which forms moats around their embayed margins (Fig. 6e). Cordierite found both within the matrix and as primary porphyroblasts is rich in graphite. Andalusite and staurolite are partially replaced by sillimanite as small crystals within microboudins and as long needles across pseudomorphs (Fig. 6e,f). Both andalusite and staurolite are wrapped by the matrix foliation whereas replacing and matrix cordierite is not. The early porphyroblast assemblage (St+And) typically forms at ~3.5-4 kbar. The late cordierite is also indicative of low pressures. A sequence involving early St+And followed by Sil+Crd is compatible with a single intrusion-related period of heating, with waning deformation.

DISCUSSION

The Takhanne River and Kluhini River map areas are characterized by roof pendants of metamorphosed siliciclastic, volcanic and carbonate rocks of the Yukon-Tanana terrane and other Paleozoic to Mesozoic units. Paleocene granodiorite enclose these pendants along with probable Late Cretaceous foliated to gneissic intermediate intrusive rocks.

Quartz-muscovite schist, amphibolite, minor marble and quartzite assigned to the Yukon-Tanana terrane are likely part of the Snowcap assemblage and possibly the Finlayson and Klinkit assemblages of the younger parts of the terrane, deformed and metamorphosed multiple times. Similar rocks are found along strike to the north of the present map area, where they are thrust over rocks of the Kluane schist (Israel and Kim, 2014). In the present map area, the Yukon-Tanana terrane is inferred to be thrust over metasedimentary Paleozoic to Mesozoic rocks. These Paleozoic to Mesozoic rocks (unit **PMS**) bear some resemblance to the Dezadeash Formation, as both units are interpreted as turbidite sequences mostly composed of sandstone, siltstone and mudstone. Correlation of unit **PMS** with the Dezadeash Formation would suggest a direct structural contact with rocks of the Yukon-Tanana terrane. Alternatively, Paleozoic to Mesozoic schist and gneiss of unit **PMS** could be part of either the Kluane schist or the Bear Creek assemblage. Both the Bear Creek assemblage and the Kluane schist are found along strike to the north; however their southern continuation into the Kluhini River and Takhanne River areas is not well understood. Where mapped in detail, the Bear Creek



Figure 5. (a) Early isoclinal folds within amphibolite orthogneiss; (b) tight to isoclinal, overturned fold with sheared upper limb located near the structural contact between the Yukon-Tanana terrane and Paleozoic to Mesozoic schist; (c) moderately northeast-dipping ductile shear zone cutting through Paleozoic to Mesozoic schist, exhibiting apparent dextral sense of motion; (d) large kyanite porphyroblasts in schist of the Yukon-Tanana terrane; (e) staurolite porphyroblasts rimmed by cordierite (white) within Paleozoic to Mesozoic schist; (f) andalusite porphyroblasts within Paleozoic to Mesozoic paragneiss.

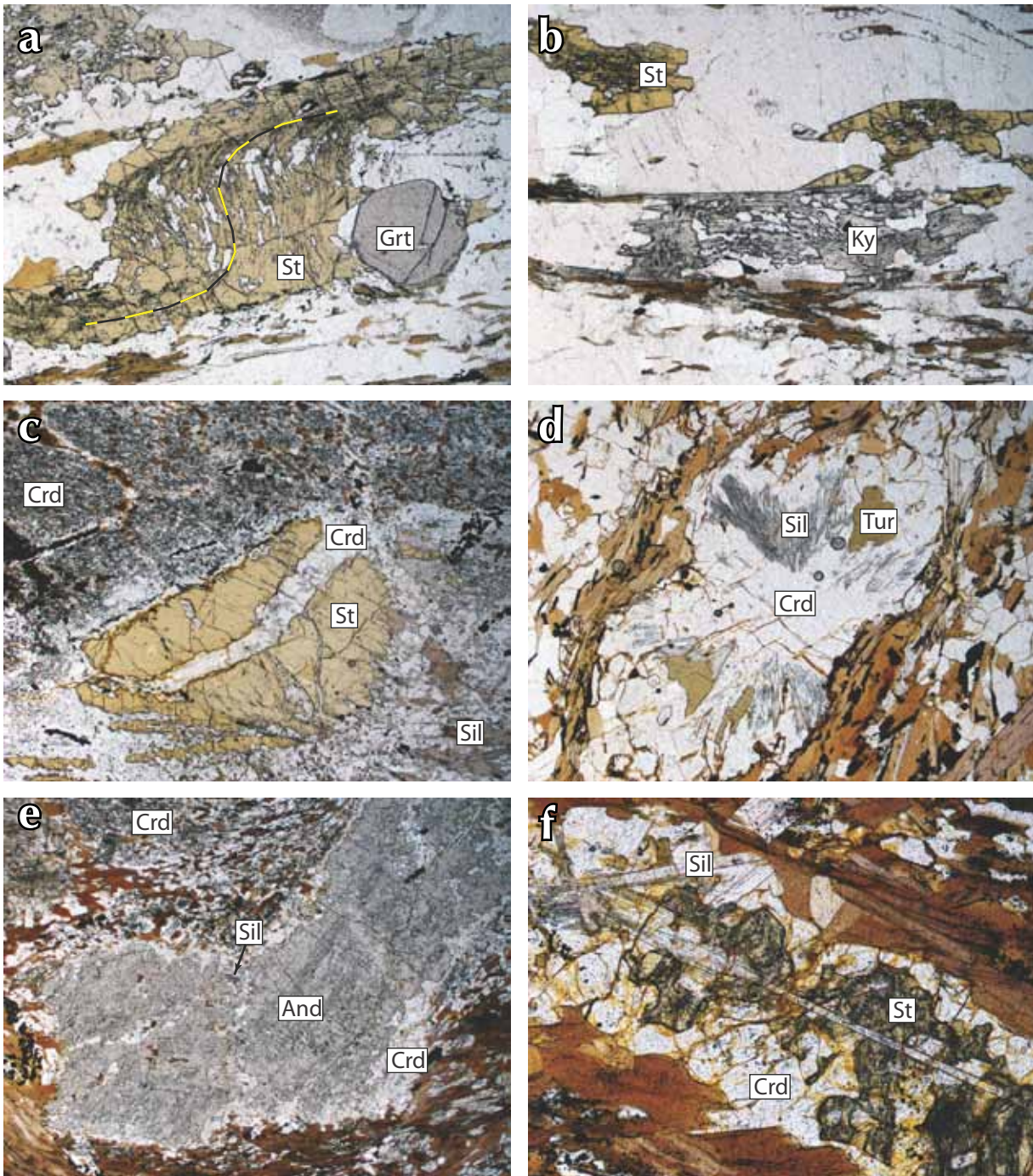


Figure 6. Photomicrographs taken in plane polarized light. (a) Staurolite and garnet porphyroblasts in sample 14-SI-088. Folded inclusion trails are preserved in the staurolite. Field of view = 3 mm. (b) Poikilitic kyanite and staurolite porphyroblasts in sample 14-SI-088. The long axis of the kyanite crystal is parallel to the foliation in the matrix, which is defined by preferentially aligned biotite and muscovite. Field of view = 3 mm. (c) Partly replaced staurolite porphyroblast in sample 14-SI-208. Inclusion-poor cordierite forms a continuous rim around staurolite. Cordierite porphyroblasts are rich in graphite inclusions. Field of view = 6 mm. (d) Nodule composed of cordierite with inclusions of radiating sillimanite and tourmaline in sample 14-SI-215. The matrix of the rock comprises biotite, quartz, plagioclase, cordierite and minor phases. Field of view = 3 mm. (e) Andalusite porphyroblast with a continuous rim of cordierite in sample 14-SI-216. Unlike the inclusion-poor cordierite that directly replaced andalusite, small cordierite porphyroblasts in the matrix are rich in graphite inclusions. Field of view = 6 mm. (f) Staurolite porphyroblast partly replaced by sillimanite (needles) and cordierite (continuous rim) in sample 14-SI-216. Field of view = 1.5 mm.

assemblage comprises mainly metamorphosed and deformed metavolcanic and metasedimentary rocks (Israel *et al.*, 2014). The metavolcanic rocks are intermediate to mafic flows and volcanoclastic rocks while the sedimentary portion of the unit is characterized by mudstone, siltstone and minor sandstone and calcareous mudstone. In other places the unit is almost entirely metabasalt structurally interleaved with thin bodies of ultramafic rocks. The Paleozoic to Mesozoic rocks in the present map area are dominantly sedimentary with no metavolcanic components; however, the sedimentary sequence is similar to that of the sedimentary portion of the Bear Creek assemblage. The Kluane schist on the other hand is dominantly a sedimentary unit. It is characterized by a fairly monotonous sequence of quartz-biotite schist, with little variation except for a paragneissic component found close to the structural boundary with the Yukon-Tanana terrane. It is possible that the Paleozoic to Mesozoic rocks found within the present map area are the southern extension of the Kluane schist. The local occurrence of carbonate horizons and the turbiditic nature of the Paleozoic to Mesozoic rocks are not really compatible with the monotonous quartz-biotite schist of the Kluane schist.

The juxtaposition of the various rock units likely occurred during southwest-directed shortening in the Late Cretaceous. The timing of deformation is probably related to foliation development within Late Cretaceous intrusive rocks structurally interleaved with Yukon-Tanana rocks. Whether this event coincided with peak metamorphic conditions is yet to be determined. Low-pressure metamorphism is likely associated with the intrusion of the large volume of the Paleocene Ruby Range suite. There is some evidence, such as locally foliated Ruby Range suite and deformed low-pressure assemblages within the Paleozoic to Mesozoic rocks, to suggest at least some deformation was occurring in the Paleocene.

Similar structural and metamorphic histories are described for rocks in southeast Alaska near the city of Juneau. In that area, rocks of Yukon-Tanana terrane are interpreted to be thrust over rocks of the Taku terrane and the Gravina assemblage (Gehrels *et al.*, 1992; Miller *et al.*, 2000). The Taku terrane is a Paleozoic to Mesozoic metasedimentary and metavolcanic assemblage (Saleeby, 2000; Gehrels, 2002) that has elements similar to the Bear Creek assemblage, and the Gravina assemblage is the along-strike equivalent to the Dezadeash Formation (McClelland *et al.*, 1992; Gehrels and Kapp, 1998).

CONCLUSION

The Kluhini and Takhanne River map areas are characterized by Yukon-Tanana terrane and Paleozoic to Mesozoic metamorphic rocks enclosed in Paleocene granodiorite of the Ruby Range suite. Late Cretaceous deformation led to the structural emplacement of Yukon-Tanana terrane over Paleozoic to Mesozoic schists and gneisses. The Paleozoic to Mesozoic rocks bear some similarities to the Dezadeash Formation, as well as the Bear Creek assemblage and the Kluane schist.

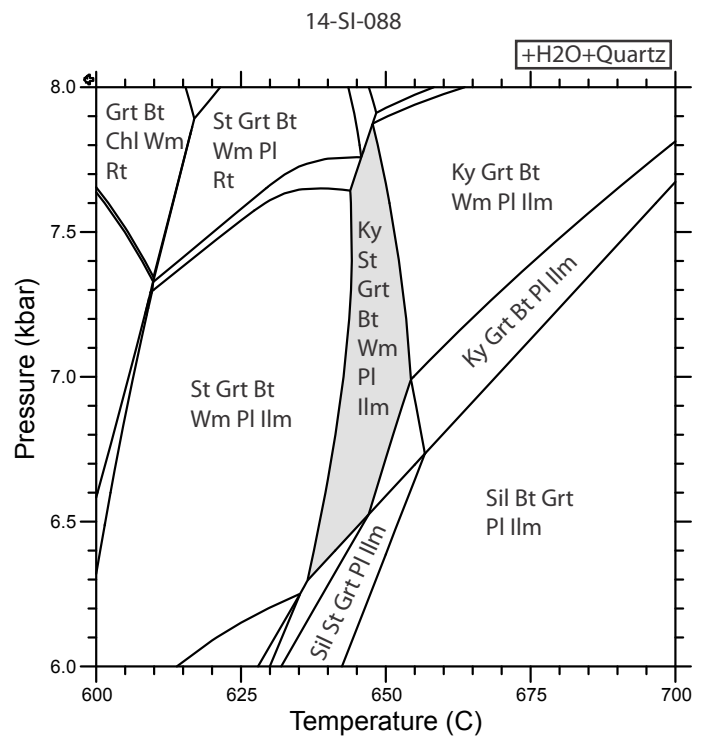


Figure 7. Equilibrium assemblage diagram for schist sample 14-SI-088. The assemblage Ky-St-Grt-Bt-Ms-Pl-Qtz-Ilm indicates that peak metamorphism took place under middle amphibolite facies, intermediate pressure conditions (~635-650°C, ~6.3-7.8 kbar). The equilibrium assemblage diagram was produced using Theriak-Domino software. Modeling was carried out in the ten-component system MnO-Na₂O-CaO-K₂O-FeO-MgO-Al₂O₃-SiO₂-H₂O-TiO₂ (MnNCKFMASH). P₂O₅ was removed from the bulk composition by projection from apatite. The thermodynamic database of Holland and Powell (1998) was used in conjunction with the solution models listed in Pattison and Tinkham (2009). A pure H₂O fluid phase was assumed to be present in excess throughout the P-T range.

REFERENCES

- Colpron, M., Nelson, J.L. and Murphy, D.C., 2006. A tectonostratigraphic framework for the pericratonic terranes of the northern Cordillera. *In: Paleozoic evolution and metallogeny of pericratonic terranes at the ancient Pacific margin of North America, Canadian and Alaskan Cordillera*, M. Colpron, J.L. Nelson and R.I. Thompson (eds.), Geological Association of Canada, Special Paper 45, p. 1-23.
- Eisbacher, G.H., 1976. Sedimentology of the Dezadeash flysch and its implications for strike-slip faulting along the Denali fault, Yukon Territory and Alaska. *Canadian Journal of Earth Sciences*, vol. 13, p. 1495-1513.
- Gehrels, G.E., 2002. Detrital zircon geochronology of the Taku terrane, southeast Alaska. *Canadian Journal of Earth Sciences*, vol. 39, p. 921-931.
- Gehrels, G.E. and Kapp, P.A., 1998. Detrital zircon geochronology and regional correlation of metasedimentary rocks in the Coast Mountains, southeastern Alaska. *Canadian Journal of Earth Sciences*, vol. 35, p. 269-279.
- Gehrels, G.E., McClelland, W.C., Samson, S.D., Patchett, P.J. and Orchard, M.J., 1992. Geology of the western flank of the Coast Mountains between Cape Fanshaw and Taku Inlet, southeastern Alaska. *Tectonics*, vol. 11, p. 567-585.
- Holland, T.J.B. and Powell, R. 1998. An internally consistent thermodynamic dataset for phases of petrological interest. *Journal of Metamorphic Geology*, vol. 16, p. 309-343.
- Israel, S., Colpron, M., Moynihan, D., Murphy, D.C. and Relf, C., 2014. Bedrock geology of the Mount Decoeli area. Yukon Geological Survey Open File 2014-18.
- Israel, S. and Kim, R., 2013. Preliminary geological map of the Granite Lake area, parts of NTS 115A/10, 11, 14, and 15. Yukon Geological Survey Open File 2013-17, 1:50000 scale.
- Israel, S. and Kim, R., 2014. Preliminary investigation into the geologic relationships in the Granite Lake area, parts of NTS 115A/10,11,14 and 15, southwest Yukon. *In: Yukon Exploration and Geology 2013*, K.E. MacFarlane, M.G. Nordling, and P.J. Sack (eds.), Yukon Geological Survey, p. 79-91.
- Israel, S., Murphy, D.C., Bennett, V., Mortensen, J.K. and Crowley, J., 2011. New insights into the geology and mineral potential of the Coast Belt in southwestern Yukon. *In: Yukon Exploration and Geology*, K.E. MacFarlane, L.H. Weston and C. Relf (eds.), Yukon Geological Survey, p. 101-123.
- Israel, S. and Westberg, E., 2011. Preliminary geological map of the northwestern Aishihik Lake area, parts of NTS 115H/12 and 13. Yukon Geological Survey Open File 2011-31, 1:50000 scale.
- Israel, S. and Westberg, E., 2012. Geology and mineral potential of the northwestern Aishihik Lake map area, parts of NTS 115H/12 and 13. *In: Yukon Exploration and Geology 2011*, K.E. MacFarlane and P.J. Sack (eds.), Yukon Geological Survey, p. 103-113.
- Kindle, E.D., 1952. Dezadeash Map-Area, Yukon Territory. Geological Survey of Canada Memoir 268, 68 p.
- Lowey, G., 2000. The Tatshenshini shear zone (new) in southwestern Yukon, Canada: Comparison with the Coast shear zone in British Columbia and southeastern Alaska and implications regarding the Shakwak suture. *Tectonics*, vol. 19, p. 512-528.
- McClelland, W.C., Gehrels, G.E. and Saleeby, J.B., 1992. Upper Jurassic-Lower Cretaceous basinal strata along Cordilleran margin: Implications for the accretionary history of the Alexander-Wrangellia-Peninsular terrane. *Tectonics*, vol. 11, p. 823-835.
- Miller, L.D., Stowell, H.H. and Gehrels, G.E., 2000. Progressive deformation associated with mid-Cretaceous to Tertiary contractional tectonism in the Juneau gold belt, Coast Mountains southeastern Alaska. *In: Tectonics of the Coast Mountains, Southeastern Alaska and British Columbia*, H.H. Stowell and W.C. McClelland (eds.), Geological Society of America, Special Paper 343.
- Nelson, J.L., Colpron, M. and Israel, S., 2013. The Cordillera of British Columbia, Yukon and Alaska: Tectonics and metallogeny. *Society of Economic Geology: Special Publication 17*, p. 53-109.
- Pattison, D.R.M. and Tinkham, D.K., 2009. Interplay between equilibrium and kinetics in prograde metamorphism of pelites: an example from the Nelson aureole, British Columbia. *Journal of Metamorphic Geology*, vol. 27, p. 249-279.

Saleeby, J.B., 2000. Geochronologic investigations along the Alexander-Taku terrane boundary, southern Revillagigedo Island to Cape Fox areas, southeast Alaska. *In: Tectonics of the Coast Mountains in southeast Alaska and British Columbia*, H.H. Stowell and W.C. McClelland (eds.), Geological Society of America, Special Paper 343, p. 107-143.

van der Heyden, P., 1992. A Middle Jurassic to early Tertiary Andean-Sierran arc model for the Coast Belt of British Columbia. *Tectonics*, vol. 11, p. 82-97.

Using terrestrial cosmogenic nuclides to constrain timing of penultimate ice advance in the Ogilvie Mountains, Yukon

L. Brown¹, B. Ward

Simon Fraser University, Department of Earth Sciences

J. Bond

Yukon Geological Survey

J. Gosse

Dalhousie University, Department of Earth Sciences

Brown, L., Ward, B., Bond, J.D and Gosse, J., 2015. Using terrestrial cosmogenic nuclides to constrain timing of penultimate ice advance in the Ogilvie Mountains, Yukon. *In: Yukon Exploration and Geology 2014*, K.E. MacFarlane, M.G. Nordling and P.J. Sack (eds), Yukon Geological Survey, p. 17-27

ABSTRACT

Throughout the Pleistocene epoch, Yukon was repeatedly influenced by glacial ice originating from the Cordilleran Ice Sheet and independent alpine glaciers. The penultimate limit in Yukon has garnered controversy in recent years, as moraines in the central region of the territory were found to be older (MIS 6) than moraines in the southwest part of the territory and Alaska (MIS 4). The Ogilvie Mountains, located east of Dawson City, have proven especially problematic for chronological studies. This study will attempt to test a relatively new dating method on penultimate surfaces in the Ogilvie Mountains; Chapman Lake is the primary study area. Using a vertical sampling method to construct a cosmogenic depth versus concentration profile in outwash gravel, this research will determine whether Marine Isotope Stage 4 or 6 provided the conditions necessary for ice nucleation to build the penultimate glacial surface. The age calculated by the depth profile is supported by radiocarbon ages and macrofossil samples, optically stimulated luminescence ages, TCN boulder dating, as well as detailed stratigraphy of significant sites near the Chapman Lake moraine. The results will help determine the effects of climate forcing in this region and its relationship to the existing glacial framework of the territory.

¹loganb@sfu.ca

INTRODUCTION

Glaciation in Yukon has proven more complex than was originally mapped by Bostock (1966) and Hughes *et al.* (1969). The Cordilleran Ice Sheet (CIS) in Yukon is divided into 5 major lobes based on source areas and flow direction: the St. Elias and Coast Mountain lobes in the southwest, the Cassiar and Selwyn lobes in central Yukon, and the Liard lobe in the southeast (Fig. 1). Initially, three major limits of the CIS were established by Hughes (1969) based on mapped correlations of moraines and geomorphic expression. The McConnell glaciation represents the most recent period of glaciation in the Canadian Cordillera and also the least extensive. The McConnell limit has been firmly dated to Marine Isotope Stage (MIS) 2, with ice sheet expansion established by ~ 24 ka (Jackson *et al.* 1991), and evidence showing that deglaciation had begun by ~ 12 ka (Stroeven *et al.*, 2010). Pre-Reid is the oldest and most extensive mapped limit. It comprises multiple advances from 2.6 Ma to the middle Pleistocene that left behind limited depositional or erosional landforms. Multiple studies (Tarnocai and Schweger, 1991; Froese *et al.*, 2000; Jackson *et al.*, 2012) have confirmed that there was more than one pre-Reid advance, spanning from 2.6 Ma (Hidy *et al.*, 2013) to the mid-Pleistocene.

Of particular interest to this work is the intermediate or penultimate limit of the Reid Glaciation, described by Bostock (1966) and others (Hughes *et al.*, 1969; Duk-Rodkin, 1999) as a single advance of the Cordilleran Ice Sheet. Timing of the penultimate advance of the CIS has been uncertain since its initial mapping. It was initially correlated to the Middle Wisconsin (MIS 4) (Bostock, 1966; Hughes *et al.*, 1969). However, the presence of the Diversion Creek paleosol on Reid deposits, which is more developed than modern soil profiles (Smith *et al.*, 1986; Tarnocai and Smith, 1989; Tarnocai and Schweger, 1991), implies a pre-last interglacial age; this suggests the Reid glaciation to be MIS 6 or older. At Ash Bend, in central Yukon, Westgate *et al.* (2001) observed the Sheep Creek tephra stratigraphically overlying Reid till. Based on a thermoluminescence age of 190 ± 20 ka for the Sheep Creek tephra (Berger *et al.*, 1996), the Reid was interpreted to be either MIS 10 or 8. Absolute $^{40}\text{Ar}/^{39}\text{Ar}$ dating to 311 ± 32 ka (Huscroft *et al.*, 2004) (later corrected to 441 ± 76 (Jackson *et al.*, 2012)) of a middle Pleistocene volcanic unit below Reid outwash at Fort Selkirk seemed to confirm an MIS 8 age for the Reid. However, Westgate *et al.* (2008) discovered several geochemically distinct

Sheep Creek tephra layers with ages ranging from 190 to 80 ka, and reinterpreted the Ash Bend site as an MIS 6 age for the Reid.

An MIS 6 age for the Reid Glaciation was confirmed by the discovery of Old Crow tephra associated with Reid deglacial deposits along the Pelly River (Ward *et al.*, 2008). The Old Crow tephra has a well-established fission track age of 124 ± 10 ka (Preece *et al.*, 2011). Demuro *et al.* (2011) also confirmed an MIS 6 age using single grain optical stimulated luminescence (OSL) dates from two glaciofluvial beds bracketing Reid till. An age of 158 ± 18 ka was obtained for the unit overlying the till, and an age of 132 ± 18 ka for the unit beneath the till (Demuro *et al.*, 2011). Although the dates were stratigraphically reversed they showed agreement within 1σ error and fit stratigraphically with the ages of the Sheep Creek tephra at Ash Bend (Westgate *et al.*, 2008).

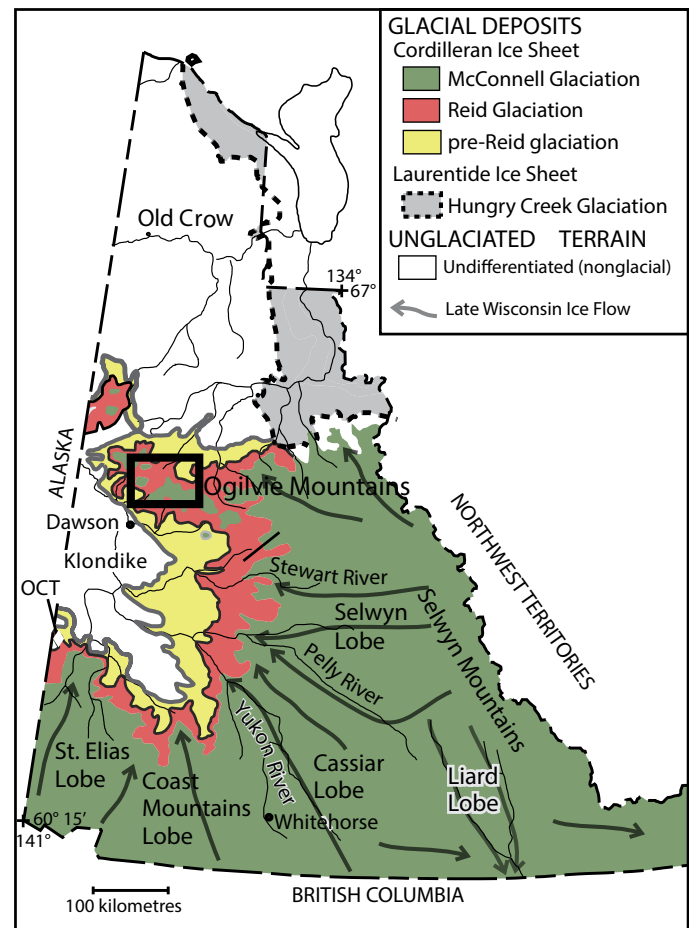


Figure 1. Map of Yukon Territory with marked glacial limits, showing McConnell, Reid and pre-Reid advances. After Duk-Rodkin (1999) and Ward *et al.*, (2007).

Although the Reid Glaciation has been shown to have achieved its maximum during MIS 6 in central Yukon, improved dating methods determined that the mapped penultimate limit is a diachronous boundary, representative of both an MIS 4 advance in southwest Yukon (Ward et al., 2007) and an MIS 6 advance in central Yukon (Ward et al., 2008; Demuro et al., 2011). Ward et al. (2007) obtained the first MIS 4 age on the penultimate glaciation in Yukon at Aishihik Lake. This region in southwest Yukon was affected by the St. Elias and Coast Mountains lobes of the Cordilleran Ice Sheet and the 'Gladstone glaciation' was assigned to this advance. It was proposed that the diachronous record was due to the precipitation limited nature of glaciers in Yukon and that variation in effective precipitation influenced glacier extents in the different source areas (Ward et al., 2007). The MIS 4 age for the penultimate limit in southwest Yukon is supported by MIS 4 advances in Alaska established by Briner et al. (2005) for three penultimate moraines using cosmogenic exposure dating. Three glacial limits, within 15 km of each other and along the White River in southwest Yukon, were deposited during MIS 2, 4 and 6 (Turner et al., 2013). These ages are based on multiple tephras and both finite and non-finite radiocarbon ages. The proximity of the MIS 2 (McConnell), MIS 4 (Gladstone) and MIS 6 (Reid) limits along the White River indicate that precipitation conditions were similar in southwest Yukon throughout the middle to late Pleistocene, allowing for continued expansion of ice sheets (Turner et al., 2013). Turner's research also demonstrates the regional variability of ice sheet growth throughout the Yukon.

Previous work indicates that precipitation acts as a major control on ice nucleation, which is largely dependent on location within the territory. This study is located in the Ogilvie Mountains east of Dawson City near the northern extent of the CIS, and will provide insight into the response of the CIS in a region with distinct ice accumulation areas and precipitation limiting conditions. Few absolute dating studies have been carried out in the region and those have yielded controversial results. The aim of this study is to provide a clear age for the penultimate advance of the CIS in the Ogilvie Mountains. Based on the findings of earlier studies, the age of the penultimate advance will likely be MIS 6, following the established pattern of MIS 4 penultimate ages found predominantly in southwest Yukon, and older MIS 6 ages being situated in central Yukon.

RESEARCH OBJECTIVES

The objective of this research is three-fold; not only does it involve solving a complex problem, but will also test an unconventional method of absolute dating. Our objectives are:

1. to determine whether the penultimate advance in the Ogilvie Mountains corresponds to MIS 4 or MIS 6, through use of a variety of Quaternary dating methods (terrestrial cosmogenic nuclide, optically stimulated luminescence and radiocarbon);
2. age fit determination within the glacial framework of the Yukon; and
3. to test the method of terrestrial cosmogenic nuclide (TCN) concentration vs. depth profile in an area with complex erosional depositional history.

STUDY AREA: CHAPMAN LAKE AND NORTH KLONDIKE RIVER

The study area is located along the Dempster Highway in the Ogilvie Mountains. The Ogilvie Mountains are located within the maximum northern limit of the CIS. Field work was completed at two locations; near the North Klondike River and at Chapman Lake (Fig. 2). The North Klondike River site is located 8.5 km beyond the MIS 2 (McConnell) limit, into the penultimate limit, and Chapman Lake is located 13 km beyond the McConnell limit. Background information and work completed at each site is described below.

CHAPMAN LAKE

The Chapman Lake area is characterized by hummocky moraine deposits, glacial fluvial and glacial lacustrine units, as well as loess and till deposits. Due to the abundant sedimentological evidence of glaciation in the area, Chapman Lake acted as the major focus area for this research.

Previous Work

Several attempts have been made to discern the absolute age of the penultimate limit at Chapman Lake; however results have proven to be conflicting. A regional cosmogenic ^{10}Be study on Yukon glacial deposits, completed by Stroeve et al. (2010), includes samples from the Ogilvie Mountains; the objective was to provide

more accurate chronological constraints on a regional scale and to establish vertical limits of glaciation. Results from their study revealed conflicting ages from samples collected from one moraine, suggesting a strong influence of exhumation of boulders and moraine degradation. Furthermore, there was noticeable disparity in some of the ages obtained, commonly due to the sampling of cobbles in the absence of boulders. In the Chapman Lake area, young ages (<10 ka) were derived for McConnell moraines suggesting the McConnell limit could be a late glacial advance, which was also proposed by Bierle (2002). The conflict in ages as a result of Holocene post-glacial processes indicate that more work needs to be carried out in the Chapman Lake area in order to constrain ages on the penultimate limit. Sediment coring of Chapman Lake completed by Bierle (2002) suggests a McConnell (MIS 2) age based on radiocarbon dating of organics in the core to 13210 ± 300 ^{14}C yr BP (Bierle, 2002). This age likely reflects the timing of sediment accumulation within the lake rather than the deposition of the moraine sediments. Work by Lacelle *et al.* (2007) on a massive ice-wedge body discovered beneath a reworked diamict called into question the proposed MIS 2 age of the Chapman Lake moraine. Using crystallographic analysis and stable isotope analysis the ice body was confirmed to be glacial in origin. High $\delta^{18}\text{O}$ values, in comparison to other MIS 2 aged ice bodies in the Canadian Arctic, suggest an MIS 4 age. A Holocene age obtained from the overlying diamict confirms that these were not deposited during the Reid, but were reworked by solifluction. The material then travelled downslope, adding more sediment on top of the ice body. This suggests that the original cover was much thinner, making it difficult to sustain the ice during more than one glacial-interglacial cycle, indicating an MIS 4 origin (Lacelle *et al.*, 2007).

NORTH KLONDIKE RIVER

The North Klondike River site is located south of the McConnell limit and within the limit of the penultimate glaciation (Fig. 2). The site is located on an irregular bedrock terrace in the valley bottom on the east side adjacent to the North Klondike River. Weathered syenite boulder erratics (NK-01 and NK-02) were identified on the bedrock, and presented

a good opportunity to use TCN dating to determine the age of the glaciation.

TOMBSTONE TERRITORIAL PARK INTERPRETIVE CENTRE

Two additional erratics (13-OG-MC-01 and 13-OG-MTB) were found within 25 km of the Tombstone Territorial Park Interpretive Centre (Fig. 2) within the penultimate limit. MC-01 is found about 5 km north of the interpretive centre between two alpine end moraines. The ground is extremely hummocky and the boulder is adjacent to a deeply incised stream. The MTB boulder is found on a moraine complex about 24 km north of the interpretive centre (Fig. 2).

METHODOLOGY

COSMOGENIC DEPTH VERSUS CONCENTRATION PROFILE

One of the primary purposes of this project is to test the TCN concentration versus depth profile method. Terrestrial cosmogenic nuclides build up in minerals as a result of prolonged exposure to secondary cosmic rays that originate from outside our solar system. When material

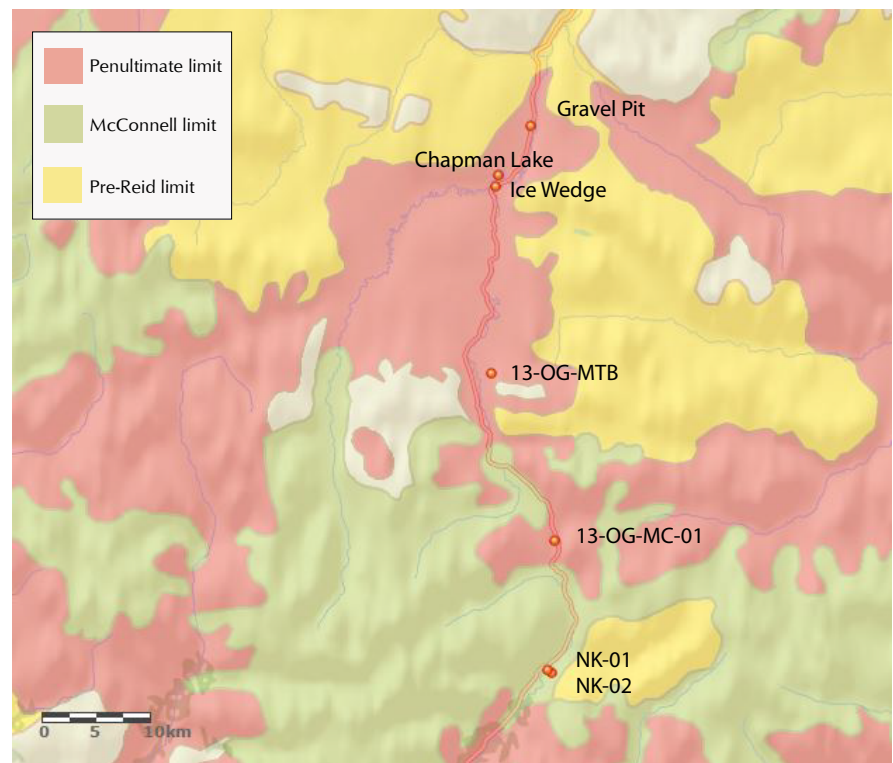


Figure 2. Map of the study area with mapped limits and location of sample sites.

is deposited under ice, TCN cannot be produced as the ice acts as a barrier. Once the ice retreats, the newly exposed sediments begin to accumulate TCN which can be measured by Accelerator Mass Spectrometry (AMS) in order to calculate an age of ice retreat.

In order to construct an accurate curve, the procedure for sampling a depth profile in the gravel unit requires collecting six, 1 kg samples of gravel in an evenly spaced, vertical sequence. In addition to those six samples, a single sample was collected ~2 m below the top of the unit in order to establish the baseline inherited TCN within the gravel unit. Finally, due to the presence of the cryoturbated zone, a swath sample was taken throughout the entire upper 60 cm of the gravel. This sample is collected because cryoturbation likely caused mixing, which would ultimately result in a fairly uniform concentration throughout the unit. It was important to obtain the swath sample as a measure of the approximate maximum concentration at the top of the unit.

Once the samples were collected, they were sent to Dalhousie University's Terrestrial Cosmogenic Nuclide Facility (CNEF) for processing. The gravel was crushed down to fine sand, sieved and magnetically separated. The samples were then treated with hydrofluoric and nitric acids in order to produce a ^{36}Cl target, comprising the ^{36}Cl from the sample with a known quantity of ^{35}Cl added during lab work. The target was then sent to Perdue University's Perdue Rare Isotope Measurement (PRIME) Lab for Accelerator Mass Spectrometry (AMS) analysis. Currently, ^{36}Cl ages are being calculated with the latest version of the CRONUS online calculator.



Figure 3. Boulder sample (13-OG-MTB). Note visible surface weathering.

BOULDER SAMPLING

Boulders used for TCN dating are carefully selected based on several significant factors. First and foremost, the boulder needs to be of sufficient size to reduce the possibility of exhumation and the likelihood of inheritance. The boulder site should have a stable surface with minimal slope. Heavily eroded boulders are not used, as removing the outermost surface with the highest TCN concentration would result in a younger age. Using a diamond-blade cut out saw, 4 to 5 parallel cuts are made ~2 to 3 cm deep and 3 to 4 cm apart into the boulder, with 2 perpendicular cuts at either end of the lines (Fig. 3). The slabs are then chiselled out, and the sample undergoes the same physical crushing, separation and chemical treatment as the TCN samples at Dalhousie University's CNEF lab.

MACROFOSSIL AND RADIOCARBON SAMPLES

Several organic horizons found in the study area were sampled (Fig. 4) in order to determine paleoenvironment of the Chapman Lake region during the Pleistocene. If sufficient organics are present in the sample, they are sent for radiocarbon dating analysis at Paleotec Labs.

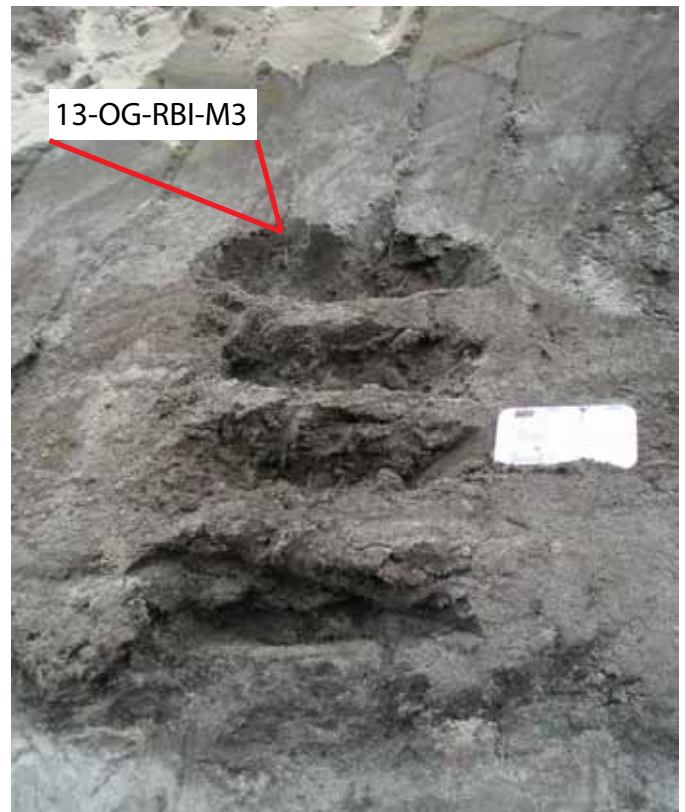


Figure 4. Samples taken within the organic horizon shown in Figure 6. The uppermost sample in the sequence (13-OG-RBI-M3), taken 45 cm above the lower contact, was sent for age dating.

OPTICALLY STIMULATED LUMINESCENCE (OSL) SAMPLES

Two OSL samples were collected in the field to act as supporting evidence for the depth profile. OSL dating is based on the principle of electrons building up in traps in crystal lattices. To be used, the sand grains need to be exposed to light to empty out the traps. The sample is then buried and the radioactive breakdown causes electrons to be dislodged and build up over time. The sand grains are illuminated with light and the radiation given off is measured. An age can then be calculated (Rhodes, 2011). Copper pipes were hammered into the sand using a rubber mallet, then carefully dug out of the section with a trowel. Both ends of the copper tube were stuffed tightly with paper to ensure the sediments would not mix, the tube was then wrapped in tape to avoid exposure to sunlight. The OSL age will be used to constrain the degree of mixing by cryoturbation in the upper part of the underlying gravel comprising Unit 1. It will also act as supporting evidence for the final age calculated from the TCN depth profile. The samples are currently undergoing analysis at the Luminescence dating laboratory (LUX) at the Université du Québec à Montréal.

RESULTS

STRATIGRAPHY: GRAVEL PIT SIT

Determining an age of the Chapman Lake site using terrestrial cosmogenic nuclides methods was challenging due to an absence of glacial erratics suitable for dating. It was decided to target the related glaciofluvial outwash gravel and use a TCN concentration versus depth profile to derive an age. Results from this part of the project are not yet available, however the site and methodology are described. An exposure was identified at a gravel pit adjacent to the Dempster Highway. The section is characterized by a 6 m unit of gravel, overlain by about 1 to 2 m of cryoturbated sand and loess (Fig. 5). It was decided that the thick gravel would prove an ideal unit in which to test the concentration versus depth profile.

Unit 1 is characterized as a sandy gravel unit and it makes up the majority of the exposure. The lower contact was not observed, so the unit is >6 m thick. Grain sizes in Unit 1 range from medium sand to ~14 cm cobbles. The subrounded to rounded clasts are randomly oriented and have weak stratification. Vertical and frost shattered

clasts are visible in the upper 15 to 60 cm of the unit and appear to be more prominent in regions where overlying sediments are thicker. Clasts are dominantly metasedimentary, with minor volcanic clasts.

Unit 2 is a medium-grained sand of variable thickness ranging from 0 to 45 cm with a sharp, irregular lower contact. The sand contains small pebbles ranging from 0.5 to 4.5 cm in size, which are more dominant in the lower 5 to 10 cm of the unit. There is no visible structure within the unit (Fig. 6).

Unit 3 is a 60 cm, fine to medium-grained sand supported diamict containing 10 to 15% clast content, with clasts ranging in size from 3 to 7 cm. Clasts are randomly oriented and are rounded to subrounded. The unit is a mottled, beige and light brown colour. The unit has an irregular lower contact with the sand unit and is massive.

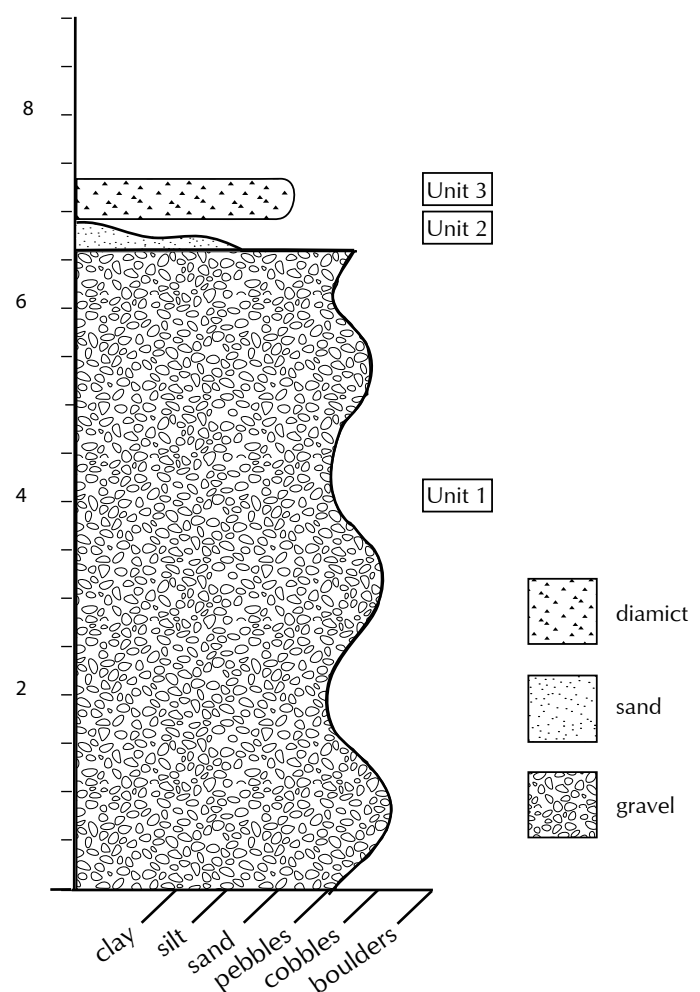


Figure 5. Schematic section of the gravel pit.

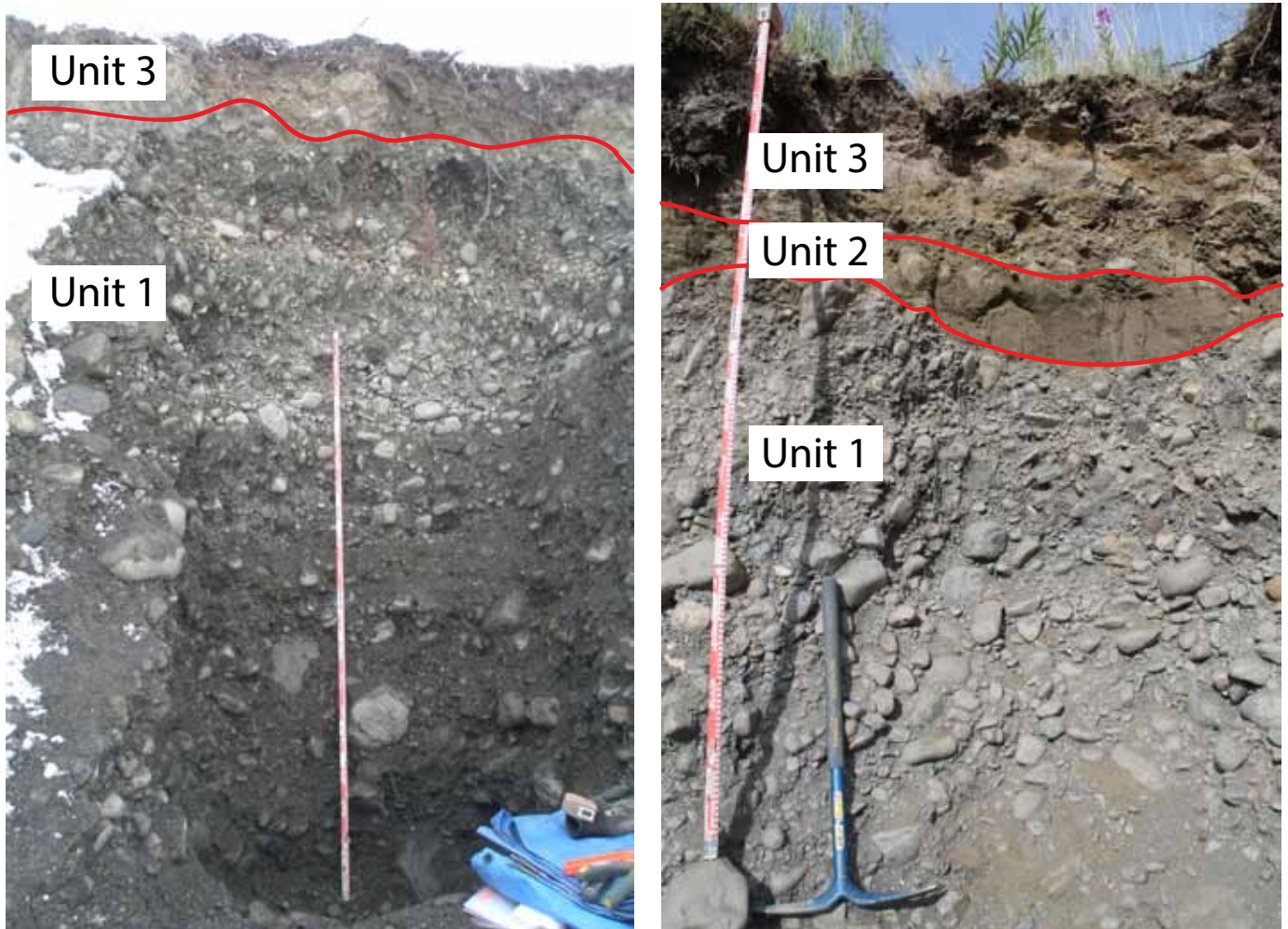


Figure 6. Comparison of two locations at the gravel pit. (a) Sample location, note that Unit 2 is not present; (b) ~5 m north from an earlier sample location. Unit 2 overlies the gravel unit.

STRATIGRAPHY: ICE WEDGE SITE

To support the TCN dating study of the glaciofluvial gravel, stratigraphic descriptions were completed at a section within the penultimate moraine at Chapman Lake. The rationale for stratigraphy is to assess the site for optical stimulated luminescence (OSL) and radiocarbon dating to use for supporting evidence from the depth profile. The Ice Wedge site is located on the south side of the Dempster Highway at the Chapman Lake road sign at kilometre 116. The section was exposed by river erosion and is named for a large ice wedge visible in the upper part of the section (Figs. 7 and 8). The section was previously reported by Duk-Rodkin (1996) who identified a diamict at the base of the section (Unit 1) and interpreted it to be a glacial till. The 3-m-thick unit has a fine-grained sand to silt matrix containing pebble to cobble-sized clasts that are well polished and display striations. The clasts display no

visible preferred orientation (however, a till fabric was not completed) and are subangular to subrounded.

Overlying the diamict is a 10 to 12 m sequence of interstratified silt and sand (Unit 2), containing multiple organic horizons. The sequence alternates between massive and laminated sub-units. Some layers are a blue-grey colour, indicative of reducing conditions, while others have been stained rusty red-brown by oxidization. Small, millimetre-scale *Psidium* shells are found in frozen, blue-grey reduced sediments throughout the unit. The organic horizons vary in thickness from 2 to 30 cm, and were sampled in order to determine macrofossil content as well as a radiocarbon age if possible (Fig. 4).

Unit 3 is a 2-m-thick fine sand and silt deposit that caps the Ice Wedge section. Unit 3 is dominantly fine-grained, loosely consolidated sand to silt and displays no visible sedimentary structures.

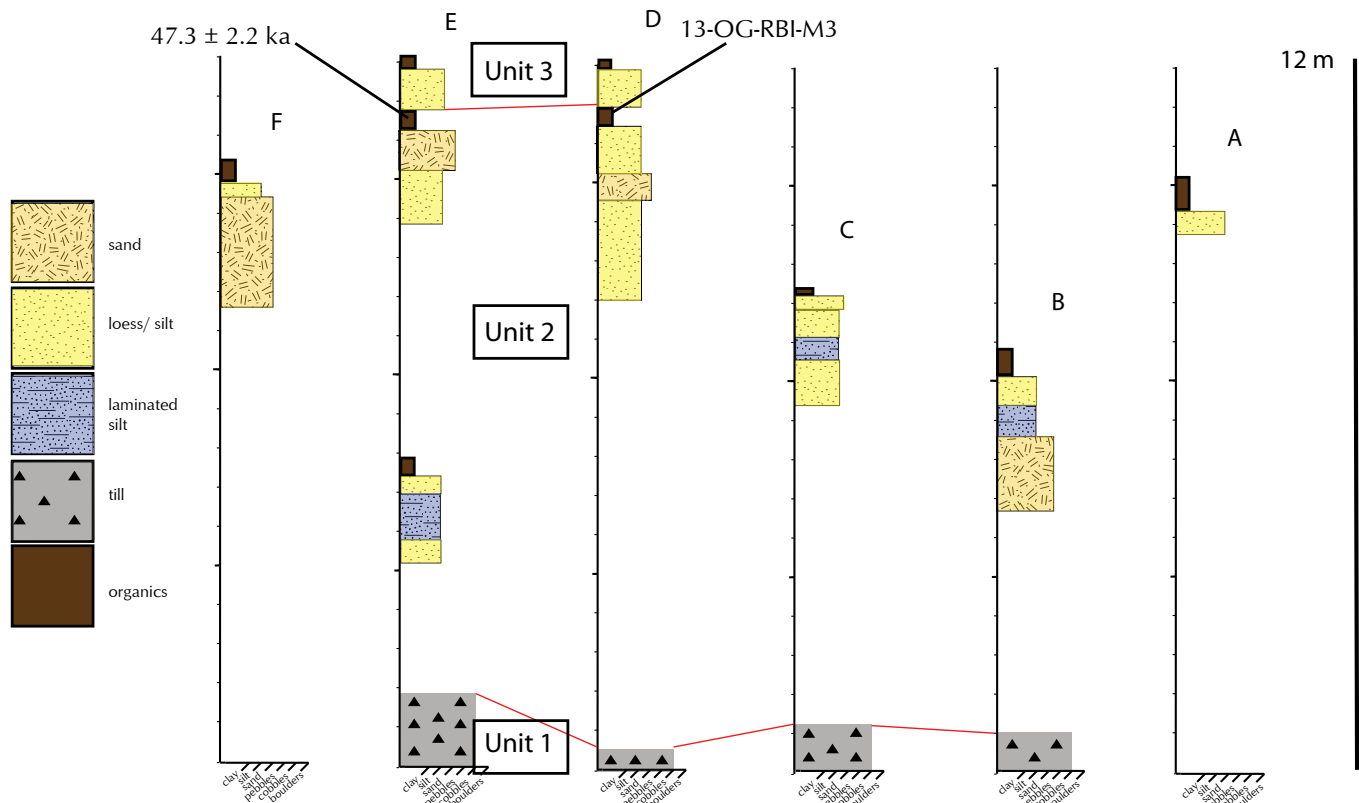
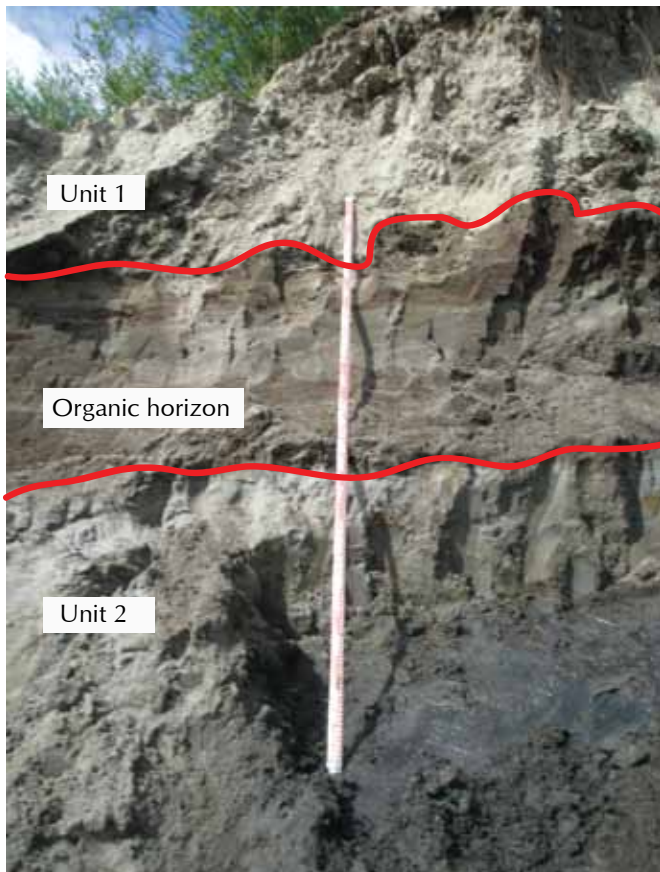


Figure 7. Schematic section of the Ice Wedge.



CURRENT AGES

Results from the gravel pit depth profile and the Ice Wedge section OSL ages are pending and not reported in this paper. Currently, several radiocarbon and boulder TCN samples have been analyzed and have had ages calculated (Tables 1 and 2). This provides initial insight into the age of the penultimate advance in the Ogilvie Mountains. None of the ages have been corrected for erosion rates and are thus minimum ages. Two North Klondike River (NK-01 (100 ka) and NK-02 (89.7 ka)) boulders fall within the range of MIS 5, and one boulder (13-OG-MTB (64.7 ka)) has an age that falls in the middle of MIS 4. The final boulder (13-OG-MC-01), unexpectedly dated to MIS 2 (18.2 ka). The anomalous young age is interpreted to be a result of the boulder having been split in two, with the second half not visible in the area, indicating that it may have been transported or exhumed.

Figure 8. The upper 3 m of the Ice Wedge section; a thick organic horizon separates the interstratified silt-sand sequence and the overlying loess.

While it is well within the penultimate limit, the MIS 2 limit is only a few kilometres away, and could represent an older advance. Boulder 13-OG-MTB is also younger than expected possibly due to surface erosion, as made evident by the rough, undulating surfaces and grus scattered nearby. This span in ages from the sampled boulders could reflect errors commonly found with the dating method, or could perhaps even suggest the presence of a minor Stage 4 advance between the Stage 2 and 6 mapped limits.

The radiocarbon ages (46.5 and 47.3 ka) obtained from organic horizons made up of predominantly aquatic mosses near the top of the Ice Wedge section are likely non-finite as they are very close to the upper limit of the technique. Their position indicates the underlying diamict is either MIS 6 or 4. If finite, the ages allow the diamict to be stage 4, with the organics representing the beginning of MIS 3. If non-finite, an MIS 6 age is more likely as the organics are likely significantly older than 45 ka.

Table 1. Boulder TCN sample ages.

Sample Number	Age	Error
13-OG-MTB	64.7 ka	± 7 ka
13-OG-MC-01	18.2 ka	± 1.9 ka
NK-01	100 ka	± 11 ka
NK-02	89.7 ka	± 9.6 ka

Table 2. Radiocarbon ages.

Sample Number	¹⁴ C Age	Error
13-OG-RBI-M3	46.5 ka	1.1 ka
128745	47.3 ka	2.2 ka

DISCUSSION

PALEOENVIRONMENT

At the gravel pit section, Unit 1 is interpreted as a glacialfluvial outwash. The site is located within the mapped penultimate limit, and was deposited as the ice began its retreat (Fig. 2). During this period the sediments were fully exposed, allowing for TCN buildup beginning at the top of the unit. Units 2 and 3 are interpreted to be loess deposited by katabatic winds following deglaciation, either the penultimate or possibly MIS 2, with Unit 3

having been reworked as a result of permafrost processes in the active layer. The presence of clasts and the inconsistent thickness of the overlying units suggest that post-glacial cryoturbation resulted in mixing, which is more evident in the upper, active layer.

Site 2, the Ice Wedge section, is interpreted as an interglacial lake sequence. At the base of the section, the diamict is interpreted to represent deposition by glacier ice during MIS 4 or 6. The likely non-finite radiocarbon ages near the top of the thick, overlying unit suggest an age of MIS 4 or older. Overlying the till, the 10 to 12 m sequence of fine-grained, stratified sediments of Unit 2 is interpreted to represent varying energy levels within a dynamic lake formed from ice damming of the Blackstone River. The massive beds of fine sand in Unit 2 represent periods where the lake experienced higher energy levels due to an increased input of meltwater. Interbedded organic horizons within the sands are indicative of periods where the lake was shallow enough to support vegetation. The material in the organic horizons was found to be aquatic mosses, which likely represent a meltwater fed paleo-lake. At the top of the Ice Wedge section, the fine sand and silt of Unit 3 is interpreted to be loess due to the massive nature and heterogeneity of the fines sediments and was likely deposited contemporaneously with the loess seen at the gravel pit section.

CONCLUSIONS

Our initial findings show that the penultimate limit occurred during MIS 6, which is consistent with the established pattern for the Selwyn lobe in central Yukon. Results from the pending TCN depth profile and OSL ages should clarify the age of the penultimate glaciation in the Ogilvie Mountains.

ACKNOWLEDGEMENTS

I would like to extend my thanks to the Yukon Geological Survey, in particular Jeff Bond for providing the project, as well as Kristen Kennedy for acting as the reviewer for this paper. I would also like to thank Brent Ward for the research opportunity and continual encouragement throughout my graduate program. Many thanks to my field assistants Stephanie Van Pelt and Sydney Van Loon for their hard work and support during the data collection process. John Gosse has been another fixture to this research, providing the lab space and equipment for the processing of the TCN samples, in addition to his countless

hours spent working on the 36-Cl calculator, and providing much-needed advice on all things TCN-related. Thank you to Alice Telka of Paleotec Labs for the macrofossil and radiocarbon analysis, as well as Michel Lamothe of the Luminescence dating laboratory (LUX) at the Université du Québec à Montréal for the OSL analysis. The Dalhousie CNEF lab procedures were compiled by Anne Reuther based on works by John Stone, Susan Ivy-Ochs, Fred Phillips and Jodie Evans. Funding was provided by the YGS, a NSERC grant to B. Ward and a Northern Scientific Training Program (NSTP) grant.

REFERENCES

- Berger, G., Péwé, T., Westgate, A. and Preece, S., 1996. Age of Sheep Creek tephra (Pleistocene) in central Alaska from thermoluminescence dating of bracketing loess. *Quaternary Research*, vol. 60, p. 63-69.
- Bierle, B., 2002. Late Quaternary glaciation in the Northern Ogilvie Mountains: revised correlations and implications for the stratigraphic record. *Canadian Journal of Earth Science*, vol. 39, p. 1709-1717.
- Bostock, H., 1966. Notes on glaciation in central Yukon Territory. Geological Survey of Canada, Paper 65-36.
- Briner, J., Kaufman, D., Manley, W., Finkel, R. and Caffee, M., 2005. Cosmogenic exposure dating of late Pleistocene moraine stabilization in Alaska. *GSA Bulletin*, vol. 117, p. 1108-1120.
- Demuro, M., Froese, D., Arnold, L. and Roberts, R., 2011. Single-grain OSL dating of glaciofluvial quartz constrains Reid glaciation in NW Canada to MIS 6. *Quaternary Research*, vol. 77, p. 305-316.
- Duk-Rodkin, A., 1996. Surficial Geology, Dawson, Yukon Territory. Geological Survey of Canada, Open File 3288.
- Duk-Rodkin, A., 1999. Glacial Limits Map of Yukon. Geological Survey of Canada, Open File 3694; Yukon Geological Survey, Geoscience Map, 1999-2, scale 1:1 000 000.
- Froese, D., Barendregt, R., Enkin, R. and Baker, J. 2000. Paleomagnetic evidence for multiple Late Pliocene- Early Pleistocene glaciations in the Klondike area, Yukon Territory. *Canadian Journal of Earth Sciences*, vol. 37, p. 863-877.
- Hidy, A., Gosse, J., Froese, D., Bond, J. and Rood, D., 2013. A latest Pliocene age for the earliest and most extensive Cordilleran Ice Sheet in northwestern Canada. *Quaternary Science Reviews*, vol. 61, p. 77-84.
- Hughes, O., Campbell, R., Muller, J. and Wheeler, J., 1969. Glacial limits and flow patterns, Yukon Territory, South of 65 degrees North Latitude. Geological Survey of Canada, Paper 68-34.
- Huscroft, C., Ward, B., Barendregt, R., Jackson Jr., L. and Opdyke, N., 2004. Pleistocene Volcanic damming of Yukon River and the maximum age of the Reid Glaciation, west-central Yukon. *Canadian Journal of Earth Science*, vol. 41, p. 151-164.
- Jackson Jr., L., Nelson, F., Huscroft, C., Villeneuve, M., Barendregt, R., Storer, J. and Ward, B., 2012. Pliocene and Pleistocene volcanic interaction with Cordilleran ice sheets, damming of the Yukon River and vertebrate Paleontology, Fort Selkirk Volcanic Group, west-central Yukon, Canada. *Quaternary International*, vol. 260, p. 3-20.
- Jackson, L., Ward, B., Duk-Rodkin, A. and Hughes, O., 1991. The Last Cordilleran Ice Sheet in Southern Yukon Territory. *Géographie physique et Quaternaire*, vol. 45, issue 3, p. 341-354.
- Lacelle, D., Lauriol, B., Clark, I., Cardyn, R. and Zdanowicz, C., 2007. Nature and origin of a Pleistocene-age massive ground-ice body exposed in the Chapman Lake moraine complex, central Yukon Territory, Canada. *Quaternary Research*, vol. 68, p. 249-260.
- Preece, S., Pearce, N., Westgate, J., Froese, D., Jensen, B. and Perkins, W., 2011. Old Crow tephra across eastern Beringia: a single cataclysmic eruption at the close of Marine Isotope Stage 6. *Quaternary Science Reviews*, vol. 30, p. 2069-2090.
- Rhodes, E.J., 2011. Optically stimulated luminescence dating of sediments over the past 200 000 years. *Annual Review of Earth and Planetary Sciences*, vol. 39, p. 461-488.
- Smith, C., Tarnocai, C. and Hughes, O., 1986. Pedological Investigations of Pleistocene Glacial Drift Surfaces in the Central Yukon. *Géographie physique et Quaternaire*, vol. 40, p. 29-37.

- Stroeven, A., Fabel, D., Codilean, A., Kleman, J., Clague, J., Miguens-Rodriguez, M. and Xu, S., 2010. Investigating the glacial history of the northern sector of the Cordilleran Ice Sheet with cosmogenic ^{10}Be concentrations in quartz. *Quaternary Science Reviews*, vol. 29, p. 3630-3643.
- Tarnocai, C. and Schweger C., 1991. Late Tertiary and Early Pleistocene Paleosols in Northwestern Canada. *Arctic Institute of North America*, vol. 44, p. 1-11.
- Tarnocai, C. and Smith, C., 1989. Micromorphology and Development of Some Central Yukon Paleosols, Canada. *Geoderma*, vol. 45, p. 145-162.
- Turner, D., Ward, B., Bond, J., Jensen, B., Telka, A., Zazula, G. and Bigelow, N., 2013. Middle to late Pleistocene ice extents, tephrochronology and paleoenvironments of the White River area, southwest Yukon. *Quaternary Science Reviews*, vol. 75, p. 59-77.
- Ward, B., Bond, J. and Gosse, J., 2007. Evidence for a 55-50 ka (early Wisconsin) glaciation of the Cordilleran Ice Sheet, Yukon Territory, Canada. *Quaternary Research*, vol. 68, p. 141-150.
- Ward, B., Bond, J., Froese, D. and Jensen, B., 2008. Old Crow tephra (140 ± 10 ka) constrains penultimate Reid glaciation in central Yukon Territory. *Quaternary Science Reviews*, vol. 27, p. 1909-1915.
- Westgate, J., Preece, S., Froese, D., Pearce, N., Roberts, R., Demuro, M., Hart, W. and Perkins, W., 2008. Changing ideas on the identity and stratigraphic significance of the Sheep Creek tephra beds in Alaska and the Yukon Territory, northwestern North America. *Quaternary International*, vol. 178, p. 183-209.
- Westgate, J., Preece, S., Froese, D., Walter, R., Sandhu, A. and Schweger, C., 2001. Dating Early and Middle (Reid) Pleistocene glaciations in central Yukon by tephrochronology. *Quaternary Research*, vol. 56, p. 335-348.

Advances in the mineralization styles and petrogenesis of the Coffee gold deposit, Yukon

E. Buitenhuis¹
Kaminak Gold Corp.

L. Boyce
Department of Earth and Atmospheric Sciences, University of Alberta

C. Finnigan (Posthumously)
Kaminak Gold Corp. and Department of Earth Sciences, Western University

Buitenhuis, E., Boyce, L. and Finnigan, C., 2015. Advances in the mineralization styles and petrogenesis of the Coffee gold deposit, Yukon. *In: Yukon Exploration and Geology 2014*, K.E. MacFarlane, M.G. Nordling and P.J. Sack (eds.), Yukon Geological Survey, p. 29-43.

ABSTRACT

Gold-bearing, arsenic-rich pyrite in association with enriched As, Sb and minor Ag is found in two separate mineralization styles at Kaminak Gold Corp.'s Coffee Gold Project, Yukon. Arsenian pyrite replaces primary metamorphic mica by sulphidizing Fe in the host, while pervasive dolomite-illite alteration destroys the host and eventually consumes early mineralized pyrite. Silicification of host rocks is observed with associated arsenian pyrite deposition due to cooling. Brecciation of silicified intervals by coarse grained hydrothermal quartz occurs later with additional pyrite deposition. Mineralized intervals are oxidized by late, meteoric fluids which consume Au-bearing pyrite and release micron-scale free gold from the pyrite crystal lattice into the remnant oxides. Sulphidized biotite within the 98 Ma Coffee Creek Granite constrains mineralization to <98 Ma. Similar metal associations (Au-As-Sb vs. Au-As-Sb-Pb-Zn-Cu) suggest Coffee potentially represents the shallower, epizonal extension of the mesozonal orogenic Boulevard gold deposit, with a late epithermal overprint.

¹ericb@kaminak.com

INTRODUCTION

Kaminak Gold Corporation's Coffee gold deposits in west-central Yukon were discovered during a spike in gold exploration activity, spurred by the rising price of gold to record-high levels from 2007 to 2010. Drilling started in 2010, and has since progressed to the completion of over 1300 diamond and reverse circulation drill holes on the property. The Coffee gold deposits currently consist of an Indicated Resource of 14 million tonnes grading at 1.56 g/t Au for 719,000 ounces, and an Inferred Resource of 79 million tonnes grading at 1.36 g/t Au for 3,434,000 ounces. The Indicated Resource contains 480,000 ounces of easily CN-leachable oxide gold, whereas the Inferred Resource contributes an additional 2,078,000 ounces of oxide gold (Makarenko *et al.*, 2014).

Recent work at the Coffee project includes MSc and BSc theses completed by the primary authors, in addition to an in-house petrographic study by Kaminak personnel and external contractors (Boyce, 2014; Buitenhuis, 2014). These researches were focused on the Latte and Double Double gold zones, in an attempt to explain the prevalence of wide intervals of disseminated mineralization at Latte, and narrow, high-grade brecciation at Double Double.

GEOLOGICAL SETTING

The Coffee gold deposits are located approximately 130 km south of Dawson City within the Yukon-Tanana terrane (YTT), a complex amalgamation of variably metamorphosed Proterozoic and Paleozoic sedimentary and igneous rocks (Fig. 1). The YTT is subdivided into four assemblages underlain by the basal Snowcap assemblage, a rifted fragment of psammitic schist, quartzite, carbonaceous schist, calc-silicate rocks, marble, and local amphibolite, greenstone, and ultramafic rocks (Piercey and Colpron, 2009). The Snowcap assemblage formed the base for the subsequent deposition of three unconformity-bound arc assemblages: the Finlayson (Upper Devonian to

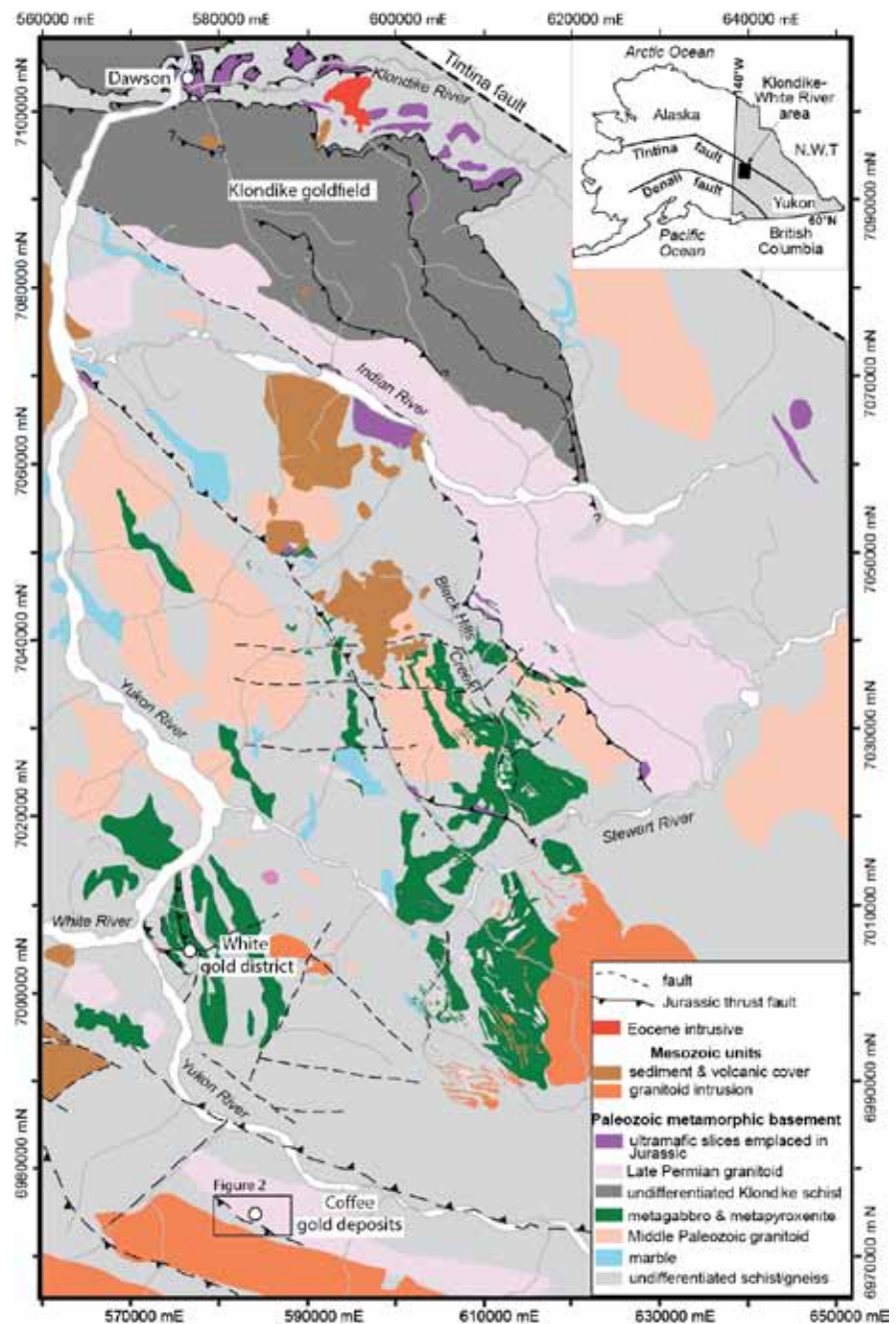


Figure 1. Location of the Coffee gold deposits within the Yukon-Tanana Terrane, 130 km south of Dawson City (from MacKenzie *et al.*, 2013).

Lower Mississippian), Klinkit (mid-Mississippian to Lower Permian), and the Klondike (Middle to Upper Permian) (Colpron *et al.*, 2007). The formation of an eastward-dipping arc along the western margin of ancestral North America, during the Late Devonian, led to the rifting of its back arc region and the formation of the Slide Mountain Ocean (SMO) by the Late Devonian-Early Mississippian (Templeman-Kluit, 1979; Mortensen, 1992; Colpron *et al.*, 2006; Nelson *et al.*, 2006).

Kilometre-scale slices of the varying YTT assemblages were thrust stacked during the Jurassic as a result of the closure of the Slide Mountain Ocean due to a reversal in subduction polarity in the Early to Middle Permian (Erdmer *et al.*, 1998; Beranek and Mortensen, 2011). Low angle, northeast-verging thrust faulting led to internal duplication of the various components of the YTT and incorporated dismembered slivers of Slide Mountain ophiolite into the local tectonic stratigraphy (MacKenzie *et al.*, 2008; MacKenzie *et al.*, 2010; Buitenhuis, 2014). Greenschist-facies metamorphism caused by low angle shearing led to sericite alteration and emplacement of orogenic quartz veins which are gold-bearing in the Klondike, but generally barren in the Coffee region. The extension resulted in the mica and amphibole in the region resetting their ages; mica at Golden Saddle is constrained to 185-170 Ma by $^{40}\text{Ar}/^{39}\text{Ar}$ dating and hornblende cooling ages of approximately 180 Ma were recorded south of Thistle Creek (Villeneuve *et al.*, 2003; Ruks *et al.*, 2006; Berman *et al.*, 2007; Beranek and Mortensen, 2011; Bailey, 2013). Mineralization in the White gold district is associated with extensional faulting and fracturing of the thickened metamorphic pile in the Late Jurassic (MacKenzie *et al.*, 2010; Bailey, 2013).

Mid-Cretaceous extension resulted in the emplacement of the Dawson Range batholith (~100 Ma) and one of its sub-phases, the Coffee Creek granite (~98 Ma), along with the development of regional-scale dextral normal faults such as the Big Creek fault, an overturned and re-activated Jurassic thrust fault to the southeast of the Coffee property (Johnston, 1995; Sanchez *et al.*, 2013). This period of extension and exhumation is contemporaneous with the formation of mineral deposits such as the Moosehorn-Longline (Au), Boulevard (Au) and Mt. Nansen (Au-Ag) deposits, but precedes the 74.3 ± 0.5 Ma Casino Cu-Mo-Au porphyry deposit and Carmacks volcanism (~70 Ma; McKenzie *et al.*, 2013; Allan *et al.*, 2013).

PROPERTY GEOLOGY

HOST ROCKS

The Coffee property is underlain by a set of metamorphic rocks which are thrust stacked to the northeast and bound to the southwest by the Coffee Creek granite, a ~98 Ma coarse-grained biotite-hornblende granite (Fig. 2). The host rocks have been traditionally divided into three main groupings listed from northeast to southwest: i) a northwest trending and moderately southwest dipping

panel of augen gneiss with minor intercalated biotite-feldspar schist; ii) a panel of southwest dipping schist varying in composition from biotite to muscovite dominant with minor mafic metavolcanics and local marble banding; and iii) the Coffee Creek granite which intrudes the metamorphic rocks.

The augen gneiss in the central to northern portion of the Coffee property is identified as the Sulphur Creek orthogneiss, a member of the Klondike assemblage, emplaced during the Klondike orogeny (Ryan *et al.*, 2013). The orthogneiss has been dated at 255 ± 3.3 Ma suggesting that the protolith granitoid was affected by Late Permian metamorphism and deformation (D_2 of MacKenzie *et al.*, 2008) shortly after emplacement (A.J. Wainwright and A. Simmons, unpublished data). The gneiss is characterized by variable amounts of foliaform quartz, biotite, and muscovite, including common quartz-alkali feldspar augens (0.5-1.5 cm). The augen content of the gneiss is variable (Cruikshank, 2011).

The swath of schistose rocks in the central region of the Coffee property consists of two main rock panels. The upper panel comprises Snowcap assemblage biotite-feldspar-quartz (\pm muscovite, \pm calcite) schist with common marble banding (Fig. 3). Thin layers of fine-grained amphibolite containing up to 30% biotite are found within the schist, interlayered on a decimetre to metre scale. Trace element geochemical analysis indicates an alkaline basalt protolith of the amphibolite within the upper panel, which exhibits within-plate and continental rift affinity (Buitenhuis, 2014). Beneath the Snowcap assemblage schist is a panel of foliated metagabbro and fine-grained amphibolite, with additional layers of amphibole-biotite schist. The metagabbro consists of coarse hornblende crystals set in a heavily altered groundmass of carbonate, epidote, and zoisite. All mafic rocks within the lower panel exhibit arc-related geochemical signatures, in direct contrast to the upper schistose rocks (Buitenhuis, 2014). Tectonically emplaced slivers of exotic ultramafic rocks, up to 20 m thick, are observed within the schistose corridor. The ultramafic bodies are thoroughly altered to magnesite and serpentinite, but are weakly foliated to unfoliated.

The Coffee Creek granite is found in the southern portion of the property in contact with the central schistose corridor. The granite exhibits an equigranular texture of 30-50% plagioclase, 20-30% K-feldspar, 20-30% quartz, and 3-5% hornblende (Wainwright *et al.*, 2011). The contact between the granite and the schistose rocks has been drilled at the Kona North prospect, and is observed to dip moderately to the south. No chill margins are

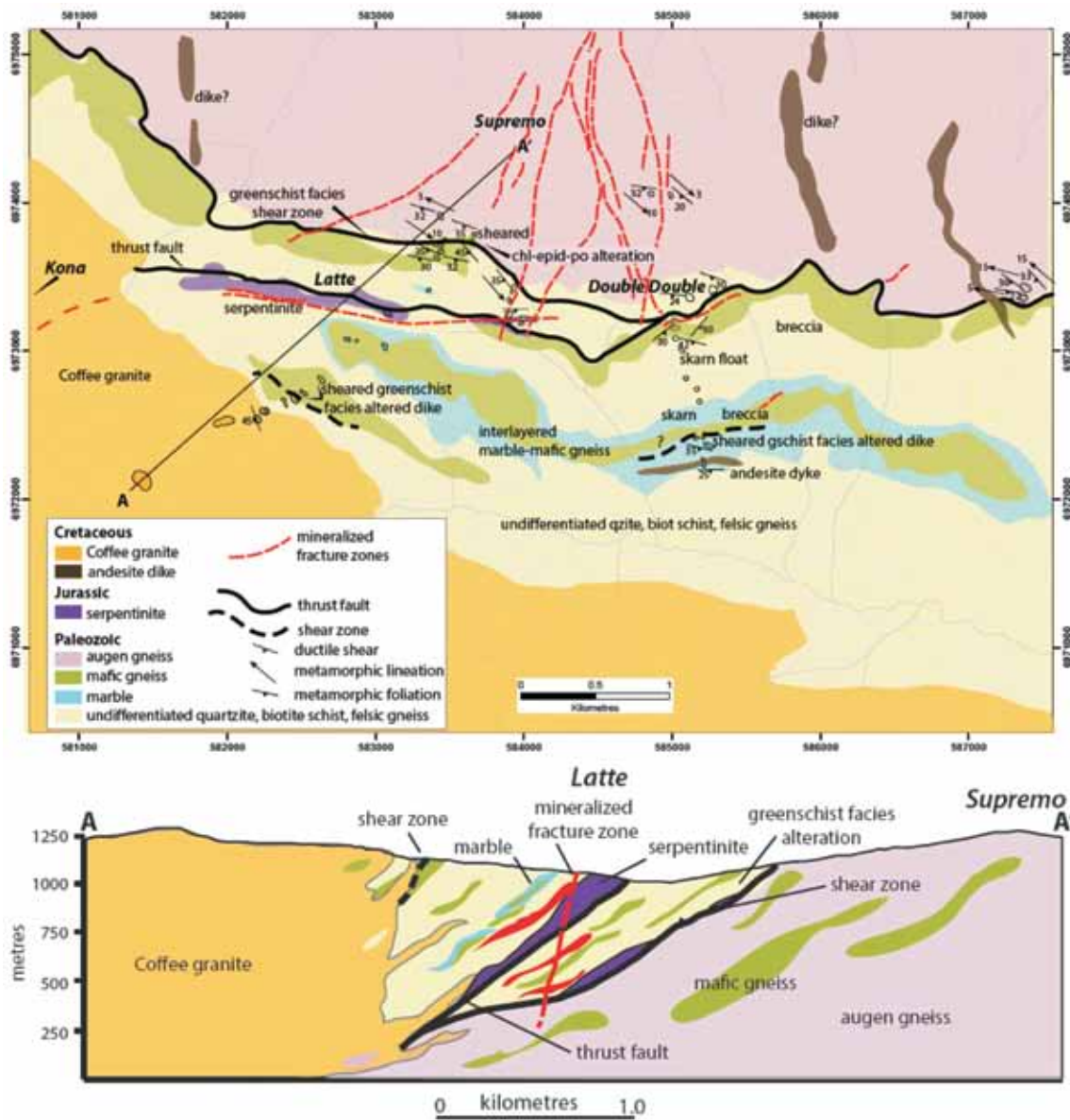


Figure 2. Geologic map and cross section of the Coffee property by MacKenzie et al. (2013).

observed within the granite approaching the contact. The immediate area of the contact, as observed in drill core, is generally obscured by widespread clay alteration and rubble.

METAMORPHISM

The Permian metamorphic rocks exhibit greenschist-facies strain and shearing along a low-angle, E striking S dipping plane. The shearing manifests itself as sericite, chlorite, epidote and actinolite ± tremolite retrogressive alteration of pre-existing amphibole and biotite present within the schistose hosts. Minor intervals of skarn are observed where these low-angle shears intersect marble horizons (MacKenzie et al., 2013). Brassy, cubic pyrite is

found throughout the schistose packages, and opaque to translucent white orogenic quartz veins associated with the shearing cut through the schist (MacKenzie et al., 2013).

MINERALIZATION STYLES

Mineralization at the Coffee property is both structurally and lithologically controlled; hosted in steeply dipping faults and fracture systems which cut all lithologies on the property. The deposits are hosted within all three lithological domains: the Sulphur Creek orthogneiss (Supremo); the mixed schistose and mafic rocks (Latte and Double Double); and the Coffee Creek granite

(Kona). Mineralization is controlled by the WNW to NW striking dextral strike-slip Coffee Creek fault system, which is interpreted as a splay off the regional-scale Big

Creek fault to the southeast (Johnston, 1995; Sanchez et al., 2013). Horsetailing splays off the Coffee Creek fault host mineralization in approximately E or W striking, steeply dipping corridors (Latte, Double Double); whereas a series of N to NNE striking brittle faults accommodate strain imposed (Fig. 4) by the dextral movement and host mineralization within the Supremo T1-T8 structures.

Two distinct styles of gold mineralization are observed across the entire property: foliation-parallel disseminations and breccia-hosted. In both styles of mineralization, gold is hosted within arsenic-rich pyrite, which releases gold from its crystal lattice upon oxidation. All gold zones are oxidized from surface; the oxidation persisting locally down to 300 m below surface.

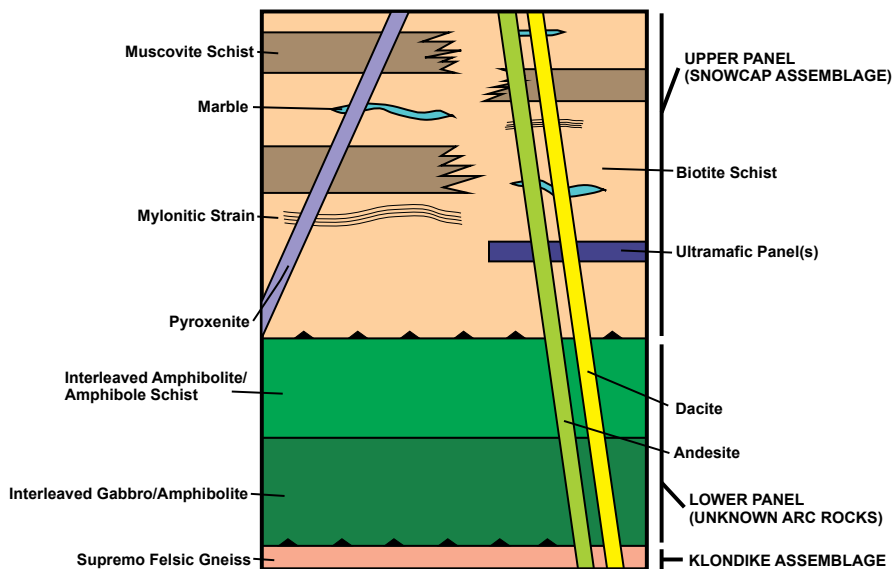


Figure 3. Tectonic stratigraphy of the central schistose corridor, centred on the Latte zone. Modified after Buitenhuis (2014).

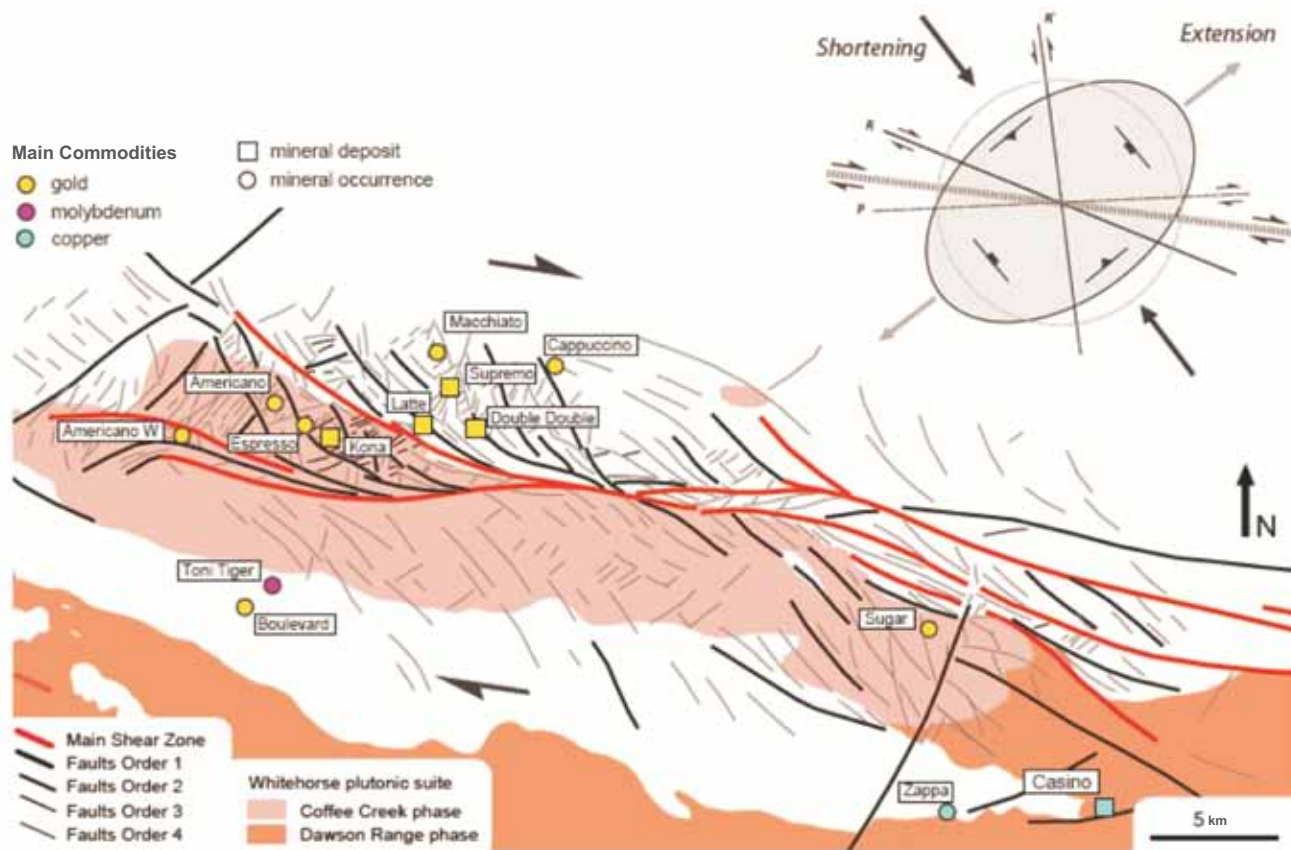


Figure 4. Fault structures at the Coffee property. Mineralized deposits and occurrences are indicated in addition to major and minor faults structures, ordered from highest to lowest confidence (1-4). From Sánchez et al. (2013).

DISSEMINATED

Disseminated mineralization is found in all zones at the Coffee property and is formed by the perfusion of a gold-rich mineralizing fluid into mica-bearing wall rocks after travelling along steep fault and fracture zones (Wainwright, 2011; Cruikshank, 2011; Boyce, 2014; Buitenhuis, 2014). Interaction of the mineralizing fluid with mica in the wall rocks forms fine-grained arsenian (up to 15 wt %) pyrite which pseudomorphs the parent mica grain and hosts Au.

As mineralizing fluid contacts the schistose wall rocks, background metamorphic biotite or phengitic muscovite is consumed through a sulphidation reaction in which Fe in the mica complexes with S in the fluid (+As and Sb). The host mica is completely replaced by fine grained white mica or illite which retains the Mg, Ti and Cr content of the parent grain (Hydrothermal 1 (HT1) of Buitenhuis, 2014), while fine-grained to blebby arsenian pyrite pseudomorphs the host mica along cleavage planes, incorporating As, Sb, Au and occasionally Ag from the fluid (Fig. 5). Au-bearing arsenian pyrite also commonly forms as rinds on unmineralized cubic pyrite found within the host metamorphic rocks. Pervasive dolomite alteration accompanies the sulphide deposition. Minor rutile forms alongside the As-rich pyrite due to the presence of Ti within the parent mica. Rare tetrahedrite has been observed in association with Au-bearing arsenian pyrite and white mica, in addition to minor Th-monzonite, zircon and barite. Rare electrum is observed within mineralized pyrites at the Supremo zone.

Continued fluid influx resulted in the formation of a second phase of white mica or illite after consumption of the primary metamorphic minerals (Hydrothermal 2 (HT2) of Buitenhuis, 2014). Electron-Probe Microanalysis (EPMA) study of fine white mica/illite within mineralized samples shows a transition from phengitic parent compositions to HT1 (lower octahedral site occupancy by Ti-Cr-Fe-Mg-Mn), and finally HT2 phase mica, which is of purely hydrothermal composition (Buitenhuis, 2014; Fig. 6). In intervals where the host rock has been fully consumed

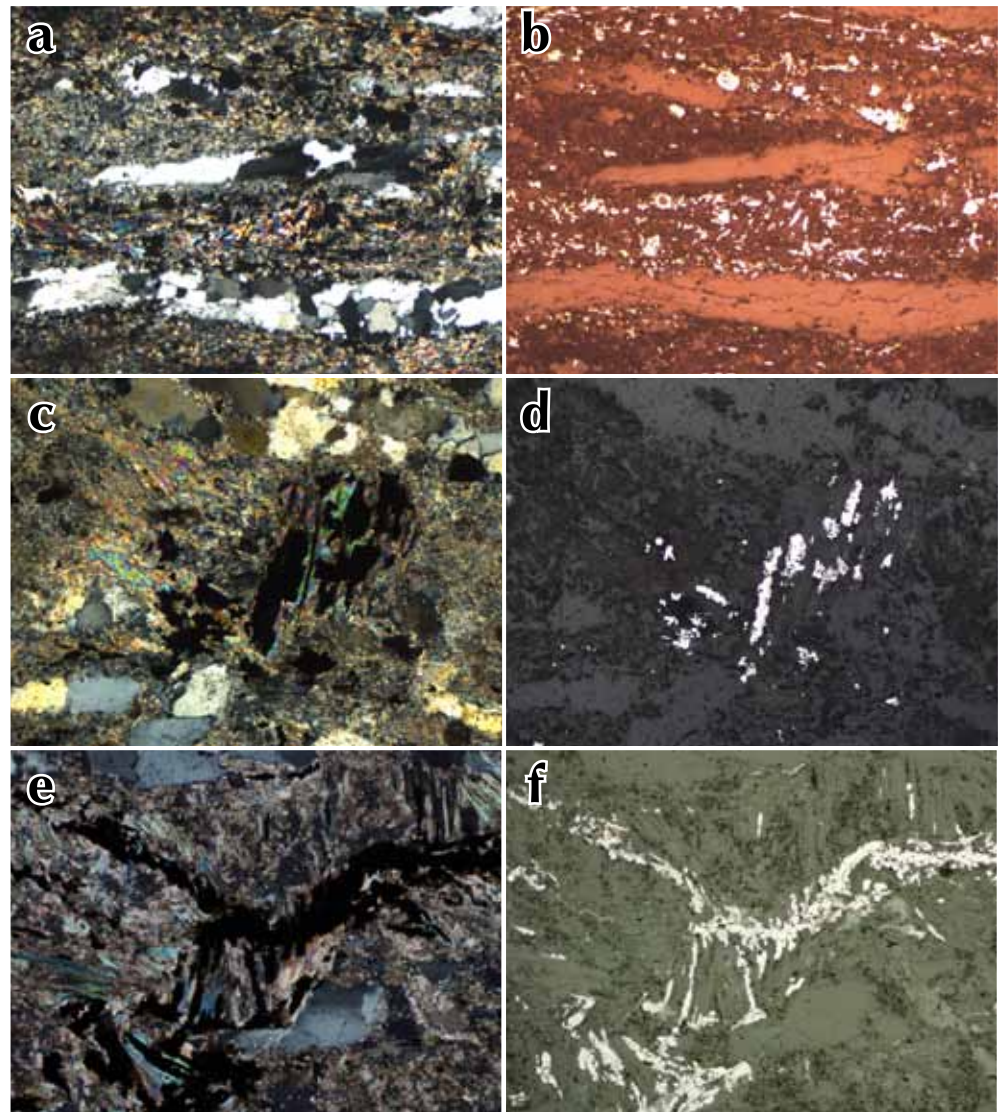


Figure 5. Examples of disseminated mineralization from the Latte (a-d) and Double Double zones (e-f). (a) Fine grained arsenian pyrite replaces primary mica in a schistose protolith, Cross polarized light (XPL); (b) same as 'a', reflected light (RL); (c) trains of arsenian pyrite which have pseudomorphed tabular grains of primary mica, XPL; (d) same as 'c', RL; (e) strong arsenian pyrite replacement of mica, with intense dolomite-illite alteration surrounding, XPL; (f) same as 'e', RL. All photomicrographs have a 4.5 mm field of view (FOV).

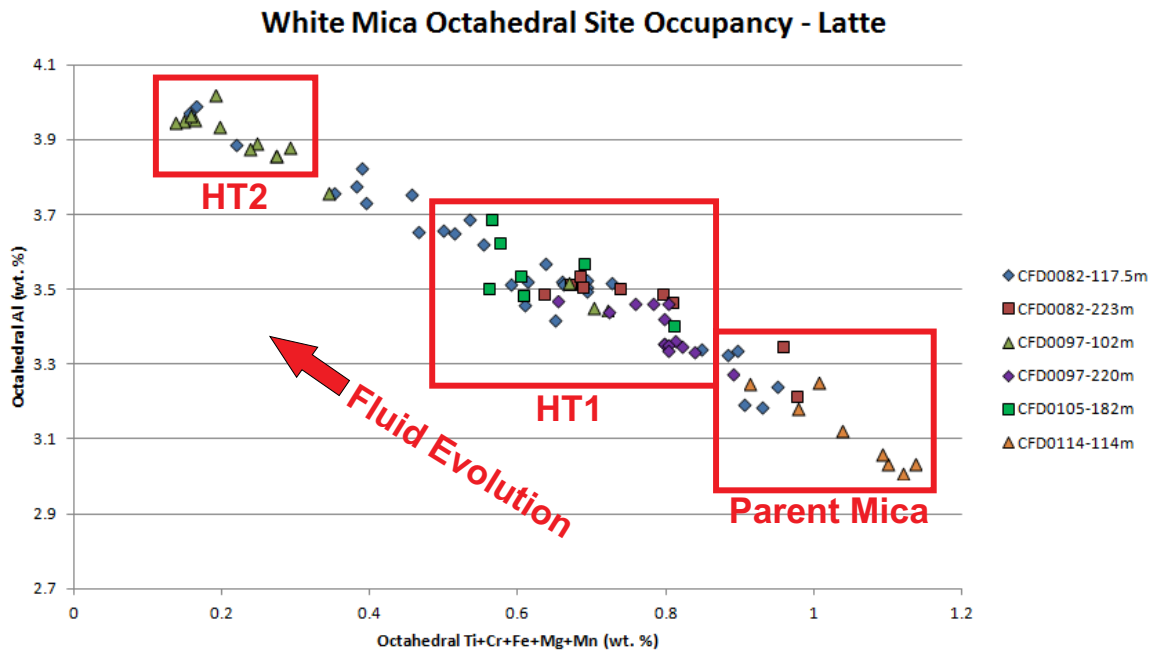


Figure 6. Plot of octahedral-site Ti, Cr, Fe, Mg and Mn vs. octahedral-site Al occupancy for white mica from the Latte zone. Mica of primary, metamorphic compositions plots in the lower right (low octahedral Al). With increasing fluid interaction, HT1 phase mica replaces parent phengite and incorporates minor Ti, Cr, Mg from the parent. Final stage mica formation is pure hydrothermal white mica (HT2) with high octahedral Al. Arsenian pyrite deposition is associated with HT1-phase white mica.

by the dolomite-illite-arsenian pyrite mineralization assemblage, continued fluid influx leads to complete breakdown of all minerals to clay and the consumption of previously deposited Au-bearing arsenian pyrite. The newly-liberated gold and sulphide is later re-deposited within thin dolomite-quartz-arsenian pyrite veinlets, which are observed to crosscut both primary disseminated mineralization and depleted, previously mineralized rock (Fig. 7).

BRECCIA-HOSTED

The structural corridors at the Coffee project have been reactivated multiple times, resulting in a number of breccia phases, both absent of, and containing, mineralization. At least two distinct phases of brecciation are observed at the Coffee property.

Samples of breccia taken from the Supremo T3 area indicate a phase of siliceous brecciation at Coffee. These breccias consist of angular heterolithic clasts of silicified wall rock set in a matrix of coarse hydrothermal quartz (Fig. 8). Clasts are multi-textured, with domains of

skeletal quartz indicative of rapid quenching and growth, intermixed with domains of extremely fine-grained silica with a mottled appearance. Both domains within the clasts contain a small proportion of fine-grained arsenian pyrite intergrown with quartz crystallites. Pyrite needles and small cubes are distributed throughout the breccia matrix, comprising approximately 25% of the matrix's volume. Pyrite is observed to rind the clasts, projecting outwards into the coarse hydrothermal quartz (Fig. 8c). Patches within the matrix contain fine grained quartz intergrown with illite which is variably replaced by kaolinite. Other clasts within the breccias include relatively un-altered fragments of the wall rock.

An additional phase of brecciation is observed throughout the property, consisting of a ferroan carbonate matrix which supports monomict clasts of the host lithology. The Fe-carbonate breccias appear to be late and cut both mineralized and unmineralized rocks (Fig. 9). No significant mineralization is associated with this late phase brecciation.

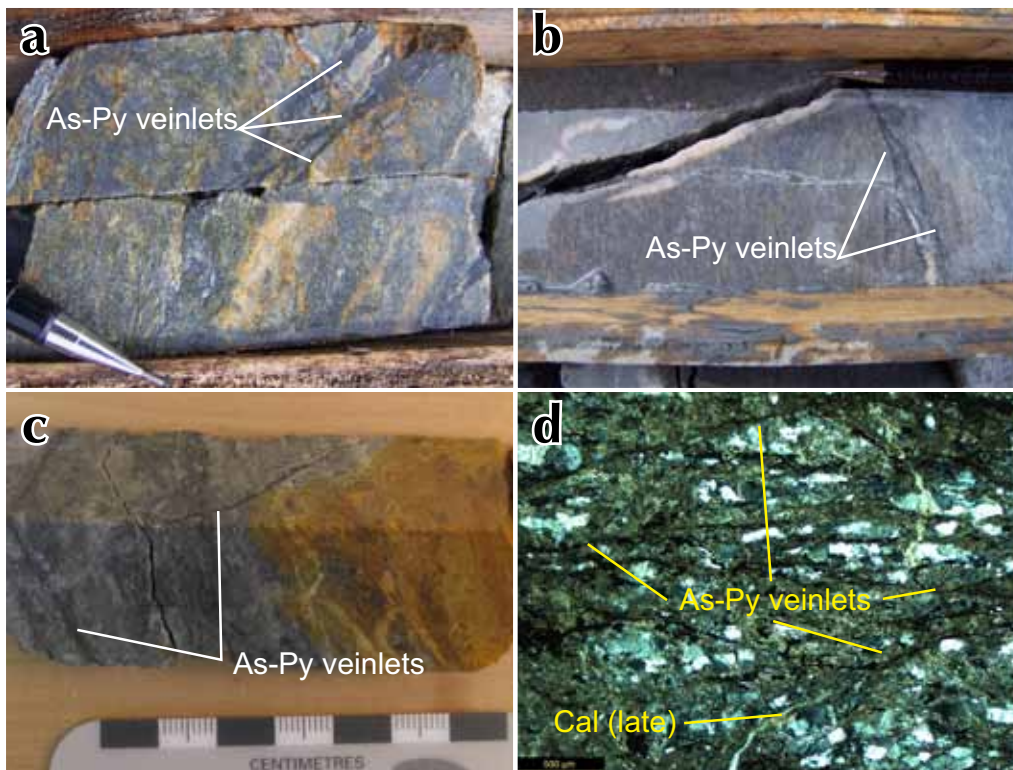


Figure 7. Thin quartz-dolomite veinlets carrying remobilized arsenian pyrite crosscutting the foliation of mineralized schists at the Latte zone. (a) CFD00115A-149.5 m, 20 g/t Au; (b) CFD0119-186.3 m, 7.07 g/t Au; (c) CFD0097-30 m, 2.07 g/t Au; (d) photomicrograph of 'c', XPL, FOV is 4.5 mm.

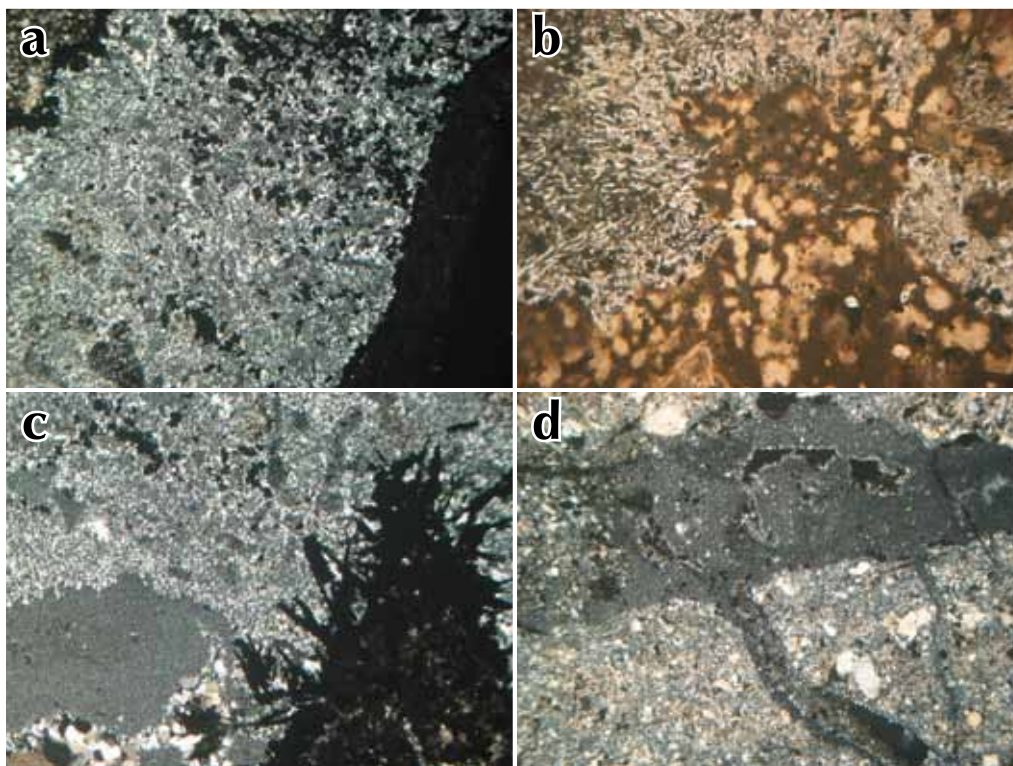


Figure 8. Examples of siliceous brecciation at the Supremo zone. All images from a surface trench sample. (a) Pervasively silicified wall rock with clusters of v. fine grained arsenian pyrite; (b) multiple textures within a clast of silicified wall rock, with visible quenching; (c) clast of wall rock with radiating needles of arsenian pyrite projecting into a super-fine matrix of quartz and pyrite; (d) polyphase brecciation within the same sample.

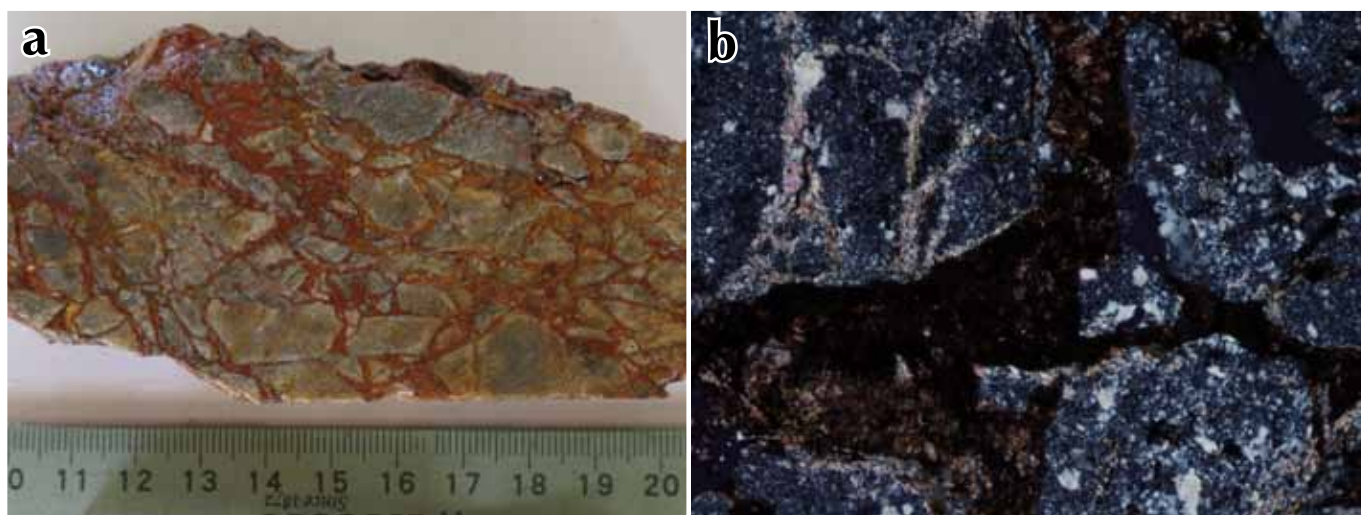


Figure 9. “Silicified clast breccia” with oxidized, ferroan carbonate matrix. Large, angular clasts within this sample do not contain appreciable sulphide, in contrast to those seen in Figure 8. (a) Hand sample; (b) XPL, FOV is 4.5 mm.

OXIDATION OF MINERALIZATION AND GOLD RECOVERY

PRIMARY MINERALIZATION

Gold at Coffee is locked within the crystal lattice of the pyrite grains due to strain imposed by the substitution of As for S ($\text{Fe}(\text{As},\text{S})_2$). This substitution allows for up to 15 weight-percent As within the pyrite, and the incorporation of significant amounts of trace metals such as Au, and including Sb, Hg, Ni, Co, Cu, Tl, Ag, Zn, W, U, Pb, Bi, Se and Te (Fleet *et al.*, 1993; Fleet and Mumin, 1997; Cline *et al.*, 2003; Emsbo *et al.*, 2003; Reich *et al.*, 2005). The exact coordination of Au within the pyrite lattice is uncertain, however, Au^{1+} most likely substitutes for Fe (Fleet *et al.*, 1993; Cline, 2001; Emsbo *et al.*, 2003; Reich *et al.*, 2005).

EPMA study of pyrites within the Supremo and Latte zones demonstrates that Au is hosted predominantly in areas of high As content (Fig. 10). It is a rare instance that a pyrite grain is enriched in As and does not contain Au. Examples of Au and As content for mineralized pyrites from Supremo and Latte are listed in Table 1 and shown in Figure 11. Generally, the higher the As content of a pyrite grain, the greater its Au content as the pyrite structure in the areas of enrichment can accommodate more Au.



Figure 10. Bands of high As content (light coloured) within a fine, rounded grain of pyrite approximately 30 microns in size from the Supremo zone.

OXIDATION

The lack of glaciation at the Coffee property has allowed for in situ weathering of the deposits from the time of formation to present. The structural regime that hosts the Coffee project was active until the Eocene (Gabrielse *et al.*, 2006), providing opportunity for meteoric oxidative fluids to percolate along the structural breaks and oxidize the Au-bearing sulphide. When meteoric fluids encounter the Au-rich arsenian pyrite, it breaks down to oxide minerals such as limonite, hematite and jarosite. As the pyrite crystalline structure is destroyed, Au^{1+} stored within the

Table 1. Spot analyses on mineralized pyrite from CFD0164-469.5 m at the Latte zone. All values reported in weight %. Note that high arsenic usually, but does not always, correlate with high Au. See Figure 10b,c for back scatter images and spot locations.

Sample	Spot	Fe	S	As	Ni	Co	Sb	Hg	Au	Total
Irregular cubic 30 micron pyrite grain (Fig. 10b)	1	46.27	52.47	1.47	0	0.06	0.04	0	0.01	100.32
	2	46.9	53.39	1.29	0	0.08	0.05	0	0.03	101.73
	3	45.86	51.28	2.81	0.01	0.1	0.03	0	0	100.09
	4	46.01	50.98	3.18	0.01	0.08	0.06	0	0	100.3
	5	42.9	44.49	9.73	0.02	0.1	0.03	0.04	0.02	97.32
	6	42.86	45.19	12.71	0.08	0.11	0.04	0	0	101
Large irreg. pyrite mass (Fig. 10c)	1	45.46	51.92	2.5	0.06	0.12	0.07	0	0.04	100.18
	2	46.43	45.62	10.57	0.05	0.08	0.05	0	0.01	99.81
	3	45.91	52.2	2.04	0.02	0.11	0.01	0	0.04	100.33
	4	43.66	46.35	10.83	0.07	0.12	0.05	0	0	101.07

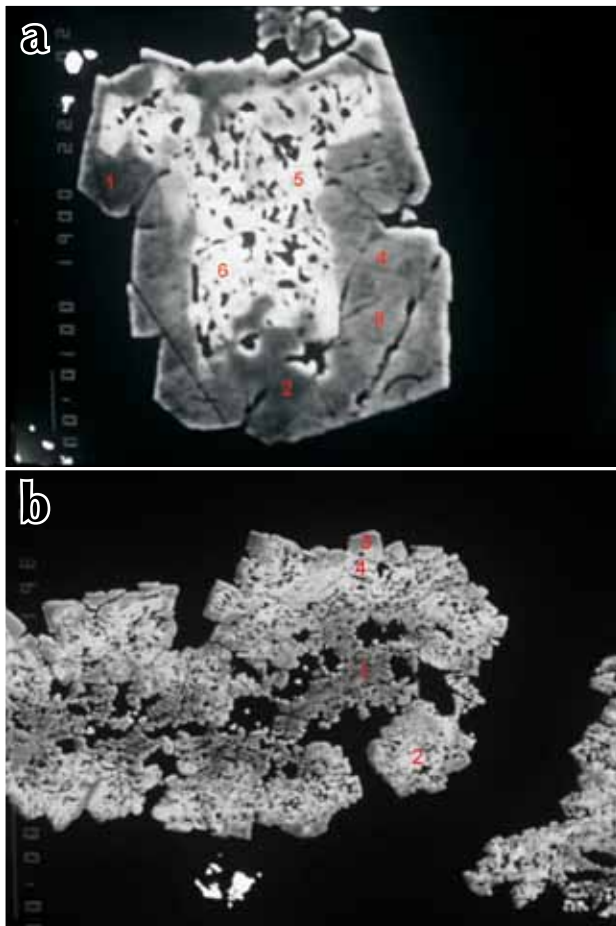


Figure 11. a) Pyrite in sample CFD0164-469.5 m from the Latte zone with spot analyses indicated, FOV is 60 microns; b) Different pyrite grain in CFD0164-469.5 m with spot analyses indicated, FOV is 0.5 mm. See Table 1 for spot results.

pyrite lattice is released. The Au coalesces into micron-scale particles of native gold, appearing as linear 'trains' of Au grains within the remnant oxide and clay (Fig. 12); where oxidation is most pervasive (e.g., upper Supremo T3 deposit) no pyrite remains. Where oxidation is less extensive or partial, the consumption of Au-bearing pyrite has not been fully completed, leaving a fraction of Au locked within the crystal lattice. No supergene enrichment or depletion of Au is observed.

A strong, late overprint of kaolinite is observed along mineralized structures. Kaolinite retrogressively replaces fine illite within both disseminated mineralization and siliceous brecciation. The kaolinite is observed to be intimately associated with Ag-phosphate, Ag-Ca-phosphate, Ag-tellurides, greenockite and baddeleyite.

RECOVERY

Metallurgical testwork completed as part of the ongoing mining feasibility studies indicate rapid and thorough gold recovery from wholly oxidized mineralization. Traditional metallurgical column CN⁺ leach test work produced gold recoveries of up to 95% after leaching with a sodium cyanide solution for up to 42 days. Column test work is dominantly conducted at a temperature of 4°C to represent the cold weather environment at the property, and crush sizes of 1/2", 1" and 6" have all been tested (Table 2).

DISCUSSION

MINERALIZATION STYLES AT COFFEE

Based on the ore-stage mineral assemblage of disseminated mineralization, a slightly acidic and reducing $H_2O-CO_2-S-As-Sb-Au-Ag$ fluid is proposed, at a temperature of approximately 220-250°C based on the stability ranges of arsenian pyrite and illite (White and Hedenquist, 1995; Buitenhuis, 2014). This fluid deposited Au-bearing arsenian pyrite while altering silicate minerals in the host rock to dolomite and illite.

Some of the highest grade mineralization at the Coffee project is hosted within polyphase siliceous brecciation (Double Double, Supremo T3). These intervals are markedly different from disseminated mineralization, and indicate the presence of a cooler, siliceous hydrothermal fluid rich in As, Sb, Au and Ag. Super-fine arsenian pyrite is found within completely silicified wall rocks and in coarse-grained, hydrothermal quartz and illite within breccia matrices at Supremo. Breccia at Double Double includes both silicification of wall rocks and later brecciation with coarse houndstooth textured carbonate infill. In the absence of metamorphic mica, the pyrite is potentially deposited by cooling of the fluid.

The temporal relationship between disseminated mineralization and siliceous brecciation is currently unclear. The differing styles may represent multiple mineralization events with different fluids; however, similar, if not identical, metal signatures in all phases (Au-As-Sb-Ag) suggest an evolving and cooling fluid. The destruction of mass amounts of silicate minerals during widespread dolomite-illite alteration during the disseminated mineralization phase would liberate significant Si, which could have been incorporated into the fluid. Although mass-balance calculations have not been completed, Si released through alteration of silicates could tip fluid composition from CO_2 -dominant to SiO_2 -dominant with a hypothetical composition of $H_2O-SiO_2-S-As-Sb-Au-Ag$. Such a fluid composition accounts for the presence of As-rich, Au-bearing pyrite within silicified wall rocks, hydrothermal quartz in breccia matrices, and low-temperature siliceous sinter textures observed in some zones at Coffee. Textural differences between the disseminations ('passive' replacement of host) and breccia-hosted mineralization (violent fracturing) could represent a transition from an early semi-ductile to later brittle regime during uplift.

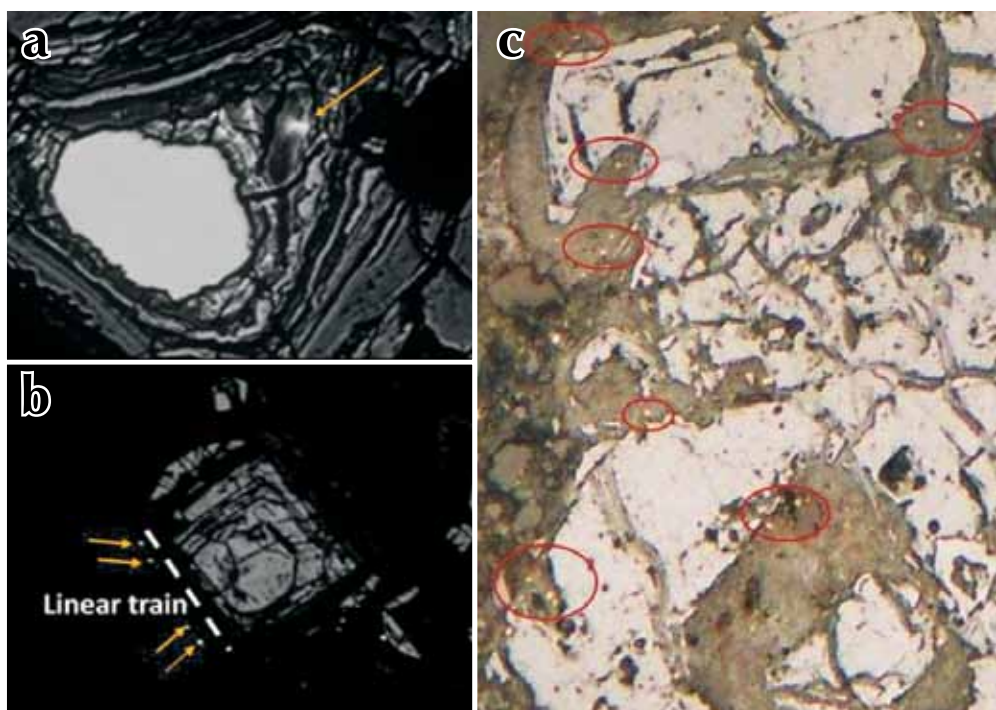


Figure 12. Backscatter (a,b) and reflected light (c) images of free gold hosted in remnant oxide and clay minerals from the Supremo zone. a) Micron-scale native gold found in the oxidized rim of an arsenian pyrite grain, FOV is 50 microns; b) Micron-scale grains of free gold in a linear train, Supremo zone, FOV is 0.1 mm; c) Free gold visible in pyrite (RL) from the Supremo zone, FOV is 0.25 mm.

RELATION TO NEARBY MINERAL DEPOSITS

Although greenschist-facies alteration, orogenic quartz veining, and pyrite formation are observed in the Coffee rocks (MacKenzie *et al.*, 2013), mineralization is constrained to <98 Ma by crosscutting relationships with the Coffee Creek granite, indicating that Coffee is not related to the nearby White Gold deposit (163-155 Ma; Bailey, 2013). The Late-Cretaceous Casino Cu-Mo-Au porphyry is located 30 km east of Coffee, but exhibits different mineralogy and metal associations than either style of Coffee mineralization. Coffee is similar to the Boulevard deposit, a Cretaceous orogenic gold deposit to

Table 2. Table of Au recoveries from column leach testwork. Columns included oxide (>90% oxidized material), upper transitional (50-90% oxidized material), lower transitional (5-50% oxidized material) and sulphide from the Latte zone (5% or less oxidized). Material is tested at 25 mm (1" inch crush), 12.5 mm (0.5" crush) and at both ambient temperature (22°C) and simulated cold climate leach temperature (4°C).

Description	Target p80 Size (mm)	Target Temp. (°C)	Calculated Head Au (g/t)	Extracted Au (g/t)	Extracted Au (%)	Consumption NaCN (kg/t)	Addition Hydrated Lime (kg/t)
Supremo, Oxide	25	4	1.573	1.455	92	0.17	1.51
Supremo, Oxide	12.5	4	1.435	1.343	94	0.28	1.5
Supremo, Oxide	12.5	22	1.547	1.471	95	0.52	1.57
Supremo, Upper Transition	12.5	4	1.488	1.081	73	0.31	1
Supremo, Lower Transition	12.5	4	1.674	0.797	48	0.38	1
Latte, Oxide	25	4	1.622	1.462	90	0.19	1.51
Latte, Oxide	12.5	4	1.54	1.382	90	0.27	1.51
Latte, Upper Transition	12.5	4	1.535	0.717	47	0.46	2.01
Latte, Lower Transition	12.5	4	1.416	0.411	29	0.64	1.51
Latte, Sulphide	12.5	4	2.365	0.126	5	0.46	1.51

the southwest of Coffee dated at ~96 Ma (McKenzie *et al.*, 2013; Buitenhuis, 2014). Metal associations at Coffee (Au-As-Sb±Ag) are similar to those seen at Boulevard (Au-As-Sb±Pb±Zn±Cu) with the exception of the minor base metals which are present within Boulevard's sheeted quartz veins. Ore-stage fluids at Boulevard are aqueous-carbonic and low-salinity, consistent with orogenic mineralizing fluids (Groves *et al.*, 2003; McKenzie *et al.*, 2013; Allan *et al.*, 2013). Though no fluid-inclusion work has been completed at Coffee, its proximity to the Boulevard deposit along with similar metal associations and a <98 Ma time domain indicates that a common origin cannot be ruled out. Coffee may also represent a separate and newly identified mineralizing event within the region.

RELEASE OF STRUCTURALLY-BOUND AU

Late stage oxidation of mineralized rocks at Coffee resulted in the breakdown of Au-bearing sulphides and release of Au from the pyrite structure. Au is then hosted within oxide and clay minerals which are amenable to

rapid leaching by CN⁻ solution. As structurally bound Au is released it coalesces into micron-scale nuggets organized in linear trains which are readily extracted by CN⁻ due to their small surface area.

CONCLUSIONS

The Coffee project is a structurally and lithologically controlled gold deposit which exhibits both epizonal orogenic and epithermal characteristics. Mineralization is hosted within brittle, near-vertical structures, which cut all lithologies on the property, and exhibits two distinct styles. The phase of disseminated mineralization was formed by the reaction of a H₂O-CO₂-S-As-Sb-Au-Ag fluid at approximately 220-250°C with mica-rich host rocks, depositing As-rich pyrite which incorporated significant Au and minor Ag within its crystal lattice. Pervasive dolomite-illite alteration accompanied sulphide deposition. Continued fluid influx in some areas led to complete obliteration of the host rock and destruction of previously deposited Au-rich pyrite, which was subsequently re-deposited in quartz-dolomite veinlets. The phase of

silicification of wall rocks and deposition of further As-rich, Au-bearing pyrite is observed along with polyphase brecciation, sealed by coarse hydrothermal quartz, fine illite, and additional As-Au bearing pyrite, which probably crystallized from the solution during cooling. The two styles of mineralization may be the result of the evolution of a single fluid from CO₂-rich to SiO₂-rich, or two separate mineralizing fluids.

Early disseminated mineralization formed at Coffee at the beginning of a transition to a brittle structural regime in an extensional tectonic environment controlled by mid-Cretaceous faulting. Breccia-hosted mineralization represents the continued mobility of Fe, S, Au, As, Sb and Ag in a SiO₂-dominant fluid which exhibits epithermal-like textures as the fluid cools.

The Coffee deposits possibly represent the shallower, epizonal extensions of the mesozonal orogenic mineralization at the Boulevard deposit to the south. Ore fluids at Boulevard may have depleted their base metal budget before advancing upwards in a regional metallogenic system, resulting in a lack of base metals at Coffee but identical Au-As-Sb enrichment. The possibility exists, however, that Coffee may represent an independent system which was active separately from the Boulevard and Toni Tiger deposits.

All gold at Coffee was initially deposited and hosted within arsenian pyrite, but oxidation by meteoric fluids destroyed the sulphide and liberated gold from within the pyrite crystal lattice. Gold in oxidized intervals is found in linear trains within oxide and clay minerals, dominantly limonite, hematite and kaolinite respectively, where it is readily liberated by cold-leach sodium cyanide (NaCN, CN⁻) solution, resulting in rapid leach kinetics and achieving column leach gold recoveries of up to 95%.

ACKNOWLEDGEMENTS

This paper is dedicated to Dr. Craig Finnigan who passed away in early 2014. Dr. Finnigan initiated much of the research presented herein, in particular conducting early petrographic, metallogenic, and mineralogical research, and acting as co-supervisor and mentor to Messrs. Buitenhuis and Boyce. The primary author would like to thank R.L. Barnett and J. Renaud for extensive EPMA and petrographic work, as well as Tim Smith, Geoff Newton, James Scott and Adam Fage for helpful reviews. A critical review by Dr. Norman Duke was much appreciated. This research was supported financially by Kaminak Gold Corporation.

REFERENCES

- Allan, M.M., Mortensen, J.K., Hart, C.J.R., Bailey, L.A., Sánchez, M.G., Ciolkiewicz, W., McKenzie, G.G. and Creaser, R.A., 2013. Magmatic and metallogenic framework of west-central Yukon and eastern Alaska. *In: Tectonics, Terranes, Metallogeny and Discovery in the northern circum-Pacific region*, M. Colpron, T. Bissig, B. Rusk and J. Thompson (eds.), Society of Economic Geologists Special Publication 17, p. 111-168.
- Bailey, L., 2013. Late Jurassic fault-hosted gold mineralisation of the Golden Saddle deposit, White Gold district, Yukon Territory. An unpublished MSc Thesis housed in the University of British Columbia library, Vancouver, Canada.
- Beranek, L.P. and Mortensen, J.K., 2011. The timing and provenance record of the Late Permian Klondike orogeny in northwestern Canada and arc-continent collision along western North America. *Tectonics*, vol. 30, TC5017.
- Berman, R.G., Ryan, J.J., Gordey, S.P. and Villeneuve, M., 2007. Permian to Cretaceous polymetamorphic evolution of the Stewart River region, Yukon-Tanana terrane, Yukon, Canada: P-T evolution linked with in situ SHRIMP monazite geochronology. *Journal of Metamorphic Geology*, vol. 25, p. 803-827.
- Boyce, L., 2014. A Paragenetic Model and Geochemistry of the Double Double Gold Zone, Kaminak's Coffee Gold Project, Yukon, Canada. An unpublished BSc Thesis housed in the University of Alberta library, Edmonton, Canada.
- Buitenhuis, E.N., 2014. The Latte Gold Zone, Kaminak's Coffee Gold Project, Yukon, Canada: Geology, Geochemistry, and Metallogeny. An unpublished MSc Thesis housed in the University of Western Ontario library, London, Canada.
- Cline, J.S., 2001. Timing of gold and arsenic sulfide mineral deposition at the Getchell Carlin-type gold deposit, north-central Nevada. *Economic Geology*, vol. 96, p. 75-89.
- Cline, J.S., Shields, D., Riciputi, L., Fayek, M., Copp, T., Muntean, J. and Hofstra, A.H., 2003. Trace element and isotope microanalyses support a deep ore fluid source at the Getchell Carlin-type gold deposit, northern Nevada. *Geological Society of America Abstracts with Programs*, vol. 35, p. 358.

- Colpron, M., Nelson, J. and Murphy, D.C., 2006. A tectonostratigraphic framework for the pericratonic terranes of the northern Canadian Cordillera. *In: Paleozoic Evolution and Metallogeny of Pericratonic Terranes at the Ancient Pacific Margin of North America, Canadian and Alaskan Cordillera*, M. Colpron and J.L. Nelson (eds.), Geological Association of Canada Special Paper 45, p. 1-23.
- Colpron, M., Nelson, J. and Murphy, D.C., 2007. Northern Cordilleran terranes and their interactions through time. *GSA Today*, vol. 17, p. 4.
- Cruikshank, P., 2011. Hydrothermal alteration and gold mineralization of the Supremo zone, Coffee property, Yukon, Canada. An unpublished BSc Thesis housed in the University of Western Ontario library, London, Canada.
- Emsbo, P., Hofstra, A.H., Lauha, E.A., Griffin, G.L., Hutchinson, R.W., John, D.A. and Theodore, T.G., 2003. Origin of high-grade gold ore, source of ore fluid components and genesis of the Meikle and neighboring Carlin-type deposits, northern Carlin Trend, Nevada. *Economic Geology*, vol. 98, p. 1069-1105.
- Erdmer, P., Ghent, E.D., Archibald, D.A. and Stout, M.Z. 1998. Paleozoic and Mesozoic high-pressure metamorphism at the margin of ancestral North America in central Yukon. *GSA Bulletin*, vol. 110, p. 615-629.
- Fleet, M.E., Chryssoulis, S.L., MacLean, P.J., Davidson, R. and Weisener, C.G., 1993. Arsenian pyrite from gold deposits; Au and As distribution investigated by SIMS and EMP and color staining and surface oxidation by XPS and LIMS. *Canadian Mineralogist*, vol. 31, p. 1-17.
- Fleet, M.E. and Mumin, A.H., 1997. Gold-bearing arsenian pyrite and marcasite and arsenopyrite from Carlin Trend gold deposits and laboratory synthesis. *American Mineralogist*, vol. 82, p. 182-193.
- Gabrielse, H., Murphy, D.C. and Mortensen, J.K., 2006. Cretaceous and Cenozoic dextral orogen-parallel displacements, magmatism, and paleogeography, north-central Canadian Cordillera. *In: Paleogeography of the North American Cordillera: Evidence For and Against Large-Scale Displacement*, J.W. Haggart, R.J. Enkin and J.W.H. Monger (eds.), Geological Association of Canada, Special Paper 46, p. 255-276.
- Groves, D.I., Goldfarb, R.J., Robert, F. and Hart, C.J.R., 2003. Gold deposits in metamorphic belts: Overview of current understanding, outstanding problems, future research, and exploration significance. *Economic Geology*, vol. 98, p. 1-29.
- Johnston, S.T., 1995. Geological compilation with interpretation from geophysical surveys of the northern Dawson Range (115-J/9, 115-J/10, and 115-I/12), central Yukon. Exploration and Geological Services Division, Yukon, Indian and Northern Affairs Canada, Open File 1995-2 (G), 1:100 000 scale.
- MacKenzie, D., Craw, D. and Mortensen, J.K., 2008. Thrust slices and associated deformation in the Klondike goldfields, Yukon. *In: Yukon Exploration and Geology 2007*, D.S. Emond, L.R. Blackburn, R.P. Hill and L.H. Weston (eds.), Yukon Geological Survey, p. 199-213.
- MacKenzie, D.J., Craw, D., Cooley, M. and Fleming, A., 2010. Lithogeochemical localisation of disseminated gold in the White River area, Yukon, Canada. *Mineralium Deposita*, vol. 45, p. 683-705.
- MacKenzie, D., Craw, D. and Finnigan, C., 2013. Structural controls on alteration and mineralization at the Coffee gold deposits, Yukon. *In: Yukon Exploration and Geology 2013*, K.E. MacFarlane, M.G. Nordling and P.J. Sack (eds.), Yukon Geological Survey, p. 119-131.
- Makarenko, M., Pilotto, D., Klingmann, S., Doerksen, G., Levy, M., Sim, R. and Lightner, F., 2014. Preliminary Economic Assessment Technical Report Coffee Project, Yukon, Canada. Technical Report Prepared for Kaminak Gold Corporation by JDS Energy & Mining Inc., Vancouver, Canada. Report Date July 8, 2014.
- McKenzie, G.G., Allan, M.M., Mortensen, J.K., Hart, C.J.R., Sanchez, M. and Creaser, R.A., 2013. Cretaceous orogenic gold and molybdenite mineralization in the Independence Creek area, Dawson Range, parts of NTS 115J/13 and 14. *In: Yukon Exploration and Geology 2012*, K.E. MacFarlane, M.G. Nordling and P.J. Sack (eds.), Yukon Geological Survey, p. 73-97.
- Mortensen, J.K., 1992. Pre-mid-Mesozoic tectonic evolution of the Yukon-Tanana Terrane, Yukon and Alaska. *Tectonics*, vol. 11, p. 836-853.

- Nelson, J., Colpron, M., Piercey, S.J., Dusel-Bacon, C., Murphy, D.C. and Roots, C.F., 2006. Paleozoic tectonic and metallogenetic evolution of pericratonic terranes in Yukon, northern British Columbia, and eastern Alaska. *In: Paleozoic Evolution and Metallogeny of Pericratonic Terranes at the Ancient Pacific Margin of North America, Canadian and Alaskan Cordillera*, M. Colpron and J.L. Nelson (eds.), Geological Association of Canada Special Paper 45, p. 323-360.
- Piercey, S.J. and Colpron, M. 2009. Composition and provenance of the Snowcap assemblage, basement to the Yukon-Tanana terrane, northern Cordillera: Implications for Cordilleran crustal growth. *Geosphere*, vol. 5, p. 439-464.
- Reich, M., Kesler, S.E., Utsunomiya, S., Palenik, C.S., Chryssoulis, S.L. and Ewing, R.C., 2005. Solubility of gold in arsenian pyrite. *Geochimica et Cosmochimica Acta*, vol. 69, p. 2781-2796.
- Ruks, T.W., Piercey, S.J., Ryan, J.J., Villeneuve, M. E. and Creaser, R.A., 2006. Mid to Late Paleozoic K-feldspar augen granitoids of the Yukon-Tanana Terrance, Yukon, Canada: Implications for crustal growth and tectonic evolution of the northern Cordillera. *GSA Bulletin*, vol. 118, p. 1212-1231.
- Ryan, J.J., Zagorevski, A., Williams, S.P., Roots, C., Ciolkiewicz, W., Hayward, N. and Chapman, J.B., 2013. Geology, Stevenson Ridge (northwest part), Yukon. Geological Survey of Canada, Canadian Geoscience Map 117 (2nd edition, preliminary), scale 1:100 000.
- Sánchez, M.G., Allan, M.A., Hart, C.J. and Mortensen, J.K., 2013. Structural Control of Mineralization Recognized by Magnetite-Destructive Faults of the Western Yukon and Eastern Alaska Cordilleran Hinterland (Poster). Society of Economic Geologists (SEG) conference, Whistler 2013: Geoscience for Discovery, September 24-27, 2013, Whistler, BC.
- Templeman-Kluit, D., 1979. Transported cataclasite, ophiolite, and granodiorite in Yukon: Evidence of arc-continent collision. Geological Survey of Canada Paper, vol. 79, p. 27.
- Villeneuve, M., Ryan, J., Gordey, S. and Piercey, S., 2003. Detailed thermal and provenance history of the Stewart River area (Yukon-Tanana terrane, western Yukon) through application of SHRIMP, Ar-Ar, and TIMS. Geological Association of Canada and Mineralogical Association of Canada Abstracts, vol. 28, p. 344.
- Wainwright, A.J., Simmons A.T., Finnigan, C.S., Smith, T.R. and Carpenter, R.L., 2011. Geology of new gold discoveries in the Coffee Creek area, White Gold District, west-central Yukon. *In: Yukon Exploration and Geology 2010*, K.E. MacFarlane, L.H. Weston and C. Relf (eds.) Yukon Geological Survey, p. 233-247.
- White, N.C. and Hedenquist, J.W., 1995. Epithermal Gold Deposits: Styles, Characteristics, and Exploration. Society of Economic Geologists Newsletter, vol. 23, p. 9-13.

Stratigraphy, geochemistry and source rock potential of the Boundary Creek Formation, North Slope, Yukon and a description of its burning shale locality

T.A. Fraser¹

Yukon Geological Survey

L. Reinhardt

German Federal Institute for Geosciences and Natural Resources

Fraser, T. and Reinhardt, L., 2015. Stratigraphy, geochemistry and source rock potential of the Boundary Creek Formation, North Slope, Yukon and a description of its burning shale locality. *In: Yukon Exploration and Geology 2014*, K.E. MacFarlane, M.G. Nordling and P.J. Sack (eds.), Yukon Geological Survey, p. 45-71.

ABSTRACT

The Cenomanian-Turonian (Upper Cretaceous) Boundary Creek Formation is a mudstone, shale and silty shale unit that is exposed in river and creek cuts on Yukon's North Slope. As part of the CASE-15 expedition, co-led by the Yukon Geological Survey and the German Federal Institute for Geosciences and Natural Resources, fieldwork in July 2013 involved measuring and sampling Boundary Creek Formation strata in two locations, and investigating a burning shale exposure near the confluence of Boundary Creek and the Big Fish River. Shale and mudstone samples were analyzed for XRF litho-geochemistry and organic matter quantity, along with thermal maturity and type using RockEval/TOC and vitrinite reflectance techniques. The Boundary Creek Formation is interpreted to have been deposited by turbidity currents moving through an outer shelf to slope environment in the distal part of the foreland basin, outboard of the Cordilleran orogeny. Litho-geochemical data suggest that at times throughout the deposition of Boundary Creek Formation shale, ocean water may have been depleted in oxygen, resulting in anoxic conditions that would have been favourable for organic matter preservation. Analyses of surface samples suggest that some areas have poor to no petroleum potential and are thermally overmature with respect to oil generation. In others, good to very good petroleum potential exists and the shale is oil to oil and gas prone and thermally mature with respect to oil generation. In these latter areas, specifically in the vicinity of the type section on Boundary Creek, the shale has the necessary components for spontaneous combustion: pyrite, organic matter and a fresh supply of oxygen provided by a landslide. Although burning shale is not unknown in northern Canada, the outcrop of burning shale on Yukon's North Slope is the first observed in shale of the Upper Cretaceous Boundary Creek Formation.

¹tiffani.fraser@gov.yk.ca

INTRODUCTION

In July 2013, an occurrence of naturally burning shale was discovered on Yukon's North Slope. The smoking exposure was sighted by helicopter while surveying Upper Cretaceous strata on the Big Fish River near the Yukon-Northwest Territories boundary. This paper discusses the sedimentology, distribution and hydrocarbon source rock potential of the Cenomanian-Turonian (Upper Cretaceous) Boundary Creek Formation, and describes the nature of the burning shale and mechanism for its formation.

STUDY BACKGROUND AND METHODS

An international consortium of geologists from Germany, France, United States and Canada conducted fieldwork on Yukon's North Slope in July 2013 as part of ongoing research on the tectonic history of the circumpolar Arctic by the German Federal Institute for Geosciences and Natural Resources (BGR). The CASE 15 (Circum-Arctic Structural Events) expedition was a collaborative project of the Yukon Geological Survey (YGS) and BGR that provided logistical support to 20 geoscientists interested in studying various aspects of Yukon's North Slope. Fieldwork was conducted from a basecamp constructed at the site of a former oil and gas exploration drilling pad near the Blow River (E-47; Fig. 1), from which daily set-outs with a contract helicopter were made. Sedimentologists and petroleum geologists from the YGS and BGR seized the opportunity to investigate sedimentary rock exposures in a relatively understudied and remote corner of the territory.

Fieldwork was conducted over a ten day period with the intent to focus on Upper Cretaceous and Tertiary siliciclastic exposures. Stratigraphic sections of the interpreted Boundary Creek Formation were measured and sampled in two main locations (BL-06 and BL-08, Fig. 1). Measured sections were described in detail and sampled to evaluate their petroleum source rock potential, mineralogy and age. Shale samples were analyzed for organic carbon quantity, thermal maturity and kerogen type using Rock-Eval pyrolysis techniques (after Espitalié *et al.*, 1977) using a Rock-Eval 6 analyzer. Total organic carbon (TOC) and total sulphur contents were determined by combustion with a LECO CS 230 carbon/sulfur analyzer. Thermal maturity was also assessed using vitrinite reflectance (VR) following the DIN 22020-5 and ASTM D7708-11 standards. X-ray fluorescence (XRF) was run on

shale samples for elemental chemistry using DIN 51418 standards. X-ray diffraction (XRD) was used to determine the preliminary mineralogy (non-quantitative) of bentonite samples using a PANalytical MPD Pro instrument on whole rock powder. Biostratigraphic and radiometric age-dating are in progress. All samples were analyzed in Germany at the BGR.

On July 18, while flying over the confluence of Boundary Creek and the Big Fish River, a plume of smoke was observed on the side of a hill. The smoke was coming from exposed shale of the Boundary Creek Formation, below which was a fan of landslide debris. The landslide appeared to be recent, as the debris fan had diverted the creek and it was unvegetated. An Aklavik resident working in camp stated that they had been aware of the burn site before this summer, however, they were unsure how long it had been burning. The burning exposure was visited and sampled for Rock-Eval/TOC and XRF elemental chemistry.

UPPER CRETACEOUS GEOLOGICAL SETTING

Upper Cretaceous strata in north Yukon were deposited in a foreland basin setting north of the active Cordilleran orogen (Dixon, 1997). In Cenomanian to Turonian time, sedimentation formed a broad belt of non-marine to inner shelf sediments close to the orogen front with progressively finer-grained sediments deposited northward. On Yukon's North Slope, the Boundary Creek Formation represents the shalier outer shelf to slope facies of this prograding clastic wedge. By the end of the Cretaceous, sedimentation had shifted northward to the subsiding continental margin of the Canada Basin where thick Paleocene to Oligocene deltas accumulated.

THE BOUNDARY CREEK FORMATION

TYPE SECTION

Young (1975) established the nomenclature of Upper Cretaceous strata on Yukon's North Slope while mapping the area along the Yukon coastal plain and the Mackenzie Delta. The Boundary Creek Formation type locality is on the north bank of Boundary Creek, adjacent the Yukon/NWT border (UTM Zone 8, 439749E, 7599615N (NAD 83); Fig. 1, BL-08 section). At this location, the formation consists of 240 m of soft, recessive, grey to black shale punctuated by beds of bentonite up to 0.3 m thick and minor carbonate beds. The weathered exposures are

oxidized to yellow, red and mahogany brown from encrustations of sulphate minerals and iron oxides (e.g., gypsum and jarosite).

DISTRIBUTION AND THICKNESS

The Boundary Creek Formation (K_{BC}) is shown by Norris (1981a,b,c) to be at surface or beneath Quaternary sediments in north Yukon between Trail River, a westerly tributary of Babbage River (NTS 117D/3), and the Mackenzie Delta in NWT (NTS 107B; Fig. 1). It has been identified in the subsurface of Yukon's North Coast, the

Mackenzie Delta and in the southeastern part of the Tuktoyaktuk Peninsula (Dixon, 1996).

On the Yukon Coastal Plain, the Boundary Creek Formation forms a northeast-thickening depositional wedge which is buried by a progressively thicker Tertiary deltaic sequence (Dixon, 1996). Three onshore wells west of Mackenzie Delta (Fig. 1) intersect the Boundary Creek Formation (Fraser and Hogue, 2007; Geoscout, 2014). Chevron Canada B-60 in NWT intersects ~232 m of Boundary Creek Formation shale beginning at a depth of 2199 m. IOE Spring River YT N-58 encountered ~76 m

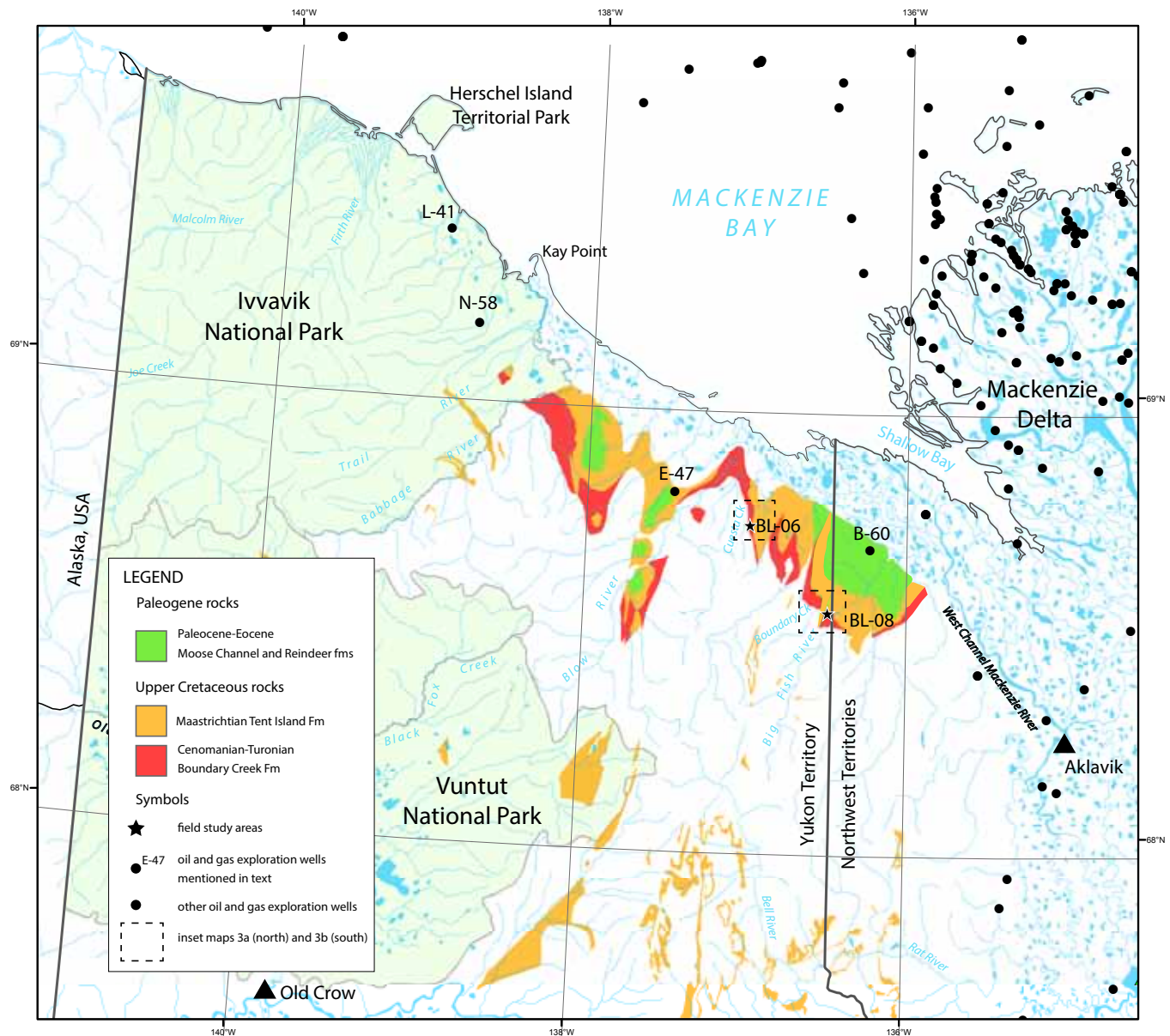


Figure 1. Regional map of northern Yukon and adjacent northwestern corner of NWT showing the distribution of Upper Cretaceous and Tertiary strata in the area, oil and gas exploration wells and location of measured sections in this report. The locations of Figures 3a and 3b are indicated by the inset boxes. Geology after Norris (1981a,b,c).

of Boundary Creek shale starting at a depth of 509 m. Roland Bay L-41 encountered ~359 m of Boundary Creek shale beginning at 352 m depth. Although the formation is almost certainly present in the Blow River E-47 well, it has not been documented to date. In the subsurface, the thickest Boundary Creek interval occurs in the central Mackenzie Valley where it is 488 m (Bruce and Parker, 1975).

In outcrop, Young (1975) measured an 1100 m section in the northern Richardson Mountains near Cuesta Creek; however, the section contains faults and may include some repeated sections.

STRATIGRAPHY AND CORRELATION

The base of the Boundary Creek Formation is marked by the major, regional mid-Cretaceous unconformity separating Lower from Upper Cretaceous rocks. Below the Boundary Creek Formation are shale and siltstone assigned to the Albian Flysch (Young, 1977). Unconformably overlying the Boundary Creek Formation are sandstones of the Cuesta Creek Member of the Maastrichtian Tent Island Formation (Fig. 2; Dixon 1992, 2004).

The Boundary Creek Formation is interpreted as an outer shelf to basinal equivalent of the lower Eagle Plain Group (Parkin and Fishing Branch formations) which occur further south in Eagle Plain basin (Dixon, 1992).

Young (1977) correlated Boundary Creek strata with the Santonian to Campanian Smoking Hills Formation which occurs within and east of the Mackenzie Delta, however, this correlation is in dispute (Dixon, 1992).

AGE

Palynomorphs and dinoflagellates are abundant in the Boundary Creek Formation and indicate a Late Cenomanian to Turonian age (after D.J. McIntyre, in Dixon *et al.*, 1985).

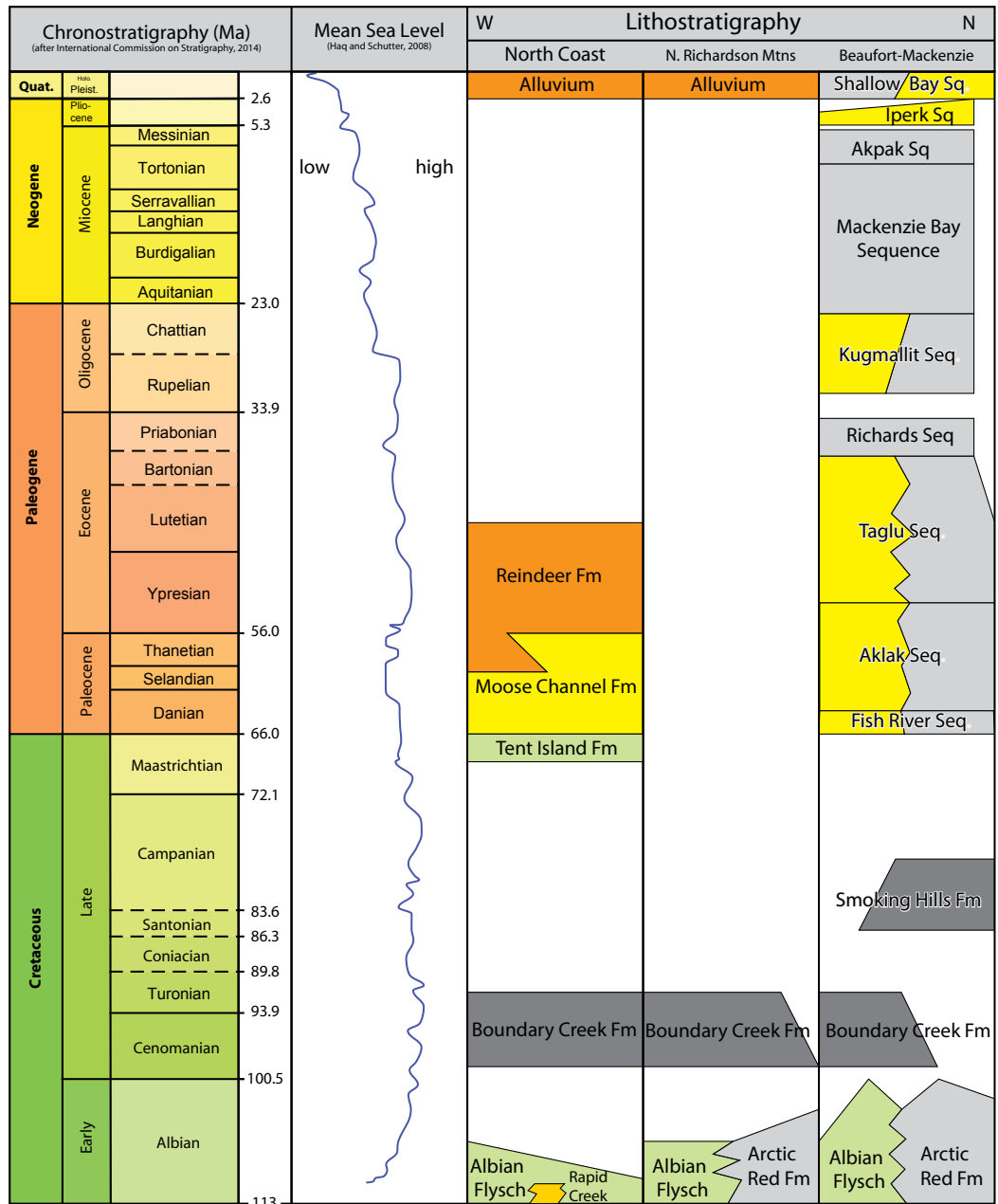
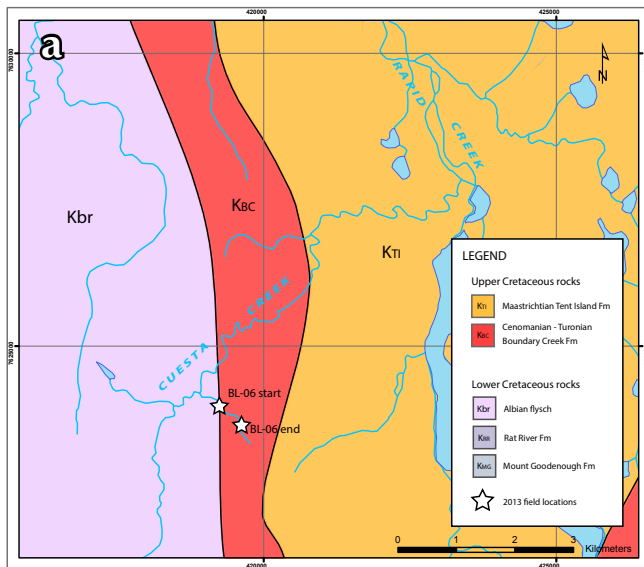


Figure 2. Table of Albian (Lower Cretaceous) and younger lithostratigraphic formations in North Yukon, northern Richardson Mountains, and Beaufort-Mackenzie Delta. Timescale after International Commission on Stratigraphy, 2014. Geology after Pigage (2007) and Dixon (1996).

2013 STUDY

MEASURED SECTIONS AND SPOT SAMPLING

Two sections of strata assigned to the Boundary Creek Formation were measured in detail at locations separated by ~32 km. The first is located in a southeasterly tributary of Cuesta Creek (BL-06; Fig. 3a) where 518 m of discontinuous shale (387 m of which is covered) was measured and sampled at intervals of ~25 m. The second is in a northern tributary of Boundary Creek, ~1.7 km northwest of the confluence of Boundary Creek and Big Fish River (BL-08A; Fig 3b). One hundred metres of shale was measured at this exposure with samples obtained at 10 m intervals. Boundary Creek Formation exposures that were spot sampled include the formation type section (BL-08C) and the location of the burning shale (BL-08B; Fig. 3b). All coordinates are given in UTM NAD83, Zone 8, and are listed in Table 1.



CUESTA CREEK SECTION (BL-06)

The majority of the Cuesta Creek section is a moderately exposed, competent to recessive, outcrop of silty shale and mudstone couplets with local carbonate concretions (Fig. 4 and 5).

Silty shale and mudstone couplets are 5-10 cm thick (Fig. 6a). Silty shale is more resistant than mudstone and comprises up to 10-25% of the exposure. It is medium grey on fresh surfaces and weathers to medium grey, yellowish brown and reddish brown. Silty shale occurs in laminated intervals up to 1 cm thick. Beds are rippled and scour into mudstone intervals below them. Upper contacts are sharp to gradational with overlying mudstone.

Mudstone comprises up to 75% of the exposure and is dark grey on fresh surfaces, weathering to medium grey, yellowish brown and reddish brown. In areas it is quasi-fissile (more shale-like) but overall, it weathers to uneven,

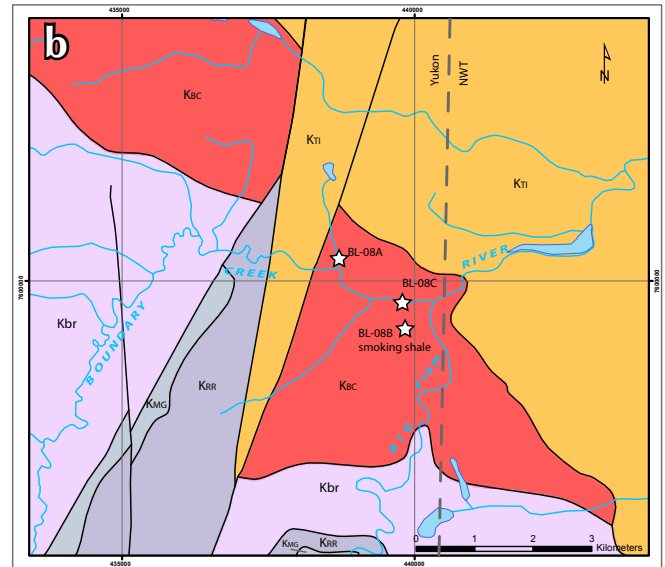
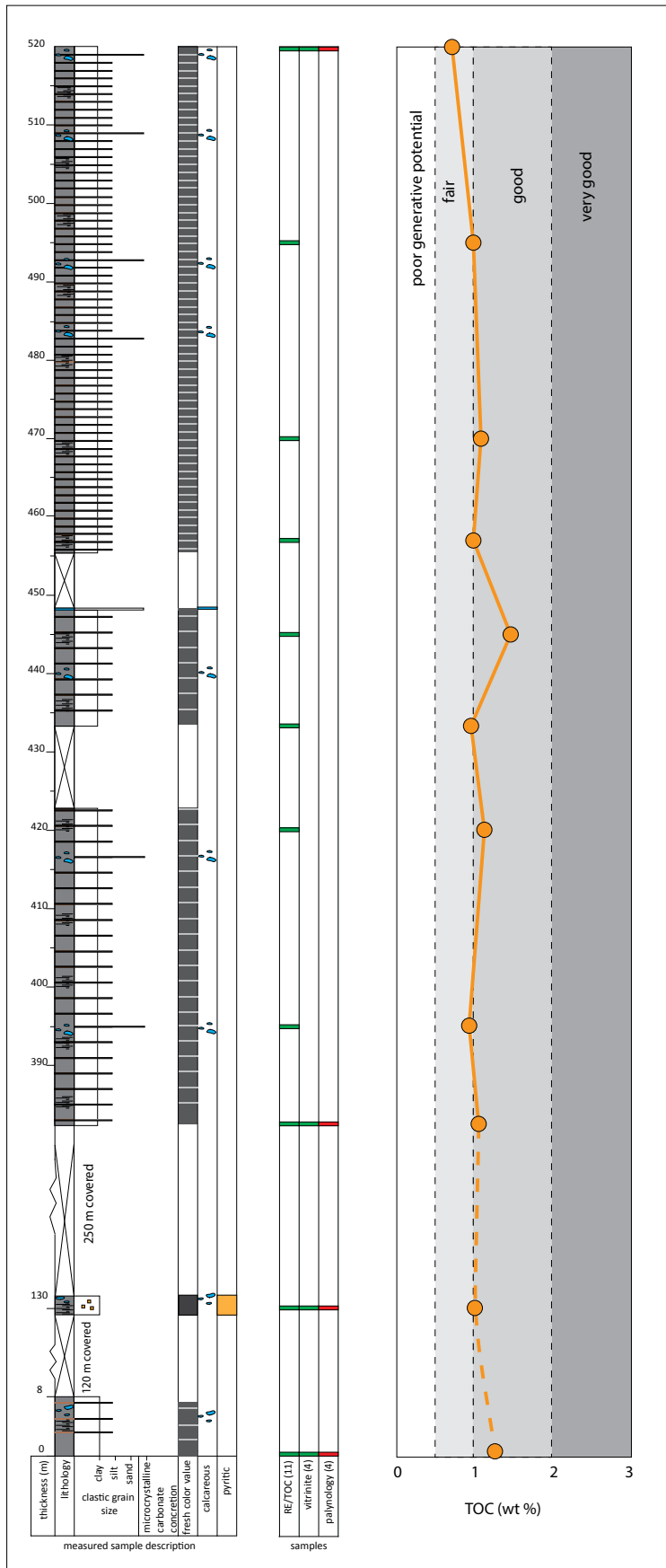


Figure 3. (a) Local geology of the Cuesta Creek area and location of BL-06 measured section. Geology after Norris (1981b). (b) Local geology of the Boundary Creek area and location of BL-08 measured section, BL-08B smoking shale locality and BL-08C (Boundary Creek Formation spot sample). Geology after Norris (1981b).

Table 1. UTM coordinates for section and sampling localities mentioned in this study.

Section	Site Description	Zone	UTM E	UTM N	Comment
TF-13-BL-06D	tributary of Cuesta Creek	8W	419631	7623659	Boundary Creek Fm (base of section 0 m)
TF-13-BL-06D	tributary of Cuesta Creek	8W	419753	7623479	Boundary Creek Fm (top of section 520 m)
TF-13-BL-08A	tributary of Boundary Creek	8W	438747	7600419	Boundary Creek Fm (base of section 0 m)
TF-13-BL-08A	tributary of Boundary Creek	8W	438854	7600461	Boundary Creek Fm (top)
TF-13-BL-08B	Boundary Creek - south	8W	439809	7599167	burning shale section
TF-13-BL-08C	Boundary Creek - north	8W	439749	7599615	Type Section of Boundary Creek Formation (Young, 1975)



LEGEND

LITHOLOGY	PRECIPITATED MINERALS
■ mudstone/shale	■ gypsum concretions
■ siltstone	■ pyrite
■ bentonite	■ carbonate concretions
■ carbonate	
SEDIMENTOLOGY	DESCRIPTORS
▨ planar-lamination	fresh color Values (Munsell)
SAMPLES	■ N5 - medium grey
■ sample location; analyzed in this study	■ N4 - medium dark grey
■ sample location; future analysis	■ N3 - dark grey
	■ N2 - greyish black
	■ N1 - black
	■ pale grayish yellow
	other
	■ calcareous
	■ pyritic

Figure 4. Graphical log of the Cuesta Creek (BL-06) measured section with accompanying sample locations and Rock-Eval derived TOC values.

small (<2 cm long) fragments. The mudstone is soft, generally breaking easily in the hands. Although highly weathered, mm-scale laminations can be observed.

Variably-sized, round to oblong carbonate concretions form up to 5% of the section. These concretions generally range in size from 60x40 cm to 10x2 cm and where present, occur semi-continuously along bedding (Fig. 6b). One distinct concretionary bed at 447 m measured depth (Fig. 4) is 30 cm thick and >3.0 m long. Like other concretions in the section, it is dark grey on fresh surfaces and weathers a distinctive greyish orange. It is dense, difficult to break with a hammer and weathers to large (30x10x10 cm) blocks. It is composed of microcrystalline carbonate and has no apparent sedimentary structures. The contacts of the concretion with the surrounding mudstone are very sharp.

In the lowest part of the section, below 130 m measured thickness, disseminated pyrite occurs on bedding surfaces.

BOUNDARY CREEK A SECTION (BL-08A)

The Boundary Creek A section (start of section at 438747E, 7600419N) comprises 100 m of shale, silty shale, bentonite and concretions (Figs. 7 and 8). Over 90% of the section is composed of shale which is black on fresh surfaces, weathers light to medium grey, and yellowish grey (jarosite-coated). Shale is overall very recessive and soft, breaking easily in the hands. Furthermore, it is fissile, weathering to small irregular pieces (<2 cm thick), wafers



Figure 5. Lower part of Cuesta Creek (BL-06) section.

or to a sticky powder. Silty shale occurs between 0 and 50 m measured depth in discrete horizons comprising ~5% of the unit. It is brownish black on fresh surfaces, and weathers rusty brown and dark reddish brown. Silty shale occurs in resistant individual laminae/beds up to 2 cm thick. These beds are, difficult to break with the hands, are



Figure 6. (a) Mudstone and silty mudstone couplets at Cuesta Creek (BL-06) section. Silty mudstone laminae are more resistant than the mudstone and can be ripple-laminated. (b) Upper part of Cuesta Creek (BL-06) section showing mudstone and weathered semi-continuous carbonate concretions.

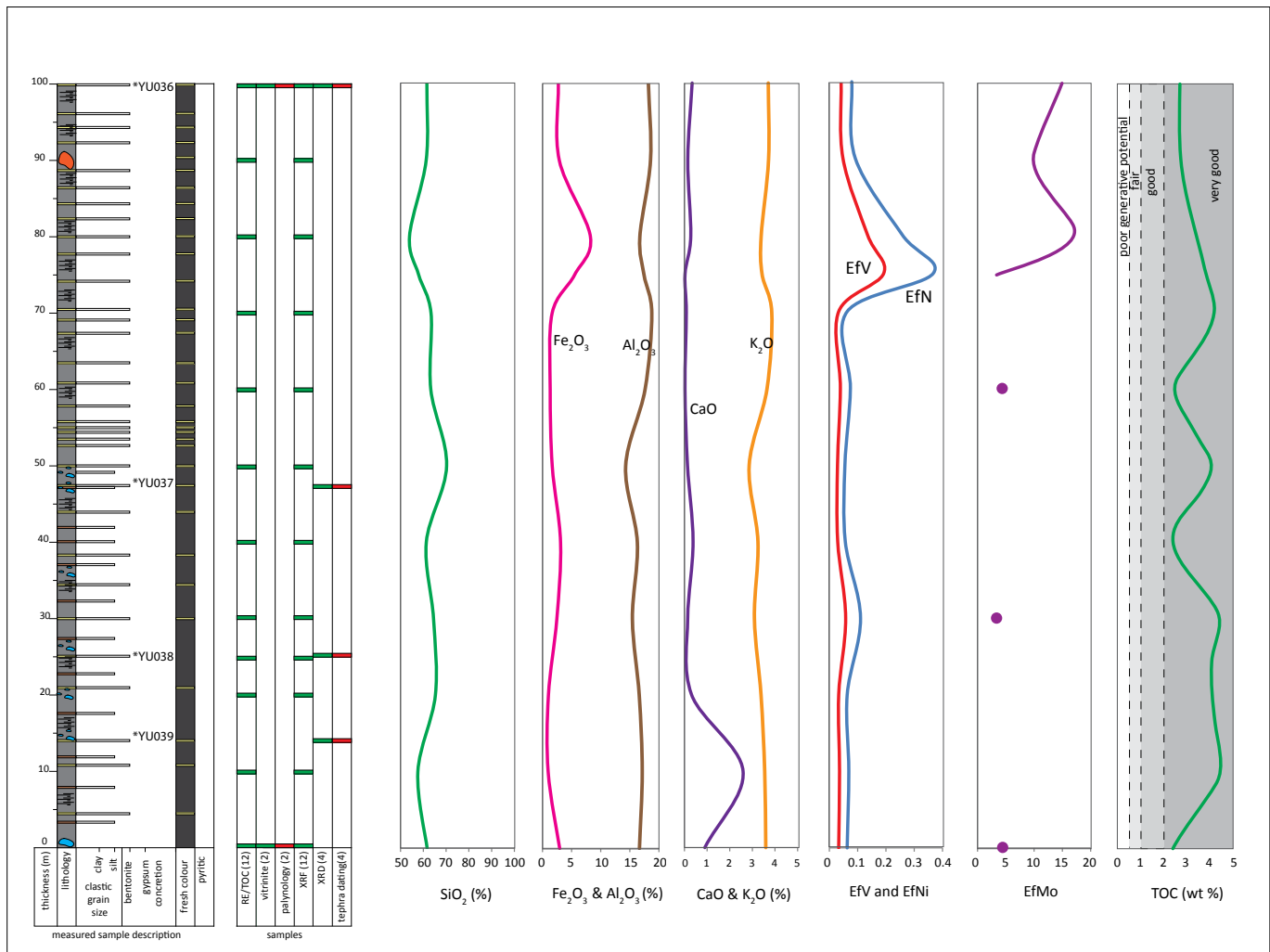


Figure 7. Graphical log of the Boundary Creek (BL-08A) measured section with accompanying sample locations, XRD geochemistry results and Rock-Eval derived TOC values. Enrichment factor (Ef) curve for Mo is broken as samples collected in this interval were below the detection limit for Mo of the XRF technique. Legend is in Figure 4. *denotes bentonite samples currently undergoing further analyses in Germany.

commonly more dense than surrounding shale and have a ferruginous smell. No sedimentary structures are observed within these intervals, however, their upper and lower contacts are sharp.

Interbedded throughout the shale are numerous discrete bentonite layers (Fig. 9a,b), ranging in average thickness from <1 cm to 3 cm but can be locally up to 40 cm thick. The horizons exhibit an apparent cyclicity on two scales: they generally occur every 30 to 50 cm, but locally more frequent, occurring every 5-15 cm. The yellowish-grey and yellowish-orange weathering (presence of iron?) of these horizons give the outcrop a striped appearance.

On fresh surfaces, the bentonites are light grey. They are unconsolidated, soft and sticky.

Rusty weathering concretionary beds are observed in up to 10% of the section. The concretions consist of shale fragments cemented by gypsum crystals and are generally rounded and <50 cm in diameter. Locally, the concretions form discrete entities along a distinct horizon; elsewhere they are amalgamated into semi-continuous beds. At the top of this section are distinctive large (>2.5 x 1.5 m), rounded concretions (Fig. 10). These particular concretions consist of black shale broken up by a dense array of gypsum crystals randomly oriented along

fractures (Fig. 11). Their orange color contrasts with the surrounding darker shale. The concretions occur within a ~10 m stratigraphic zone, but are not assigned to one specific bed. They form resistant features on the exposure, however, are soft and easy to sample with a hammer.



Figure 8. Exposure of Boundary Creek Formation at BL-08A. Large concretions are those shown in Figure 10.



Figure 9. (a) Cyclical nature of the shale of the Boundary Creek Formation at BL-08A. Light yellow horizons are bentonites. Orange-stained horizons are generally concretionary but may also include weathered bentonites. (b) Close-up of bentonite at Boundary Creek section (BL-08A).

BOUNDARY CREEK C EXPOSURE (BL-08C)

The Boundary Creek C locality is Young's (1975) type section (439832E, 7599204N; Fig. 3 in Young, 1975). It was visited to investigate and sample a ~50 cm-thick tephra bed visible from the helicopter (Fig. 12). At this site, >10 m of Boundary Creek Formation shale is exposed, punctuated by bentonite layers. Although not measured in detail, the shale is similar to the BL-08A section in that it is black on fresh surfaces and weathers pale yellowish grey (indicating possible presence of jarosite). The shale is fissile and has visible laminations. Furthermore, it is a soft shale that breaks easily by hand and weathers to small angular pieces. Round concretions form ~5% of unit, and are mainly up to 40 cm in diameter. Like the smaller concretions at the BL-08A section, they are semi-continuous along bedding.



Figure 10. Large gypsiferous concretions in the upper part of the Boundary Creek (BL-08A) measured section.



Figure 11. Close-up photograph of the internal structure of the gypsiferous concretions shown in Figure 10.

BOUNDARY CREEK B EXPOSURE (BL-08B)

Across the creek from the type section is an exposure of Boundary Creek shale that was burning in summer 2013 (439832E; 7599204N). A general site description is given in a subsequent section. Adjacent to the burning exposure, are small (<2 m) outcrops of fresh, black, fissile shale that were sampled for this study.

GEOCHEMISTRY AND MINERALOGY

LITHOGEOCHEMISTRY

Twelve samples from the BL-08A section were analyzed for elemental geochemistry by XRF (Appendix A). Major oxides (SiO_2 , Al_2O_3 , Fe_2O_3 , CaO and K_2O) and the enrichment factors (due to anoxia) of V and Ni are shown in Figure 7. SiO_2 is the dominant oxide with a range of 53-70%, followed by Al_2O_3 (14-19%), Fe_2O_3 (1-8%), K_2O (3-4%) and CaO (<1%, except at 10 m where it is 2.6%). Values for all oxides are fairly consistent; the 80 m sample showing a slight decrease in SiO_2 , Al_2O_3 and K_2O and slight increases in Fe_2O_3 and CaO . CaO also doubles in value at the 10 m stratigraphic level, but decreases again for the remainder of the section.

Enrichment factors (Ef) for the redox sensitive elements Mo, V and Ni were measured using calculations by Tribouillard *et al.* (2006). Values of >1 suggest enrichment of the trace element due to anoxia. The Ef values for V are <0.2 and for Ni are <0.4 suggesting a lack of anoxic conditions during deposition of the shale at this section, however, oxygen levels appear to fluctuate with an interpreted decrease in oxygenated water conditions at the ~75–80 m stratigraphic level. Ef values for Mo, while incomplete due to the detection limits of the XRF

(values <6), suggest conditions of anoxia for seven samples, with more extreme conditions at the 80 m and higher stratigraphic levels.

One shale sample from the Boundary Creek C (BL-08C) section was analyzed; all XRF-derived elemental data fit within the ranges of the BL-06A section, with the exception of Cr, Sr and loss-on-ignition (LOI) which had slightly lower values (Appendix A). Ef values for Ni and V were comparable to the BL-08A section, showing no evidence for anoxia. The Ef value for Mo was indeterminate due to the detection limits of the XRF.

Two samples were analyzed from fresh (unburned) shale at the Boundary Creek B (BL-08B) exposure adjacent the burning shale site (Appendix A). The major element compositions of these two samples were generally within the range of the BL-08A section with the exception of significantly elevated Fe_2O_3 , P_2O_5 , MnO , Co , Ni and Zn , and minor elevated values of MgO . In sample BL-08B1, SiO_2 and Zr were slightly lower and Ba remarkably lower than at BL-08A. In sample BL-08B2, TiO_2 and Al_2O_3 were slightly elevated compared to the BL-08A samples. Ef values for Ni (0.46-0.64) and V (0.24-0.34) are notably higher than samples from the BL-08A and BL-08C exposures suggesting a decrease in oxygen in the sea water compared to the other sites. The Ef value for one Mo sample is 5.79 suggesting anoxia.

To assess the origin of the silica in the samples, a cross-plot of SiO_2 and Zr can be used as a proxy for biogenic versus detrital sources, under the premise that Zr is transported into a basin rather than sourced from local biological sources (Hall *et al.*, 2013). Figure 13 shows a positive SiO_2 vs. Zr trend suggesting the silica in the Boundary Creek region is of a detrital origin.

LECO-DERIVED SULPHUR AND SEAWATER OXYGENATION

The relationship between C_{org} and total sulphur can be used to evaluate seawater oxygenation. Berner and Raiswell (1983) empirically determined a C_{org} /sulphur relationship of 2.8 and 3.5 for normally oxygenated marine conditions in modern and in Upper Cretaceous time, respectively. Total sulphur (organic + inorganic) values determined by LECO measurements range from 0.27 to 0.58 wt % for the Cuesta Creek (BL-06) samples and from 0.75 to 10.20 wt % for the Boundary Creek (BL-08) samples. The cross-plot of C_{org} versus sulphur (Fig. 14) indicates that the Cuesta Creek samples (BL-06) plot on or adjacent to Berner and Raiswell's (1983)



Figure 12. Bentonite horizon at Boundary Creek type section (Young, 1975; our section BL-08C). View to the north across the creek from the smoking shale location.

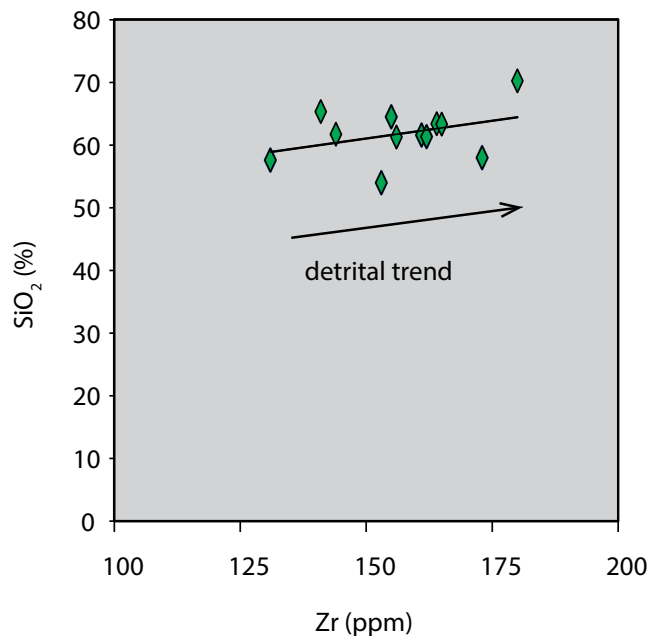


Figure 13. SiO_2 vs. Zr: samples display a positive trend suggestive of a detrital origin for silica in the Boundary Creek Formation samples from section BL-08. Elemental chemistry derived from XRF. Interpretation after Hall *et al.* (2013).

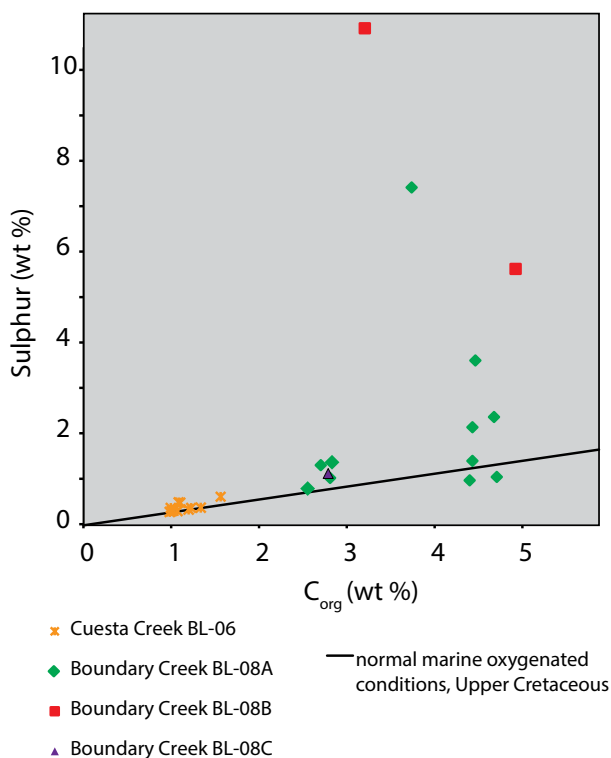


Figure 14. C_{org} vs. sulphur showing variance of Boundary Creek Formation samples around the normally oxygenated marine conditions in Upper Cretaceous time. C_{org} is derived from Rock/Eval and sulphur from LECO analyses. The normal marine line is from Berner and Raiswell (2013).

Upper Cretaceous, normally oxygenated, marine line (C_{org}/S -relation = 3.5). In contrast, Boundary Creek region values show a range from just below the normal line to significantly above, indicating a range of marine oxygenation conditions from normal to depleted.

XRD MINERALOGY

Four bentonite layers from the BL-08A section (YU036, YU037, YU038, YU039) and one from BL-08C (YU041) were analyzed for XRD mineralogy (Fig. 7). All samples are mineralogically similar, composed mainly of illite/montmorillonite-mixed-layer minerals and possibly rectorite (alternating illite/smectite), containing minor amounts of quartz, feldspar, kaolinite, jarosite and gypsum (Appendix B). Trace minerals in some samples include jarosite, quartz, gypsum, feldspar, kaolinite and possibly goethite.

The clay mineralogy of Boundary Creek Formation shale is given in Young (1975; Table 2). Minerals include quartz, feldspar, illite, chlorite, gypsum, montmorillonite (2 samples indicating the presence of bentonites), pyrite, dolomite and siderite, in order of abundance.

PETROLEUM POTENTIAL

Petroleum potential including quantity, maturity and type of organic matter were assessed by RockEval/TOC pyrolysis techniques which provide measured values of S1, S2, S3, TOC, Tmax and derived values of HI (hydrogen index), OI (oxygen index) and PI (production index). The method consists of the programmed-temperature heating (25°C/minute up to 600°C) of a small sample of rock to quantitatively determine: i) the free and adsorbed hydrocarbons (gas and oil) contained in the rock samples (S1); ii) the hydrocarbon-bearing compounds that are expelled from the rock during the cracking of kerogen (S2); and iii) the oxygen-bearing compounds (CO_2) that are expelled from the rock during the cracking of kerogen (S3; after Espitalié *et al.*, 1977; Figure 15). Tmax is the oven temperature when the S2 peak is achieved and corresponds to the temperature at which thermal cracking of kerogen releases the largest amount of hydrocarbons. TOC is determined by adding the organic carbon content remaining in the sample after pyrolysis (residual organic carbon) to the organic carbon content determined during pyrolysis. Derived values from RockEval pyrolysis include HI ($S2/\text{TOC} \times 100$) which is a proxy for determining the H/C atomic ratio in a sample and expresses the “useable” fraction of organic content in a sample; OI ($S3/\text{TOC} \times 100$) which is a proxy for determining the O/H atomic ratio in

Table 2. Comparison of Boundary Creek and Smoking Hills formation characteristics compiled from Dixon (1992, 2004), Dixon et al. (1992), Mathews and Bustin (1984), Young (1975), Saison (2010) and this study.

	Boundary Creek Formation on Boundary Creek	Smoking Hills Formation, Smoking Hills, NWT
age	Cenomanian/Turonian	Santonian/Campanian
depositional environment	outer shelf to slope/basin; probable anoxic intervals	outer shelf to slope/basin; anoxic intervals
lithology	black, organic-rich shale with mm to m thick bentonite horizons and concretions	black, organic-rich shale with mm to m thick bentonite horizons and concretions
mineralogy	illite, chlorite, montomorrillonite; minor feldspar, quartz, pyrite, dolomite, siderite, gypsum	smectite; minor mica (muscovite), quartz, pyrite, gypsum/bassanite, jarosite
	unburned, fresh and/or weathered samples (this study)	unburned, fresh and/or weathered samples (Mathews and Bustin, 1984)
LOI (%)	10.2-14.5	14.5-43.8
Fe₂O₃ or Fe (%)	0.97-13.11 (Fe ₂ O ₃)	5.0-14.2 (Fe)
SiO₂ (%)	50.4-66.6	30.3-56.7
Al₂O₃ (%)	14.3-18.8	8.3-14.4
TOC (wt %)	2.5-4.6	4-6
S1 mg HC/g rock	0.19-1.72	0.16-2.28
S2 mg HC/g rock	1.54-8.61	1.14-25.64
S3 mg HC/g rock	0.01-0.31	0.15-4.40
Tmax (°C)	427-449	429-443
PI	0.04-0.22	0.04-0.08
HI	57-209	92-474
OI	0-12	3-192
VR (%Ro)	1.12-1.16 (oil window)	<0.7 (immature to early oil window)

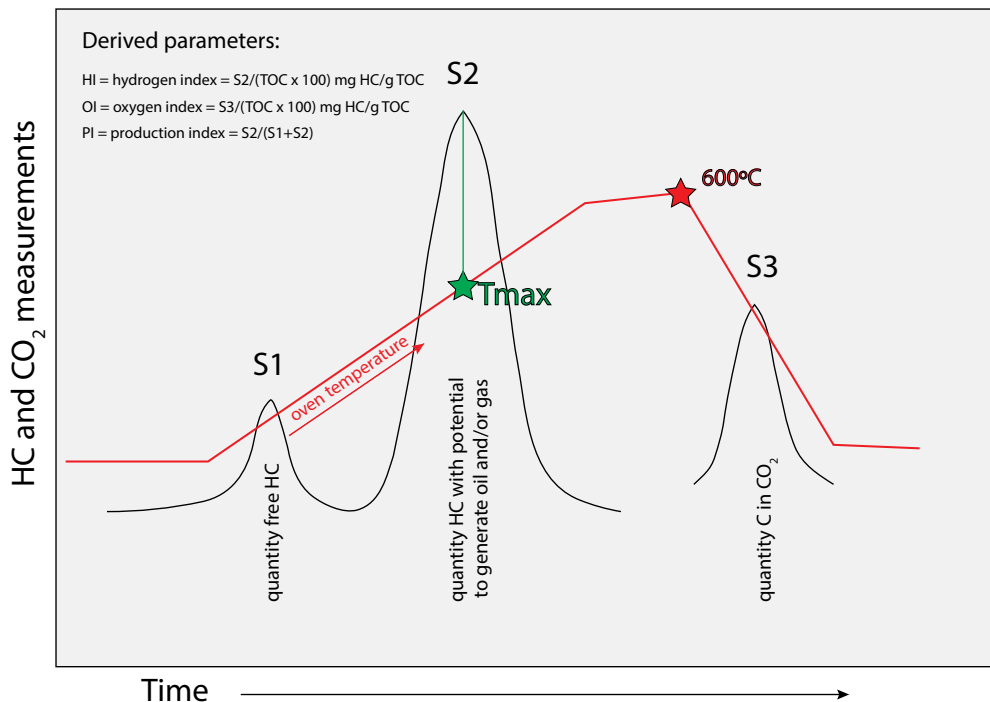


Figure 15. Schematic RockEval plot displaying the type of result that can be obtained from pyrolysis or programmed-temperature heating of a shale sample. S1 and S2 peaks are measured in mg hydrocarbons (HC) per g rock. S3 peak is measured in mg CO₂ per g rock. Tmax in degrees Celcius (°C). Derived values include hydrogen and oxygen indices (HI and OI respectively, measured in mg HC/g TOC) and the production index (PI). Description of parameters is after Espitalié et al. (1977) and is summarized in the text.

a sample and corresponds to the quantity of CO₂ relative to TOC; and PI (S1/S1+S2) which is the proportion of free hydrocarbons in a sample in relation to the total amount of hydrocarbons obtained during pyrolysis. An HI vs. OI crossplot (pseudo van Krevelen diagram) can be used to determine the type of organic matter in a sample (Types I, II, III and IV) which correspond to types of hydrocarbons expected to be generated (oil, oil, gas and none, respectively) under ideal thermal conditions (Espitalié *et al.*, 1977).

Vitrinite reflectance was also used to determine thermal maturity of organic matter in shale. The following petroleum potential interpretations are summarized in Peters (1986) and Peters and Cassa (1994) unless referenced otherwise.

QUANTITY OF ORGANIC MATTER

Rock-Eval/TOC analyses were conducted on 11 Cuesta Creek samples (BL-06) and 15 Boundary Creek area samples (12 BL-08A, 2 BL-08B and 1 BL-08C). Plots depicting organic matter quantity indicators (TOC, S1 and S2) are shown in Figure 16a and tabulated results in Appendix C. The data reveal important differences between the Cuesta Creek and the Boundary Creek samples. Cuesta Creek samples have TOC values ranging from 0.9-1.5% suggesting fair to good petroleum-generating potential. The Boundary Creek area samples have higher TOC values ranging from 2.4-4.6%, all suggestive of very good petroleum-generating potential. S1 and S2 values for Cuesta Creek samples are ≤ 0.18 mg hydrocarbons (HC)/g rock suggesting poor petroleum generative potential. In contrast, S1 and S2 values for Boundary Creek area samples are higher having values of 0.2-1.7 and 1.5-8.6 mg HC/g rock, respectively. These values indicate poor to good generative potential.

MATURITY OF ORGANIC MATTER

Organic maturity can be evaluated using both vitrinite reflectance measurements or indirectly by calculations of Tmax and PI from RockEval/TOC pyrolysis data. However, RockEval-derived Tmax is an unreliable indicator of thermal maturity if S2 values are < 0.2 mg HC/g rock, as in the case of the Cuesta Creek samples.

Plots of organic material thermal maturity indicators are shown in Fig. 16b. For the Boundary Creek samples, Tmax values range from 427-449°C. Using Tmax temperatures

of 435-470°C to delineate the mature stage of thermal maturity for oil or "oil window", the majority of Boundary Creek area samples are mature (80%) and the minority immature (20%). Likewise, 80% of Boundary Creek PI values fall within the oil generation window (0.1-0.4) and 20% are immature (< 0.1). VR values for two Boundary Creek samples had values of 1.12 and 1.16%Ro and are within the late mature stage of thermal maturity for oil.

PI values for Cuesta Creek samples indicate immature organic matter in shale samples whereas VR are 1.65 and 2.00%Ro, which indicate a post-mature stage of thermal maturity for oil.

TYPE OF ORGANIC MATTER

Plots of organic matter type indicators are shown in Figure 16c. Interpretation of HI and S2/S3 values indicate that Cuesta Creek samples contain Type IV kerogen (inert) and would not expel any hydrocarbons at peak maturity. HI values for the Boundary Creek area samples indicate mainly Type III and lesser Type II/III kerogen, which would expel gas and mixed oil and gas respectively, at peak maturity. S2/S3 values indicate mostly Type II kerogen with lesser Types II and II/III, indicating they are prone to expulsion of mixed oil and gas and oil products at peak maturity.

A pseudo-Van Krevelen Plot (Espitalié *et al.*, 1977) displays the Cuesta Creek samples along the HI-axis indicating they are Type IV (inert). Boundary Creek area samples plot along the Type I and Type II curves, both of which are oil-prone.

BURNING SHALE

TERMINOLOGY

Actively burning or combusting shale exposures are sometimes referred to as "bocannes" after Selwyn (1877, in Crickmay, 1967) who first used the term for smoking outcrops on the Smoky River, Alberta. Crickmay (1967) suggests that the term derives from "boucanes", French-Canadian for clouds of smoke. Active bocannes are characterized by fumes or smoke of hot, sulfurous gas, high ground temperatures and red, bleached or fused shale (Mathews and Bustin, 1984). Extinct bocannes are marked by discoloured and/or fused shale (klinker) and do not release gas.

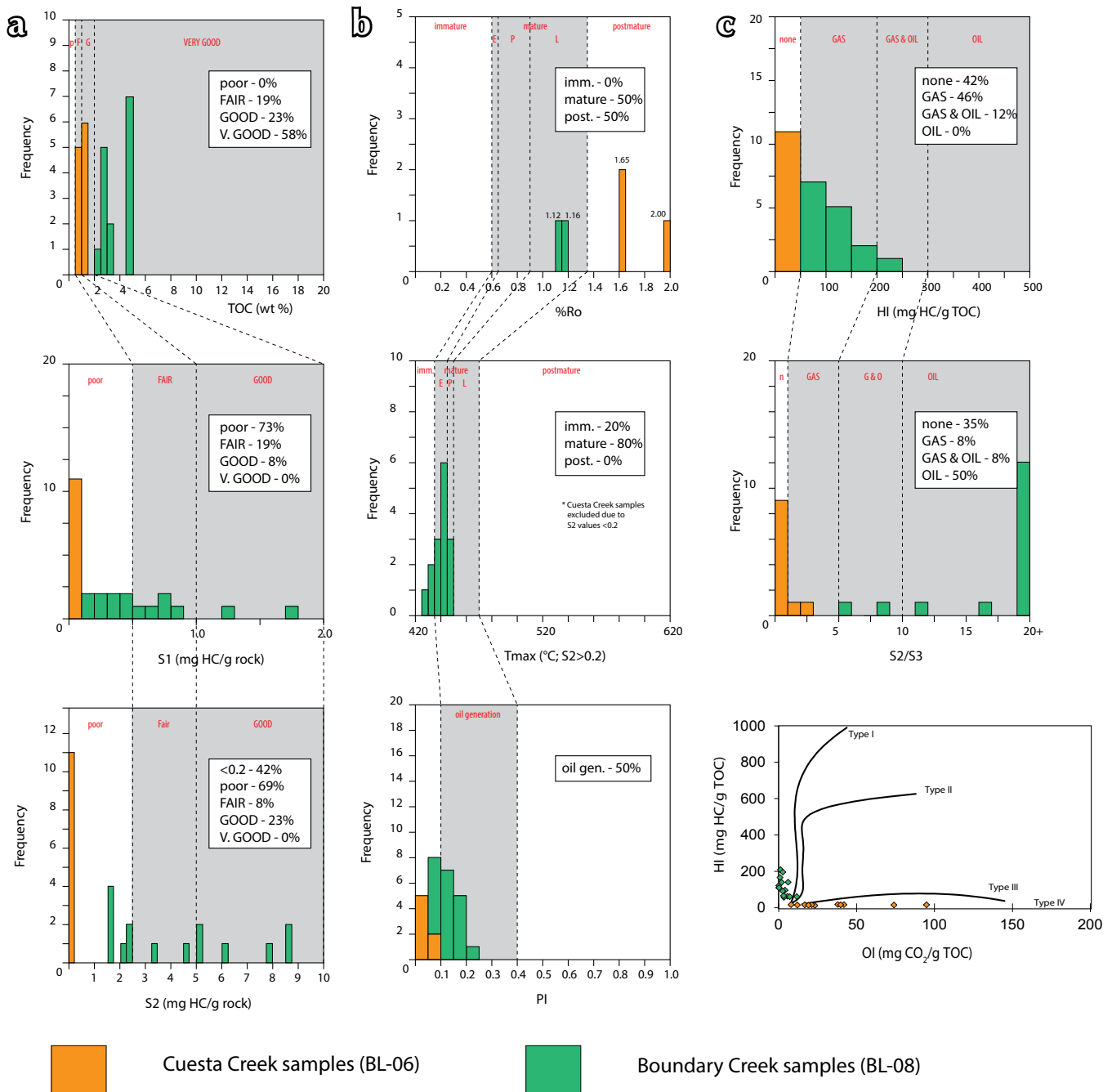


Figure 16. (a) Rock-Eval-derived indicators of the quantity of organic matter (TOC, S1 and S2); (b) organic matter thermal maturity indicators derived from RockEval (Tmax, PI) and vitrinite reflectance (%Ro); (c) rock-Eval-derived kerogen type and interpreted generated petroleum (HI, S2/S3 and HI vs. OI or pseudo van Krevelen plot).

Pyrometamorphism is a rock-modifying process that occurs at ultra-high temperatures (>1000°C) and low pressures (1 kbar) and often results in fusion of near-surface sediments (Cosca *et al.*, 1989). Pyrometamorphism is sometimes referred to as combustion metamorphism.

Pyrometamorphic rocks are commonly associated with near-surface basaltic intrusions; however, they are also associated with combusted bituminous sedimentary rocks and coal beds. The latter have been referred to as 'fire-baked rocks' (e.g., Mathews and Bustin, 1984).

OCCURRENCES

Smoking shale or evidence of previous shale burns is not uncommon in northern Canada or Alaska, nor is it a recent phenomenon. Franklin and Richardson observed smoking shale exposures on the Arctic Coast of present-day NWT during their 1825-27 expedition (Richardson, 1851), as did McConnell (1891) near the confluence of the Bear and Mackenzie rivers during his field exploration of northern Yukon and the Mackenzie basins in 1888-89. The former location is now referred to as the 'Smoking Hills' where Upper Cretaceous shale of the Smoking Hills Formation is burning today, 190 years after it was first reported.

Upper Paleozoic organic-rich shales show evidence of pyrometamorphism along the Dempster Highway (inactive; Devonian Canol Formation; Fraser and Hutchison, 2014), in the southern Richardson Mountains (active and inactive; Devonian-Mississippian Ford Lake Shale Formation and Mississippian Hart River Formation; Allen *et al.*, in press), in Kandik Basin, and in eastern Yukon (inactive; Ford Lake Shale Formation; first author observation in summer 2014). An active bocanne is currently burning Ford Lake Shale Formation shale in Kandik Basin, western Alaska, ~10 km from the Yukon border, that has been referred to as the "Yukon-Charley volcano" after the national preserve in which it resides (Rozell, 2014).

As part of the 2013 expedition on Yukon's North Slope, evidence for pyrometamorphosed shale was observed in several outcrops of the Tertiary Reindeer Formation. At these locations, intercalated coal seams appear to be the fuel source contributing to temperatures that were high enough to melt adjacent rocks to paralava (Fig. 17).



Figure 17. Pyrometamorphosed shale (klinker) in the Tertiary Moose Channel Formation, North Slope, Yukon.

2013 LOCATION AND SITE DESCRIPTION

The naturally-burning shale exposure was identified by helicopter reconnaissance near the confluence of the Boundary Creek and the Big Fish River at the border between the Yukon and NWT (Figs. 1 and 3). The exposure is marked by a prominent smoke plume above an apron of landslide-induced colluvium (Fig. 18). The smoke plume was previously observed early in 2013 (local Aklavik resident working for the project, *pers. comm.*).

The burning exposure occurs on the south bank of Boundary Creek. At this location, an un-vegetated lobate debris apron occurs below an ~80 m exposure of shale. The apron displays compression structures in its middle and lower parts and has diverted the flow of Boundary Creek (Fig. 19). The head of the landslide is marked by an irregularly shaped cliff that is several metres high, composed of scattered shale blocks that show minimal movement and still carry their original plant cover.



Figure 18. Burning shale location on Boundary Creek immediately upstream from its confluence with the Big Fish River. Note the landslide apron, diversion of Boundary Creek and smoke plume approximately one third of the way down the escarpment. View towards southwest. Helicopter circled for scale.

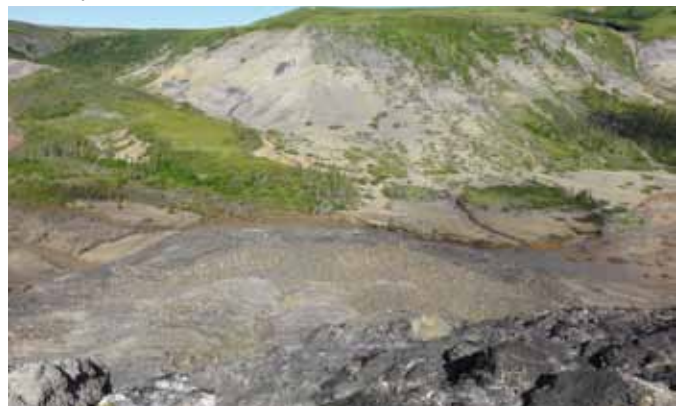


Figure 19. View of the diversion of Boundary Creek from the smoking shale site. Young's (1975) Boundary Creek type section is across the creek. View is northeast.

The debris apron appears to be a quite recent feature as only the outermost part of the apron on the valley floor has been eroded by Boundary Creek and the lobe itself remains un-vegetated. It is probable that it was a result of a landslide during the summer of 2012 (one year earlier; Figs. 18 and 19). Initiation of the landslide was likely triggered by a combination of creek-bank-undercutting by Boundary Creek and permafrost thaw, reducing the stability of the slope. Thawing permafrost is visible throughout the region and locally on the southern creek bank where an active slump has formed, exposing a headwall of melting ice and frozen shale. Combined with creek-undercutting, permafrost-thawing could facilitate a landslide event.



Figure 20. (a) Smoke plumes at the burning shale exposure (BL-08B); (b) Smoke plumes emanating from linear vents at the burning shale exposure (BL-08B).

SMOKE PLUME

The site of the smoke plume was accessed by foot from a helicopter landing site at the top of the creek bank above the burning shale. The smoke occurs in the upper one-third of the landslide debris zone and emanates randomly from discrete vents and cracks on the rubbly surface (Fig. 20a,b). Wind blowing up from the creek bottom significantly fans the combustion process. The wind also helped blow potentially noxious, likely sulphuric (rotten-egg smell) fumes away from the site so that it could be closely examined. No open flames were visible, only grey-white smoke exhausted from cracks and vents. The surface itself was hot but could be touched with bare hands.

The smoke vents are surrounded by slightly 'baked' shales, which have been changed from their original dark grey to black color to a red, orange or tan hue (Fig. 21). No fused rock was found at any of the smoking exposures. Soft white, grey and brown ash-like combustion products are widespread around the actively smoking site and were easily picked up by the wind. Each of the smoking cracks and vents are rimmed with yellow and white crystals (Fig. 22a,b), likely a variety of sulfur minerals.

MECHANISM OF FORMATION

Richardson (1828) attributed the burning shale at the Smoking Hills to the combustion of fine-grained sulphur and bitumen. Referring to extinct bocannes at the Smoky River in Alberta, Dawson (1881) identified very finely divided pyrite and carbonaceous matter in the shale that were sufficient to account for the slow combustion. Mathews and Bustin (1984) offer a modern explanation backed by analytical data, but do recognize the astuteness



Figure 21. Pyrometamorphosed shale at the burning shale exposure (BL-08B).

of these older observations and compliment the early explorers in the conclusions of their paper. Their study identifies the fuel of the smoke and burned shale to be self-sourced. Rapid oxidization of pyrite and high organic material found in the shale can create enough energy to burn, bake and even fuse rocks (pyrometamorphism). Their studies suggest that there could be enough energy in the shale to raise temperatures 2000-5000°C, but 300°C is all that is needed to cause shale discoloration. To initiate instantaneous combustion, they suggest that exposure of fresh rock by landsliding is all that is required, exposing the organic material and pyrite to oxygen. Landslides

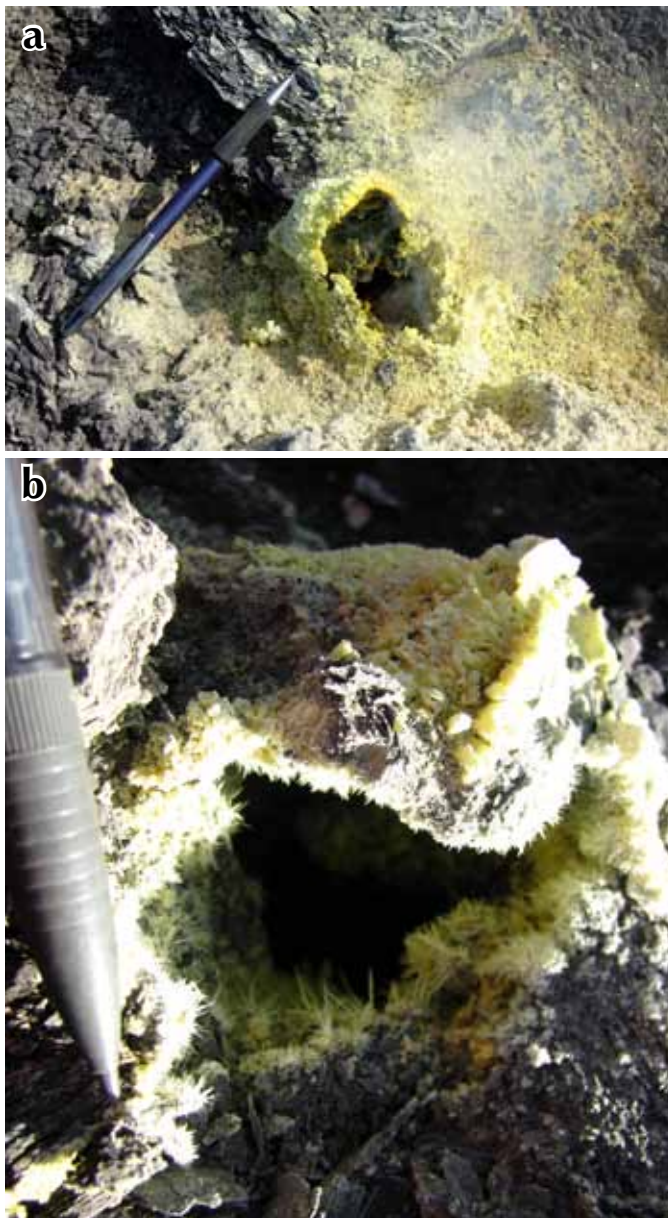


Figure 22. Photos (a) and (b) show smoke vents with sulphurous mineral rims at the burning shale exposure (BL-08B).

are a common phenomenon in northern Canada where permafrost or ice-rich surficial deposits are thawing. Following combustion and burning, the residual materials left in place depends on temperatures reached and include white/grey ash, red and white/grey rock, paralava and klinker.

Although slightly different in age, the smoking shale on Boundary Creek is in many ways similar to the shale of the Smoking Hills Formation (Table 2) and the mechanism of formation is inferred to be the same. Both formations are lithologically and mineralogically similar and interpreted to be deposited in similar outer shelf to slope depositional settings. Both formations contain pyrite (see Young, 1975 for Boundary Creek Formation) and organic material. Landslides are present at both locations and are the likely trigger for combustion. One difference is that the temperature of the shales appears to be lower in the Boundary Creek shale as no evidence for pyrometamorphism was observed as in the Smoking Hills area. This may be due to the longer duration of burning at Smoking Hills or variations in local organic content, but these are speculations at this time.

DISCUSSION

DEPOSITIONAL SETTING FOR THE BOUNDARY CREEK FORMATION

Lithology and sedimentology of the Boundary Creek Formation exposures examined for this study suggest an outer shelf to slope depositional environment. The cyclical nature of the fine-grained sedimentation and the presence of detrital SiO_2 and Al_2O_3 suggest a steady supply of fine-grained clastic sediment, likely transported by turbidity currents outboard of the Cordilleran orogeny. This study, however, was restricted in scope. To establish a depositional framework and paleogeographic setting, more work and research is necessary to confirm such an interpretation.

COMPARISON OF BOUNDARY CREEK FORMATION MEASURED SECTIONS (BL-06 AND BL-08A)

The Boundary Creek Formation was observed in two areas where it was mapped by Norris (1981b). Despite similarities in interpreted depositional environments, the geology of the two areas is remarkably different. The Boundary Creek location (BL-08A) has an abundance of bentonite horizons, has very good oil to mixed oil/

gas generating potential and is marked by an abundance of gypsum concretions, some of them exceeding 2 m in diameter. In contrast, the Cuesta Creek exposure (BL-06) lacks bentonite horizons, has a lower petroleum potential and consequent petroleum-generating capability, is thermally overmature ($\%Ro \geq 1.65$) and has only minor carbonate concretions.

More information is required in order to fully understand the differences between the two sites. A simple explanation, however, is that the sections are not coeval and do not share a thermal or depositional history. For example, the Cuesta Creek sediments could be older than in the Boundary Creek area, with their overmaturity due to a deeper depth of burial. Cuesta Creek samples may have been deposited in a more proximal setting, which could explain the siltier nature of the sediments and lower TOC values, as organic material is better preserved in quiescent environments. A deeper environment for the Boundary Creek area sediments is indicated by the preservation of tephra, the higher TOC values and the finer grain size of these exposures. In addition, the BL-08B section has elevated enrichment factors of V and Ni demonstrating that paleo-oceanographic oxygen conditions vary within the formation. The enrichment factor for Mo combined with C_{org} vs. S plots suggest that anoxic conditions were attained at least for some of the Boundary Creek samples, particularly adjacent to the smoking shale site (BL-08B) and the upper part of the measured section (BL-08A). Age determinations, geochemical analysis and mapping would be required to establish how each isolated section relates to the others.

PETROLEUM POTENTIAL OF THE BOUNDARY CREEK FORMATION

The petroleum potential of the Boundary Creek Formation has been evaluated from wells in the Mackenzie Delta and southern Tuktoyaktuk Peninsula (Bruce and Parker, 1975; Snowdon, 1980; Creaney, 1980); however, until now it has not previously been evaluated in Yukon. In NWT, subsurface Boundary Creek shale is immature with respect to oil generation (Creaney, 1980). In contrast, our study shows that at least part of the Boundary Creek Formation is optimally mature for oil generation in Yukon. The shales observed in the vicinity of the Boundary Creek type section in Yukon have good to very good petroleum potential and are oil to mixed oil and gas prone. The burning shale exposure nearby is also evidence for a

hydrocarbon fuel source in this formation. In the Cuesta Creek area, the petroleum potential is poor, likely due to overmaturity. Whether optimal maturity exists in the Yukon subsurface is unknown at this time.

Saison (2010) studied the petroleum genetic potential within the Smoking Hills Formation in the Mackenzie Delta and found that it varies widely from one sample to another and even between adjacent layers from excellent to no potential. Given that the Boundary Creek Formation is similar to the Smoking Hills Formation, the comparison is instructive. Saison (2010) attributes this variation in petroleum potential to changing environmental conditions in regions of low sedimentation rates, where bottom current speeds and redox conditions can selectively sort, transport and preserve organic material on one hand, and episodic marine and/or fresh water incursions may flush them out on the other. This situation leads to vertical and horizontal variations in organic material preservation in the rock record.

Other environmental factors also influence the deposition and preservation of organic matter. Sea-level changes could influence oxygen availability and the influx of terrestrial material; a high terrestrial input dilutes the concentration of organic material. Volcanic ashfall is also a consideration, as regular inputs could influence seawater chemistry; dissolved O_2 can be consumed by silicate-bound Fe^{2+} in tephra which could lead to enhanced preservation of organic material in marine sediments (Hembury *et al.*, 2012). Detailed sampling and facies mapping of the formation would provide better insight into petroleum "sweet" spots, how they vary in time and space and the factors controlling their variability.

BURNING SHALE

To our knowledge, the exposure of burning shale described in this study is the only shale fire reported in the Upper Cretaceous Boundary Creek Formation. The characteristics of the shale, combined with the recent landslide event suggest the smoking shale site formed similarly to the Smoking Hills site in NWT, as described by Mathews and Bustin (1984), involving the rapid oxidization of pyrite and organic matter. Young (1975) documented pyrite in Boundary Creek shale samples from XRD mineralogy in the region. We have not observed pyrite in fresh shale samples from the site but suspect its presence as weathering products of pyrite including gypsum ($CaSO_4 \cdot 2H_2O$), iron oxide (Fe_2O_3), and jarosite

($\text{KFe}^{3+}_3(\text{OH})_6(\text{SO}_4)_2$) all are all present (e.g., Pye and Miller, 1990). RockEval-derived S values from samples in fresh outcrop near the burn site are 5-10% indicating that the rock was enriched in sulfide (pyrite) or sulphate (pyrite weathering products). Furthermore, organic material is in good supply having values averaging 3.5% in the Boundary Creek area. Spontaneous shale combustion would therefore only require oxygen; landsliding provides a mechanism for the rapid exposure of fresh rock to oxygen and is a common event in permafrost regions.

One might speculate that recent warmer mean summer temperatures may have been responsible for the landslide that initiated the combustion process. However, heat released by oxidation of organic matter and pyrite alone appears to be sufficient, as is shown by an example of naturally burning coal scree at the rim of the Prince of Wales ice field in colder climatic conditions on southern Ellesmere Island (Reinhardt *et al.*, 2013). That being said, global warming may lead to more landslides in areas of melting permafrost which may lead to more burning shale sites.

TEPHRA STUDIES

Upper Cretaceous (Cenomanian–Turonian) strata in north Yukon record an active history of volcanism in the form of cyclical tephra horizons in marine shale. More detailed analyses of the bentonite layers are underway including additional XRF, ICP-MS litho-geochemistry and scanning electron microscopy (SEM). These data will provide a geochemical fingerprint to compare with candidate volcanic source areas and help determine the suitability of individual tephra layers for radiometric age dating.

CONCLUSION AND FUTURE WORK

The Boundary Creek Formation on Yukon's North Slope is an Upper Cretaceous mudstone, shale and silty shale deposited by turbidity currents along an outer shelf to slope environment in the distal part of the foreland basin, outboard of the Cordilleran orogeny forming to the south. At times throughout its deposition, ocean water may have been depleted in oxygen, resulting in anoxic conditions that would have been favourable for organic matter preservation. The results of analyses of surface samples suggest that some areas have poor to no petroleum potential and are thermally overmature with

respect to oil generation. In others, good to very good petroleum potential exists because the shale is oil to oil and gas prone and thermally mature with respect to oil generation. In these latter areas, specifically in the vicinity of the type section on Boundary Creek, the shale has the necessary ingredients for spontaneous combustion: pyrite, organic matter and a fresh supply of oxygen provided by a landslide. Although burning shale is not unknown in northern Canada, the outcrop of burning shale on Yukon's North Slope is the first observed in shale of the Upper Cretaceous Boundary Creek Formation.

In light of the reconnaissance nature of this study, some recommendations to expand this research to improve the understanding of Upper Cretaceous stratigraphy in North Yukon include:

- detailed correlation of the Boundary Creek Formation in the subsurface, from Yukon to NWT, to determine its regional distribution;
- evaluation of the Boundary Creek Formation as a subsurface petroleum source rock in Yukon;
- mapping of thermal maturity parameters to assist with an understanding of the Upper Cretaceous thermal maturation history in the region;
- refining the shale stratigraphy and bedrock mapping on the north coast; and
- dating and typing thicker bentonite layers and linking these to the regional tectonic story.

ACKNOWLEDGEMENTS

Thank you to Georg Scheeder and Jolanta Kus from BGR's sub-department "Resource Geochemistry" for handling of the geochemical and microscopic analyses. Review by Don Murphy, Yukon Geological Survey is greatly appreciated. Tammy Allen is acknowledged and thanked for field support. Olwyn Bruce is a GIS-wizard. Field work during 2013 on the Yukon North Slope was completed as part of the CASE 15 expedition of the Federal Institute for Geosciences and Natural Resources (BGR, Hannover, Germany) led by M. Colpron (YGS, Whitehorse, Canada) and K. Piepjohn (BGR, Hannover, Germany) and co-funded by the BGR, YGS and Université Pierre et Marie Curie (Paris, France).

REFERENCES

- Allen, T.L., Fraser, T.A., Hutchison, M.P., Dolby, G., Reyes, J. and Utting, J., *in press*. Stratigraphy, age, and petroleum potential of Upper Devonian black shale (unit 'Cf'), east Richardson Mountains and Peel Plateau, Yukon. Yukon Geological Survey, Open File with Appendices.
- ASTM D7708-11. Standard Test Method for Microscopical Determination of the Reflectance of Vitrinite Dispersed in Sedimentary Rocks, ASTM International, West Conshohocken, PA, 2011, www.astm.org.
- Berner, R.A. and Raiswell, R., 1983. Burial of organic carbon and pyrite sulfur in sediments over phanerozoic time: a new theory. *Geochimica et Cosmochimica Acta*, vol. 47, p. 855-862.
- Bruce, C.J. and Parker, E.R., 1975. Structural Features and Hydrocarbon Deposits in the Mackenzie Delta. *In: Proceedings of the Ninth World Petroleum Congress Tokyo, 1975, Volume 2: Geology, Applied Science Publishers Ltd.*, p. 251-261.
- Crickmay, C.H., 1967. A note on the term bocanne. *American Journal of Science*, vol. 265, p. 626-627.
- Cosca, M.A., Essene, E.J., Geissman, J.W., Simmons, W.B. and Coates, D.A., 1989. Pyrometamorphic rocks associated with naturally burned coal beds, Powder River Basin, Wyoming. *American Mineralogist*, vol. 744, p. 85-100.
- Creaney, S., 1980. The Organic Petrology of the Upper Cretaceous Boundary Creek Formation, Beaufort-Mackenzie Basin. *Bulletin of Canadian Petroleum Geology*, vol. 28, p. 112-129.
- Dawson, G.M., 1881. Report on the exploration of Fort Simpson on the Pacific coast to Edmonton on the Saskatchewan, embracing a portion of the northern part of British Columbia and the Peace River country, 1879. Geological Survey of Canada, Report of Progress, 1879-1880, Part B.
- DIN 22020-5, 2005. Rohstoffuntersuchungen im Steinkohlenbergbau - Mikroskopische Untersuchungen an Steinkohle, Koks und Briketts - Teil 5: Reflexionsmessungen an Vitriniten (Investigations of the raw material in hard-coal-mining - Microscopical examinations of hard coal, coke and briquettes - Part 5: Reflectance measurements on vitrinites). DIN 22020-5:2005-02, DIN Deutsches Institut für Normung e. V.
- DIN 51418 (Teile 1 und 2), 2008. Röntgenspektralanalyse - Röntgenemissions- und Röntgenfluoreszenz-Analyse (RFA) - Teil 1: Allgemeine Begriffe und Grundlagen.
- Röntgenspektralanalyse - Röntgenemissions- und Röntgenfluoreszenz-Analyse (RFA) - Teil 2: Begriffe und Grundlagen zur Messung, Kalibrierung und Auswertung, DIN 51418 (Teile 1 und 2), DIN Deutsches Institut für Normung e. V.
- Dixon, J., 1992. A review of Cretaceous and Tertiary stratigraphy in the northern Yukon and adjacent Northwest Territories. Geological Survey of Canada, Paper 92-2, 79 p.
- Dixon, J., 1997. Cretaceous and Tertiary. *In: The Geology, Mineral and Hydrocarbon potential of Northern Yukon Territory and Northwestern District of Mackenzie*, Geological Survey of Canada, Bulletin 422, p. 301-317.
- Dixon, J., 2004. Lower Cretaceous (Albian) to Tertiary strata, Yukon Territory - Northwest Territories (a contribution to the geological atlas of the Northern Canadian Mainland sedimentary basin). Geological Survey of Canada, Open File 4633, 45 p.
- Dixon, J., Dietrich, J.R., McNeil, D.H., McIntyre, D.J., Snowdon, L.R. and Brooks, P., 1985. Geology, biostratigraphy and organic geochemistry of Jurassic to Pleistocene strata, Beaufort-Mackenzie area, northwest Canada. Canadian Society of Petroleum Geologists Course Notes, 65 p.
- Dixon, J., 1996 (editor). Geological Atlas of the Beaufort-Mackenzie Area. Geological Survey of Canada, Miscellaneous Report 59, 173 p.
- Espitalié, J., Laporte, J.L., Madec, M., Marquis, F., Leplat, P., Paulet, J. and Boutefeu, A., 1977. Méthode rapide de caractérisation des roches mères, de leur potentiel pétrolier et de leur degré d'évolution. *Oil and Gas Science and Technology - Revue de l'Institut Français du Pétrole*, vol. 32, p. 23-42.
- Fraser, T.A. and Hogue, B., 2007. List of Wells and Formation Tops, Yukon Territory, version 1.0. Yukon Geological Survey, YGS Open File 2007-05, 1 p. plus spreadsheet.
- Fraser, T.A. and Hutchison, M., 2014. Petroleum potential of the Middle-Upper Devonian Canol Formation in north Yukon: report on field investigations in 2013. Canadian Society of Petroleum Geologists Annual Convention, May, 2014, Abstract.

- Geoscout, 2014. Northern Canada well database, current to 2014/08/12. Proprietary software of Geologic Systems Ltd., accessed on December 12, 2014 through purchased licensing arrangement.
- Hall, D., Sterner, M. and Shukla, R., 2013. Application of cuttings gas/oil analysis, rapid XRF and high-resolution photography to reservoir evaluation. *World Oil*, April 2013 issue, p. 163-168.
- Haq, B.U. and Schutter, S.R., 2008. A chronology of Paleozoic sea-level changes. *Science*, vol. 322, p. 64-68.
- Hembury, D.J., Palmer, M.R., Fones, G.R., Mills, R.A., Marsh, R. and Jones, M.T., 2012. Uptake of dissolved oxygen during marine diagenesis of fresh volcanic material. *Geochimica et Cosmochimica Acta*, vol. 84, p. 353-368.
- International Commission on Stratigraphy, 2014. International Chronostratigraphic Chart v2014/10. <http://www.stratigraphy.org/index.php/ics-chart-timescale>, accessed on December 12, 2014.
- Mathews, W.H. and Bustin, R.M., 1984. Why do the Smoking Hills smoke? *Canadian Journal of Earth Sciences*, vol. 21, p. 737-742.
- McConnell, R.G., 1891. Report on an exploration in the Yukon and Mackenzie Basins, N.W.T. Geological Survey of Canada, Annual Report 1888-89, vol. 4, p. 1D-163D.
- Norris, D.K., 1981a. Geology, Herschel Island and Demarcation Point, Yukon Territory. Geological Survey of Canada, "A" Series Map 1514A, 1 sheet.
- Norris, D.K., 1981b. Geology, Blow River and Davidson Mountains, Yukon Territory-District of Mackenzie. Geological Survey of Canada, "A" Series Map 1516A, 1 sheet.
- Norris, D.K., 1981c. Geology, Aklavik, District of Mackenzie. Survey of Canada, "A" Series Map 1517A, 1 sheet.
- Peters, K.E., 1986. Guidelines for Evaluating Petroleum Source Rock Using Programmed Pyrolysis. *American Association of Petroleum Geologists Bulletin*, vol. 70, p. 318-329.
- Peters, K.E. and Cassa, M.R., 1994. Applied source-rock geochemistry. *In: The Petroleum System - From Source to Trap*, L.B. Magoon and W.G. Dow (eds.), American Association of Petroleum Geologists Memoir 60, p. 93-120.
- Pigage, L., 2007. Yukon Stratigraphic Correlation Chart, version 3.0. Yukon Geological Survey and Oil and Gas Management Branch, Yukon Geological Survey, Open File 2007-2.
- Pye, K. and Miller, J.A., 1990. Chemical and biochemical weathering of pyritic mudrocks in a shale embankment. *Quarterly Journal of Engineering Geology and Hydrogeology*, vol. 23, p. 365-382.
- Reinhardt, L., Andruleit, H. and Rippington, S., 2013. Coal scree found burning in August 2011 on southern Ellesmere Island (Nunavut, Arctic Canada). *In: 25. Internationale Polartagung, Changing Polar Regions, Hamburg, 17.-22. März 2013, Berichte zur Polar- und Meeresforschung / Reports on Polar and Marine Research*, Pfeiffer, E.-M. et al. (eds.). Bremerhaven, Alfred-Wegener-Institut, German Society for Polar Research, vol. 659, p. 136.
- Richardson, J., 1828. Narrative of the eastern detachment of the expedition. *In Narrative of a second expedition to the shores of the polar sea in the years 1825, 1826, 1827*. Edited by J. Franklin. Greenwood Press, New York. P. 187-283.
- Richardson, J.S., 1851. Arctic Searching Expedition: a journal of a boat-voyage through Rupert's Land and the Arctic Sea, in search of the discovery of ships under the command of Sir John Franklin, Vol. II. Longman, Green and Longmans, London.
- Rozell, N., 2014. Fire on the mountain near the Yukon River. *Alaska Science Forum*, Article #2241, Geophysical Institute, University of Alaska, Fairbanks. October 9, 2014. <http://www.gi.alaska.edu/AlaskaScienceForum/article/fire-mountain-near-yukon-river>, accessed December, 12, 2014.
- Saison, A., 2010. Petroleum Potential of Cretaceous and Tertiary sediments of the Mackenzie Delta (Canada). Influence of organic facies variations and gas system. PhD Thesis, Technische Universität Berlin, 167 p.
- Selwyn, A.R.C., 1877. Report on exploration in British Columbia. Geological Survey of Canada, Report of Progress 1875-1876, p. 28-86.
- Snowdon, L.R., 1980. Petroleum Source Potential of the Boundary Creek Formation, Beaufort-Mackenzie Basin. *Bulletin of Canadian Petroleum Geology*, vol. 28, p. 46-58.

Tribovillard, N., Algeo, T.J., Lyons, T. and Riboulleau, A., 2006. Trace metals as paleoredox and paleoproductivity proxies: An update. *Chemical Geology*, vol. 232, p. 12-32.

Young, F.G., 1975. Upper Cretaceous stratigraphy, Yukon coastal plain and northwestern Mackenzie Delta: Geological Survey of Canada, Bulletin 249, 83 p.

Young, F.G., 1977. The Mid-Cretaceous flysch and phosphatic ironstone sequence, northern Richardson Mountains, Yukon. Geological Survey of Canada, Report of Activities Part C, Paper no. 77-1C, p. 67-74.

APPENDIX A: XRF lithochemistry data

Sample #	Sample ID	Measured Section (m)	Location	UTM E	UTM N	Comments
TF-13-BL-08A	TF-13-BL-08A 0	100	Tributary of Boundary Creek	438854	7600461	measured section
TF-13-BL-08A	TF-13-BL-08A 10	90	Tributary of Boundary Creek	438845	7600455	measured section
TF-13-BL-08A	TF-13-BL-08A 20	80	Tributary of Boundary Creek	438835	7600462	measured section
TF-13-BL-08A	TF-13-BL-08A 25	75	Tributary of Boundary Creek			measured section
TF-13-BL-08A	TF-13-BL-08A 30	70	Tributary of Boundary Creek	438821	7600461	measured section
TF-13-BL-08A	TF-13-BL-08A 40	60	Tributary of Boundary Creek	438806	7600458	measured section
TF-13-BL-08A	TF-13-BL-08A 50	50	Tributary of Boundary Creek	438795	7600436	measured section
TF-13-BL-08A	TF-13-BL-08A 60	40	Tributary of Boundary Creek	438786	7600438	measured section
TF-13-BL-08A	TF-13-BL-08A 70	30	Tributary of Boundary Creek	438777	7600437	measured section
TF-13-BL-08A	TF-13-BL-08A 80	20	Tributary of Boundary Creek	438768	7600424	measured section
TF-13-BL-08A	TF-13-BL-08A 90	10	Tributary of Boundary Creek	438765	7600422	measured section
TF-13-BL-08A	TF-13-BL-08A 100	0	Tributary of Boundary Creek	438747	7600419	measured section
TF-13-BL-08B	TF-13-BL-08B shale 1	n/a	Confluence Boundary Ck and Big Fish R.	439809	7599167	burning shale section
TF-13-BL-08B	TF-13-BL-08B shale 2	n/a	Confluence Boundary Ck and Big Fish R.	439809	7599167	burning shale section
TF-13-BL-08C	TF-13-BL-08C	n/a	Confluence Boundary Ck and Big Fish R.	439749	7599615	near thick tephra

UTM NAD 83, zone 8

Sample ID	Sum_RF (%)	LOI (%)	SiO ₂ (%)	Al ₂ O ₃ (%)	Fe ₂ O ₃ (%)	CaO (%)	K ₂ O (%)	MnO (%)	MgO (%)	Na ₂ O (%)	P ₂ O ₅ (%)
TF-13-BL-08A 0	99.61	10.2	61.57	18.19	2.72	0.34	3.703	0.003	0.96	0.69	0.075
TF-13-BL-08A 10	99.64	10.34	61.27	18.55	2.88	0.147	3.716	0.004	0.99	0.62	0.079
TF-13-BL-08A 20	99.64	14.45	53.94	16.72	8.23	0.279	3.389	0.027	0.87	0.62	0.054
TF-13-BL-08A 25	99.62	12.54	57.94	17.44	5.5	0.025	3.428	0.013	1.13	0.7	0.065
TF-13-BL-08A 30	99.66	9.19	63.38	18.77	1.65	0.082	3.857	0.004	0.96	0.74	0.056
TF-13-BL-08A 40	99.63	11.21	63.28	17.61	1.32	0.023	3.647	0.004	0.9	0.79	0.052
TF-13-BL-08A 50	99.67	7.88	70.23	14.28	1.67	0.134	2.859	0.003	0.91	0.92	0.049
TF-13-BL-08A 60	99.67	12.34	61.31	16.29	3.1	0.38	3.247	0.003	0.97	0.97	0.075
TF-13-BL-08A 70	99.71	11.26	64.49	15.44	2.46	0.143	3.09	0.009	0.97	0.93	0.048
TF-13-BL-08A 80	99.67	10.16	65.3	16.62	1.01	0.313	3.382	0.002	0.96	0.94	0.04
TF-13-BL-08A 90	99.68	13.05	57.6	17.13	0.97	2.589	3.545	0.003	0.97	0.81	0.039
TF-13-BL-08A 100	99.66	10.2	61.68	16.65	2.95	0.899	3.592	0.004	1.01	1.02	0.066
TF-13-BL-08B shale 1	99.64	14.06	50.44	15.47	13.11	0.273	3.062	0.155	1.27	0.66	0.217
TF-13-BL-08B shale 2	99.64	13.9	55.86	15.35	7.92	0.374	2.9	0.038	1.27	0.86	0.279
TF-13-BL-08C	99.69	9.12	66.57	16.48	1.39	0.079	3.205	0.007	1.02	0.95	0.057

Sample ID	TiO ₂ (%)	Cl (%)	F (%)	SO ₃ (%)	As ppm	Ba ppm	Bi ppm	Ce ppm	Co ppm	Cr ppm	Cs ppm	Cu ppm
TF-13-BL-08A 0	0.849	0.004	<0,05	0.29	51	1429	<6	85	<7	124	<66	14
TF-13-BL-08A 10	0.876	0.002	<0,05	0.13	26	1370	<6	70	<7	127	<66	22
TF-13-BL-08A 20	0.791	<0,002	<0,05	0.26	32	1249	<7	63	11	109	<65	89
TF-13-BL-08A 25	0.736	0.003	<0,05	0.1	36	1358	<6	83	16	119	<65	58
TF-13-BL-08A 30	0.861	<0,002	<0,05	0.07	21	1282	<6	86	<7	122	<66	22
TF-13-BL-08A 40	0.787	0.003	<0,05	0.03	14	1394	<6	68	<7	103	<65	20
TF-13-BL-08A 50	0.661	0.003	<0,05	0.1	15	1206	<6	63	<7	92	<66	11
TF-13-BL-08A 60	0.731	<0,002	<0,05	0.24	17	1230	<6	90	<7	102	<65	21
TF-13-BL-08A 70	0.741	<0,002	<0,05	0.1	12	1117	<6	<50	<7	101	<65	26
TF-13-BL-08A 80	0.77	<0,002	<0,05	0.17	10	1248	<6	66	<7	106	<65	18
TF-13-BL-08A 90	0.718	<0,002	<0,05	2.23	8	1302	<6	81	<7	101	<66	12
TF-13-BL-08A 100	0.796	0.003	<0,05	0.81	8	1154	<6	77	<7	114	<66	10
TF-13-BL-08B shale 1	0.67	0.004	<0,05	0.31	39	981	<7	72	40	105	<66	82
TF-13-BL-08B shale 2	0.654	0.004	<0,05	0.24	30	1139	<6	56	23	109	<65	85
TF-13-BL-08C	0.742	<0,002	<0,05	0.07	14	1316	<6	67	<7	87	<65	19

APPENDIX A (continued): XRF lithochemistry data

Sample ID	Ga ppm	Hf ppm	La ppm	Mo ppm	Nb ppm	Nd ppm	Ni ppm	Pb ppm	Rb ppm	Sb ppm	Sc ppm	Sm ppm
TF-13-BL-08A 0	27	<17	42	41	22	<37	11	32	166	<89	<24	<40
TF-13-BL-08A 10	29	<17	49	25	23	<37	13	33	165	<89	28	<40
TF-13-BL-08A 20	25	<18	43	42	18	<37	33	28	148	<88	<23	<43
TF-13-BL-08A 25	30	<17	49	9	21	<37	49	23	148	<88	<23	<41
TF-13-BL-08A 30	28	<16	56	<6	21	<36	9	19	161	<89	<24	<38
TF-13-BL-08A 40	26	<16	54	11	20	<36	10	34	158	<88	<23	<38
TF-13-BL-08A 50	24	<16	<40	<6	22	<36	6	22	128	<89	<24	<39
TF-13-BL-08A 60	27	<16	58	<7	17	<36	7	24	147	<88	<24	<39
TF-13-BL-08A 70	25	<16	42	7	19	<36	13	19	143	<87	<23	<39
TF-13-BL-08A 80	25	<16	<40	<6	17	<36	8	18	154	<88	<24	<38
TF-13-BL-08A 90	27	<16	47	<6	17	<36	9	20	156	<89	<24	<38
TF-13-BL-08A 100	26	<17	<41	11	19	<37	8	28	150	<90	<24	<40
TF-13-BL-08B shale 1	24	<19	<40	<7	17	<38	76	18	131	<88	<24	<47
TF-13-BL-08B shale 2	24	<18	<40	13	17	<37	54	21	134	<87	<24	<43
TF-13-BL-08C	28	<16	<40	<6	17	<36	8	17	137	<88	<24	<38

Sample ID	Sn ppm	Sr ppm	Ta ppm	Th ppm	U ppm	V ppm	W ppm	Y ppm	Zn ppm	Zr ppm	EfNi	EfV	EfMo
TF-13-BL-08A 0	<36	130	<11	18	<9	325	<10	26	31	161	0.08	0.04	15.41
TF-13-BL-08A 10	<36	118	<12	13	<10	280	<11	25	24	156	0.09	0.05	9.22
TF-13-BL-08A 20	<36	112	<13	18	<10	236	<11	28	53	153	0.26	0.13	17.18
TF-13-BL-08A 25	<36	143	<12	20	<10	231	<11	42	65	173	0.37	0.19	3.53
TF-13-BL-08A 30	<36	129	<11	18	<9	253	<10	31	27	164	0.06	0.03	
TF-13-BL-08A 40	<36	128	<11	18	<9	226	<10	27	18	165	0.07	0.04	4.27
TF-13-BL-08A 50	<36	91	<11	13	<9	190	<10	24	16	180	0.05	0.03	
TF-13-BL-08A 60	<36	140	<12	15	<9	212	<10	28	14	162	0.06	0.03	
TF-13-BL-08A 70	<35	107	<11	15	<9	211	<10	24	18	155	0.11	0.06	3.10
TF-13-BL-08A 80	<36	91	<11	15	<9	239	<10	20	16	141	0.06	0.03	
TF-13-BL-08A 90	<36	107	<11	12	<9	263	<10	18	13	131	0.07	0.04	
TF-13-BL-08A 100	<36	188	<12	14	<10	240	<10	22	18	144	0.06	0.03	4.52
TF-13-BL-08B shale 1	<36	90	<14	17	<11	224	<12	29	179	126	0.64	0.34	
TF-13-BL-08B shale 2	<36	118	<13	14	11	227	<11	35	173	141	0.46	0.24	5.79
TF-13-BL-08C	<36	88	<11	15	<9	195	<10	24	16	153	0.25	0.03	

EfNi, EfV and EfMo are derived values

APPENDIX B: XRD mineralogy of tephra samples

Sample #	Location	Measured Section (m)	UTM E	UTM N	Comments	Principal and minor minerals	Trace minerals
YU036	BL-08A - 5 m	95	438854	7600461	measured section	Rectorite or illite/ montmorillonite-mixed-layer? kaolinite; gypsum	jarosite; quartz; goethite
YU037	BL-08A - 35 m	65	438806	7600458	measured section	quartz; illite/montmorillonite- mixed-layer?	jarosite; gypsum; feldspar?
YU038	BL-08A - 85 m	15	438765	7600422	measured section	illite/montmorillonite-mixed- layer?	kaolinite; quartz; jarosite; feldspar
YU039	BL-08A - 95 m	5	438747	7600419	measured section	illite/montmorillonite-mixed- layer?; kaolinite; quartz	feldspar; gypsum
YU041	BL-08C	n/a	439749	7599615	Type section of Young (1975)	quartz; illite/montmorillonite- mixed-layer?	gypsum; feldspar; kaolinite; jarosite

UTM NAD 83, zone 8

APPENDIX C: RockEval/TOC data

Sample #	Sample ID	Measured Section (metre)	Location	UTME	UTM N	Lithology	Rock Unit	Description/Notes	VR %Ro	C total (%)	C _{org} (%)	S total (%)	S1 (mg/g)	S2 (mg/g)	S3 (mg/g)	Tmax (°C)	PI	HI	OI
TF-13-BL-08A	TF-13-BL-08A 0	100	Tributary of Boundary Creek	438854	7600461	shale	Boundary Creek Fm	measured section	1.12	2.65	2.65	1.29	0.19	1.62	0.31	441	0.10	61	12
TF-13-BL-08A	TF-13-BL-08A 10	90	Tributary of Boundary Creek	438845	7600455	shale	Boundary Creek Fm	measured section		2.63	2.63	0.97	0.2	1.65	0.15	432	0.11	63	6
TF-13-BL-08A	TF-13-BL-08A 20	80	Tributary of Boundary Creek	438835	7600462	shale	Boundary Creek Fm	measured section		3.5	3.5	6.93	0.37	2	0.12	439	0.16	57	3
TF-13-BL-08A	TF-13-BL-08A 25	75	Tributary of Boundary Creek			shale	Boundary Creek Fm	measured section		4.18	4.18	3.38	0.54	5.1	0.01	442	0.10	122	0
TF-13-BL-08A	TF-13-BL-08A 30	70	Tributary of Boundary Creek	438821	7600461	shale	Boundary Creek Fm	measured section		2.51	2.51	1.23	0.18	1.65	0.08	443	0.10	66	3
TF-13-BL-08A	TF-13-BL-08A 40	60	Tributary of Boundary Creek	438806	7600458	shale	Boundary Creek Fm	measured section		4.16	4.15	1.32	1.27	5.8	0.08	446	0.18	140	2
TF-13-BL-08A	TF-13-BL-08A 50	50	Tributary of Boundary Creek	438795	7600436	shale	Boundary Creek Fm	measured section		2.41	2.39	0.75	0.45	2.29	0.1	441	0.16	96	4
TF-13-BL-08A	TF-13-BL-08A 60	40	Tributary of Boundary Creek	438786	7600438	shale	Boundary Creek Fm	measured section		4.47	4.41	0.99	1.72	6.2	0.27	433	0.22	141	6
TF-13-BL-08A	TF-13-BL-08A 70	30	Tributary of Boundary Creek	438777	7600437	shale	Boundary Creek Fm	measured section		4.18	4.15	2.01	0.68	4.56	0.01	444	0.13	110	0
TF-13-BL-08A	TF-13-BL-08A 80	20	Tributary of Boundary Creek	438768	7600424	shale	Boundary Creek Fm	measured section		4.19	4.12	0.92	0.7	8.61	0.05	449	0.08	209	1
TF-13-BL-08A	TF-13-BL-08A 90	10	Tributary of Boundary Creek	438765	7600422	shale	Boundary Creek Fm	measured section		4.38	4.38	2.22	0.37	8.56	0.12	447	0.04	195	3
TF-13-BL-08A	TF-13-BL-08A 100	0	Tributary of Boundary Creek	438747	7600419	shale	Boundary Creek Fm	measured section	1.16	2.53	2.53	1.23	0.24	1.54	0.18	427	0.13	61	7
TF-13-BL-08B	TF-13-BL-08B shale 1	n/a	Confluence Boundary Ck and Big Fish R.	439809	7599167	shale	Boundary Creek Fm	burning shale section		3	3	10.2	0.71	3.28	0.01	438	0.18	109	0
TF-13-BL-08B	TF-13-BL-08B shale 2	n/a	Confluence Boundary Ck and Big Fish R.	439809	7599167	shale	Boundary Creek Fm	burning shale section		4.61	4.61	5.26	0.89	7.67	0.04	438	0.10	166	1
TF-13-BL-08C	TF-13-BL-08C	n/a	Confluence Boundary Ck and Big Fish R.	439749	7599615	shale	Boundary Creek Fm	Type section of Young (1975)		2.61	2.61	1.06	0.46	2.39	0.07	442	0.16	92	3
TF-13-BL-06D	TF-13-BL-06D 0	520	Tributary of Cuesta Creek	419753	7623479	shale	Boundary Creek Fm	measured section	1.65	0.93	0.92	0.27	0	0.16	0.35	>600	0.00	17	38

APPENDIX C (continued): RockEval/TOC data

Sample #	Sample ID	Measured Section (metre)	Location	UTM E	UTM N	Lithology	Rock Unit	Description/Notes	VR %Ro	C total (%)	C _{org} (%)	S total (%)	S1 (mg/g)	S2 (mg/g)	S3 (mg/g)	Tmax (°C)	PI	HI	OI
TF-13-BL-06D	TF-13-BL-06D 25	495	Tributary of Cuesta Creek	419735	7623505	shale	Boundary Creek Fm	measured section		0.99	0.99	0.46	0	0.17	0.08	>600	0.00	17	8
TF-13-BL-06D	TF-13-BL-06D 50	470	Tributary of Cuesta Creek	419709	7623537	shale	Boundary Creek Fm	measured section		1.13	1.12	0.32	0.01	0.17	0.83	>600	0.06	15	74
TF-13-BL-06D	TF-13-BL-06D 63	457	Tributary of Cuesta Creek	419694	7623540	shale	Boundary Creek Fm	measured section		1.02	0.99	0.37	0.01	0.16	0.94	>600	0.06	16	95
TF-13-BL-06D	TF-13-BL-06D 75	445	Tributary of Cuesta Creek	419683	7623551	shale	Boundary Creek Fm	measured section		1.46	1.46	0.58	0.01	0.18	0.34	>600	0.05	12	23
TF-13-BL-06D	TF-13-BL-06D 87	433	Tributary of Cuesta Creek	419671	7623567	shale	Boundary Creek Fm	measured section		0.94	0.94	0.29	0.01	0.15	0.2	>600	0.06	16	21
TF-13-BL-06D	TF-13-BL-06D 100	420	Tributary of Cuesta Creek	419655	7623602	shale	Boundary Creek Fm	measured section		1.13	1.13	0.34	0.01	0.18	0.19	>600	0.05	16	17
TF-13-BL-06D	TF-13-BL-06D 125	395	Tributary of Cuesta Creek	419639	7623640	shale	Boundary Creek Fm	measured section		0.93	0.93	0.35	0.01	0.16	0.39	>600	0.06	17	42
TF-13-BL-06D	TF-13-BL-06D 138	382	Tributary of Cuesta Creek	419631	7623659	shale	Boundary Creek Fm	measured section	1.65	1.09	1.03	0.46	0.01	0.16	0.41	>600	0.06	16	40
TF-13-BL-06E	TF-13-BL-06E	130	Tributary of Cuesta Creek	419354	7623879	shale	Boundary Creek Fm	measured section		1	1	0.29	0	0.15	0.12	>600	0.00	15	12
TF-13-BL-06F	TF-13-BL-06F	0	Tributary of Cuesta Creek	49236	7623972	shale	Boundary Creek Fm	measured section	2	1.25	1.25	0.36	0	0.17	0.24	>600	0.00	14	19

Palaeoenvironment, palaeohydrography and chemostratigraphic zonation of the Canol Formation, Richardson Mountains, north Yukon

M.P. Hutchison¹ and T.A. Fraser
Yukon Geological Survey

Hutchison, M.P. and Fraser, T.A., 2015. Palaeoenvironment, palaeohydrography and chemostratigraphic zonation of the Canol Formation, Richardson Mountains, north Yukon. *In: Yukon Exploration and Geology 2014*, K.E. MacFarlane, M.G. Nordling and P.J. Sack (eds.), Yukon Geological Survey, p. 73-98.

ABSTRACT

Sedimentological and geochemical results from samples in the Richardson Mountains indicate that siliceous shales and chert of the Canol Formation were deposited in stratified, oxygen-depleted waters that favoured the preservation of organic matter. Dilution by terrigenous input was minimal; however, fluctuating palaeoproductivity resulted in significant biogenic silica enrichment that reduced porosity. The Canol Formation was divided into four regionally correlatable chemostratigraphic zones. Each zone was characterized by up-section profiles of: decreasing biogenic silica enrichment, increasing proportions of siliceous shale relative to chert, decreasing redox-sensitive Mo, U and V enrichment factors and decreasing Mo/TOC (total organic carbon) ratios. A preliminary sequence stratigraphic framework was constructed and eustasy invoked as the dominant allogenic control. Mo/TOC ratios are indicative of a silled, restricted basin with euxinic deepwater. The overall decrease up-section of these ratios suggests increasing restriction over time, associated with relative sea-level fall. Comparison of north Yukon data with similar modern and ancient basins has constrained preliminary reconstructions of Canol basin palaeohydrography.

¹matt.hutchison@gov.yk.ca

INTRODUCTION

In 2013, Yukon Geological Survey initiated the 'North Yukon Upper Palaeozoic Shale Project' as a continuation of the Geological Survey of Canada's GEM-Energy 'Yukon Basins Project' which concluded earlier that year. The project's aim is to further the understanding of the petroleum potential of Devonian-Carboniferous shale sequences in north Yukon, with a focus on the: upper Road River Group, Canol Formation, Ford Lake Shale and Blackie formations. The Canol Formation was targeted as the first priority for lithological characterization, refinement of age and stratigraphic relationships and assessment of source rock and shale gas reservoir potential. Analytical results from outcrop and diamond drillhole core work undertaken in 2012 and 2013 (Fraser *et al.*, 2012; Fraser and Hutchison, 2014; Hutchison and Fraser, 2014), suggest that the Canol Formation is highly prospective as a dry gas source rock in north Yukon (e.g., %Ro>1.8, 4.3% average TOC). The formation also exhibited comparable maturity, TOC and silica enrichment to both idealized and major North American shale gas plays, including the Marcellus Shale (eastern US) and Horn River Formation (British Columbia).

STUDY AIMS

Work to understand the depositional environment, palaeohydrography and controls on organic richness of the formation has not been undertaken until now (although lithofacies observations from Trail River were reported by Fraser in 2014). This study therefore aims to provide an integrated, detailed, palaeoenvironmental assessment of the Canol shales based on facies analysis and interpretation of lithogeochemical data collected from the 2013 work program. Results from this study are anticipated to enhance palaeohydrographic reconstructions of the Canol basin during the upper Palaeozoic, and impact the prediction of source rock/reservoir distribution and quality for future exploration in the region. The lithogeochemical database will also be interrogated to provide a chemostratigraphic zonation for the Canol Formation. This zonation scheme can then be used in future studies to facilitate both inter and intra-formational correlation between the surface and subsurface, where these data exist, both within north Yukon and in the wider regional context of the Late Devonian Seaway/Western Canada Sedimentary Basin.

AREA AND STRATIGRAPHY OF INTEREST

A full geological appraisal of the Canol Formation has previously been reported in Fraser *et al.*, (2012) and Fraser (2014), and as such only a brief summary of its distribution and stratigraphic relationships is provided here. The Canol Formation is a siliceous and organic-rich black shale that documents marine basinal sedimentation across northern Yukon during Middle to Late Devonian (Fig. 1). It has been dated as Givetian-Frasnian at its type locality in the Northwest Territories by Gal *et al.*, (2009). The formation is coeval with, and may have been laterally continuous with, other stratigraphic units in Yukon, including the 'unnamed shale unit' and Prongs Creek Formation (Norris 1968) and the Earn Group of Selwyn basin (Campbell, 1967). Potential correlative and coeval strata in southern Kandik Basin and eastern Alaska (the McCann Hill Chert, e.g., Van Kooten *et al.*, 1997), Liard and Horn River basins (the Muskwa Member of the Horn River Formation – F. Ferri, *pers. comm.*, 2014) and on Banks Island in the Arctic suggest an extensive, possibly interconnected system of basins in western North America during the Middle to Upper Devonian transition.

In Yukon, the Canol Formation typically overlies either Middle Devonian platform carbonates of the Ogilvie or Hume formations, or Road River Group limestone and shales in the Richardson Mountains (Fig. 1). The nature of the formation's basal contact is currently unclear, but has been interpreted as both conformable and unconformable in previous work (Pugh, 1983). At several locations in Yukon, the contact between the Road River Group and Canol Formation is marked by metre-scale carbonate concretions and Mo-Ni-Zn-PGE mineralization (Hulbert *et al.*, 1992; Goodfellow *et al.*, 2010; Balgord *et al.*, 2009). High abundances of trace metals noted in the interpreted Road River-Canol contact zone at Trail River suggest the presence of this horizon in the Peel Plateau and Richardson Mountains area (Fraser and Hutchison, 2014). At the zone's type section, on the Nick mineral exploration property in the Wernecke Mountains, analytical results from detailed lithogeochemical and rhenium-osmium (Re-Os) and $\delta^{13}\text{C}_{\text{org}}$ isotope sampling in the summer of 2014 are anticipated to provide new insights into the absolute age, stratigraphic context and depositional environments of this contact zone in Yukon (see Fraser *et al.*, 2014).

Recent (2014) field observations in the Richardson Mountains highlighted the presence of a thin, lithologically distinctive shale unit between the Road River Group and

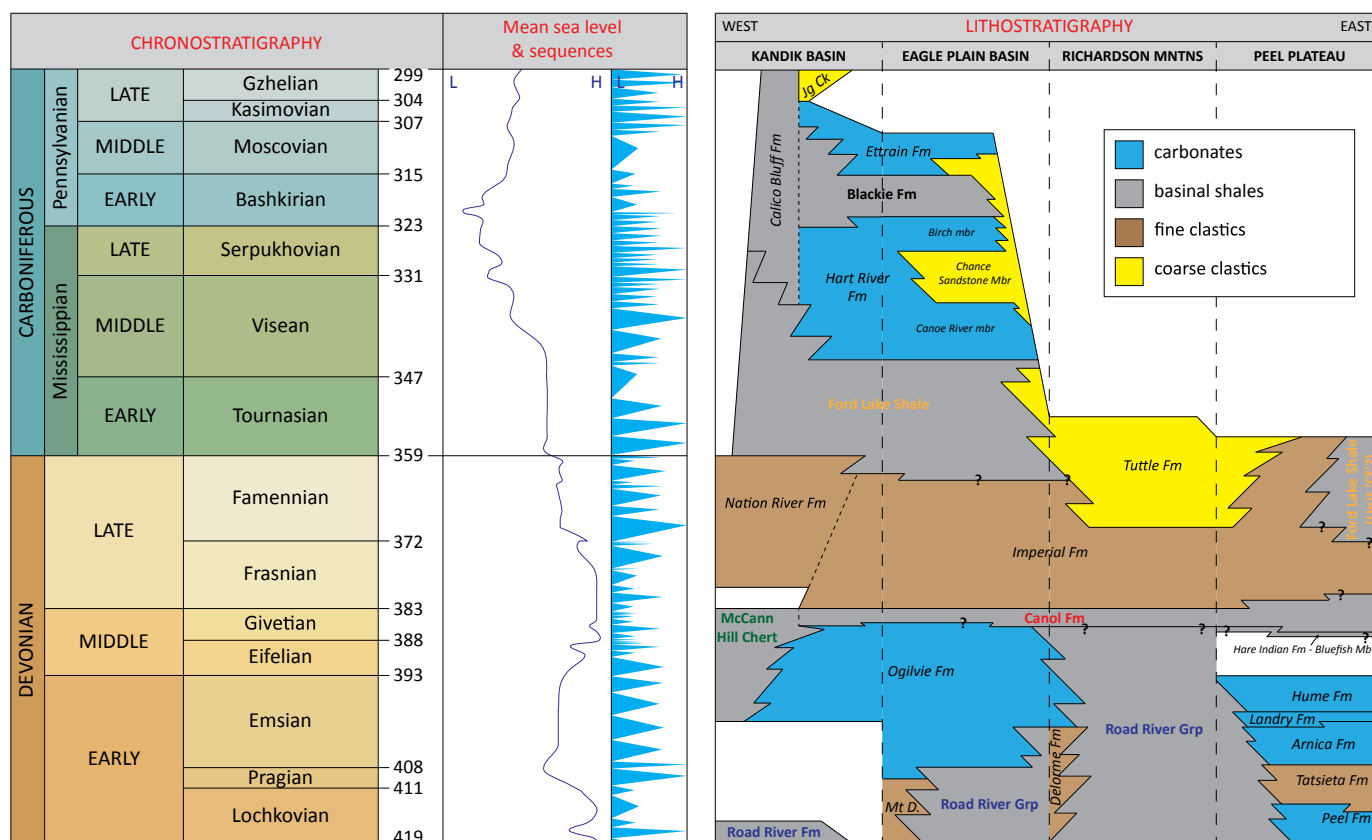


Figure 1. Generalized north Yukon stratigraphy. Chronostratigraphy from Cohen et al. (2013), mean sea level and sequences from Haq and Schutter (2008), Yukon lithostratigraphy modified from Pigage (2007) and east Alaskan stratigraphy in Kandik Basin from Van Kooten et al. (1997).

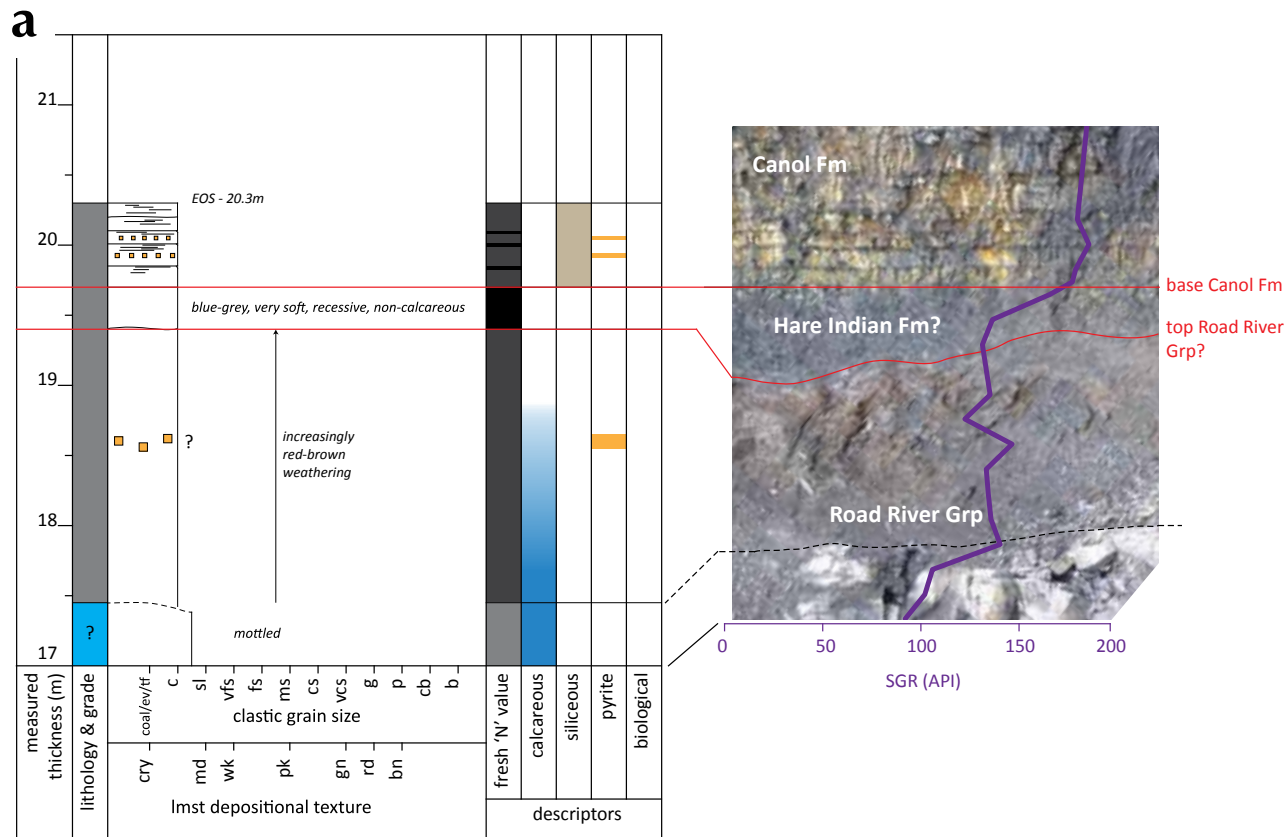
Canol Formation that may be correlative to strata of the lower Hare Indian Formation in the Northwest Territories (Fig. 2a; also see Fraser et al., 2014). Field observations in the Northern Ogilvie Mountains subsequently highlighted the presence of a soft, carbonaceous, in-part highly radioactive shale intercalated within the uppermost Ogilvie Formation carbonate sequence (Fig. 2b). Both sets of observations, combined with ongoing work at the Nick property type zone, suggest a more regionally-complex basal stratigraphic architecture and palaeogeography of the formation than previously recognized. At its upper contact, the Canol Formation is conformably overlain by clastic strata of the Imperial and Ford Lake Shale formations.

UTILITY OF LITHOGEOCHEMICAL DATA IN SHALE STUDIES

Lithogeochemical data have been used to define chemostratigraphic correlations in the petroleum industry for over a decade (Ratcliffe et al., 2010). This technique relies upon delineating changes in elemental

concentrations over time, and using these to model and constrain depositional controls such as changes in palaeoclimate and provenance (Ratcliffe et al., 2010). Lithogeochemical datasets routinely collected from organic-rich shales are also utilized to facilitate the interpretation of palaeoredox conditions during oceanic anoxic events (e.g., Tribouillard et al., 2006 and Algeo and Tribouillard, 2009). By increasing the range of elements and elemental ratios analyzed in the dataset, lithogeochemical data have been successfully used to create regional correlation frameworks, assess mineralogical variability and rock brittleness, assess the origins of silica and interpret levels of terrigenous clastic influx as a proxy for shoreline proximity (Ratcliffe et al., 2010).

Source rock and shale reservoir exploration requires an understanding of palaeoredox conditions, as high total organic carbon (TOC) values are only typically found in sediments where bottom conditions were anoxic (Ratcliffe et al., 2010). Redox-sensitive trace metals, e.g., uranium (U), vanadium (V) and molybdenum (Mo), tend to be more



b



Figure 2. (a) Detailed 2014 sedimentary and spectral gamma ray log across the Road River Group to Canol Formation contact at Trail River (14-TF-001). Lower-resolution work in 2013 did not identify the distinctive soft, blue-grey, high-radioactive shale in the contact zone that may be a lateral equivalent of the Hare Indian Formation (Bluefish Member). (b) Photo of interbedded, highly radioactive, soft, black shales in the uppermost carbonate succession of the Ogilvie Formation in the Northern Ogilvie Mountains (geologist for scale).

soluble under oxidizing conditions and less soluble under reducing conditions, resulting in authigenic enrichments in oxygen-depleted sedimentary facies (Tribovillard *et al.*, 2006). In addition, some elements, e.g., nickel (Ni) and cobalt (Co), are delivered to the sediment in association with organic matter and these can be used as relatively good proxies for organic carbon richness. Redox-sensitive trace elements can also typically be found in early-formed sedimentary pyrite (e.g., Large *et al.*, 2014) following organic matter (OM) decay in reduced sediment. It should be noted, however, that the covariation of U, V and Mo and their enrichment factors (redox sensitive trace elements normalised to aluminium content that is assumed to represent detrital influx - see calculation below) with TOC does not increase in strength linearly as oxygen depletion increases in restricted and stratified basins (Tribovillard *et al.*, 2006; Algeo and Lyons, 2006; Fig. 3).

- Enrichment factor (Ef) = $(TE_{\text{sample}}/Al_2O_{3\text{sample}})/(TE_{\text{avshale}}/Al_2O_{3\text{avshale}})$, where TE is the redox-sensitive trace element concentration. Average shale values and equation taken from Tribovillard *et al.* (2006). An Ef value of greater than 1 indicates enrichment due to anoxia.

Where litho-geochemical data are unavailable, uranium can also be derived from spectral gamma ray data collected by a hand-held spectrometer at outcrop. In a similar manner to analyzing elemental enrichment concentrations rather than simply the elemental concentration itself,

excess uranium (Uxs) can be calculated from uranium and thorium (Th) data based on Myers and Wignall's (1987) technique for assessing variations in U concentration against the thorium value as a quantitative reference. The calculation (see equation below) requires a 'normal' shale Th/U ratio value to be set at 3 (after Rider, 2002, based on empirical data originally collected by Adams and Weaver in 1958) and deviations lower than this value are essentially a result of excess/enriched uranium precipitated in association with reducing organic matter, rather than variations in thorium. The validity of this technique is documented by Uxs spikes found in association with condensed sequences in the marine realm (e.g., Rider, 2002).

- $Uxs \text{ (ppm)} = U - (Th/3)$ from Rider (2002), after Myers and Wignall (1987)

In modern low-oxygen marine systems, patterns of Mo-U covariation have also been linked to variation in benthic redox conditions and basin palaeohydrography Algeo and Tribovillard (2009). The degree of enrichment of authigenic Mo and U, and the Mo/U ratio of the sediment relative to the molar ratio of modern seawater can be used to distinguish open-ocean systems with unrestricted circulation from restricted, deepwater circulation in silled basins. By comparison of these elemental data between modern basins such as the Black Sea and anoxic facies from the Late Devonian Seaway, Algeo and Tribovillard (2009) demonstrate that authigenic Mo-U relationships

between modern and ancient systems document similar redox and hydrographic controls on deposition. This ability to use modern analogues to facilitate the interpretation of ancient systems has profound implications for the temporal and palaeogeographic prediction of organic richness and, therefore, both source rock and shale reservoir distribution and quality in ancient settings.

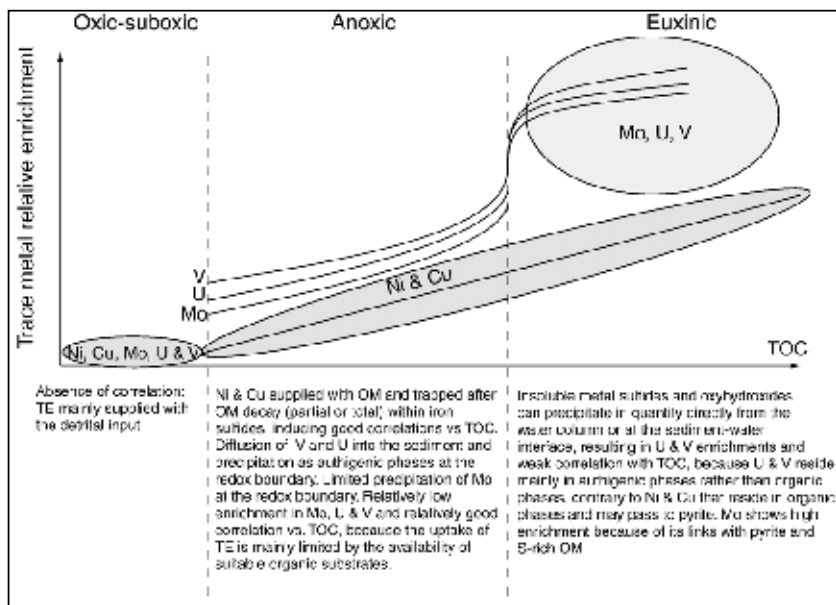


Figure 3. Schematic diagram illustrating the relative enrichment of Ni, Mo, U and V against TOC (from Tribovillard *et al.*, 2006). Note TE stands for trace elements and OM for organic matter.

DEPOSITIONAL CONTROLS ON ORGANIC RICHNESS

The organic richness of a rock is typically measured in or expressed as its TOC content. The accumulation of organic matter in depositional environments is controlled by complex interactions between three main controls: rates of production, destruction and dilution (e.g., Tyson, 2005; Katz, 2005; Passey *et al.*, 2010 – Fig. 4).

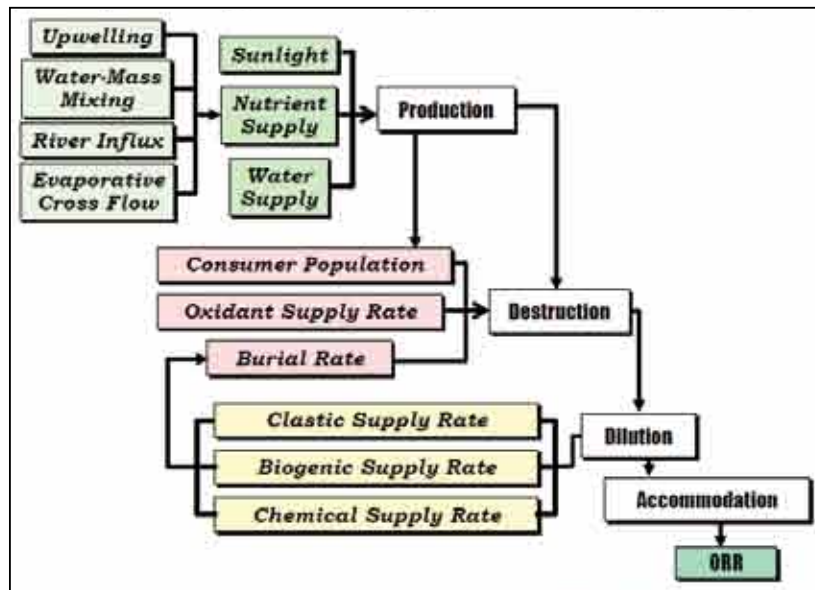


Figure 4. Schematic flow-diagram outlining the interconnected, tripartite controls on organic richness: production, destruction and dilution (from Passey *et al.*, 2010).

With sufficient accommodation rates to accumulate significant sediment thicknesses, the enrichment of organic matter is most likely to occur under conditions where production is maximized, destruction minimized and dilution by clastic or biogenic (*i.e.*, non hydrocarbon-based) material optimized. However, very high rates of production are detrimental to TOC enrichment. In this event, significant dilution by non-hydrocarbon-rich biogenic material (*e.g.*, silica tests of radiolarians) occurs and recent studies (*e.g.*, Bohacs *et al.*, 2005) demonstrate that moderate productivity is more conducive to forming an organic-rich rock. Dilution rates are also increased in areas of high terrigenous clastic influx, suggesting in general that as proximity to shoreline increases, organic matter will become less enriched. The key factor for preservation of organic matter is the maintenance of low oxidant concentrations in the sediment pore-water system, which is achieved via water column stratification (Passey *et al.*, 2010).

DATA AND METHODOLOGY

SECTION LOCATIONS

The Canol Formation has been mapped at surface between 65° and 67°N, and is documented in oil and gas wells in and near the exploration regions of Eagle Plain Basin, Peel Plateau and Plain basins and northeast

Kandik Basin (Fig. 5). Data for this study are taken from one measured outcrop section (Trail River), accessed via helicopter in the east Richardson Mountains, and from one exploration diamond drillhole core (RI07-07A) drilled on Quetzal Energy Ltd.'s Rich property (Yukon MINFILE 116I085) in 2007 (Fig. 5) to target the Mo-Ni-Zn-PGE mineralization discovered further south in Selwyn basin. Section location information is presented in Table 1.

The Canol Formation at Trail River is 227.3 m thick, and is considerably thicker than exposures located on the carbonate platforms both east and west of the former Richardson trough. The drill core from the Rich property comprises 158.6 m of Canol Formation. In both sections, the formation is underlain by calcareous shales of the upper Road River Group, and at Trail River the Canol Formation is overlain by mudstones of the Imperial Formation. Palynomorphs collected by Norris (1985) from this section provide a late Givetian or early Frasnian date. Affirmation of this age comes from palynomorphs more recently recovered from the uppermost Road River Group (Middle? Devonian), and lowermost Imperial Formation (Frasnian: Dolby, 2013). The Rich core currently has no age control. For further detail on the overall section description for Trail River see Fraser (2014).

DATA COLLECTION

The Trail River section was measured, described and sampled by a team of four YGS geologists in the summer of 2013. The Rich property drill core was similarly worked on by one YGS field assistant in the summer of 2014. At Trail River, detailed lithological observations enabled construction of a graphical sedimentary log and a facies analysis to be undertaken. Spectral gamma ray data were collected at 1 m intervals at the Trail River section using a hand-held spectrometer (Radiation Solution's RS-230 BGO Super-SPEC spectrometer with a 0.103 litre BGO crystal). Individual concentrations of potassium (K), uranium and thorium were then proportionally summed using the equation below to give an overall standard gamma ray (SGR) count in API units. Spectral gamma ray data were not collected from the Rich core – the small volume of rock available for the meter to 'read' from a 41.9 mm diamond drillhole core was considered insufficient from

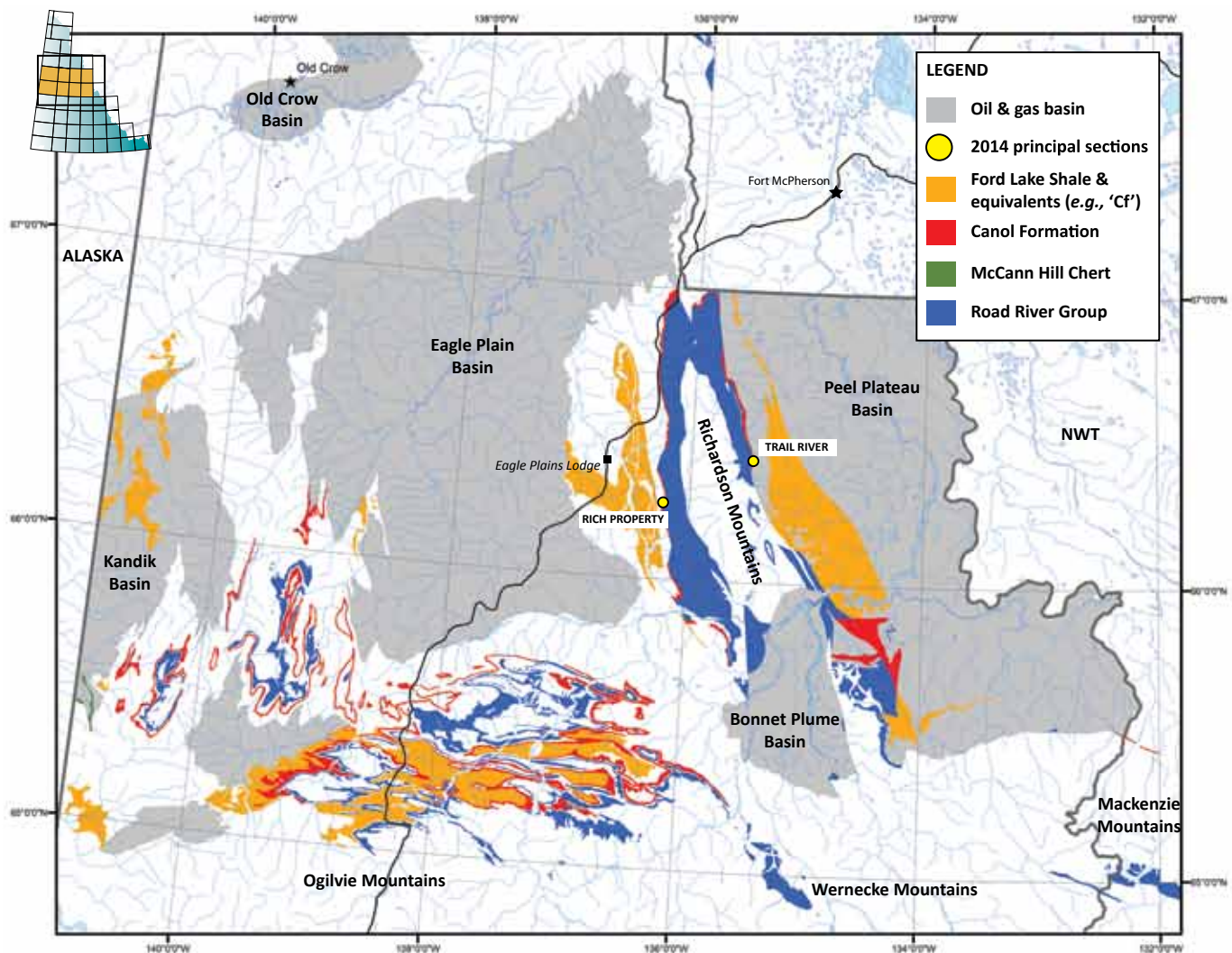


Figure 5. North Yukon area map with locations of the Trail River outcrop and Rich Property drillhole core sections. Surface extent of formations after Gordey and Makepeace (2003).

which to obtain an accurate value (based on conclusions in Hutchison, 2014 from a study attempting to measure SGR on half-cut and/or resin slabbed cores from North Sea condensate fields).

- $SGR (API) = 16.32 \times K (\%) + 8.09 \times U (ppm) = 3.93 \times Th (ppm)$ (from Rider, 2002)

Rock chip samples were collected through 2 m intervals (Trail River) and 1 m intervals (Rich core) and subsequently sent for RockEval/TOC analysis at the Organic Petrology Laboratory (Geological Survey of Canada, Calgary) and inductively coupled plasma-emission/mass spectroscopy (ICP-ES/MS) litho geochemistry by ACME Laboratories Ltd. in Vancouver. Every other 1 m sample from the Rich core was used for analysis to replicate the 2 m

sample spacings used at outcrop. The methodologies for individual interpretative techniques utilized in this study are described at their point of presentation in the results section.

RESULTS AND INTERPRETATION

FACIES ANALYSIS AND ORGANIC RICHNESS ASSESSMENT

The Canol Formation at Trail River is a resistant shale sequence that is characterized by rhythmically bedded siliceous shale and chert lithofacies (Fraser, 2014). It was noted in the field that these two facies delineated two depositional end-members, where interbedded

Table 1. Location and section information for Trail River and the Rich Property (note the contacts are given in measured thickness from base (Trail River) and downhole depth (Rich core)).

Section ID	Type	Easting	Northing	UTM Zone	NTS Mapsheet	Base Canol Fm (m)	Top Canol Fm (m)	Canol Fm Thickness (m)
Trail River	outcrop	477796	7366173	NAD83, zone 8	106L/6 (Lusk Lake)	19.7	247.0	227.3
Rich Property	DDH core	444721	7355752	NAD83, zone 8	116I/8 (Mount Raymond)	158.6	0.0	158.6

units display differences in relative end-member facies proportion, bed thickness and lateral intra-bed facies variability. Elongate concretions, up to 2.5 m long and 0.9 m wide, were noted to occur at specific stratigraphic horizons in the section. Fine-grained pyrite was common in the formation where it was either concentrated along bedding planes or disseminated in shale. A pyrite nodule 35 cm long and 3 cm wide was noted at 25 m. The updated (from Fraser, 2014) graphical sedimentary log is presented in Figure 6.

For this study's facies analysis and assessment of organic richness, Fraser's (2014) four original lithofacies will be compressed to three: siliceous shale, interbedded siliceous shale and chert (with variable percentages of each greater than 10%), and chert. The concretions will also be analyzed as a separate lithofacies. The pyrite will be interpreted within the interbedded lithofacies as this was where the aforementioned nodule was recorded. Key lithofacies observations are tabulated with accompanying representative photos (Fig. 7). A brief lithofacies interpretation and summary are also included in Figure 7 for completeness, but is expanded upon below.

Siliceous shale

The black colouration of this facies is attributed to a high TOC content (average 3.77 wt % - Table 2), with the organic material deposited in sediments with a very low to absent oxidant concentration (e.g., Passey *et al.*, 2010), preventing decay. The thin planar lamination and fine-grained nature of this facies suggest deposition from suspension in a quiescent environment, with the laminae separating upon surface exposure and subsequent weathering to give the facies its characteristic fissility (e.g., Ingram, 1953 and Weaver, 1989). In terms of Passey *et al.*'s (2010) model for achieving organic richness (Fig. 4), the relatively high TOC content of this facies is attributed to high primary productivity (hydrocarbon-based producers such as algae), low secondary productivity and dilution by silica-based producers (such as radiolaria) and relatively low dilution by clastic influx (Fig. 7).

The variability in bed thickness and associated competency within this facies is difficult to interpret without the availability of SEM sections or high-resolution sampling. If increased competency is attributed to the presence of increased silica (sourced from re-precipitated radiolarian test material within the sediment, e.g., Blood *et al.*, 2013), then these thicker beds are the depositional product of greater secondary palaeoproductivity than their soft, thinner, recessive facies counterpart. Blood *et al.* (2013) describe similar siliceous shales from the Marcellus Formation in the eastern US where the enrichment of biogenic silica is linked to transgressive episodes that re-supply nutrients to formerly restricted basins, which re-stimulates productivity in the photic zone. Hall *et al.* (2011) also describe potential biogenic silica enrichment of the Muskwa Member (Canol Formation equivalent) of the Horn River Formation in British Columbia, although the authors note that skeletal remains of the actual siliceous organisms are rare.

Chert

The black colouration of this facies is again attributed to organic richness; deposition and decay prevention occurs in sediments with low oxidant concentrations. The very thin to thin lamination again suggests a quiescent environment and deposition from suspension. However, the absence of fissility along the laminae, laminae rarity and the relatively thick nature of the beds for such a low-energy setting is evidence for post-depositional modification of these sediments. This process, akin to early-diagenetic cementation, imparts homogeneity to the rock which is expressed in its conchoidal fracture and ability to weather to irregular blocks.

In their respective analysis of Marcellus and Muskwa shales, Blood *et al.* (2013) and Hall *et al.* (2011) use SEM analysis to determine that authigenic quartz derived from re-precipitated siliceous organisms is able to permeate the clay mineral fabric, forming a pervasive and continuous high-modulus (competent) medium which is ultimately conducive to artificial stimulation during

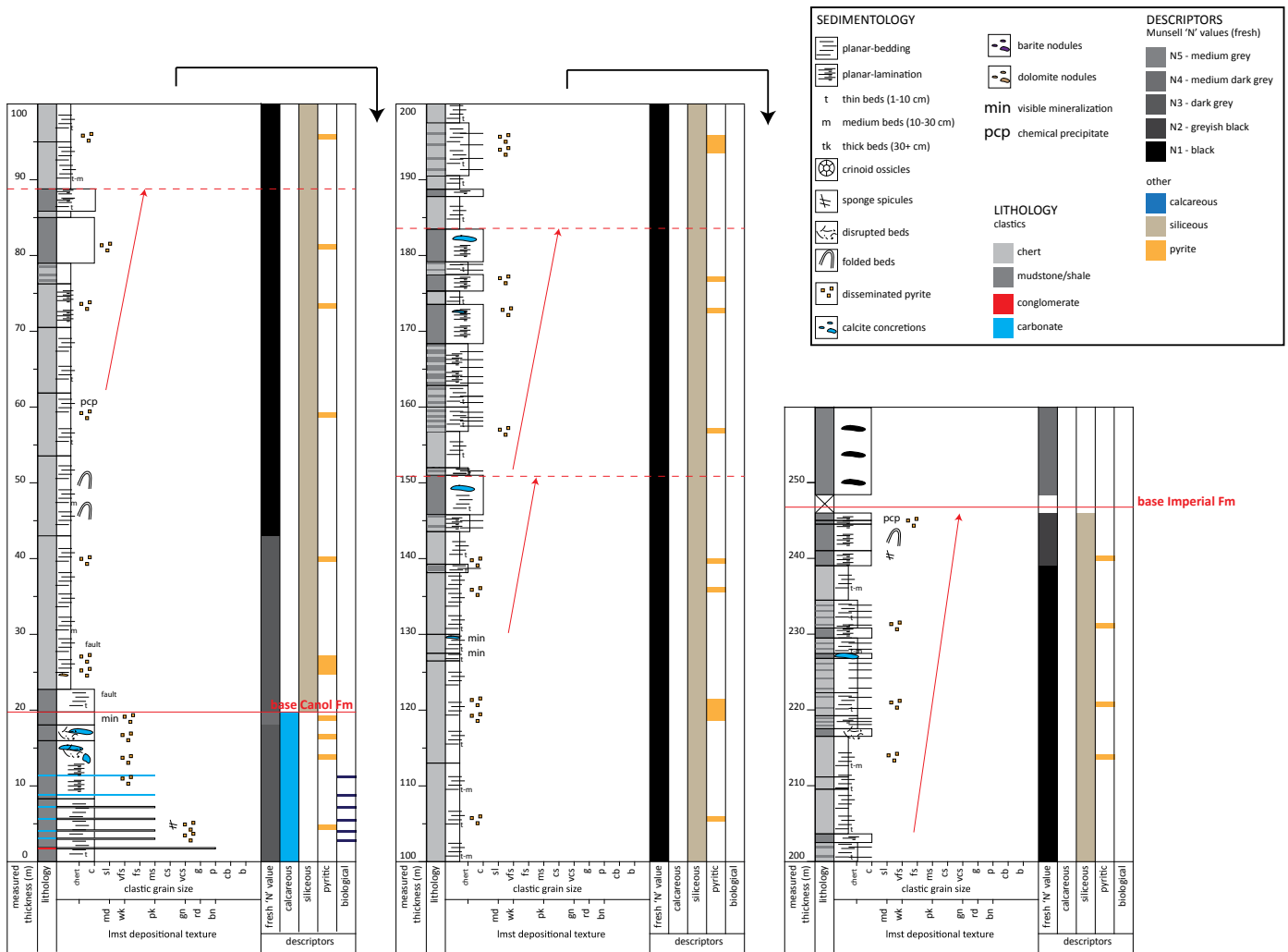


Figure 6. Sedimentary log of the Road River Group to Imperial Formation section measured at Trail River. The red arrows highlight four sequences of increasing siliceous shale proportion up-section, with the dashed horizontal red lines at the top of these sequences correlating to the lithogeochemical zone boundaries defined in Figure 8.

hydraulic fracturing. Hall *et al.* (2011) also demonstrate the utility of SEM analysis to differentiate between biogenic (authigenic) and detrital quartz. In this facies, it is considered unlikely (in consideration of the prevalent post-depositional modification) that the highly siliceous nature is a product of increased clastic influx. The absence of crosscutting, chert-filled veins furthermore suggests that the silicification was not a product of hydrothermal fluid alteration during later burial.

Although the factors discussed thus far are suitable for the occurrence of highly enriched organic matter in this facies, the fact that it is so siliceous as to be termed ‘chert’ in the field suggests that secondary productivity and subsequent

dilution by silica-based material (Fig. 7) would be expected to have had a significant impact on limiting the potential organic richness of this facies (e.g., Bohacs *et al.*, 2005), although this is not seen in the facies’ TOC statistics presented in Table 2. The presence of minor, thinly bedded partings of the siliceous shale facies suggests, however, that palaeoproductivity was variable, and occasionally favoured against radiolarian productivity. The rhythmical deposition of these shale partings, forming either the top or base of individual chert bed depositional events, further suggests cyclicity in watermass chemistry that may be influenced by eustatic or tectonic events.





LITHOFACIES	PHOTO	OBSERVATIONS	INTERPRETATION	
Chert		<ul style="list-style-type: none"> • Black colour • Beds 1-10 cm, max 16 cm thick • Rare planar lamination • Conchoidal fracture • <10% siliceous shale partings 	Quiescent, low advection, suspension deposition Low oxidant conc. in sediment pore-water system Low destruction of organic matter	50% chert Increasing primary productivity (carbon-producers) Decreasing secondary productivity (biogenic SiO ₂ - rads?) Decreasing dilution of organic matter
Interbedded chert & siliceous shale		<ul style="list-style-type: none"> • Rhythmically interbedded • Variable composition • ≥10% chert • ≥10% siliceous shale 		
Siliceous shale		<ul style="list-style-type: none"> • Black colour • Competent beds <10 cm thick • Soft beds <3 cm thick & planar laminated • <10% chert beds 		
Concretions		<ul style="list-style-type: none"> • Elongate • <2.5 m long, <0.9 m wide • typically flat bases, domed tops, laminae traced into body • dolomitic composition 		

Figure 7. Canol Formation facies analysis from Trail River.

Interbedded siliceous shale and chert

This lithofacies encompasses the range of variable percentages of interbedded siliceous shale and chert end-members described above and, although the controls on deposition and enhancement of organic richness are the same for each facies type, the higher frequency of change of these controls is expressed in the rock record by the high degree of interbedding. TOC contents therefore exhibit a much higher variability than for either end-member facies (Table 2), although the average TOC content is not dissimilar to that of the other two facies.

Table 2. TOC statistics for individual facies at Trail River.

	Facies TOC (wt %)		
	Chert	Interbedded chert & siliceous shale	Siliceous shale
<i>n</i>	38	58	18
<i>min</i>	2.80	2.33	1.85
<i>max</i>	5.71	6.16	5.33
<i>range</i>	2.91	3.83	3.48
<i>mean</i>	3.80	3.81	3.77
<i>st dev</i>	0.64	0.76	1.04

The pyrite in this (and all facies) is typical of sedimentary pyrite formation in seafloor muds when hydrogen sulphide, produced by the microbial reduction of marine sulphate, reacts with iron (Large *et al.*, 2014). The various fine-grained textures observed (Fig. 7) are typical of syngenetic sedimentary origins (e.g., small nodules and framboids); late stage diagenetic pyrite also occurs, overgrowing earlier pyrite generations, resulting in elongate nodular forms. Blood *et al.* (2013) also demonstrates that pyrite can completely replace radiolarian material in various states of dissolution in the Marcellus Shale. The abiotic processes that occur during the formation of pyrite are particularly efficient under reducing, anoxic conditions (e.g., Tribovillard *et al.*, 2006 and Brocculeri and Foos, 1987). Consequently, trace-element enrichments in both pyrite and their host sediment should mirror these specific palaeoredox conditions that prevailed at the time of Canol Formation deposition and early diagenesis.

Concretions

The origin of the concretions in the Canol Formation at Trail River is not clear. Fraser (2014) suggested that their flat bases and domed upper contacts (Fig. 7) are indicative of formation as a syn-sedimentary or early

diagenetic feature on or just beneath the seafloor rather than growth after burial during late stage diagenesis. The reddish-brown weathering, local association with discrete iron-rich horizons and dolomitic composition are suggestive of ferroan dolomite fluid flow along bedding planes acting to cement the sediment. Early cementation is also indicated by the preservation of laminae within the concretion body. This mode of formation, termed pervasive growth (Raiswell and Fisher 2000), functions by the infilling of pore space by precipitating minerals and occurs simultaneously throughout the entire volume of rock rather than concentrically from a nucleus. Both a coarser-grained sediment and/or an absence of siliceous test material would seem pre-requisite for this process to occur, which may explain the occurrence of concretions in the uppermost siliceous shale (rather than chert) unit of a sequence (Fig. 6). Their distinctive mound shape may be explained by formation just beneath the seafloor, where the more indurated and dewatered underlying sediment promoted growth upwards into softer muds.

The concretion's mineralogy and elongate orientation is analogous to the early diagenetic dolostone 'doggers' of the Kimmeridge Clay Formation source rocks in northwest Europe described by Morgans-Bell *et al.* (2001). Literature on the genesis of concretions, exclusive of mineralogical composition, suggests that favourable conditions for growth would be met primarily by diminished sedimentation (such as the formation of hardgrounds, or on the crests of less subsident submerged fault blocks; e.g., Scotchman, 1989) and a long-term stable redox boundary within the sediment (e.g., Witkowska, 2012). However, Scotchman (1991) also proposes that the specific development of similar complex and concretionary dolomites in the Kimmeridge Clay are related to high sedimentation rates and organic matter enrichment commonly found across the deep shelf.

LITHOGEOCHEMISTRY

Palaeoredox conditions

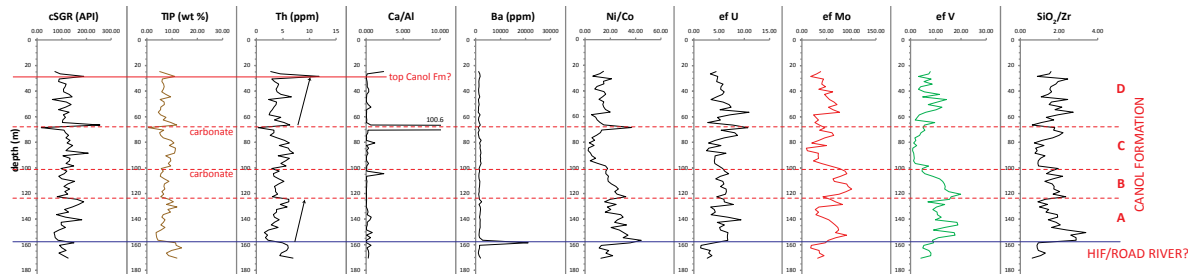
Enrichment factors (Ef) of Mo, U and V are elevated in both sections of the Canol Formation, relative to underlying Road River and overlying Imperial sediments, suggesting that, in general, anoxic conditions prevailed during deposition of the Formation (Fig. 8). A distinctive four-zone division is also evident that suggests redox conditions fluctuated over time in response to changing long-term controls (e.g., Algeo and Lyons, 2006) where

zones B and D show the greatest enrichment of these elements and zone B shows the highest enrichment of the four zones (although caution in translating this directly to the section's highest TOC contents is advised – see discussion below). The enrichment profiles of U and Mo especially document an extremely rapid onset of anoxia at the base of the Canol in zone A. The Ni/Co ratio profile (Fig. 8), also used as a proxy to indicate anoxic conditions (Rimmer, 2003), documents the same overall trends of zoned anoxia in the Canol. In the Horn River Group reference section in the Mackenzie Valley in Northwest Territories, V enrichment and elevated Ni/Co ratios are used to characterize the Canol Formation (Pyle *et al.*, 2014), although a correlation between NWT and Yukon suggests that the entire formation in NWT correlates into only the lower two zones of the Trail River section (zones A and B; Fig. 9). The serrated enrichment profiles of zone A, B and D suggest a secondary, shorter-term variability in anoxia or basin stratification/restriction. In contrast, the less-anoxic zone C profile is more subdued (especially evident in V concentrations) suggesting that the basin was either less restricted during this time, or that the degree of flux from dysoxic to anoxic was so rapid that the fluctuations were not able to be observed in a homogenized 2 m sample interval.

Mo-TOC and EfMo-EfU covariation patterns can be used to assess the degree of basinal deepwater restriction and its differentiation between anoxic or euxinic (dominated by H₂S rather than O₂) redox potential. At Trail River, the Mo/TOC ratio profile (Fig. 10a; see also Fig. 8) highlights a long-term trend towards lower ratios suggestive of an overall increase in basin restriction during deposition of the Canol Formation. The average Mo/TOC ratio is 8.66 (10⁻⁴) which indicates that the basin was silled and had strongly restricted, and therefore sulphidic, deepwater that was able to preserve organic matter (Algeo and Lyons, 2006). A distinct higher Mo/TOC ratio in zone B is indicative of a transition into a less restricted basin, which then subsequently becomes more restricted again up-section. Further evidence for rapid flooding and then onset of anoxia in the basal Canol strata is provided by the Mo/TOC spike at 19.8 m (Fig. 10a).

The degree of basin restriction can also be assessed using EfMo-EfU covariance relative to that of modern seawater derived from analogues (e.g., Algeo and Tribovillard, 2009). EfMo-EfU cross-plots in Figure 10b show a positive correlation coefficient between enrichment factors in both sections, despite the coefficients only being moderate

RICH PROPERTY (west)



TRAIL RIVER (east)

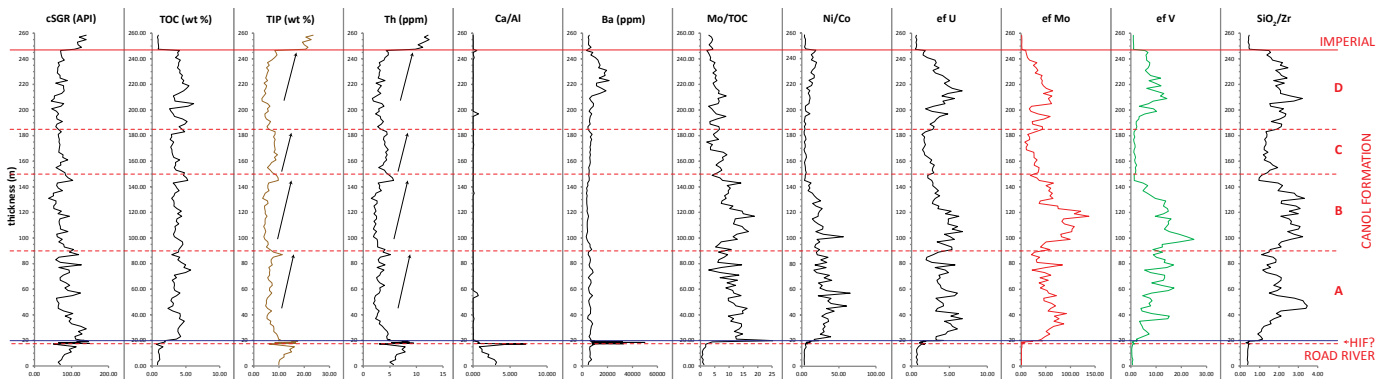


Figure 8. Lithochemical correlation between sections in the Richardson Mountains. It is uncertain if the top Canol Formation contact is present in the Rich core section, although the thermal index and Th profiles suggest its location as indicated. cSGR is the SGR value calculated from elemental lithochemical (rather than hand-held gamma ray meter) data using the equation in the text. HIF refers to the Hare Indian Formation.

to weak ($R^2=0.57$ at Trail River and 0.24 in the Rich core). The Canol Formation of both sections exhibits EfMo/EfU ratios that are elevated above the modern seawater molar ratio (approximately 7.5-7.9; Algeo and Tribovillard, 2009) and has trend line gradients that also approximately parallel those of modern seawater (Fig. 10b). This characteristic is similar to that documented from deepwater cores in the Cariaco Basin and from the Late Devonian Chattanooga Shale basin in the southern US (Algeo and Tribovillard, 2009). It is attributed to both benthic redox variation at the sediment-water interface (*i.e.*, relative enrichment of both Mo and U as redox conditions become anoxic, with Mo enrichment outpacing that of U once bottom waters become sulphidic) and Mn-Fe redox cycling within the water column that also contributes to the preferential enrichment of Mo over U. Critically, the effectiveness of Mn-Fe redox cycling may be enhanced by strong variations in water-column redox conditions at short to intermediate timescales (*e.g.*, 50-100 years in the Cariaco Basin; Algeo and Lyons, 2006);

a factor which also supports the previously proposed shorter-term variability in Canol basin restriction.

The effects of long-term aqueous Mo drawdown and the Mo-TOC relationship to hydrographic dynamics in the Canol Formation can be further tested by analysis of Mo-TOC covariation on a three point running-averaged sample-by-sample depth basis (Fig. 11). Although Mo-TOC covariation at Trail River might initially appear to be random, 64% of Canol sample-to-sample paths are positively covariant (reflective of either organic matter preservation or dilution variability). The long-term decrease in Mo/TOC ratios observed throughout the Canol (also see Figs. 8 and 10a) is similar to that predicted by Algeo and Lyons, (2006) in their 'basin reservoir effect' based on modern analogues studies. To illustrate this long-term drawdown of aqueous Mo up-section in the plot, samples from each of the four zones are differentially colour-coded and the zone contact depths are highlighted. Finally, the covariation paths also document the onset of deepwater restriction and development of benthic anoxia between

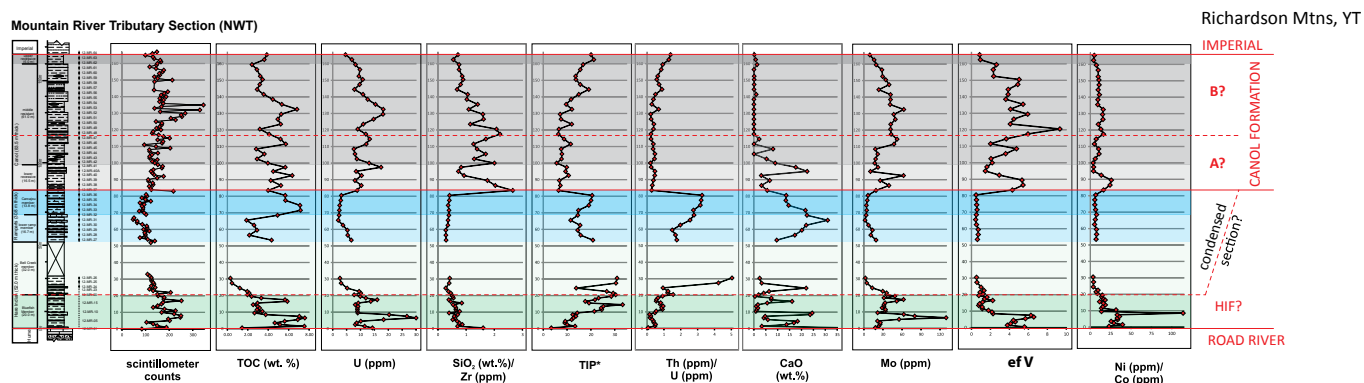


Figure 9. Horn River Group reference section in NWT (modified from Pyle *et al.*, 2014), with lithogeochemical profiles correlated to the north Yukon zonation. Note that only two of the Yukon Canol Formation zones appear to be represented to the east in NWT and the 'missing' Bell Creek Member and Ramparts Formation is potentially represented as a condensed section in Yukon.

the Road River and Canol Formation (blue to dashed-black path) and the return to oxic conditions of Imperial Formation deposition (yellow path). The onset of Imperial Formation deposition is also recorded in the uppermost Canol zone D, where the relatively consistent decrease in Mo/TOC ratio between 219 m and 246.5 m suggests increasing detrital terrigenous influx.

Terrigenous influx

Two lithogeochemical proxies were used to assess the degree of terrigenous influx during deposition of the Canol Formation: thorium concentration (positively correlated to clay volume – Ratcliffe *et al.*, 2010) and 'terrigenous input profile – TIP' (Hildred and Rice, 2012). The TIP was also used by Pyle *et al.* (2014) in their analysis of Northwest Territories' Devonian stratigraphy to illustrate the fluctuations in major oxides related to land-derived sediments. In this study, the TIP is the summed weight percent of Al_2O_3 , TiO_2 , K_2O and Na_2O (the Fe_2O_3 concentration is included by Pyle *et al.*, 2014, but is omitted here due to the perceived solubility and mobility of iron during sedimentation and diagenesis). Elements such as aluminium and titanium are commonly of detrital origin and are usually immobile during diagenesis (Tribovillard *et al.*, 2006). Figure 8 highlights the similarity in average Th (3.27 ppm at Trail River, 4.08 ppm in the Rich core) and TIP (6.33 wt % at Trail River, 7.16 wt % in the Rich core) concentrations between the two sections.

At Trail River, TIP values are very low throughout the Canol Formation, but increase significantly below the basal contact, over a 2.35 m thick package of rock that also

exhibits low SiO_2/Zr ratios. Here it is tentatively correlated to the Bluefish Member of the Hare Indian Formation (HIF; Fig. 9). High TIP values (relative to the overlying Canol Formation) are also characteristic of the Bluefish Member in the Mountain River Tributary reference section (Pyle *et al.*, 2014; Fig. 9). At the top of the Canol Formation in Trail River, a relatively sharp increase in TIP values marks the onset of siliclastic Imperial Formation deposition, although this progradational sequence (also observable in the sedimentary log – Fig. 6) appears less gradual than that observed in NWT. Thorium concentrations are seen to mirror the TIP trends at Trail River and suggest that any terrigenous material reaching this distal area of the basin is dominated by clay grade sediment only. Terrigenous influx proxies in the Rich core document the same trends; higher TIP and Th concentrations of the possible Bluefish Member are distinctly observed at the base of the section (Fig. 8). This corresponds to a drill core interval of relatively high silt contents and slightly lighter shades of grey colouration than the overlying Canol Formation. The higher average clastic influx proxies and serrated nature of the Rich core profiles are also suggestive of a closer depositional proximity to shoreline.

The TIP and thorium concentration profiles were used to zone the Canol Formation at Trail River into a dominant series of stacked, progradational (*i.e.*, increasingly more terrigenous up-section) sequences that are also defined by decreasing Mo/TOC ratios and Mo and U enrichment factors (Fig. 8). These sequences correlate to the section's sedimentary log where the nature of the sequence is characterized by gradual up-section increases

of siliceous shale proportion relative to chert. The four flooding surfaces, at the very base of the Canol and at approximately 90, 145 and 185 m, represent decreases in terrigenous influx, likely associated with relative sea-level rise which retrograde the submarine sediment delivery systems and result in a less restricted basin.

The sharpness of the kick in Th and TIP concentrations at the base of the Canol suggests that this flooding event may have been fairly rapid and may actually be a maximum flooding surface. This sequencing can be correlated to the

Rich core, where the progradational sequences are more distinctive but gradual. The sequences in zones B and C exhibit ‘reversed’ upper TIP and Th profiles relative to their correlative zones at Trail River. This is due to the presence of thinly laminated, wackestone turbidite packages, 1-3 m in thickness, that perhaps mark the distal representation of shoreline progradation in this area of the basin. These intervals also correspond to distinct peaks in the CaO/Al₂O₃ ratio at these horizons in the Rich core (see mineralogical results below).

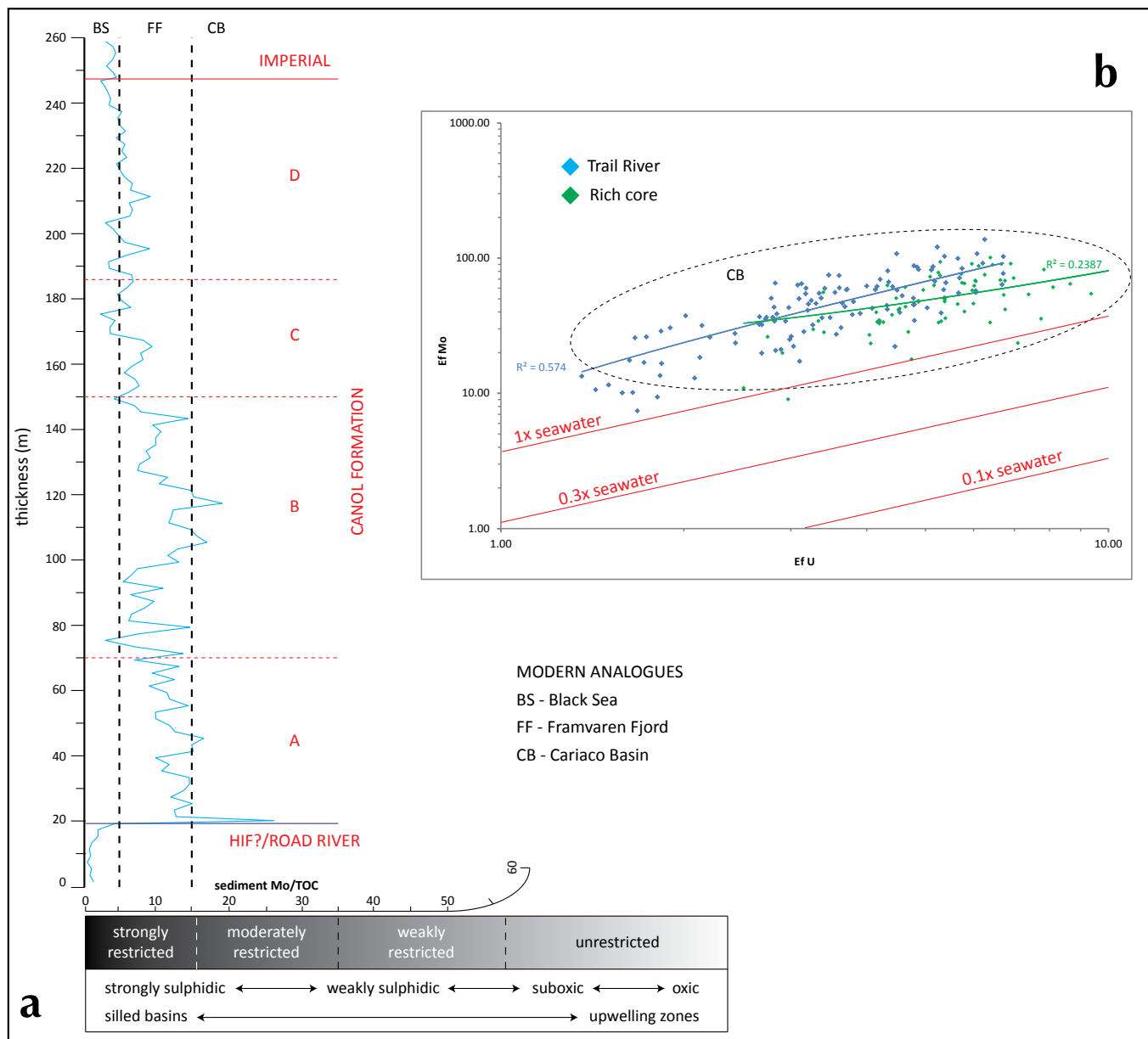


Figure 10. (a) Mo/TOC ratio profile from Trail River with superimposed zonation scheme from Figure 8. Palaeoredox, palaeohydrography and modern analogues from Algeo and Lyons (2006). (b) Mo and U enrichment factor (Ef) cross-plots and comparison to modern seawater molar ratios. Seawater trend lines and Cariaco Basin data cluster from Algeo and Tribouillard (2009).

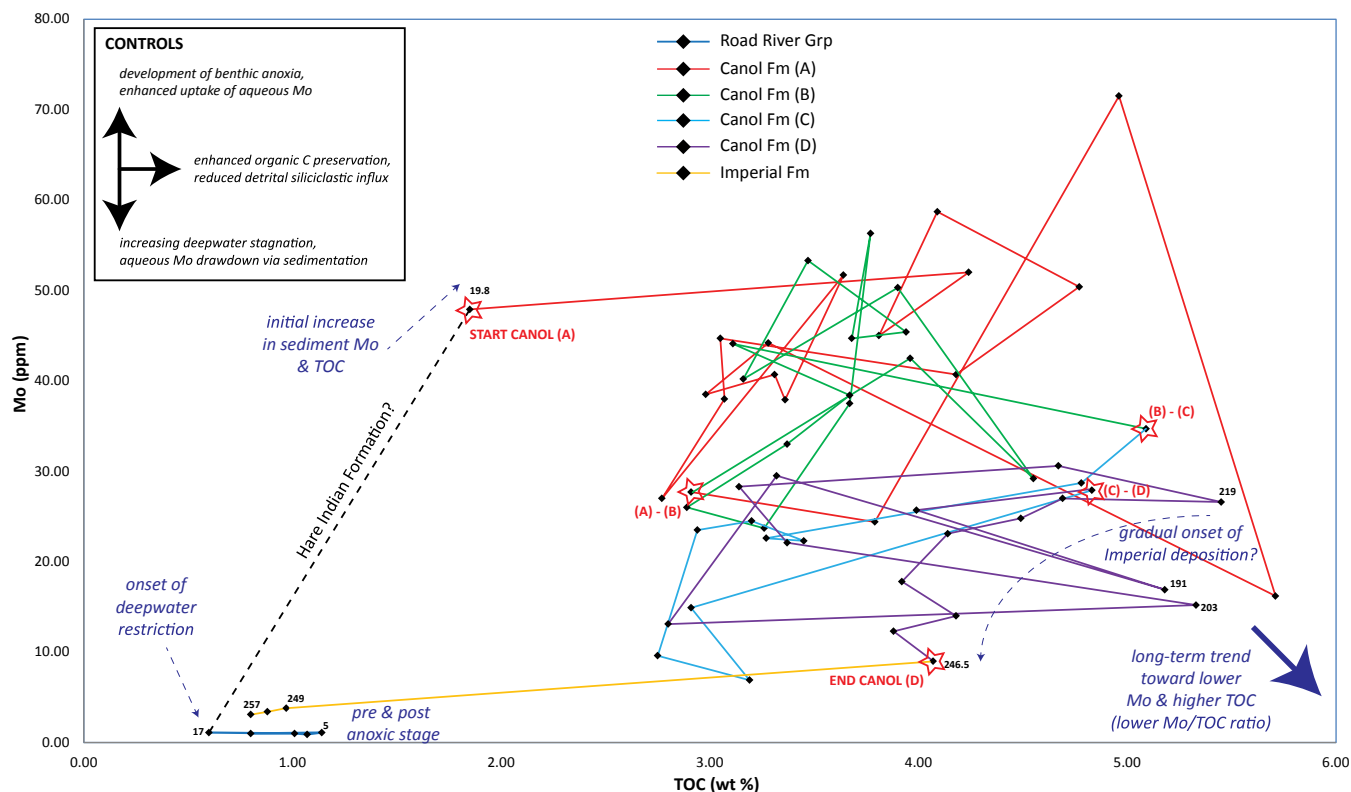


Figure 11. Mo/TOC covariance in the Canol Formation at Trail River. For clarity, sample points have been averaged using a three-point running average method and plotted every 12 m with key depths numbered. Starred depths highlight chemostratigraphic zonal changes. Note the onset and return from benthic anoxia in the Road River Group and Imperial Formation and the general trend towards lower Mo/TOC ratios throughout the Canol Formation zones. Interpreted controls from Algeo and Lyons (2006).

Silica origin

Although a brittle, silica-rich mineralogical composition is important for successful hydraulic fracturing in shales, the origin of the silica is also important to understand watermass chemistry and productivity (biogenic silica) and/or establishing palaeoshoreline proximity (terrestrially derived). The differentiation of detrital from biogenic silica is achieved by the use of silica (SiO_2) and zircon (Zr) cross-plots (Fig. 12). In these plots (e.g., as utilized by Hall *et al.*, 2013), biogenic silica is suggested by a shallow, negative SiO_2/Zr slope in contrast to terrestrially derived silica which exhibits a steeper, positive correlation. The Canol Formation SiO_2/Zr data from Trail River and the Rich core both delineate a shallow, negative trend indicative of biogenic silica enrichment. The Trail River data also show a stronger negative correlation ($R^2=0.56$) relative to the Rich core data ($R^2=0.03$); the less constrained Rich dataset suggesting a greater influence of terrestrially derived silica despite the presence of the negatively sloped trend (Fig. 12). The very high silica composition (averaging

83%) of the Trail River Canol Formation is supported both by facies proportions (siliceous shale comprises only 15% of the formation) and by XRD mineralogy results that indicate a quartz content average of 93% (Fraser and Hutchison, 2014).

In the litho-geochemical profiles for the two sections (Fig. 8), the high SiO_2/Zr ratio, suggestive of biogenic silica enrichment, is characteristically higher in the Canol Formation than the underlying Road River Group and overlying Imperial Formation shales. This is consistent with that observed by Pyle *et al.* (2014) at the Mountain River Tributary Canol Formation section in NWT, which displays the same prominent peaks in this ratio at the base of zone A and in zone B as Trail River and the Rich core (Figs. 8 and 9). The gradual decrease in SiO_2/Zr ratio up-section in zones A and B correlates well to both increasing TIP and decreasing Mo/TOC ratios that characterize these zones. There is no evident comparison between the upper Canol Formation in Trail River and the Mountain River Tributary sections, as the Trail River section is characterized by a

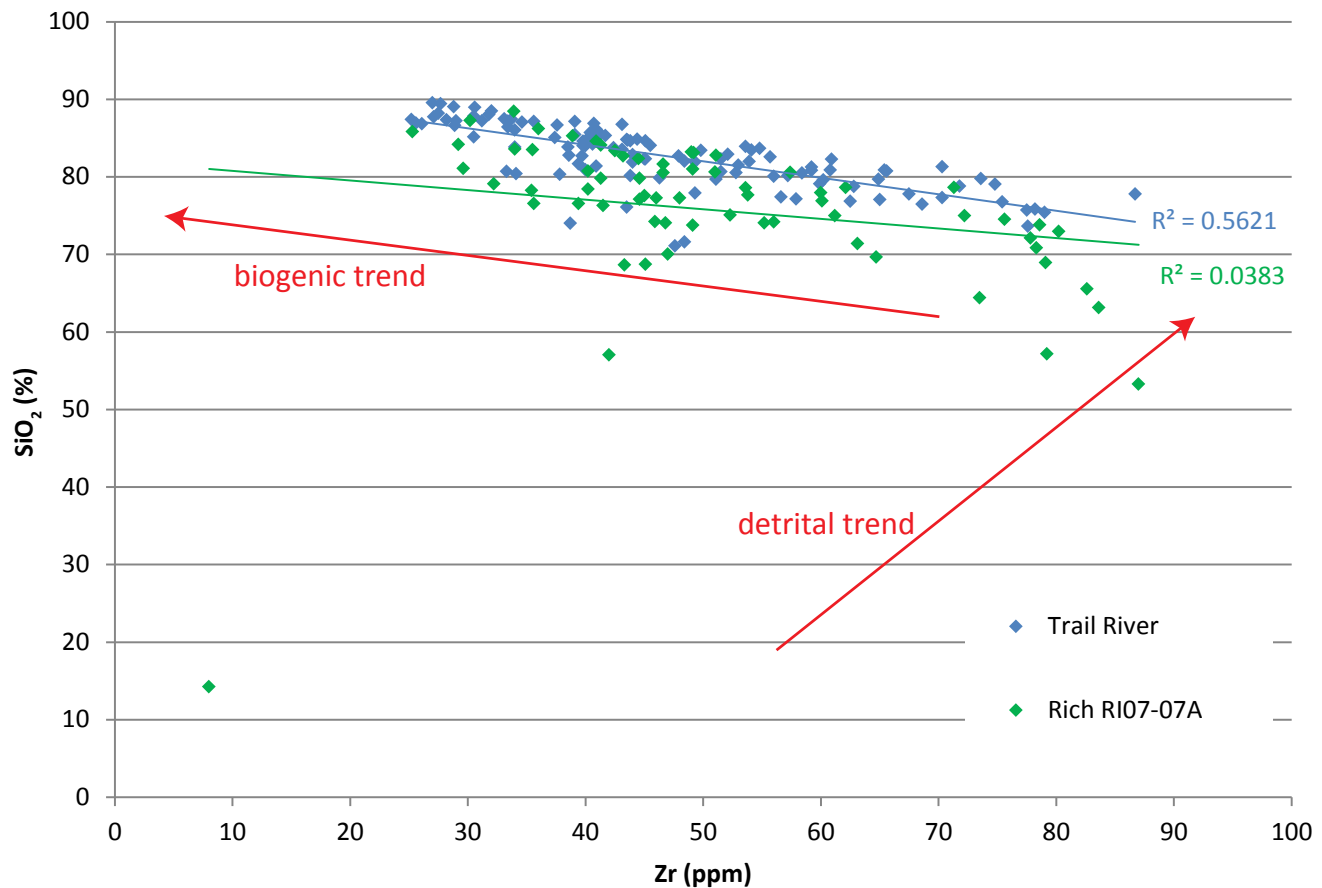


Figure 12. SiO_2/Zr cross-plot highlighting the dominance of biogenic silica in the Canol Formation.

return to biogenic silica enrichment up-section. In contrast, the Mountain River Tributary section documents a gradual, but punctuated, SiO_2/Zr ratio decrease (increase in terrestrially-derived silica) up-section into the Imperial Formation that corresponds to an overall coarsening-up (progradational) sequence in the sedimentological log.

The 20 cm interval sampling program across the Road River Group-Canol Formation contact zone at Trail River enabled a distinctive 2.35 m package of low SiO_2/Zr ratio sediments to be resolved, which is also observed below the basal Canol contact at 158.64 m in the Rich core (Fig. 8). A similar trend occurs below the Canol Formation in the NWT section, with low ratios in the Bluefish and Bell Creek members of the Hare Indian Formation (Pyle *et al.*, 2014; Fig. 9). Although these units are more likely to contain higher carbonate levels, owing to their eastern location nearer to the carbonate platform shoreline, it is

conceivable that their distal equivalents may be present to the west in Yukon. Black to dark grey, soft, non-calcareous shales with an elevated SGR signature observed in the uppermost 'Road River Group' at Trail River are similar to those described by Pyle *et al.* (2014) from the Bluefish Member in the western Mackenzie Valley.

Carbonate, phosphorus and barium

Carbonate-rich intervals can be identified using calcium oxide (CaO) concentrations in the geochemical dataset, although differentiation between bedded, diagenetic (concretionary) or fracture infill carbonates is not possible without sedimentological control from outcrop or core. $\text{CaO}/\text{Al}_2\text{O}_3$ ratios can also be used as a clay-carbonate proxy; an increase in this ratio infers increasing carbonate and decreasing clay contents (Ratcliffe *et al.*, 2010). The $\text{CaO}/\text{Al}_2\text{O}_3$ ratios presented in Figure 8

document very low carbonate concentrations relative to clay. This is supported by XRD mineralogy results of four samples taken from the Canol Formation at Trail River (at depths of 23, 138.5, 241 and 244-245 m) that contain no calcite or dolomite and an average of only 4% muscovite). The complete absence of carbonate and low overall formational CaO (averaging 0.13 wt % excluding concretionary outliers) from Trail River, is unexpected considering the fact that the up-dip and underlying depositional basement consists of carbonate-prone lithologies. The absence suggests that the carbonate platforms surrounding the former Richardson trough were also flooded, and that the location of Trail River in the resultant basin was too remote to experience erosion and transport of carbonate material down-dip from the western palaeoshoreline. Another possible contributing factor to this absence is that carbonate dissolution is promoted by acidic conditions associated with redox processes in high TOC facies (Ver Straeten *et al.*, 2011).

The CaO/Al₂O₃ ratio spikes in the Trail River profile are related primarily to logged areas of 'chemical precipitate' that is probably dolomite based on associated MgO and Fe₂O₃ spikes (e.g., at 197 m and 54-58 m) and the dolomitic concretionary lense in the upper Road River Group at approximately 17 m. The ratio spikes in the Rich core section at 67-70 m and 104-105 m are associated with carbonate turbidite units (Fig. 8), the presence of which further supports a more proximal location for the Rich area in the basin.

Barium, another proxy element linked to palaeoproductivity, has been documented by Tribovillard *et al.*, (2006) as being unreliable in organic-rich sediments that are typically present in high-productivity platforms. Therefore, barium will not be discussed further in a palaeoenvironmental context. However, highly-elevated barium concentrations, observed in the potential Bluefish Member in both sections, provide a stratigraphic marker horizon that will facilitate the differentiation of this member from the surrounding black shales of the Canol Formation and uppermost Road River Group in the field and in core/cuttings (Fig. 8).

DISCUSSION

STRATIGRAPHIC FRAMEWORK

The proposed chemostratigraphic zonation of the Canol Formation fits directly into a preliminary sequence stratigraphic framework. Each sequence is typically

characterized by:

- increasing facies proportions of siliceous shale relative to chert (suggestive of decreasing silica dilution as the basin becomes more restricted and productivity decreases);
- decreasing SiO₂/Zr ratios and TIP values (indicative of decreasing productivity and biogenic silica enrichment, and/or increasing influx of terrigenous material); and
- decreasing Mo/TOC ratios (suggestive of increasing basin restriction and euxinic palaeoredox conditions up-section that may enhance the preservation of organic matter).

The nature of the lithochemical and sedimentological sequences suggests the Canol Formation was dominantly deposited during sea-level highstand and the flooding event at the base of zone A is proposed as the maximum flooding surface for the section (Fig. 8). The long-term decrease in Mo/TOC ratios reflects the nature of these tracts, as the very slow to non-existent rates of relative sea-level change results in increasing restriction and less deepwater renewal through time. The sharpness of the basal Canol contact at Trail River and absence of the intervening NWT platform stratigraphy between Bluefish Member and Canol Formation (Fig. 9) is also suggestive of hardground development that marks the beginning of Canol depositional 'time'.

PALAEOHYDROGRAPHY

The chert lithofacies from Trail River is similar to chert rocks described by Bramlette (1946) from the Monterey Formation of California (although in this case the silica was diatomaceous in origin). During the Miocene, chert deposition was within a series of extensional, interconnected deep basins that were separated from nearby land, from each other and from the open ocean by relatively shallow and narrow seaways (*i.e.*, sills). Reed and Hollister (1936) hypothesized that the active faulting and associated volcanic activity at the beginning of the middle Miocene acted to disintegrate many of the major drainage systems, resulting in capture of sediment on land rather than distribution into the Monterey sea. In the deeper, restricted basins, this lack of terrigenous influx would have favoured the accumulation of highly organic-rich rocks by reducing organic matter dilution (e.g., Passey *et al.*, 2010). Finally, Bramlette (1946) concludes that the rates of accumulation of siliceous material required to

form such thick deposits as recorded in the Monterey (and potentially at the previously-noted anomalously thick Trail River section) was "not very much slower than the rate of accumulation of many clastic deposits".

In order to supply such a large volume of siliceous material to these basins, Bramlette (1946) hypothesises that, rather than *in situ* basinal changes in watermass chemistry favouring renewed episodes of productivity (e.g., as previously discussed when interpreting the chert lithofacies at Trail River), it was the drifting of these organisms in currents from the open ocean into coastal catchment areas of restricted water during transgressive episodes that allowed the accumulation of the thick chert deposits. However, the author offers no explanation as to the ultimate control on this drifting, and if this hypothesis is applied to the Canol Formation in north Yukon, both eustasy and tectonics may offer a competing influence. In this case, sea level rise enables greater circulation between basins and the open ocean by deepening the intervening shallow seaward sills, and faulting results in palaeobathymetric reorganization affecting ocean current patterns. The presence of siliceous shale, together with the varying degrees of lithofacies interbedding with chert at Trail River, suggests that whichever control is invoked, it was periodic to cyclical.

Reference to interpreted Phanerozoic sequences and short to intermediate-term Phanerozoic sea level cycles (e.g., Haq and Schutter, 2008) indicates that this periodic control was probably eustatically-driven. For example, there are 14 sequences recorded in the Givetian-Frasnian interval that correspond to 14 short-term cycles of sea-level change (Fig. 1). The lack of documented tectonic or volcanic activity in north Yukon during this time cautions against using Reed and Hollister's (1936) interpretation of drainage disruption to achieve this. It also adds further support for eustasy as the dominant control that allows periodic reconnection and renewal of restricted basin waters during deposition of the Canol. The use of the Mo-TOC sample-to-sample covariance path technique in association with radiocarbon-dating of sediments in modern basin cores also enabled variation seen in Mo/TOC ratios to be linked to significant palaeohydrographical events such as glacio-eustatic changes during the Holocene ice ages, or more recent anthropogenic sill dredging activities (Algeo and Lyons, 2006). It is therefore anticipated that with complete $\delta^{13}\text{C}$ -isotope profiles through these Canol sections (results pending), potential hydrographic variations interpreted in Mo-TOC covariance paths or in lithofacies distribution can be linked to well-

documented, global or local allogenic controls during the Middle-Late Devonian.

The degree of restriction indicated by the Canol Formation's Mo/TOC ratios is most similar to that recorded in the modern anoxic marine environment of the Framvaren Fjord (a 5-8 km² fjord in southern Norway with a total depth of 183 m and a sill depth of 2.5 m; Algeo and Lyons, 2006). Occasional transitions of this ratio to values similar to the less restricted Cariaco Basin of Venezuela (*i.e.*, between Trail River depths of 100-122 m, and initially at 19.8 m) or the more restricted Black Sea (typically between 170-205 m at Trail River) document variability in Canol basin palaeohydrography and its controls. Due to the very strong correlation coefficient ($R^2=0.9$) between Mo/TOC and deepwater renewal time (itself an indicator of basin restriction) derived from these modern analogue studies (Algeo and Lyons, 2006), together with their documented appropriateness for use in ancient basin systems (e.g., Algeo and Tribovillard, 2009), the Canol Formation average Mo/TOC can be used to estimate average deepwater renewal times in the basin. Renewal time estimates in the order of 100-1000 years (the ratio of 8.66×10^{-4} gives a specific value of 400 years) fall within the range of times modeled from modern sediments of both the Black Sea and Framvaren Fjord (Algeo and Lyons, 2006). These modern analogues also provide a means to cautiously estimate both sill/total depth and chemocline/total depth ratios, where the chemocline is the depth at which the water column becomes euxinic (*i.e.*, sulphidic). Data from Algeo and Lyons (2006) and references therein suggest sill depth/total depth ratios of 0.01-0.1 and chemocline depth/total depth ratios of 0.01-0.2 may be appropriate for use in reconstructing the basin's palaeohydrography in the vicinity of the Trail River section.

The Mo-TOC relationships described thus far have important implications for the use of Mo (and U, and therefore SGR) as a palaeoredox, and therefore TOC richness proxy, where SGR and Uxs data can be derived from either spectral gamma meter or lithochemical data. Examples of very weak positive correlation coefficients with TOC ($\text{Mo}=0.01$, $\text{SGR}_{\text{gamma}}=0.07$, $\text{Uxs}_{\text{gamma}}=0.08$ and $\text{Uxs}_{\text{chem}}=0.09$) suggest that although organic richness is often qualitatively linked to enriched Mo and U concentration (and therefore high SGR), the lack of any quantitative correlation means that such comparisons should be viewed with extreme caution. In addition, the fact that the calculated SGR value also comprises contributions from potassium and thorium (commonly associated with detrital influx and therefore

expected to be inversely correlated to TOC) suggests that it is not actually possible to achieve a strong SGR-TOC correlation.

The very weak Mo and Uxs-TOC coefficients are also reflective of the non-linear relationship between Mo, U and TOC recorded in modern seawater from anoxic marine basins and provide support for interpreting a euxinic, restricted depositional system (Algeo and Tribovillard, 2009; Tribovillard *et al.*, 2006; Algeo and Lyons, 2006). In terms of Mo concentrations preserved in ancient sediments, the amount of Mo taken up under anoxic conditions is dependent not only on the concentration of organic matter (*i.e.*, host availability), but also on the concentration of aqueous Mo in the water column (*i.e.*, source ion availability). In euxinic, silled basins such as that proposed during Canol deposition, the rate of Mo removal typically exceeds the rate of resupply via deepwater renewal events leading to reduced aqueous Mo availability and subsequent reduced Mo uptake by sediment per unit organic matter (termed 'basin reservoir effect' by Algeo and Lyons, 2006).

IMPLICATIONS FOR PETROLEUM POTENTIAL

The understanding of palaeoredox conditions is a key component to successfully identifying source rock and shale reservoir potential since high total organic carbon (TOC) values are only typically found in sediments where bottom conditions were anoxic (Ratcliffe *et al.*, 2012a). In this study, the presence of dark grey to black, siliceous shales and chert, together with elevated TOC contents and Mo, U and V enrichment in the Canol Formation (relative to the Road River Group and Imperial Formation) is strongly suggestive of oxygen-depleted bottom waters. In addition, the absence of a strong correlation between Mo and TOC is further suggestive of restricted, euxinic basin conditions, and this was supported by Algeo and Lyons' (2006) conclusions that Mo uptake in the sediment is controlled primarily by the degree of watermass restriction rather than the organic richness of the sediment. In the case of the Canol Formation, this is seen when basin restriction is predicted to increase up-section following maximum flooding at its basal contact as Mo concentration decreases but TOC contents remain consistently high. Where basin restriction is initially suspected from outcrop distribution maps, and then corroborated by Mo/TOC data, the actual prediction of organic richness from redox sensitive elements cannot, therefore, be performed with any degree of quantitative accuracy. The best method for modelling TOC in such a

basin is still considered to be a combination of lithofacies analysis and interpretation, using the tripartite controls outlined by Passey *et al.* (2010) with TOC data measured directly from the rock (*e.g.*, by Rock-Eval).

The lithogeochemical dataset can provide information such as biogenic silica enrichment and potential mineralogical composition without the initial requirement for costly XRD analysis. The recognition of zones with high biogenic silica is critical to determine reservoir quality in shales, as it affects porosity, brittleness and log response during well analysis (Ratcliffe *et al.*, 2012b). Very high silica concentrations, such as found in the chert lithofacies in Trail River, may result in low porosities, especially if the specific organic richness of this facies is found to be diluted by radiolarian test material during intervals of high productivity.

In a compilation of 'ideal' shale reservoir characteristics, based largely on the 'Magnificent Seven' shale plays in North America, brittle mineral content (*i.e.*, proxied by SiO₂ and CaO) should be greater than 40% (but can be less if the silica is of biogenic origin) with corresponding porosities of greater than 2% (Zou, 2013; Passey *et al.*, 2010; Blood *et al.*, 2013). Preliminary porosity results from a chert plug sample taken from the Trail River section at 23.3 m in Canol Formation zone A and Rich core samples taken from 45.9, 84.1 and 88.3 m give a maximum porosity of 1% and an average value of 0.9% (AGAT, 2014), both of which are less than the 'ideal' minimum of producing shale plays. The same list of characteristics also suggests that clay mineral content should be less than 30-50% of the rock composition (Zou, 2013). XRD studies in the Canol from Trail River document average quartz contents of 93%, which indicates that the minor clay composition of the Canol Formation is also atypical when compared to known producing shale plays in North America. It is likely that more conducive properties for shale reservoir exploitation may be found closer to the basin margins where the degree of restriction and its effects were less marked.

RECOMMENDATIONS FOR FURTHER WORK

Field and core/cuttings studies

This study of the Canol Formation focuses on one core section and just one outcrop section, albeit the best exposed and most complete located by the Yukon Geological Survey in north Yukon. Its findings are therefore accurate to the best interpretation of the data collected, but interpreted palaeohydrographic

reconstructions must be viewed as a preliminary basis from which to build from in future work. Systematic lithogeochemical data, hopefully tied to $\delta^{13}\text{C}$ isotope profiles, are considered the most flexible and chrono-allostratigraphically relevant data with which to establish both long and short-term depositional controls and assess basin palaeohydrography in the upper Palaeozoic of north Yukon. As such, the primary recommendation for further work is to continue to construct a geo-referenced Canol Formation lithogeochemical database from all visited outcrops, 'Nick' zone exploration diamond drill cores and oil and gas well cuttings/core from north Yukon. The increase in data density will subsequently allow for a more 'grounded' constraint of Middle to Late Devonian palaeogeography than the preliminary interpretation provided herein.

High resolution TOC-lithofacies analysis

The low variability in organic richness between facies, as demonstrated in Table 2, is expected from a limited spectrum of deep-water sediments, although lower average TOC values were expected from the chert facies due to the potential aforementioned dilution effects. The technique of continuous interval sampling is likely to homogenise TOC contents for each 2 m section, however, and it is therefore still unclear as to whether a specific relationship exists between silica-dilution levels and TOC contents (Hutchison and Fraser, 2014). High resolution, point sampling on a bed-to-bed scale would facilitate this investigation (similar 'microhorizon' work has been carried out on the Upper Devonian Torquay Formation of southeastern Saskatchewan to determine kerogen types – Wielgoz and Bend, 2014). Such a study is recommended in the Canol Formation as a focus for further targeted work, as it has profound implications for reservoir volume estimations (Fig. 13).

Analogue comparisons

Reconstruction data, such as ratios of sill/total depth and chemocline/total depth derived from modern restricted basin analogues, are exceptionally useful in their ability to facilitate constraint of the basin palaeohydrography during Canol Formation deposition. Algeo and Lyons (2006) and Algeo and Tribouillard (2009) demonstrate that watermass restriction and the chemical attributes that define it are relatively independent of such factors as basin scale, climatic setting or run-off/discharge rates. More significantly, they are similar over geological time: ancient shale basins of the Late Devonian Seaway give

predictable results when analyzed with modern analogue data due to their well-documented basinal configuration. The north Yukon basin where Canol Formation sediments were deposited is interconnected within the Late Devonian Seaway to other major North American shale plays (e.g., the Chattanooga Shale and Ohio Shale of the Southern Appalachian Basin) that form within bathymetric depressions along this marine corridor (Fig. 14). These ancient analogues also have the advantage of vastly increased density of data due to their previous exploitation history, and as such, lithogeochemical trends and their controls, interpreted here, are likely to help 'bridge' interpretation gaps in the comparatively disparate north Yukon dataset.

CONCLUSIONS

The Canol Formation in the Richardson Mountains is a resistant shale sequence that is characterized by rhythmically bedded siliceous shale and chert. These facies exhibit characteristics indicative of deposition in a deep water, quiescent environment. Oxygen-depleted bottom waters (supported by Mo, U and V enrichment) resulted in ideal conditions for the preservation of organic matter, and dilution by terrigenous clastic influx was minimal. The key control on facies variability between the two end-members at Trail River was fluctuating palaeoproductivity, and variation in water chemistry (due to periodic deepwater renewal) was anticipated to result in the pervasive dilution of organic matter via reprecipitation of siliceous radiolarian material, despite bulk-sample TOC concentrations remaining relatively constant (averaging 4.3%) during Canol deposition. This silica enrichment also appears to result in low porosities (averaging 0.9%), which are lower than those of 'ideal' producing shale plays in North America (>2%). The 2 m interval homogenized sampling program resulted in an unclear silica enrichment-TOC relationship at the individual facies level, and further high-resolution sampling is suggested to test this dilution-effect hypothesis.

A chemostratigraphic analysis of the Formation at Trail River (east Richardson Mountains) highlighted four distinct zones (A-D) that were successfully correlated to the Rich property drill core section on the western side of the Richardson Mountains. These zones were characterised by chemostratigraphic up-section profiles of: decreasing biogenic silica enrichment indicative of decreasing productivity, together with slightly increasing terrestrial influx profiles (TIPs), decreasing redox-

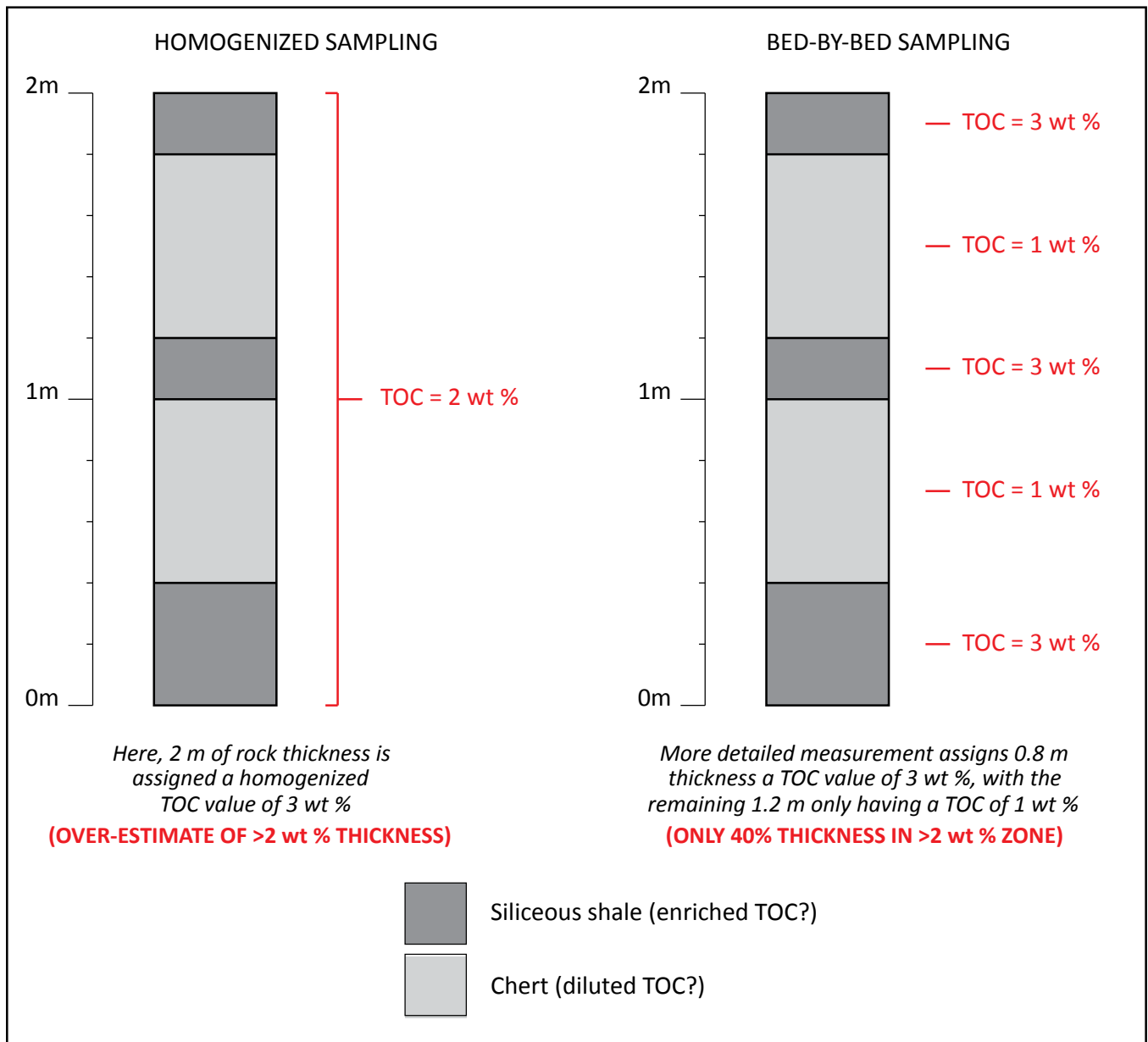


Figure 13. Implications for shale reservoir volume when using TOC percentages from homogenized 2 m sample intervals (assuming that TOC contents in the chert facies are biogenic silica-diluted).

sensitive trace element (Mo, U and V) enrichments factors and decreasing Mo/TOC ratios. Both section's chemostratigraphic profiles suggested the first evidence for the Bluefish Member of the Hare Indian Formation underlying the Canol Formation in the Richardson Mountains.

Distal carbonate turbidites recorded at the tops of Canol zones B and C in the Rich core, together with a greater degree of profile variability up-section, suggest

a more proximal location in the basin compared with Trail River. These zones were also successfully correlated to parasequences interpreted from the respective sedimentary logs where the siliceous shale facies increases in proportion up-section relative to chert. The nature of change of all key profiles listed above is consistent with relative sea-level fall resulting in an increasingly restricted basin. This observation enabled the construction of a preliminary sequence stratigraphic framework for the Formation. This consisted of a flooding surface marking

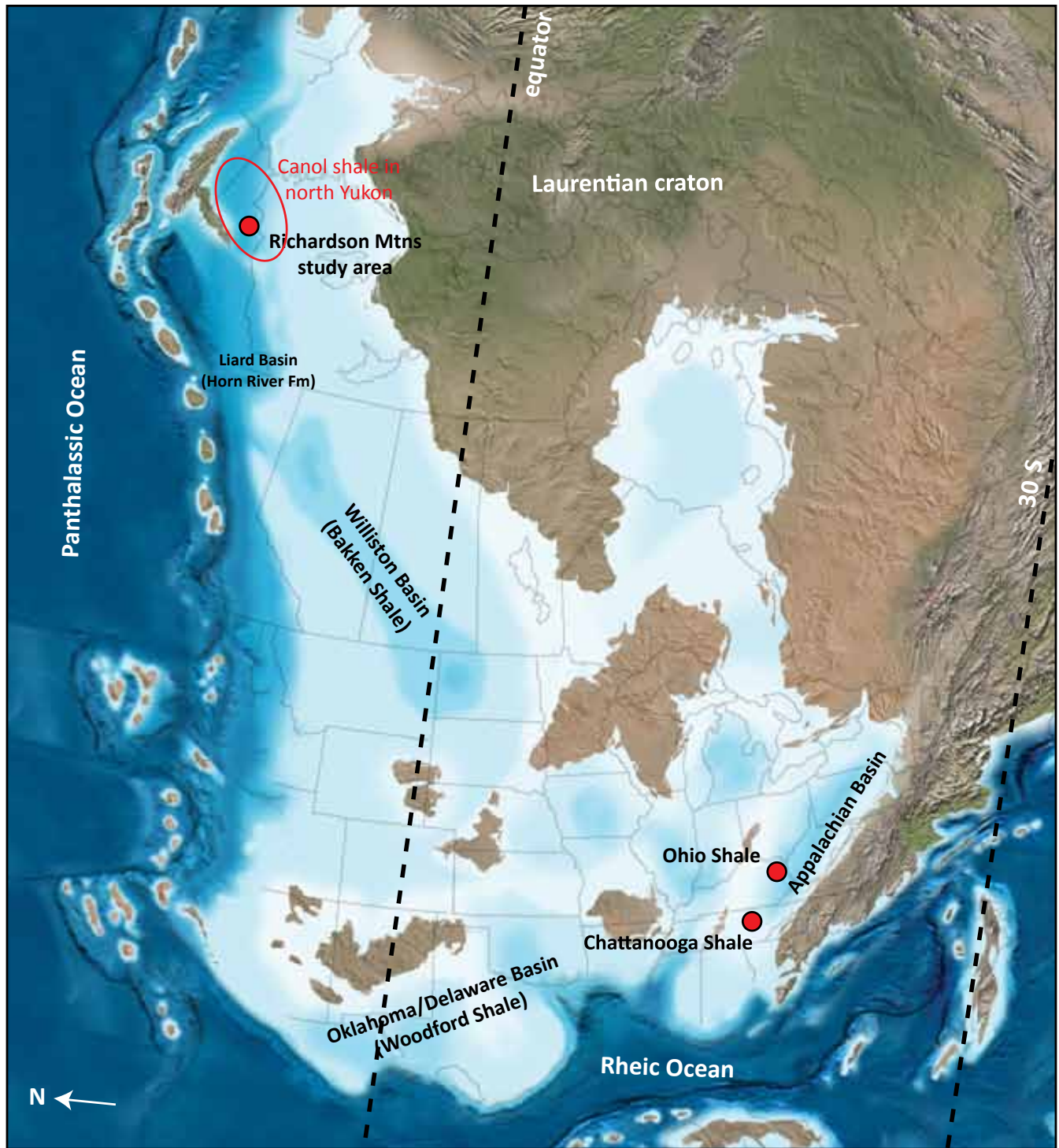


Figure 14. Palaeogeography of the Late Devonian Seaway of North America (base map from Blakey, 2014), with the Richardson Mountains study area, north Yukon Canol basin and its closest analogues based on EfMo-EfU covariance (the Chattanooga and Ohio shales) highlighted. US basin locations from Algeo and Tribovillard (2009).

the base of the Canol and deposition of the formation occurring during long-term sea-level highstand. Eustatic variability operating on both long and short-term frequencies was invoked as the primary allogenic control on these sequences.

On average, low Mo/TOC ratios for the Canol Formation were indicative of a silled, restricted basin with euxinic (sulphidic) deepwater. Relatively high Mo/TOC in the lower Canol zones (A and B) suggest that the basin was less restricted during early Canol Formation, but became more so up-section. Comparison to similarly restricted modern basin analogues (e.g., Framvaren Fjord in Norway and the Cariaco Basin in Venezuela) has constrained preliminary reconstructions of basin palaeohydrography. The pervasive presence of biogenically enriched siliceous facies (e.g., chert) was also recognized from the Monterey Formation of California, where interconnected basins were interpreted to be restricted and shallow-silled. Due to the fact that Mo concentration decreases relative to TOC under increasing restriction (a process supported in this study by very weak Mo-TOC and Uxs-TOC correlation coefficients), caution should be used when using redox-sensitive trace elements to predict TOC in north Yukon basins characterized by this inferred palaeohydrography.

ACKNOWLEDGEMENTS

Trans North Helicopters Ltd. is thanked for safe and competent flying during summer fieldwork. Eagle Plains Lodge are also thanked for provision of accommodation, both inside and out. Marisa Hindemith, Patrick Sack, Monica Nordling and Tammy Allen provided field assistance. Don Murphy, Patrick Sack, Fil Ferri, Luke Beranek, Thomas Hadlari and Leanne Pyle are thanked for thought-provoking and informative discussions on the Canol Formation that led to some of the research presented here. The paper was greatly improved thanks to Don Murphy's critical review.

REFERENCES

Adams, J.A. and Weaver, C.E., 1958. Thorium-to-uranium ratios as indicators of sedimentary processes: Example of concept of geochemical facies. *American Association of Petroleum Geologists Bulletin*, vol. 42, p. 387-430.

AGAT, 2014. Final core analysis report – miscellaneous outcrop samples 14-TF-001 Trail River and 14-TF-RI07-07A Rich Property. AGAT Laboratories Ltd., Report number RC31215.

Algeo, T.J. and Lyons, T.W., 2006. Mo-total organic carbon covariation in modern anoxic marine environments: Implications for analysis of paleoredox and paleohydrographic conditions. *Paleoceanography*, vol. 21, PA1016, p. 1-23.

Algeo, T.J. and Tribovillard, N., 2009. Environmental analysis of paleoceanographic systems based on molybdenum-uranium covariation. *Chemical Geology*, vol. 268, p. 211-225.

Balgord, E.A., Mahoney, J.B., Hooper, R.L. and Groat, L., 2009. Examining the genesis of the Middle Devonian NiMo deposit, Selwyn Basin, Yukon. *In: Cordilleran Roundup 2009*, poster presentation.

Blakey, R., 2014. Colorado Plateau Geosystems website – Paleogeography and Geologic Evolution of North America (Late Devonian 360Ma map), <<http://cpgeosystems.com/namD360.jpg>> (accessed December 12, 2014).

Bohacs, K.M., Grabowski Jr., G.J., Carroll, A.R., Mankiewicz, P.J., Miskell-Gerhardt, K., Schwalbach, J.R., Wegner, M.B. and Simo, J.A., 2005. Production, Destruction, and Dilution – The Many Paths to Source-Rock Development. *In: Deposition of Organic-Carbon-Rich Sediments: Models*, N.B. Harris (ed.), Society for Sedimentary Geology, Special Publication, no. 82, p. 61-101.

Blood, R., Lash, G. and Bridges, L., 2013. Biogenic silica in the Devonian shale succession of the Appalachian Basin, USA. *In: Search and Discovery Article #50864* (2013), American Association of Petroleum Geologists 2013 Annual Convention and Exhibition, 19-22 May 2013, Pittsburgh, USA.

Bramlette, M.N., 1946. The Monterey Formation of California and the origin of its siliceous rocks. United States Geological Survey, Professional Paper 212, 57 p.

Brocculeri, T. and Foos, A.M., 1987. Depositional environment and early diagenetic controls on mineralogy of Kittanning Formation, Allegheny Group, eastern Ohio. *In: Search and Discovery Article #91041* (1987), American Association of Petroleum Geologists 1987 Eastern Section Meeting, 7-10 October 1987, Columbus, USA.

Campbell, R.B., 1967. Geology of Glenlyon map-area, Yukon Territory (105L). Geological Survey of Canada, Memoir 352, p. 1-92.

- Cohen, K.M., Finney, S.C., Gibbard, S.L. and Fan, J-X., 2013. The ICS International Chronostratigraphic Chart. Episodes, vol. 36, p. 199-204.
- Dolby, G., 2013. Palynological analysis of 22 outcrop samples from the 2013 Yukon field season. Internal Yukon Geological Survey report.
- Fraser, T.A., 2014. Field descriptions of the Middle-Upper Devonian Canol Formation on Trail River, east Richardson Mountains, Yukon. *In: Yukon Exploration and Geology 2013*, K.E. MacFarlane, M.G. Nordling and P.J. Sack (eds.), Yukon Geological Survey, p. 53-68.
- Fraser, T.A. and Hutchison, M.P., 2014. Petroleum potential of the Middle-Upper Devonian Canol Formation in north Yukon: report on field investigations in 2013. Poster presentation, Canadian Society of Petroleum Geologists 2014 GeoConvention, 12-14 May 2014, Calgary, Canada.
- Fraser, T.A., Allen, T.L., Lane, L.S. and Reyes, J.C., 2012. Shale gas potential of Devonian shale in north Yukon: Results from a diamond drillhole study in western Richardson Mountains. *In: Yukon Exploration and Geology 2011*, K.E. MacFarlane and P.J. Sack (eds.), Yukon Geological Survey, p. 45-74.
- Fraser, T.A., Hutchison, M.P., Murphy, D.C., Sack, P.J., Beranek, L. and Hadlari, T., 2014. Characterizing Devonian-Carboniferous stratigraphy at the Nick Property, Wernecke Mountains. Poster Presentation at 2014 Yukon Geoscience Forum, 15-19 November 2014, Whitehorse, Canada.
- Gal, L.P., Allen, T.L., Hadlari, T. and Zantvoort, W.G., 2009. Chapter 10 – Petroleum Systems Elements. *In: Regional Geoscience Studies and Petroleum Potential, Peel Plateau and Plain, Northwest Territories and Yukon: Project Volume*, L.J. Pyle and A.L. Jones (eds.), Northwest Territories Geoscience Office and Yukon Geological Survey, NWT Open File 2009-02 and YGS Open File 2009-25, p. 477-549.
- Goodfellow, W.D., Geldsetzer, H., Gregoire, C., Orchard, M. and Cordey, F., 2010. TGI-3 Workshop: Public geoscience in support of base metal exploration programme and abstracts. Geological Association of Canada, Cordilleran Section 2010, p. 15-18.
- Gordey, S.P. and Makepeace, A.J. (comps.), 2003. Yukon digital geology, v. 2.0. Geological Survey of Canada Open File D1749 and YGS Open file 2003-9(D), 2 CD-ROMs.
- Hall, C.D., Jennings, D. and Miller, R., 2011. Comparison of the reservoir properties of the Muskwa (Horn River Formation) with other North American gas shales. *In: Canadian Society of Petroleum Geologists, Canadian Society of Exploration Geophysicists, Canadian Well Logging Society Convention 2011*, Calgary, Canada, online abstract (www.cspg.org/cspg/Conferences/Geoconvention/2011_Abstract_Archives.aspx).
- Hall, D., Sterner, M. and Shukla, R., 2013. Application of cuttings gas/oil analysis, rapid XRF and high-resolution photography to reservoir evaluation. *World Oil*, April 2013, p. 163-168.
- Haq, B.U. and Schutter, S.R., 2008. A chronology of Paleozoic sea-level changes. *Science*, vol. 322, p. 64-68.
- Hildred, G.V. and Rice, C., 2012. Using high resolution chemostratigraphy to determine well-bore pathways in multilateral drilling campaigns: an example from the Horn River Formation, British Columbia, Canada. *In: Canadian Society of Petroleum Geologists 2012 GeoConvention, May 2012*, Calgary, Canada, online abstract (cseg.ca/resources/2012-conference-abstracts-a-to-l).
- Hulbert, L.J., Gregoire, D.C., Paktunc, D. and Carne, R.C., 1992. Sedimentary nickel, zinc and platinum-group element mineralization in Devonian black shales at the Nick Property, Yukon, Canada: a new deposit type. *Exploration Mining Geology*, vol. 1, p. 39-62.
- Hutchison, M.P., 2014. The sedimentological and petrophysical characterisation of dryland mudstones. Unpublished PhD Thesis, University of Aberdeen, Aberdeen, UK, 211 p.
- Hutchison, M.P. and Fraser, T.A., 2014. North Yukon Upper Palaeozoic Shale Project – 2014 update. Poster Presentation at 2014 Yukon Geoscience Forum, 15-19 November 2014, Whitehorse, Canada.
- Ingram, R.L., 1953. Fissility of mudrocks. *Geological Society of America, Bulletin*, vol. 64, p. 869-878.
- Jackson, D.E. and Norford, B.S., 2004. Biostratigraphical and ecostratigraphical significance of Tremadoc (Ordovician) graptolite faunas from the Misty Creek Embayment and Selwyn Basin in Yukon and Northwest Territories. *Canadian Journal of Earth Science*, vol. 41, p. 331-348.

- Katz, B.J., 2005. Controlling Factors on Source Rock Development – A Review of Productivity, Preservation, and Sedimentation Rate. *In: Deposition of Organic-Carbon-Rich Sediments: Models*, N.B. Harris (ed.), Society for Sedimentary Geology, Special Publication, vol. 82, p. 7-16.
- Large, R.R., Halpin, J.A., Danyushevsky, L.V., Maslennikov, V.V., Bull, S.W., Long, J.A., Gregory, D.D., Lounejeva, E., Lyons, T.W., Sack, P.J., McGoldrick, P.J. and Calver, C.R., 2014. Trace element content of sedimentary pyrite as a new proxy for deep-time ocean-atmosphere evolution. *Earth and Planetary Science Letters*, vol. 389, p. 209-220.
- Morgans-Bell, H.S., Coe, A.L., Hesselbo, S.P., Jenkyns, H.C., Weedon, G.P., Marshall, J.E.A., Tyson, R.V. and Williams, C.J., 2001. Integrated stratigraphy of the Kimmeridge Clay Formation (Upper Jurassic) based on exposures and boreholes in south Dorset, UK. *Geological Magazine*, vol. 138, p. 511-539.
- Myers, K.J. and Wignall, P.B., 1987. Understanding Jurassic organic-rich mudrocks – new concepts using gamma spectrometry and palaeoecology: examples from the Kimmeridge Clay of Dorset and the Jet Rock of Yorkshire. *In: Marine and clastic sedimentology: new developments and concepts*, J.K. Leggett (ed.), p. 172-189.
- Norris, A.W., 1968. Reconnaissance Devonian stratigraphy of northern Yukon Territory and northwestern District of Mackenzie (Operation Porcupine area). *Geological Survey of Canada, Memoir*, vol. 410, p. 1-81.
- Norris, A.W. 1985. Stratigraphy of Devonian outcrop belts in northern Yukon Territory and northwestern District of Mackenzie (Operation Porcupine area). *Geological Survey of Canada, Memoir* 410, 81 p.
- Passey, Q.R., Bohacs, K.M., Esch, W.L., Klimentidis, R. and Sinha, S., 2010. From oil-prone source rock to gas-producing shale reservoir – geological and petrophysical characterization of unconventional shale-gas reservoirs. Society of Petroleum Engineers, CPS/SPE International Oil and Gas Conference and Exhibition, Beijing, China, 8-10 June 2010, SPE 131350, p. 1-29.
- Pigage, L., 2007. Yukon Stratigraphic Correlation Chart, v. 3.0. Yukon Geological Survey and Oil and Gas Management Branch, YGS Open File 2007-2.
- Pugh, D.C., 1983. Pre-Mesozoic geology in the subsurface of Peel River map area, Yukon Territory and District of Mackenzie. *Geological Survey of Canada, Memoir*, vol. 401, p. 1-61.
- Pyle, L.J., Gal, L.P. and Fiess, K.M., 2014. Devonian Horn River Group: A reference section, lithogeochemical characterization, correlation of measured sections and wells, and petroleum-potential data, Mackenzie Plain area (NTS 95M, 95N, 96C, 96D, 96E, 106H, and 106I), NWT. Northwest Territories Geoscience Office, Open File 2014-06, p. 1-70.
- Raiswell, R. and Fisher, Q.J., 2000. Mudrock-hosted carbonate concretions: a review of growth mechanisms and their influence on chemical and isotopic composition. *Journal of the Geological Society of London*, vol. 157, p. 239-251.
- Ratcliffe, K.T., Wright, A.M. and Schmidt, K., 2010. Application of inorganic whole-rock geochemistry to shale resource plays: an example from the Eagle Ford Shale Formation, Texas. *Society for Sedimentary Geology, The Sedimentary Record*, June 2012, p. 4-9.
- Ratcliffe, K.T., Wright, A.M. and Spain, D., 2012a. Unconventional methods for unconventional plays: using elemental data to understand shale resource plays – Part 1. *Petroleum Exploration Society of Australia, News Resources*, February/March 2012, p. 89-93.
- Ratcliffe, K.T., Wright, A.M. and Spain, D., 2012b. Unconventional methods for unconventional plays: using elemental data to understand shale resource plays – Part 2. *Petroleum Exploration Society of Australia, News Resources*, March/April 2012, p. 89-93.
- Reed, R.D. and Hollister, J.S., 1936. Structural evolution of southern California. *American Association of Petroleum Geologists Bulletin*, vol. 20, p. 1693-1704.
- Rider, M., 2002. *The Geological Interpretation of Well Logs*, 2nd Edition. Rider-French Consulting, Sutherland, UK, 290 p.
- Rimmer, S.M., 2003. Geochemical paleoredox indicators in Devonian-Mississippian black shales, Central Appalachian Basin (USA). *Chemical Geology*, vol. 206, p. 373-391.
- Scotchman, I.C., 1989. Diagenesis of the Kimmeridge Clay Formation, onshore UK. *Journal of the Geological Society of London*, vol. 146, p. 285-303.

- Scotchman, I.C., 1991. The geochemistry of concretions from the Kimmeridge Clay Formation of southern and eastern England. *Sedimentology*, vol. 38, p. 79-106.
- Tribovillard, N., Algeo, T.J., Lyons, T. and Riboulleau, A., 2006. Trace metals as paleoredox and paleoproductivity proxies: An update. *Chemical Geology*, vol. 232, p. 12-32.
- Tyson, R.V., 2005. The "Productivity Versus Preservation" Controversy: Cause, Flaws, and Resolution. *In: Deposition of Organic-Carbon-Rich Sediments: Models*, N.B. Harris (ed.), Society for Sedimentary Geology, Special Publication, vol. 82, p. 17-33.
- Van Kooten, G.K., Watts, A.B., Coogan, J., Mount, V.S., Swenson, R.F., Daggett, P.H., Clough, J.G., Roberts, C.T. and Bergman, S.C., 1997. Geologic investigations of the Kandik area, Alaska and adjacent Yukon Territory, Canada. Alaska Division of Geological and Geophysical Surveys, Report of Investigations 96-6a, sheet 1 of 3.
- Ver Straeten, C.A., Brett, C.E. and Sageman, B.B., 2011. Mudrock sequence stratigraphy: a multi-proxy (sedimentological, paleobiological and geochemical) approach, Devonian Appalachian Basin. *Palaeogeography, Palaeoclimatology, Palaeoecology*, vol. 304, p. 54-73.
- Weaver, C.E., 1989. Clays, muds and shales. *Developments in Sedimentology*, vol. 44, p. 1-819.
- Wielgoz, N.T. and Bend, S.L., 2014. Petroleum source rock analysis of the Upper Devonian Torquay Formation of south eastern Saskatchewan. *In: Canadian Society of Petroleum Geologists 2014 GeoConvention*, 12-14 May 2012, Calgary, Canada, online abstract, www.cspg.org/cspg/Conferences/Geoconvention/2014_GeoConvention.aspx
- Witkowska, M., 2012. Palaeoenvironmental significance of iron carbonate concretions from the Bathonian (Middle Jurassic) ore-bearing clays at Gnaszyn, Kraków-Silesia Homocline, Poland. *Acta Geologica Polonica*, vol. 62, p. 307-324.
- Zou, C., 2013. *Unconventional Petroleum Geology*. Elsevier, San Diego, USA, 373 p.

The Bear Creek assemblage: A latest Triassic volcano-sedimentary succession in southwest Yukon

S. Israel, M. Colpron
Yukon Geological Survey

J. Cubley
Yukon College

D. Moynihan, D.C. Murphy, C. Relf
Yukon Geological Survey

Israel, S., Colpron, M., Cubley, J., Moynihan, D., Murphy, D.C. and Relf, C., 2015. The Bear Creek assemblage: A latest Triassic volcano-sedimentary succession in southwest Yukon. *In: Yukon Exploration and Geology 2014*, K.E. MacFarlane, M.G. Nordling and P.J. Sack (eds.), Yukon Geological Survey, p. 99-112.

ABSTRACT

The bedrock geology in the Mount Decoeli area of southwest Yukon is characterized by Paleozoic to Triassic stratigraphy of the Alexander terrane, Wrangellia and the Bear Creek assemblage, overlain and intruded by Jurassic and younger rocks. Alexander terrane rocks comprise mainly Devonian mafic to intermediate volcanic and volcanoclastic rocks overlain by thick successions of carbonate and phyllite. Wrangellia is characterized by Mississippian to Permian volcanic and siliciclastic rocks of the Station Creek and Hasen Creek formations, overlain by Upper Triassic basalts and calcareous rocks of the Nikolai and McCarthy formations respectively. The Alexander terrane and Wrangellia are separated by the Duke River fault, a mainly Late Cretaceous northeast-verging thrust fault. To the northeast, Wrangellia is separated from the Bear Creek assemblage by the Denali fault, a strike-slip fault with as much as 400 km of right-lateral motion.

The Bear Creek assemblage comprises metamorphosed and deformed siltstone, mudstone and sandstone interlayered with mafic to intermediate volcanic and volcanoclastic rocks. Preliminary ages suggest the Bear Creek assemblage is Late Triassic (ca. 204 Ma). Regional correlation of the Bear Creek is unclear, but similarities between the assemblage and rocks of the Taku and Alexander terranes suggest possible linkages. Correlation with Upper Triassic rocks of Wrangellia is less favourable.

¹ steve.israel@gov.yk.ca

INTRODUCTION

During ten days of fieldwork in early June 2014, the Yukon Geological Survey undertook an accelerated 1:50 000-scale bedrock mapping project of the Mt. Decoeli area in southwest Yukon. The purpose of this project was to characterize the succession of enigmatic metavolcanic and metasedimentary rocks in the Bear Creek assemblage, found west-southwest of Haines Junction (Fig. 1). These rocks are associated with anomalous gold in regional geochemical samples and volcanogenic massive sulphide occurrences. Their characterization will help refine current understanding of the regional tectonic and stratigraphic framework of southwest Yukon.

Vehicle access to the area is limited to an all-wheel drive road in the southeast, through the Bear Creek subdivision and along the Dezadeash River, south of the Alaska Highway. Less maintained roads are present in the areas of Kimberly and Telluride creeks, however their condition is unknown and are likely only useable by quads or walking. Helicopter is the only means of access to most of the area, and is only a short distance from Haines Junction. Exposure is excellent in the southeast and southwest parts of the area and very poor in the northeast and northwest. This report highlights the preliminary findings of this mapping project and serves as companion to YGS Open File 2014-18 (Israel *et al.*, 2014a).

REGIONAL GEOLOGY

Southwest Yukon is characterized by several Paleozoic to Mesozoic terranes, assembled into larger composite terranes and accreted to one another in the Middle Jurassic or earlier (McClelland *et al.*, 1992; van der Heyden, 1992; Nelson *et al.*, 2013). The Intermontane terranes, which in southwest Yukon includes Yukon-Tanana and Stikinia, formed a western continental margin in Mesozoic to which the Insular terranes, Alexander and Wrangellia, were accreted. This led to mountain building, exhumation and erosion of both tectonic elements. The detritus shed from the uplifted terranes was deposited in a series of Jura-Cretaceous basins along the tectonic boundary (McClelland *et al.*, 1992; Umhoefer *et al.*, 2002; Nelson *et al.*, 2013). These basins include rocks of the Dezadeash Formation and the Kluane schist, both located in southwest Yukon (Fig. 1). The Dezadeash Formation is sourced from the Insular terranes and overlaps these terranes as well as rocks assigned to the Yukon-Tanana terrane (Eisbacher, 1976; Gehrels and

Saleeby, 1987). The Kluane schist is sourced from the Intermontane terranes, more specifically the Yukon-Tanana terrane, as well as post-amalgamation plutons that intrude the terrane (Israel *et al.*, 2011). The Yukon-Tanana terrane was subsequently thrust over the Kluane schist in Late Cretaceous. This structural boundary is intruded by Paleocene granodiorite of the Ruby Range suite.

The present boundary between Insular and Intermontane terranes is defined by the Denali fault, a continental-scale dextral strike-slip fault with as much as 400 km of movement from the latest Cretaceous (?) to the present (Fig. 1). Other large structures in the region include the Duke River fault, a northeast-directed thrust fault that places rocks of the Alexander terrane over Wrangellia and that was mainly active in Late Cretaceous through the present (Cobbett, 2011). The Shakwak and Tatshenshini faults, northeast of the Denali (Fig. 1), are not well constrained, but together with the Denali fault they bound a structural wedge between the Intermontane and Insular terranes that is underlain by enigmatic rocks of the Bear Creek assemblage.

LITHOLOGY

A preliminary bedrock geology map of the Mt. Decoeli area is shown in Figure 2. The area can be divided into three geographically distinct stratigraphic successions separated by major faults, from southwest to northeast: 1) Alexander terrane; 2) Wrangellia; and 3) the Bear Creek/Dezadeash succession. The Duke River fault separates Alexander from Wrangellia, and Wrangellia is juxtaposed to the Bear Creek/Dezadeash succession along the Denali fault (Fig. 2). An extensive description of lithologies from the Bear Creek/Dezadeash succession, the focus of the project, is provided below, but only brief descriptions of Alexander terrane and Wrangellia are given here. The reader is referred to Dodds and Campbell (1992a), Israel *et al.* (2006, 2014b), and Israel and Cobbett (2008) for more detailed descriptions of Alexander and Wrangellia regional stratigraphy.

ALEXANDER TERRANE

The Alexander terrane in the map area is composed mainly of Silurian to Devonian sedimentary and minor volcanic and volcanoclastic rocks, as seen in the exposed hanging wall of the Duke River fault (Fig. 2). Limited amount of work was done on Alexander rocks within this project; our limited observations were compiled with the more detailed work by Dodds and Campbell (1992b,c). Three main units were identified in the Alexander terrane.

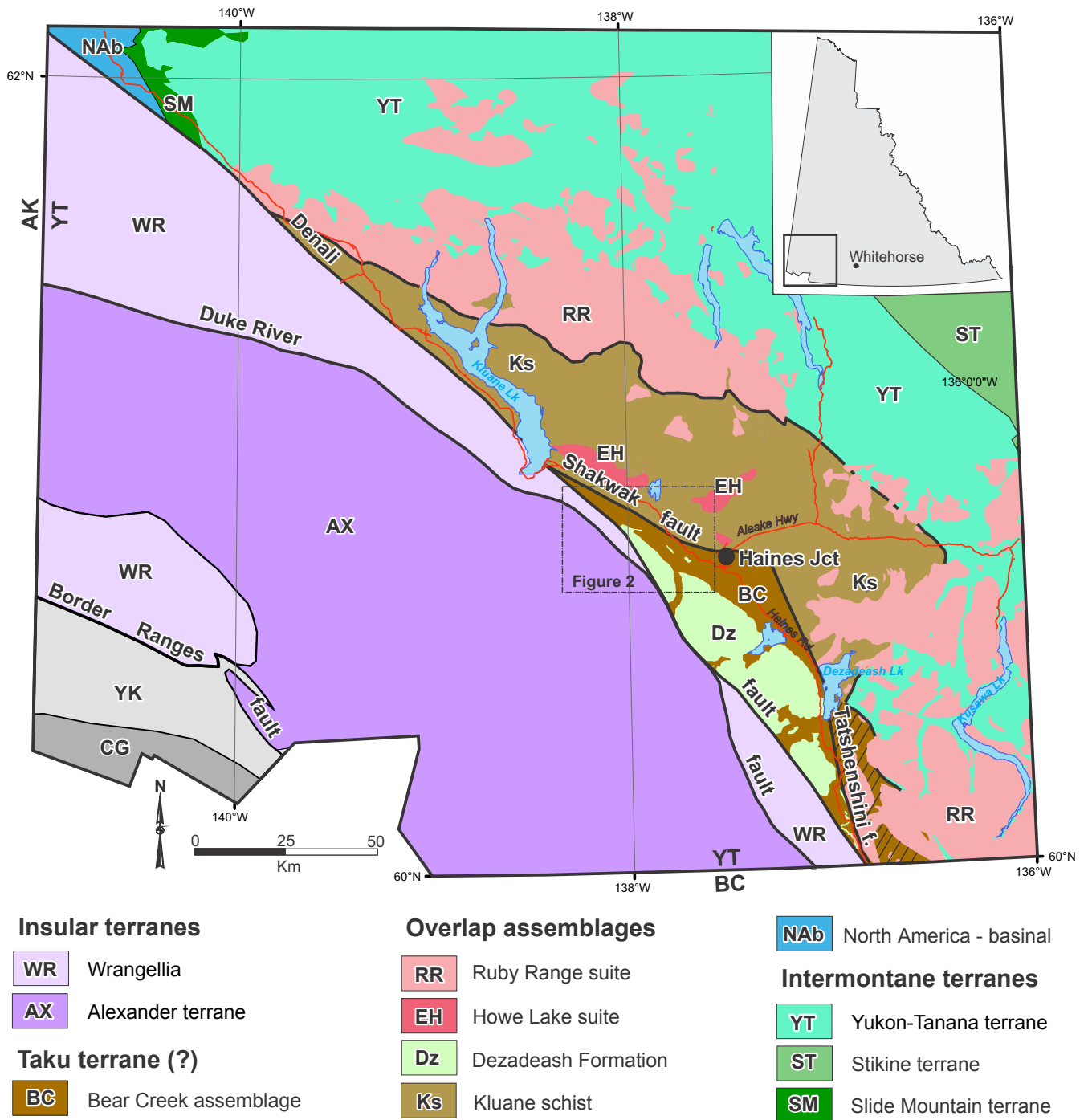


Figure 1. Terrane map of southwest Yukon (modified after Colpron and Nelson, 2011). Inset map shows location with respect to the rest of Yukon. Location of the study area (Fig. 2) is shown by dashed line box. AK-Alaska, YT-Yukon Territory, BC-British Columbia.

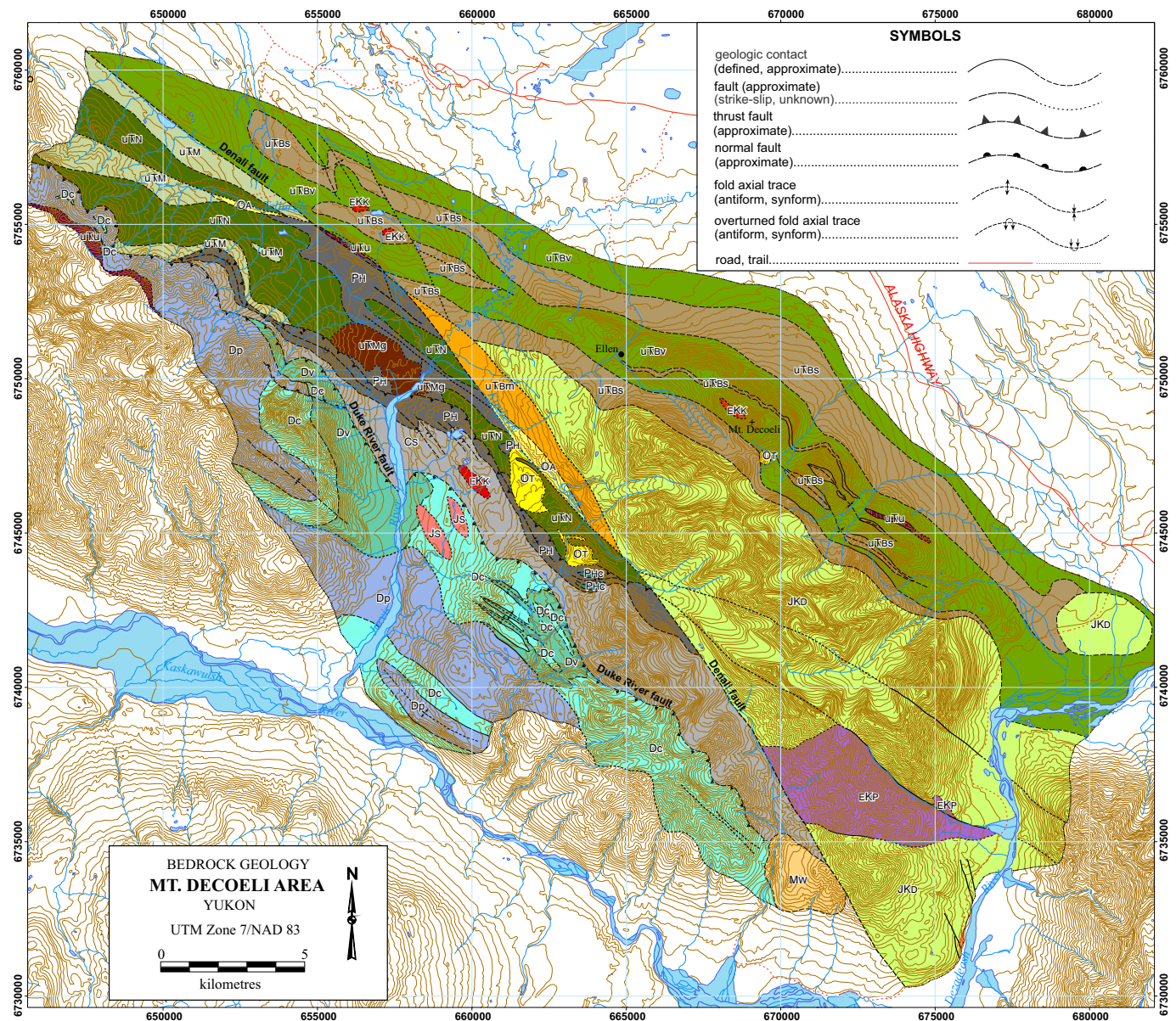


Figure 2. Generalized bedrock geology map of the Mt. Decoeli area, parts of NTS 115A/12, 13 and 115B/9, 16. Legend is on opposite page.

The oldest exposed parts of the Alexander terrane occur within tight antiforms on a northeast-trending ridge between the Kaskawulsh River and Kimberly Creek and on steep slopes west of the Jarvis River (Fig. 2). Mixed, interlayered volcanoclastic and hornblende-phyric mafic flows dominate this succession (Fig. 3a). The volcanic rocks become strongly foliated greenschist near faults and within tight fold axes. Locally thin layers of intermediate to felsic metavolcanic rocks occur within the mafic rocks. The age of these volcanic rocks is not known.

The volcanic rocks are overlain by a thick sequence of marble, which occurs as coherent, bedded carbonate, carbonate breccia and calcareous phyllite assigned to the informal Bullion Creek assemblage of Dodds and Campbell (1992a). It commonly forms large, mountain-scale exposures several hundreds of metres thick (Fig. 3b), and laterally continuous for several kilometres. Several fossils collected from within the Bullion Creek assemblage yielded Late Silurian to Devonian ages (Dodds *et al.*, 1993).

LEGEND

OVERLAP ASSEMBLAGES

MIOCENE (?)

WRANGELL VOLCANICS

MW coherent flow-banded andesitic to dacitic lavas and subvolcanic intrusions; silicic tuff and lapilli tuff

OLIGOCENE

OA pebble to cobble and locally boulder, clast supported conglomerate; clast types include well-rounded to subangular rock types found in the immediate area including mafic to intermediate volcanic and intrusive rocks, fine-grained clastic rocks and marble

TKOPE SUITE (ca. 34-23 Ma):

OT medium to coarse-grained, plagioclase, quartz porphyry

EARLY CRETACEOUS

KLUANE RANGES SUITE (ca. 124 - 116 Ma):

EKK medium to coarse-grained, strongly foliated, hornblende, biotite granodiorite to quartz diorite

PYROXENITE CREEK SUITE (ca. 124 Ma):

EKP fine to coarse-grained, strongly foliated to massive hornblende, biotite granodiorite; white to beige weathered, salt and pepper fresh; garnet is common

DEZADEASH FORMATION:

JKD interbedded light to dark buff-grey lithic greywacke, sandstone, siltstone, thin dark grey shale, argillite and conglomerate; mass-flow conglomerate; rare light grey tuff

UNKNOWN TECTONIC AFFINITY

LATE TRIASSIC

BEAR CREEK ASSEMBLAGE

uTKBm foliated and faulted melange-like assemblage of medium to dark green, medium to coarse-grained clastic or volcanoclastic rocks and lesser grey chert and mudstone, with local highly foliated, cm- to dm-scale, cream-coloured layers and lenses of more felsic composition (tuff?)

uTKBs fine-grained meta-siltstone, mudstone and sandstone; phyllitic to schistose, locally more massive; abundant pyrite cubes observed in mudstone

uTKBv fine to medium-grained, strongly foliated to massive intermediate to mafic metavolcanic rocks; greenschist near fault zones; interlayered with metasedimentary rocks of uTKBs and thin carbonate horizons; locally pillowed

LEGEND EXPLANATION

PLUTONIC SUITES: grouping of plutonic rock units based on age, regional distribution and in some cases composition

LAYERED ROCK ASSEMBLAGES: regionally mappable units generally of Group or Formation rank

WRANGELLIA

LATE TRIASSIC

MAPLE CREEK GABBRO: (ca. 232 Ma)

uTKMg medium to coarse-grained, gabbro and diorite; massive to strongly foliated near fault zones

KLUANE MAFIC/ULTRAMAFIC SUITE: (ca. 232-228 Ma)

uTKu medium to fine-grained peridotite, dunite and gabbro; where deformed abundant serpentinite

MCCARTHY FORMATION

uTKM fine-grained calcareous to carbonaceous mudstone and siltstone; massive beige to cream weathered carbonate; white to light grey, strongly deformed evaporite

NIKOLAI FORMATION

uTKN dark green to maroon, massive to locally foliated, amygdaloidal and vesicular basalt; rare pillow and volcanic breccia

MISSISSIPPIAN TO PERMIAN

HASEN CREEK FORMATION

PHc beige to white weathered, laterally discontinuous carbonate; light to dark grey banded to massive

PH fine-grained, mudstone, siltstone and sandstone; minor volcanoclastic rocks; locally phyllitic

STATION CREEK FORMATION

Cs dark green metabasalt, volcanic breccia, greenschist; minor carbonate and fine-grained siliciclastic rocks

ALEXANDER TERRANE

JURASSIC

SAINT ELIAS SUITE: (ca. 152-148 Ma)

JS coarse-grained, dark brown-black, hornblende +/- biotite granodiorite and quartz diorite

SILURIAN TO DEVONIAN (?)

SDp fine-grained, dark to light grey phyllite and calcareous phyllite

BULLION CREEK ASSEMBLAGE

SDc fine to medium-grained, grey-cream weathered, light grey to white marble; internally strongly deformed

SDv dark green metabasalt, meta-volcanoclastic rocks, greenschist

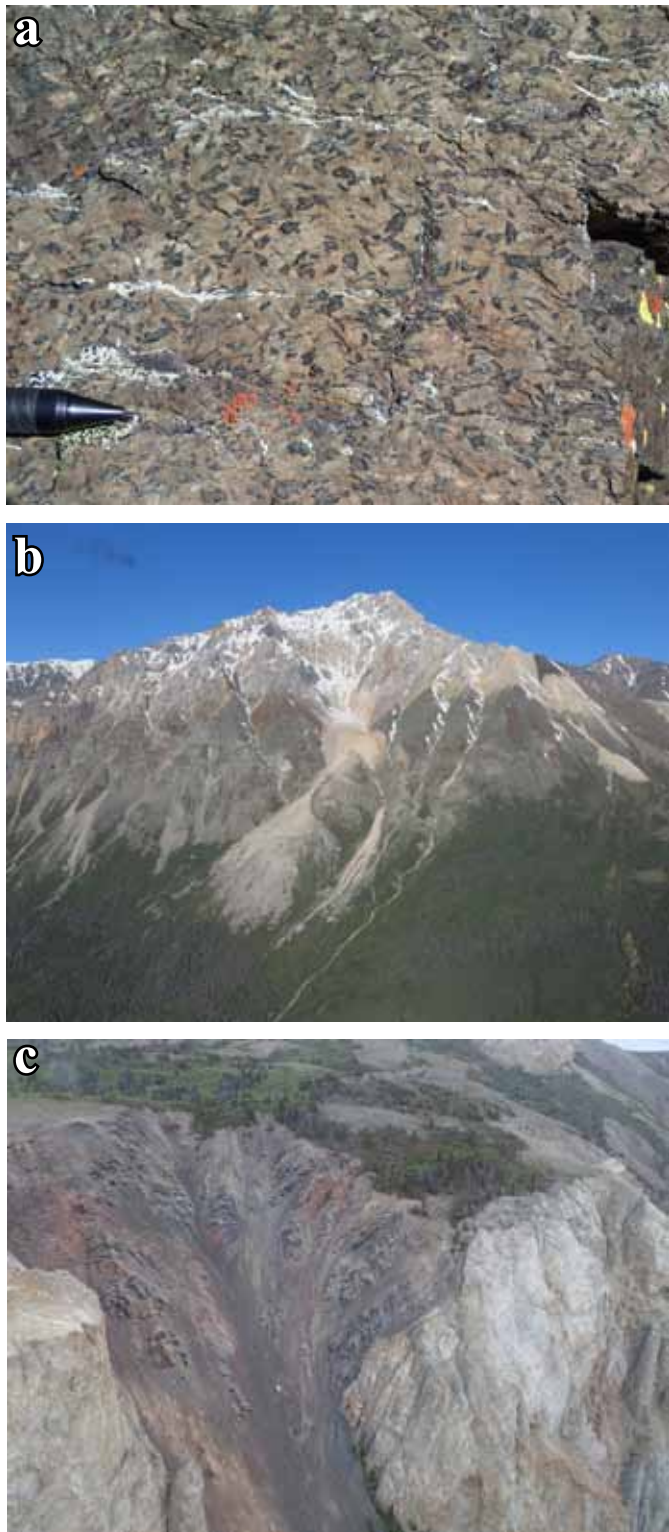


Figure 3. (a) Hornblende-phyric metabasalt of unit Dv of the Alexander terrane; (b) several hundred metres-thick carbonate of unit Dc of the Alexander terrane capping an unnamed mountain west of the Jarvis River, view looking south; (c) bedded, dark grey calcareous phyllite of unit Dp overlying Dc carbonate.

A thick succession of calcareous phyllite overlies the marble and is faulted against the older volcanic succession (Figs. 2 and 3c). The phyllite is light to dark grey banded and locally black and graphitic. Thin bands of cherty layers also occur locally. Total thickness of this unit is not known but must be at least several hundred metres based on exposures on steep mountain sides west of the Jarvis River. The age of the phyllite is Devonian based on several fossil localities within the unit (Dodds *et al.*, 1993).

WRANGELLIA

Rocks assigned to Wrangellia occur structurally sandwiched between the Duke River fault and the Denali fault (Fig. 2). The rocks are consequently strongly deformed and generally form overturned folds with northeast vergence. Wrangellia is well exposed near the Duke River fault, but exposures are sparse in areas of low topographic relief, such as the flats surrounding Telluride Creek.

In the Mt. Decoeli area, the oldest rocks in Wrangellia are mafic to intermediate volcanic breccia, volcanoclastic rocks and flows of the Station Creek Formation (Fig. 2). Breccia comprise pyroxene-phyric basaltic clasts within a fine-grained matrix of similar composition (Fig. 4a). Brown to grey carbonate clasts are common within the breccia (Fig. 4a) and carbonate occurs as thin layers within the volcanoclastic sequence. Flows are generally strongly deformed and schistose but locally occur as massive greenstone. The greenstone is locally pyroxene-phyric. The age of the Station Creek Formation is Mississippian to Pennsylvanian (Israel *et al.*, 2014). Metasedimentary rocks of the Hasen Creek Formation overlie the Station Creek Formation. The contact between the two formations was not observed in the Mt. Decoeli area, but elsewhere in southwest Yukon this contact is gradational. The Hasen Creek Formation comprise siltstone, mudstone, sandstone and carbonate. Carbonate is thickest (up to 10 m) near the top of the unit where it is interlayered with black mudstone and siltstone (Fig. 4b). Abundant fossil collections throughout southwest Yukon constrain the age of the Hasen Creek Formation as Permian.

The Nikolai formation unconformably overlies the Hasen Creek Formation (Fig. 2). It is characterized by a thick sequence of highly vesicular to amygdaloidal mafic volcanic rocks that weather a distinct dark green to maroon colour that are easily distinguished from volcanic rocks of the Station Creek Formation (Fig. 4c). Massive flows are dominant but volcanic breccia and rare pillow basalt occur locally near the base of the unit. The thickness

of the Nikolai formation in the Mt. Decoeli area is not well constrained but in other parts of southwest Yukon the basalt can be up to 3000 m thick (Read and Monger, 1976). The age of the Nikolai formation is Late Triassic (Carnian to Norian) based on dating of associated gabbro and ultramafic rocks, and on conodont collections from interlayered carbonate near the top of the unit (Greene *et al.*, 2009). A mixed sequence of carbonate and calcareous to graphitic mudstone overlies the basalt. The carbonate is likely part of the Chitistone Limestone, a Norian limestone unit well documented elsewhere in southwest Yukon, and the mudstone is part of the McCarthy Formation, which is also Norian. Poor exposure and structural interleaving of these units made it difficult to separate them into different units on the map so they are included together as the McCarthy Formation (Figs. 2 and 4d).

BEAR CREEK ASSEMBLAGE

The Bear Creek assemblage is found north of the Denali fault where it occupies much of the low land north of Telluride Creek and the peaks and front slopes of the mountains surrounding Mt. Decoeli (Fig. 2). The assemblage is characterized by strongly deformed metasedimentary and metavolcanic rocks. Metasedimentary rocks appear to underlie the volcanic rocks, however there is some interlayering of the two higher up in the sequence.

Metasedimentary rocks included within the Bear Creek assemblage are characterized by thinly bedded to massive siltstone, mudstone and sandstone (uTBS; Figs. 2 and 5a). Beds range in thickness from centimetre to metre-scale. Original sedimentary features, such as graded beds and



Figure 4. (a) Pyroxene-phyric volcanic clasts within volcanic breccia of the Station Creek Formation, note brown weathered carbonate clast; (b) folded metasilstone, mudstone and carbonate of the Permian Hasen Creek Formation; (c) Upper Triassic dark green, amygdaloidal basalt of the Nikolai formation; (d) mixed carbonate, evaporite and bedded carbonaceous limestone of the McCarthy Formation and the Chitistone Limestone.

soft sediment deformation structures, are locally preserved (Fig. 5b). Elsewhere the rocks are more graphitic and deformed resulting in a black phyllite horizon that is easily identifiable in the field (Fig. 5c). Pyrite cubes up to 2-3 mm in size are commonly found within the black phyllite. Dark to light grey banded marble of variable thickness is interlayered with the phyllite and less deformed clastic sedimentary rocks (Fig. 5d). Marble occurs within the sedimentary horizons that are interlayered with the volcanic rocks near the top of the assemblage.

Intermediate to mafic volcanic rocks gradationally overlie the sedimentary portion of the Bear Creek assemblage (uTbV; Fig. 2). Similarly, thin horizons of metasedimentary rocks are interlayered with the volcanic rocks near the top of the sequence. The volcanic rocks are also highly deformed and often form greenschist. They are locally

interlayered with carbonate bands (Fig. 6a). Pillows are preserved in areas of lesser deformation (Fig. 6b,c). More volcanoclastic-like material is found throughout the massive flows, likely representing tuffaceous deposits. Andesitic to basaltic compositions dominate the volcanic succession; however, more felsic, plagioclase and quartz-phyric horizons occur locally (Fig. 6d).

An enigmatic succession of metasedimentary rocks located next to the Denali fault, just north of Kimberly Creek, is tentatively assigned to the Bear Creek assemblage (uTbM; Fig. 2). A strand of the main Denali fault separates these rocks from the Dezadeash Formation in the north and they are unconformably overlain by Oligocene Amphitheatre deposits in the south (Fig. 2). The rocks within this fault sliver are a highly deformed and metasomatically altered succession of melange-like, medium to dark green,

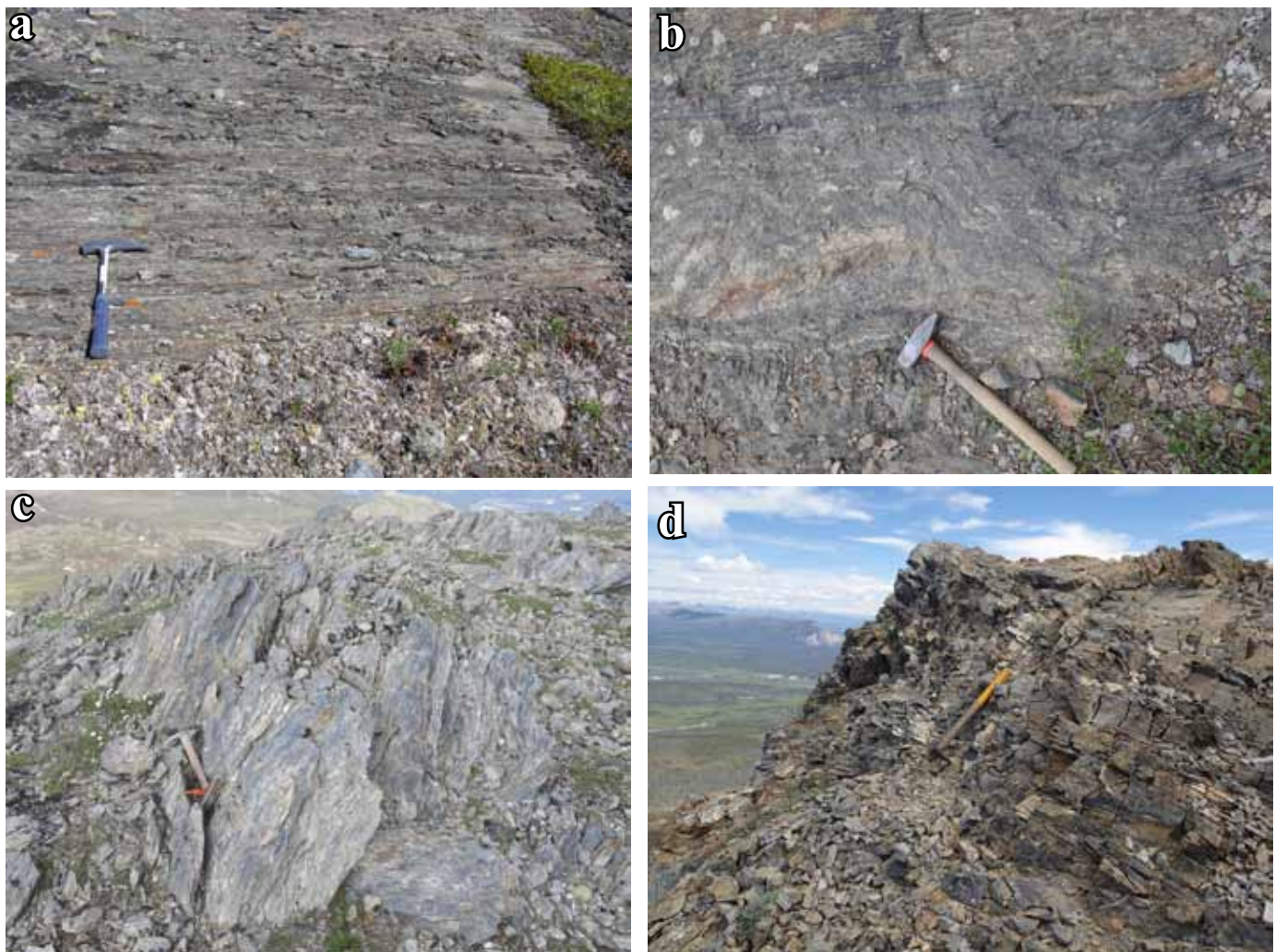


Figure 5. (a) Interlayered, deformed and metamorphosed siltstone, mudstone and sandstone of the Bear Creek assemblage; (b) soft sediment slump folds within uTbS of the Bear Creek assemblage; (c) black phyllite typical of uTbS; (d) dark grey, bedded carbonate interlayered with siltstone and mudstone of uTbS.

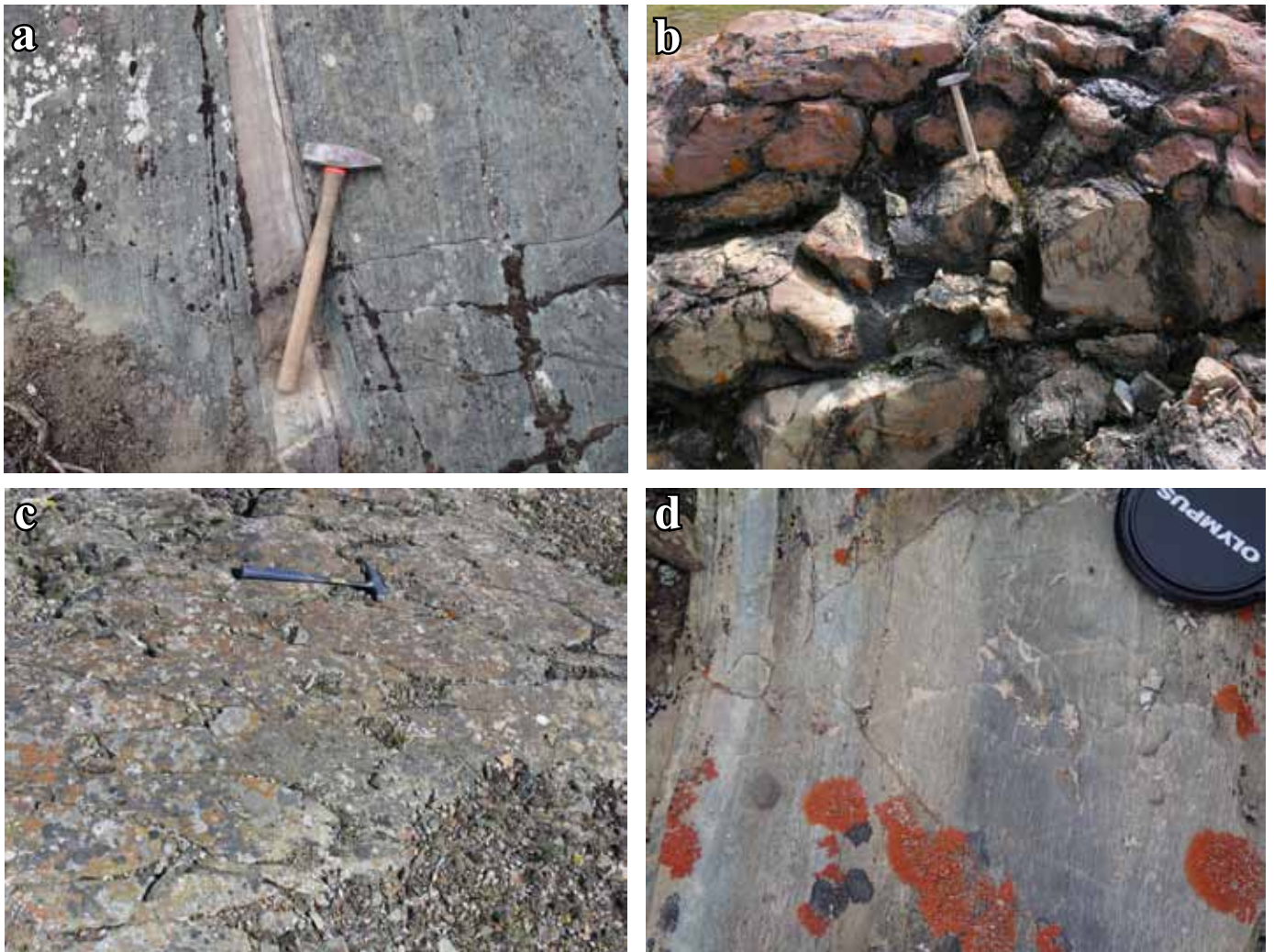


Figure 6. (a) Thin, grey weathered carbonate horizon within greenschist of uTBV; (b) strongly deformed pillows in the volcanic portion of the Bear Creek assemblage; (c) typical outcrop of deformed pillow basalt of uTBV; (d) quartz and plagioclase-phyric intermediate to felsic meta-tuff within uTBV.

medium to coarse-grained siliciclastic and volcanoclastic rocks with lesser amounts of grey chert and mudstone (Fig. 7a). This succession includes centimetre to decimetre-scale layers of cream coloured rock that may be felsic tuff. This unit is locally conglomeratic, containing angular to subrounded clasts of variable compositions ranging from less than one centimetre to fifty centimetres (Fig. 7b). Stratigraphic relationships with other surrounding units are unclear. This unit does not look like Dezadeash Formation, nor does it resemble other units within the Bear Creek assemblage. However, its unconformable relationship with the Amphitheatre Formation suggests it is an older unit, and may be an unidentified part of the Bear Creek, perhaps an extremely altered and structurally modified part of the lower clastic unit.

A strongly deformed felsic tuff layer within the volcanic portion of the Bear Creek assemblage returned a U-Pb zircon age of ~204 Ma (J.L. Crowley, *pers. comm.*, 2014). The degree of deformation at this locality obscures original relationships and the felsic layer could also be a dike intruding the mafic volcanic rocks, so this date is considered the youngest age limit for this unit.

DEZADEASH FORMATION

The Dezadeash Formation outcrops north of the Denali fault where it seems to unconformably overlie the Bear Creek assemblage (Fig. 2). The formation consists of at least several hundred metres of siltstone, mudstone and sandstone, interpreted to be part of a submarine fan, turbidite succession (Eisbacher, 1976). Sandstone beds

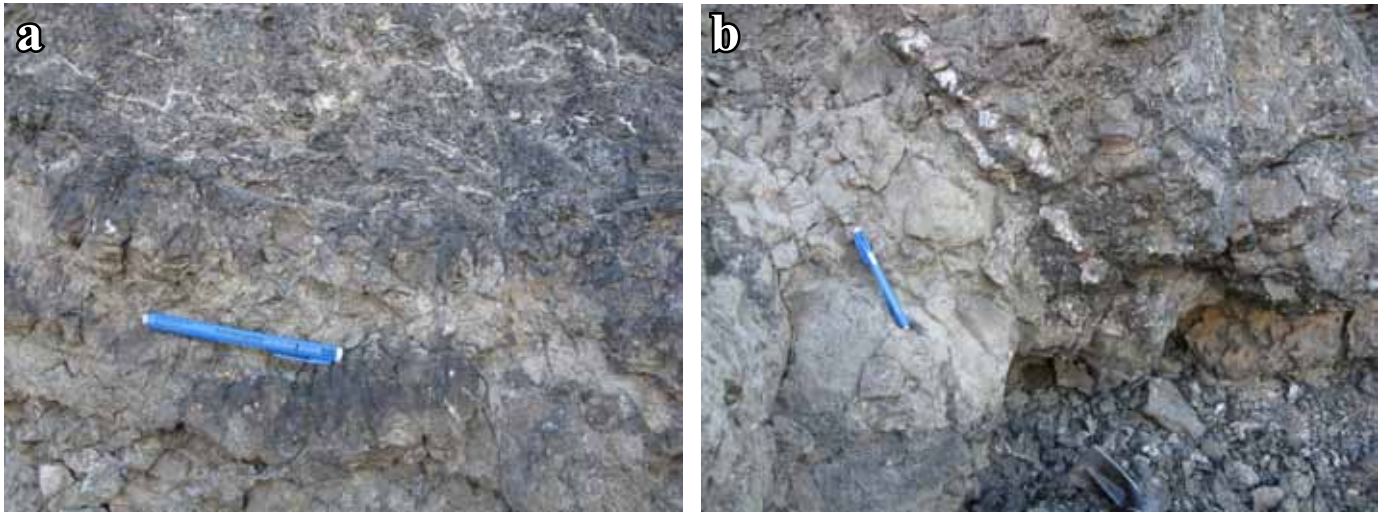


Figure 7. (a) Convolute layering within metamorphosed and altered sedimentary rocks of **uTBM**; (b) large clast of possible granitic material (white) within the conglomeratic portion of **uTBM**.

range in thickness from less than one metre to several tens of metres. Graded beds, cross-laminations and other sedimentary structures are common. The unit is highly deformed, exhibiting at least two phases of folding. The first is a north-trending, tight, upright to overturned phase that is responsible for repeated stratigraphy, very steep bedding and a regionally developed penetrative cleavage. A second phase of folding trends northwest, is more open and re-folds the earlier phase. The Dezadeash Formation is Late Jurassic (Oxfordian) to Early Cretaceous (Valanginian) based on numerous fossil collections (Eisbacher, 1976).

AMPHITHEATRE FORMATION

The Amphitheatre Formation outcrops exclusively within the Denali fault zone, where it unconformably overlies enigmatic rocks assigned to the Bear Creek assemblage (**uTBM**) and is faulted against rocks of Wrangellia (Fig. 2). The unit comprises poorly sorted conglomerate, with well-rounded to subangular clasts ranging in size from less than one centimetre to twenty centimetres (Fig. 8). Clast types include compositions similar to almost all local bedrock units. It is likely that the conglomerate is related to movement along the Denali fault, deposited as a fault scarp breccia/conglomerate. The steep orientation of the unconformable contact with underlying rocks and the presence of deformed clasts indicates movement on the fault continued after deposition of the Amphitheatre. The Amphitheatre Formation is Oligocene, based on regional fossil collections (Ridgway *et al.*, 1992).



Figure 8. Well-rounded to subangular clasts of metamorphic country rocks within poorly sorted conglomerate of the Oligocene Amphitheatre Formation.

INTRUSIVE ROCKS

Several ages and compositions of intrusive rocks are found throughout the Mt. Decoeli area (Fig. 2). The oldest of these rocks are the granodiorite to quartz diorite of the St. Elias suite, which intrude the Alexander terrane south of the Duke River fault (Fig. 2). Regionally these range from 155-148 Ma (Dodds and Campbell, 1988). Three main intrusive suites are found within Wrangellia. These include the Late Triassic Maple Creek suite, the Early Cretaceous Kluane Ranges suite and the Oligocene Tkope suite.

The Maple Creek suite includes ca. 232 Ma medium to coarse-grained, pyroxene-hornblende gabbro (Mortensen and Hulbert, 1991). The Klwane Ranges suite includes granodiorite and hornblende quartz diorite ranging in age from 124 to 116 Ma. It mainly intrudes Wrangellia but may also include small intrusions within the Bear Creek assemblage just west of the Jarvis River. The youngest plutons to intrude Wrangellia are Oligocene quartz-plagioclase porphyries that are assigned to the Tkope suite. These rocks are found near the Denali fault and may have been intruded during deformation along the fault.

A large pyroxenite body intrudes the Dezadeash Formation west of the Dezadeash River (Fig. 2). These rocks have been assigned to the Pyroxenite Creek suite and are interpreted as Early Cretaceous based on K-Ar dates on hornblende and biotite (Dodds and Campbell, 1988).

DISCUSSION

REGIONAL STRATIGRAPHIC RELATIONSHIPS OF THE BEAR CREEK ASSEMBLAGE

The role of the Bear Creek assemblage in the overall stratigraphic and tectonic framework of the northern

Cordillera is unclear. Other Upper Triassic rocks in the region include the Nikolai formation of Wrangellia, the Perseverance Group of the Taku terrane, and Upper Triassic stratigraphy of the Alexander terrane. Below we describe the general stratigraphy of each of these tectonic entities and compare them to the Bear Creek assemblage.

The Nikolai formation of southwest Yukon includes up to ~3000 m of subaerial to subaqueous basalt flows with locally preserved Middle Triassic mudstone below the basalt (Read and Monger, 1976; Israel *et al.*, 2006, 2007). Pillows are very rare in the Nikolai formation in southwest Yukon and found mainly near the base of the sequence. Thick accumulations of carbonate with lesser evaporites of the Chitistone Limestone and calcareous mudstone and siltstone of the McCarthy Formation overly the basalt (Fig. 9). The basalt is interpreted as the surficial expression of ca. 232-228 Ma mafic and ultramafic intrusions found throughout Wrangellia.

The thick accumulation of basalt and capping limestone of the Wrangellia does not fit with the stratigraphy observed within the Bear Creek assemblage. Also, no large mafic intrusions, similar to those of the Maple Creek suite in Wrangellia, have been observed within the Bear Creek assemblage. Small, highly deformed and altered ultramafic

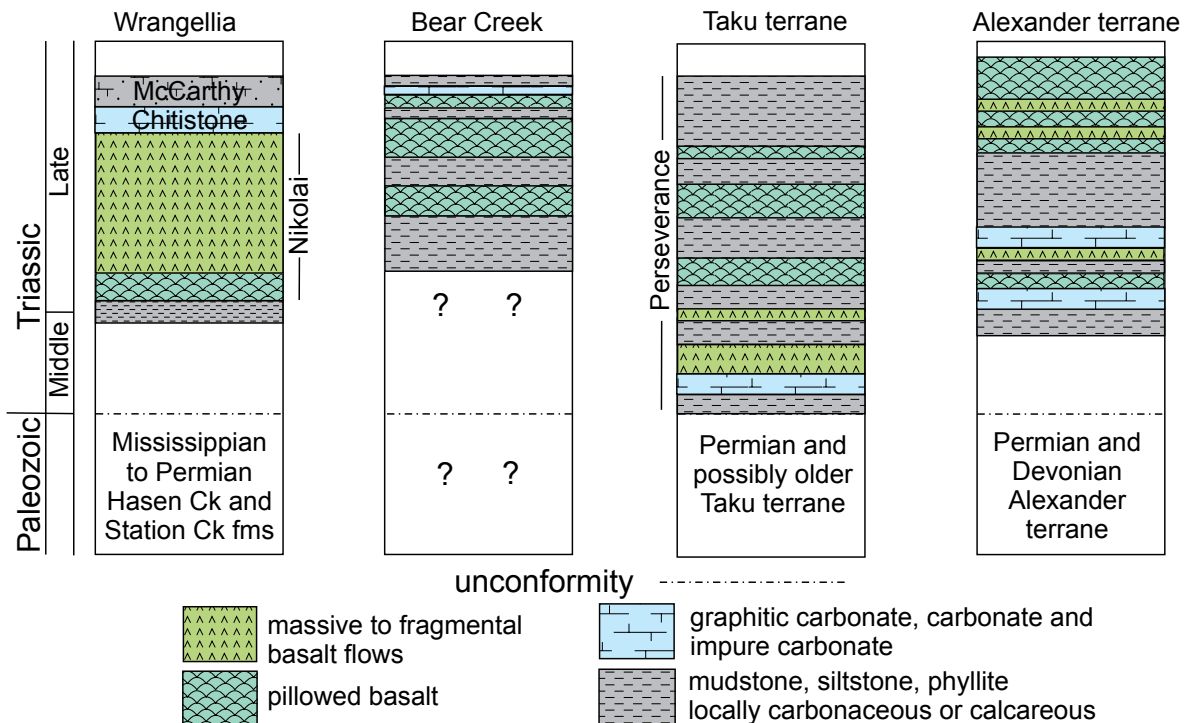


Figure 9. Comparative, schematic stratigraphic sections through Upper Triassic Wrangellia, the Bear Creek assemblage, Taku terrane and Alexander terrane. Section for the Alexander terrane from Taylor *et al.* (2005); Wrangellia, Israel *et al.* (2005); Taku terrane, Gehrels *et al.* (1992).

bodies are present in the Bear Creek assemblage, but it is unclear whether these are intrusions or tectonic slivers. Furthermore the ultramafic rocks associated with the Nikolai formation are almost entirely found within the underlying Paleozoic sequence, and never in Upper Triassic sedimentary rocks. The ultramafic rocks in the Bear Creek assemblage are found within the Triassic volcanic/sedimentary sequence (Fig. 2). Finally the age of the Nikolai (~232-228 Ma) does not overlap the age for the Bear Creek assemblage. Overall Wrangellia is not a good match for the Bear Creek assemblage.

Upper Triassic rocks in the Alexander terrane are mainly preserved in southeast Alaska and northwestern British Columbia. The sequence of Late Triassic stratigraphy in the Alexander terrane is laterally variable. It generally consists of Upper Triassic calcareous shale and mudstone, arkose, dolomitic limestone, basalt and local conglomerate and mafic/ultramafic intrusions, overlying a section of Paleozoic basement rocks (Fig. 9; Taylor *et al.*, 2005). The clastic rocks are primarily Carnian and Norian in age (237-205 Ma) with interlayered basalt, limestone and arkose. Basalt flows overlying calcareous mudstone containing upper Norian fossils cap the sequence. Mafic and ultramafic intrusions occur throughout these rocks, including within the upper basalt, and are possibly similar to ultramafic bodies found within the Bear Creek assemblage. The Upper Triassic stratigraphy of the Alexander terrane is known for its volcanogenic massive sulphide deposits (e.g., Windy Craggy, Greens Creek). The Bear Creek assemblage is host to VMS-style mineralization at the Ellen prospect, just west of the Jarvis River (Fig. 2). It is possible the Bear Creek assemblage is a fault sliver of the northern extension of Upper Triassic Alexander terrane.

The Taku terrane is a sequence of Paleozoic to early Mesozoic rocks found in southeast Alaska, structurally juxtaposed between the Yukon-Tanana and Alexander terranes (Saleeby, 2000; Gehrels, 2002). Only brief summaries of its stratigraphy have been published: a Permian to possibly slightly older sequence of metamorphosed turbidites, marble and metabasalt, is overlain by Middle to Upper Triassic mudstone, calcareous and carbonaceous phyllite, carbonate and basalt of the Perseverance Group (Fig. 9; Gehrels *et al.*, 1992; Gehrels, 2002). The interlayered nature of the basalt and mudstone/phyllite is very similar to that observed in the Bear Creek assemblage. The carbonate within the Perseverance Group may also be similar to the carbonate found in the Bear Creek assemblage. The position of the

Taku terrane between the Alexander and Yukon-Tanana terranes, as well as the similarities in stratigraphy, makes correlation with the Bear Creek assemblage attractive.

CONCLUSIONS

The Mt. Decoeli area is underlain by Paleozoic to Mesozoic rocks of the Alexander terrane, Wrangellia and the Bear Creek assemblage. These tectonic entities are separated by terrane bounding faults, such as the Duke River and Denali faults, which were mainly active in Late Cretaceous and Cenozoic. The Bear Creek assemblage is an enigmatic succession of metamorphosed and deformed clastic sedimentary rocks interlayered with mafic to intermediate volcanic rocks. These rocks appear to be unconformably overlain by Jura-Cretaceous turbidites of the Dezadeash Formation. Age determination from the Bear Creek assemblage suggests a Late Triassic age for the sequence. Correlation of the Bear Creek assemblage is unclear; however, preliminary indications suggest possible ties with the Taku or Alexander terranes. Correlation with Wrangellia is less favourable.

ACKNOWLEDGEMENTS

Thanks to all who contributed as field assistants, too many to name. Thanks to all the staff at the Kluane Lake Research Station, especially Sian Williams and Lance Goodwin for providing a great place to stay. Trans North helicopters out of Haines Junction provided excellent air support. M. Colpron is thanked for reading an earlier version of the manuscript. Final review and edits by K. MacFarlane is much appreciated.

REFERENCES

- Cobbett, R., 2011. Timing and kinematics of the Duke River fault; insights into the evolution of the Insular terrane, southwest Yukon. Unpublished MSc Thesis. University of British Columbia, 140 p.
- Colpron, M. and Nelson, J.L., 2011. A digital atlas of terranes for the northern Cordillera. Yukon Geological Survey, [Dec. 2014], (*also, BC Geological Survey, Geofile 2011-11*).
- Dodds, C.J. and Campbell, R.B., 1988. Potassium-argon ages of mainly intrusive rocks in the Saint Elias Mountains, Yukon and British Columbia. Geological Survey of Canada, Paper 87-16, 43 p.

- Dodds, C.J. and Campbell, R.B., 1992a. Overview, legend, and mineral deposit tabulations for geology of SW Kluane Lake (115G and G[E1/2]), Mount Saint Elias (115B and C[E1/2]), SW Dezadeash (115A), NE Yakutat (114O), and Tatshenshini (114P) map areas, Yukon Territory and British Columbia. Geological Survey of Canada, Open Files 2188-2191, 85 p.
- Dodds, C.J. and Campbell, R.B., 1992b. Geology of SW Dezadeash map area (115A), Yukon Territory. Geological Survey of Canada, Open File 2190, 85 p., 1 sheet.
- Dodds, C.J. and Campbell, R.B., 1992c. Geology of the Kluane Lake map area (115G and F[E1/2]), Yukon Territory. Geological Survey of Canada, Open File 2188, 85 p., 1 sheet.
- Dodds, C.J., Campbell, R.B., Read, P.B., Orchard, M.J., Tozar, E.T., Bamber, E.W., Pedder, A.E.H., Norford, B.S., McLaren, D.J., Harker, P., McIver, E., Norris, A.W., Ross, C.A., Chatterton, B.D.E., Cooper, G.A., Flower, R.H., Haggart, J.W., Uyeno, T.T. and Irwin, S.E.B., 1993. Macrofossil and conodont data from: SW Kluane Lake (115G and F[E1/2]), Mount St. Elias (115B and C[E1/2]), SW Dezadeash (115A), NE Yakutat (114O) and Tatshenshini River (114P) map areas, southwestern Yukon and northwestern British Columbia. Geological Survey of Canada, Open File 2731, p. 137.
- Eisbacher, G.H., 1976. Sedimentology of the Dezadeash flysch and its implications for strike-slip faulting along the Denali fault, Yukon Territory and Alaska. *Canadian Journal of Earth Sciences*, vol. 13, p. 1495-1513.
- Gehrels, G.E., 2002. Detrital zircon geochronology of the Taku terrane, southeast Alaska. *Canadian Journal of Earth Sciences*, vol. 39, p. 921-931.
- Gehrels, G.E., McClelland, W.C., Samson, S.D. and Patchett, P.J., 1992. Geology of the western flank of the Coast Mountains between Cape Fanshaw and Taku Inlet, southeastern Alaska. *Tectonics*, vol. 11, p. 567-585.
- Gehrels, G.E. and Saleeby, J.B., 1987. Geology of southern Prince of Wales Island, southeastern Alaska. *Geological Society of America Bulletin*, vol. 98, p. 123-137.
- Greene, A.R., Scoates, J.S., Weis, D. and Israel, S., 2009. Geochemistry of Triassic flood basalts from the Yukon (Canada) segment of the accreted Wrangellia oceanic plateau. *Lithos*, vol. 110, p. 1-19.
- Israel, S., Colpron, M., Cubley, J., Moynihan, D., Murphy, D.C. and Relf, C., 2014a. Preliminary bedrock geology of the Mt. Decoeli area, parts of NTS (115A/12, 13 and 115B/9, 16). Yukon Geological Survey Open File 2014-18.
- Israel, S., Beranek, L.P., Friedman, R.M. and Crowley, J.L., 2014b. New ties between the Alexander terrane and Wrangellia and implications for North America Cordilleran evolution. *Lithosphere*, vol. 6, p. 270-276.
- Israel, S. and Cobbett, R., 2008. Kluane Ranges bedrock geology, White River area (Parts of NTS 115F/9, 15 and 16; 115G/12 and 115K/1, 2). *In: Yukon Exploration and Geology 2007*, D.S. Emond, L.R. Blackburn and L.H. Weston (eds.), Yukon Geological Survey, p. 153-167.
- Israel, S., Cobbett, R. and Fozard, C., 2007. Bedrock geology of the Miles Ridge area, Yukon (parts of NTS 115F/15, 16 and 115K/1, 2). Yukon Geological Survey, Open File 2007-7, 1:50 000 scale.
- Israel, S., Murphy, D.C., Bennett, V., Mortensen, J.K. and Crowley, J., 2011. New insights into the geology and mineral potential of the Coast Belt in southwestern Yukon. *In: Yukon Exploration and Geology 2010*, K.E. MacFarlane, L.H. Weston and C. Relf (eds.), p. 101-123.
- Israel, S., Tizzard, A.M. and Major, J., 2005. Geological map of the Duke River area (parts of NTS 115G/2, 3, 5, 6, 7) Yukon. Yukon Geological Survey, Open File 2005-11, 1:50 000 scale.
- Israel, S., Tizzard, A.M. and Major, J., 2006. Bedrock geology of the Duke River area, parts of NTS 115G/2, 3, 4, 6 and 7, southwest Yukon. *In: Yukon Exploration and Geology 2005*, D.S. Emond, G. Bradshaw, L.L. Lewis and L.H. Weston (eds.), Yukon Geological Survey, p. 139-154.
- McClelland, W.C., Gehrels, G.E. and Saleeby, J.B., 1992. Upper Jurassic-Lower Cretaceous basinal strata along Cordilleran margin: Implications for the accretionary history of the Alexander-Wrangellia-Peninsular terrane. *Tectonics*, vol. 11, p. 823-835.
- Mortensen, J.K. and Hulbert, L.J., 1991. A U-Pb zircon age for a Maple Creek gabbro sill, Tatamagouche Creek area, southwest Yukon Territory. *Radiogenic Age and Isotopic Studies: Report 5*. Geological Survey of Canada, Paper 91-2, p. 175-179.

- Nelson, J.L., Colpron, M. and Israel, S., 2013. The Cordillera of British Columbia, Yukon and Alaska: Tectonics and metallogeny. Society of Economic Geology, Special Publication 17, p. 53-109.
- Read, P.B. and Monger, J.W.H., 1976. Pre-Cenozoic volcanic assemblages of the Kluane and Alsek Ranges, southwestern Yukon Territory. Geological Survey of Canada, Open File 381, 96 p.
- Ridgway, K.D., DeCelles, P.G., Cameron, A.R. and Sweet, A.R., 1992. Cenozoic syntectonic sedimentation and strike-slip basin development along the Denali fault system, Yukon Territory. *In*: Yukon Exploration and Geology 1992, Yukon Geological Survey, p. 1-26.
- Saleeby, J.B., 2000. Geochronologic investigations along the Alexander-Taku terrane boundary, southern Revillagigedo Island to Cape Fox areas, southeast Alaska. *In*: Tectonics of the Coast Mountains in southeast Alaska and British Columbia, H.H. Stowell and W.C. McClelland (eds.), Geological Society of America, Special Paper 343, p. 107-143.
- Taylor, C.D., Premo, W.R., Meier, A.L. and Taggart, J.E., 2005. The metallogeny of Late Triassic rifting of the Alexander terrane in southeastern Alaska and northwestern British Columbia. *Economic Geology*, vol. 103, p. 89-115.
- Umhoefer, P.J., Schiarizza, P. and Robinson, M., 2002. Relay Mountain Group, Tyaughton-Methow basin, southwest British Columbia: a major Middle Jurassic to Early Cretaceous terrane overlap assemblage. *Canadian Journal of Earth Sciences*, vol. 39, p. 1143-1167.
- van der Heyden, P., 1992. A Middle Jurassic to early Tertiary Andean-Sierran arc model for the Coast Belt of British Columbia. *Tectonics*, vol. 11, p. 82-97.

Summary of Yukon Geological Survey permafrost monitoring network results, 2008-2013

P.S. Lipovsky
Yukon Geological Survey

Lipovsky, P.S., 2015. Summary of Yukon Geological Survey permafrost monitoring network results, 2008-2013. *In: Yukon Exploration and Geology 2014*, K.E. MacFarlane, M.G. Nordling and P.J. Sack (eds.), Yukon Geological Survey, p. 113-122.

ABSTRACT

Up to six years of data have been collected at seven stations within Yukon Geological Survey's permafrost monitoring network between 2008 and 2013. Warm permafrost conditions ($>-0.5^{\circ}\text{C}$) governed by latent heat effects exist at the Whitehorse, Watson Lake, Ross River School and Dawson School monitoring stations, while average permafrost temperatures in Faro are only marginally cooler at -0.6°C . Mean annual ground temperatures at the Beaver Creek and the Dawson dump forest monitoring stations are much colder at -2.9 and -2.0°C respectively. Most sites show either insignificant or very slight short term permafrost warming trends, although slight cooling is apparent at Ross River School, and rapid warming has occurred at Beaver Creek over the monitoring period. Opportunities to expand the network and collaborate with external parties operating similar monitoring stations should be further explored to facilitate more complete and representative reporting on the thermal state of permafrost in Yukon.

¹ panya.lipovsky@gov.yk.ca

INTRODUCTION

The Yukon Geological Survey (YGS) has maintained a permafrost monitoring network in or near several Yukon communities (Whitehorse, Beaver Creek, Dawson, Faro and Ross River) since 2007 (Fig. 1). Additional monitoring stations have since been added to the network in undisturbed forest near the Dawson dump (in November 2008) and Watson Lake (in October 2009). The monitoring stations consist of shallow boreholes 2-13 m deep that are instrumented with temperature sensors and data loggers which record hourly air temperatures and ground temperatures at various depths. The boreholes do not extend to the base of permafrost at any site, so temperature measurements are only representative of near-surface permafrost conditions.

The Whitehorse and Watson Lake stations are located within the sporadic discontinuous permafrost zone, where 10-50% of the terrain is underlain by permafrost (Fig. 1; Heginbottom *et al.*, 1995) and the Faro and Ross River sites straddle the boundary between sporadic and extensive discontinuous permafrost (where 50-90% of the terrain is underlain by permafrost) (Fig. 1; Heginbottom *et al.*, 1995). The Dawson and Beaver Creek sites are located

within the extensive discontinuous permafrost zone (Fig. 1; Heginbottom *et al.*, 1995), however new modeling by Bonnaventure *et al.* (2012) suggests that the Beaver Creek site is located at the southern boundary of an isolated region of continuous permafrost which underlies >90% of the local terrain.

The primary purpose of the monitoring network is to collect baseline data in order to characterize local permafrost thermal conditions and detect any changes that may emerge. Subject to funding availability, it is YGS's intent to maintain and upgrade the network as required in order to continue gathering data for the long term.

The network is also used to engage local school students in related outreach activities. It was set up as part of the Permafrost Outreach Program, in collaboration with the University of Alaska Fairbanks, which operates a similar and much larger network throughout Alaska and around the circumpolar north. Within this program, permafrost monitoring stations and frost tubes are installed near participating schools so that students can be actively engaged in the data collection.

This brief paper provides a snapshot of current permafrost conditions by summarizing the thermal state of permafrost

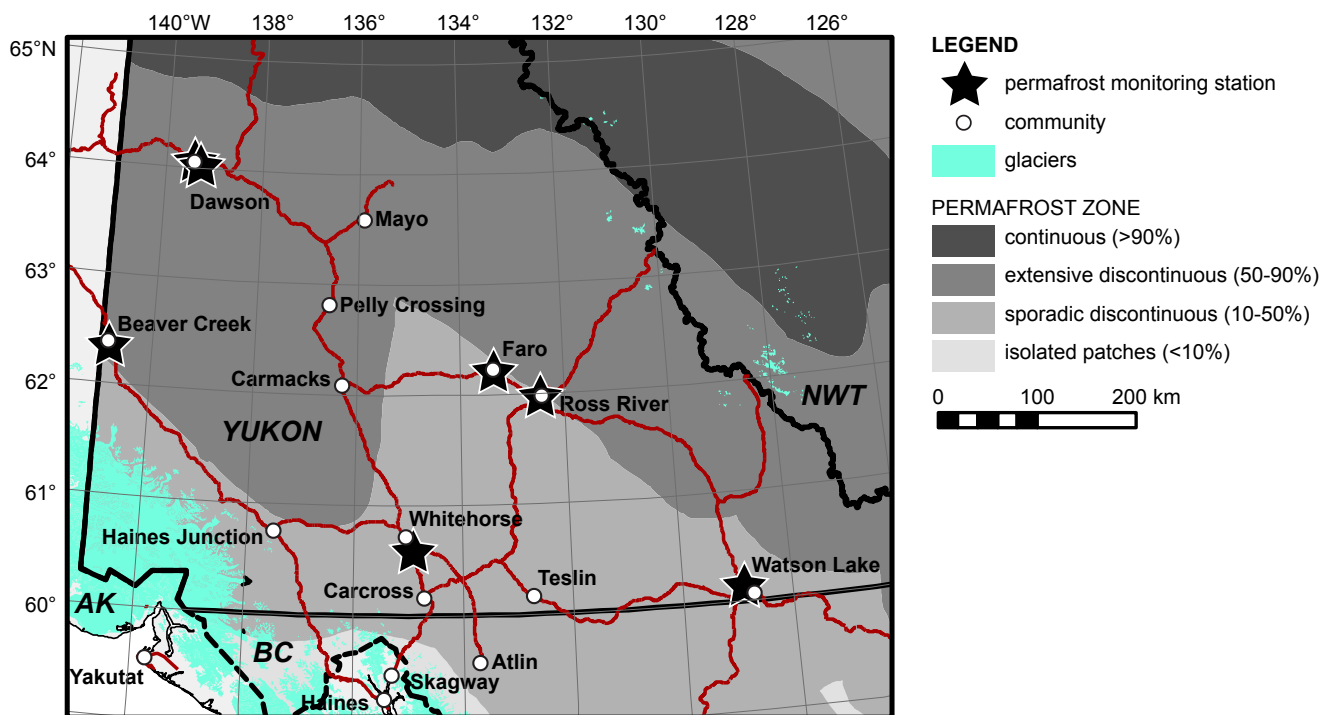


Figure 1. Map of southern Yukon and surrounding jurisdictions showing locations of permafrost monitoring stations with respect to generalized permafrost zones (after Heginbottom *et al.*, 1995). AK: Alaska; BC: British Columbia; and NWT: Northwest Territories.

for each monitoring station for the period 2008-2013. Background information on the Permafrost Outreach Program, monitoring station installation methods, instrumentation and detailed site characteristics are outlined in Lipovsky and Yoshikawa (2009).

RESULTS

Ground thermal conditions are depicted graphically in Figures 2 and 3 which present ground temperature envelopes and mean annual temperature time series for each station. Ground temperature envelopes were generated from mean monthly temperatures, while the mean annual temperature time series were derived by averaging mean daily data for each year. Where gaps in the data collection exist (as described in Data Limitations below) missing values are modeled or interpolated where they could be reasonably predicted. Where this was not possible, incomplete data are omitted for particular years and/or depths. The incorporation of modeled data is indicated by the larger data point markers in Figures 2 and 3.

Table 1 provides a summary of site location data and a variety of parameters commonly used to characterize permafrost conditions; note that due to gaps in data, the data summary period varies slightly for some stations. Highlights of these data are outlined and discussed below.

Mean annual air temperature (MAAT) is the primary control on regional permafrost distribution (Smith and Riseborough, 2002; Lewkowicz *et al.*, 2012) and colder MAATs are generally associated with colder permafrost temperatures (Throop *et al.*, 2012). MAAT, averaged over the data summary period for each monitoring station, ranged between -4.8°C in Beaver Creek and -2.0°C in Whitehorse. The colder MAATs measured in Beaver Creek and Dawson (-4.4°C) reflect their greater continentality and higher latitudes with respect to the remaining sites. The MAAT of -2.0°C measured at the Whitehorse monitoring station is significantly colder than the -0.2°C measured nearby at Whitehorse airport by Environment Canada over the same period, likely due to its forested location.

Mean annual ground surface temperature (MAGST) was also averaged over the data summary period for each site. At undisturbed sites, MAGST varied between -1.7°C in Beaver Creek and 0.6°C in Faro. At disturbed sites which

lack natural vegetation and ground cover, higher mean annual ground temperatures were recorded, with 3.5°C at Dawson School and 0.7°C at Ross River School.

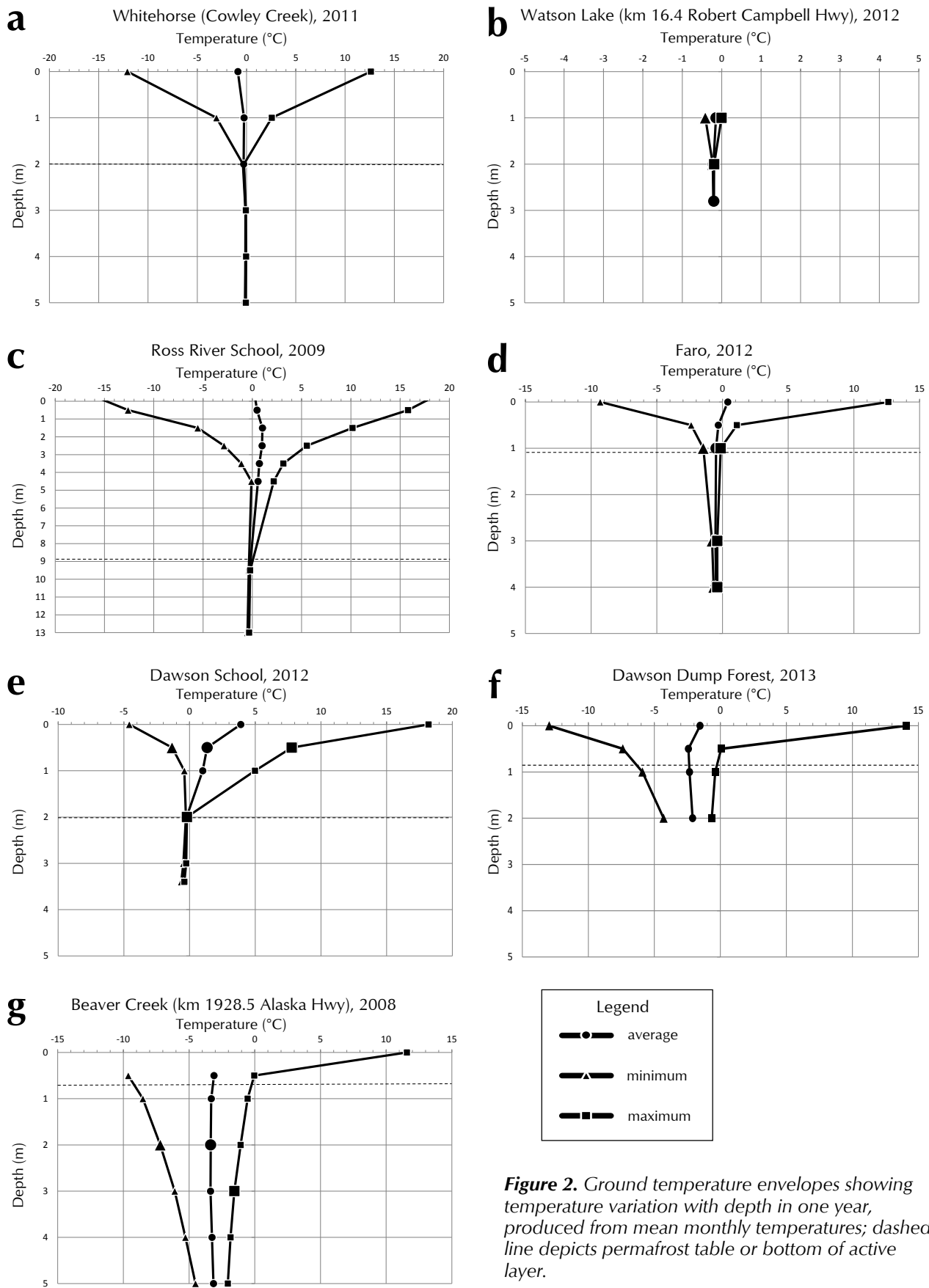
The thickness of the active layer (AL; the ground surface layer above permafrost which thaws and refreezes annually) was interpolated from average monthly ground temperature data measured at depths above and below the permafrost table. At sites with natural organic cover, active layer thicknesses varied between 0.5 m at Beaver Creek and 1.9 m in Whitehorse. At disturbed sites, active layers ranged from 1.9 m at Dawson School to 8.7 m at Ross River School.

Mean annual ground temperature at the top of permafrost (TTOP) (*i.e.*, the permafrost table or the bottom of the active layer) was averaged over the data summary period for each site. TTOP was -0.2°C in Watson Lake and at Dawson school, -0.3°C in Whitehorse and at Ross River School, -0.6°C in Faro, -2.1°C at the Dawson dump forest and -2.7°C in Beaver Creek.

Mean annual ground temperatures at 3 m depth (MT3M), averaged over the data summary period for each site, were: 0°C in Beaver Creek; -0.1°C in Whitehorse; -0.2°C in Watson Lake; -0.4°C at Dawson School; -0.6°C in Faro; and +0.8°C at Ross River School.

The depth of zero annual amplitude (ZAA; where seasonal temperature variation is <0.1°C) was approximately 2.0 m in Whitehorse (Fig. 2a) and Watson Lake (Fig. 2b), and 9.5 m in Ross River (Fig. 2c); however, since the accuracy of the temperature sensors is >0.1°C (as discussed in Data Limitations below), there is some uncertainty with these ZAA values. ZAA was not encountered at any of the other stations. Mean annual ground temperatures at the depth of zero annual amplitude (MTZA) were -0.2°C in Watson Lake, and -0.3°C in Whitehorse and at Ross River School.

Mean annual ground temperatures at the deepest sensor for each station's borehole (MAGT), averaged over the data summary period, were: -2.9°C (at 5 m) in Beaver Creek; -2.0°C (at 2 m) at the Dawson dump forest; -0.6°C (at 3.4 m) at Dawson School; -0.6°C (at 4 m) in Faro; -0.5°C (at 13 m) at Ross River School; -0.2°C (at 2.8 m) in Watson Lake; and -0.1°C (at 5 m) in Whitehorse. Where colder permafrost exists at the Dawson dump forest and in Beaver Creek, the ground temperature envelopes (Fig. 2f,g respectively) show greater temperature variation below the active layer due to the lack of latent heat effects (discussed further below).



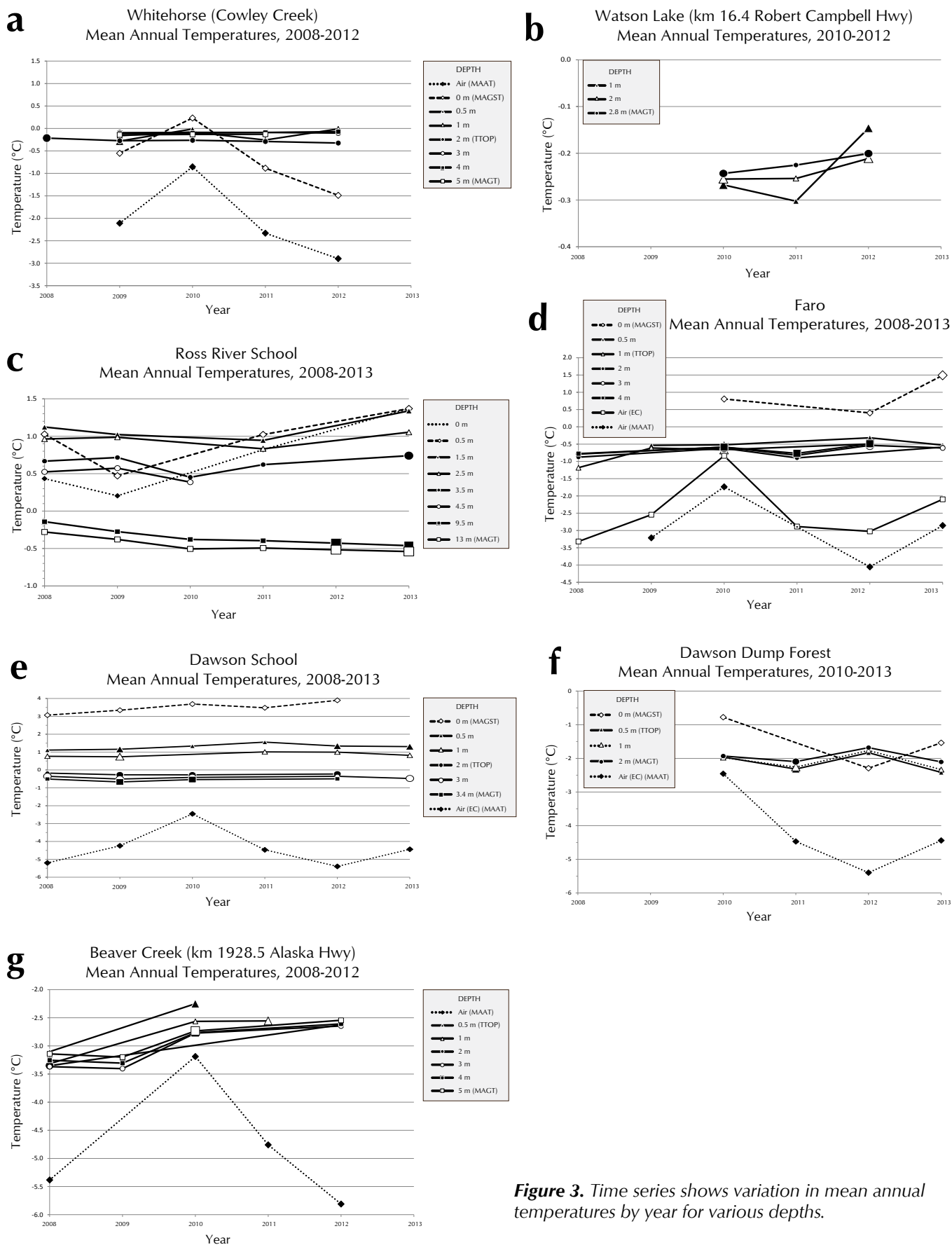


Figure 3. Time series shows variation in mean annual temperatures by year for various depths.

Table 1. Summary of permafrost monitoring station site characteristics and key thermal regime parameters (averaged over the data summary period). EC = Environment Canada climate station.

Station Name	Beaver Creek	Whitehorse	Ross River School	Faro
STATION LOCATION AND CHARACTERISTICS				
location	40 m west of Alaska Highway at km 1928.5 (5 km south of Beaver Creek)	40 m southeast of Salmon Trail, 40 m east of Cowley Creek	15 m west of gym doors	between Blind Creek Rd and Douglas Drive
latitude	62°20'16"N	60°35'35"N	61°58'46.5"N	62°13'24.5"N
longitude	140°50'9"W	134°54'18"W	132°27'9.5"W	133°20'31.3"W
elevation (m)	700	712	659	720
disturbed site?	no	no	yes	no
depths of temperature sensors (m)	air, 0, 0.5, 1.0, 2.0, 3.0, 4.0, and 5.0 m	air, 0, 0.5, 1.0, 2.0, 3.0, 4.0, and 4.95 m	0.5, 1.5, 2.5, 3.5, 4.5, 9.5, and 13.0 m	air, 0, 0.5, 1.0, 2.0, 3.0, and 3.9 m
vegetation	tussocky muskeg with black spruce	mature drunken white spruce forest	patchy grass	young white spruce forest (following 1969 forest fire)
ground cover	moss (15 cm)	moss (10 cm)	gravel	moss (10 cm)
substrate	silt and clay	4 m silt and fine sand underlain by 1 m clay	4 m sand overlying 2 m gravel overlying 14 m silt and clay	4 m fine sandy silt, underlain by gravel
THERMAL REGIME				
data summary period	2008-2012	2009-2012	2008-2013	2008-2013
active layer thickness (depth of permafrost table) (m) - AL	0.5	1.9	8.7	0.9
depth of zero annual amplitude (m) (<0.1 C variation) - ZAA	>5.0	2.0	9.5	no data
mean annual air temperature (°C) - MAAT	-4.8	-2.0	no data	-3.0
mean annual ground temperature (°C):				
at ground surface - MAGST	-1.7 (May 2007-2008)	-0.7	0.7	0.6
at top of permafrost - TTOP	-2.7	-0.3	-0.3	-0.6
at 3m depth - MT3M	-3.0	-0.1	0.8	-0.6
at depth of zero annual amplitude - MTZA	no data	-0.3	-0.3	no data
at deepest sensor in borehole - MAGT	-2.9 (at 5 m)	-0.1 (at 5 m)	-0.5 (at 13 m)	-0.6 (at 4 m)
rate of change over data summary period (°C/decade)	+2.0 (at 3, 4 and 5 m)	no change (at 2, 3, 4 and 5 m)	-0.5 (at 9.5 and 13 m)	+0.4-0.5 (at 2, 3 and 3.9 m)
surface offset (MGST - MAAT)	3.1	1.3	no data	3.6
thermal offset (TTOP - MAGST)	-1.0	0.4	-1.0	-1.2

Surface offset is a parameter which characterizes heat transfer between the air and the ground surface, and is defined as the difference between the mean annual ground surface temperature (MAGST) and mean annual air temperature (MAAT). Snow cover has the greatest influence on surface offsets due to its insulating capacity which restricts heat loss from the ground during the winter (Smith and Riseborough, 2002), but vegetation and subsurface conditions (e.g., soil moisture) are also important (Karunaratne and Burn, 2004). Surface offsets at the monitoring stations, averaged over the data summary

period, were 7.9°C at Dawson School, 3.6°C at Faro, 3.1°C at Beaver Creek, 2.7°C at the Dawson dump forest and 1.3°C at Whitehorse.

Thermal offset is defined as the difference between mean annual ground temperature at the top of permafrost (TTOP) and mean annual ground surface temperature (MAGST). A negative value is most common and indicates that the ground surface is warmer than the permafrost surface, while a positive value indicates the reverse situation. Thermal offset is the result of seasonal variations in the thermal conductivity of the active layer when it is

Table 1 (continued).

Station Name	Dawson School	Dawson Dump Forest	Watson Lake
STATION LOCATION AND CHARACTERISTICS			
location	5 m south of Queen Street, midway between 4th & 5th Ave. at Robert Service School	600 m along Dawson dump road, 25 m on NW side	100 m south of Robert Campbell Hwy at km 16.4
latitude	64°03'40.0"N	64°01'54.7" N	60°9'7.2"N
longitude	139°25'49.1"W	139°17'41.1" W	128°53'7.7"W
elevation (m)	320	344	670
disturbed site?	yes	no	no
depths of temperature sensors (m)	air, 0, 0.5, 1.0, 2.0, 3.0, and 3.4 m	0, 0.5, 1.0, and 2.0 m	0, 1.0, 2.0, and 2.8 m
vegetation	none	spruce forest	mature drunken white spruce forest
ground cover	30 cm mulch and topsoil overlying 40 cm gravel	moss	moss (20 cm)
substrate	3 m organic-rich silt underlain by gravel	sandy silt	silt
THERMAL REGIME			
data summary period	2008-2013	2010-2013	2010-2012
active layer thickness (depth of permafrost table) (m) - AL	1.9	0.6	<1.0
depth of zero annual amplitude (m) (<0.1 C variation) - ZAA	no data	no data	2.0
mean annual air temperature (°C) - MAAT	-4.4 (EC)	-4.2 (EC)	-2.1 (EC)
mean annual ground temperature (°C):			
at ground surface - MAGST	3.5	-1.5	no data
at top of permafrost - TTOP	-0.2	-2.1	-0.2
at 3m depth - MT3M	-0.4	no data	-0.2 (at 2.8 m)
at depth of zero annual amplitude - MTZA	no data	no data	-0.2
at deepest sensor in borehole - MAGT	-0.6 (at 3.4 m)	-2.0 (at 2 m)	-0.2 (at 2.8 m)
rate of change over data summary period (°C/decade)	no change (at 2, 3 and 3.4 m)	no change (at 0.5, 1 and 2 m)	insufficient data
surface offset (MGST - MAAT)	7.9	2.7	no data
thermal offset (TTOP - MAGST)	-3.7	-0.6	no data

frozen and thawed (Romanovsky and Osterkamp, 1995; Smith and Riseborough, 2002) and arises because the thermal conductivity of ice is four times greater than that of water. Thermal offset effectively allows permafrost to develop or persist even if the MAGST is above 0°C (Burn and Smith, 1988; Osterkamp and Romanovsky, 1999; Smith and Riseborough, 2002), which is the case at the Ross River School, the Dawson School and in Faro. Thermal offsets at the monitoring stations, averaged over the data summary period, were -3.7°C at Dawson School, -1.2°C in Faro, -1.0°C in Beaver Creek and at Ross River School, -0.6°C at the Dawson dump forest and +0.4°C in Whitehorse.

DATA LIMITATIONS

Readers must be cautioned that the data presented portray very site specific permafrost conditions only and do not necessarily apply to surrounding areas. Permafrost temperature is very sensitive to microclimate and physical site conditions (e.g., slope, aspect, exposure, elevation, vegetation, organic cover and surficial geology stratigraphy), and may vary both spatially and temporally across relatively small areas. This is illustrated by noting the large differences in ground temperature parameters between the “disturbed” Dawson School and the “natural” Dawson dump forest site.

It must also be emphasized that our data only represent near-surface permafrost conditions. While permafrost thickness is unknown at each of the monitoring stations, it has been reported to be in the range of 2-20 m in warm ($>-0.5^{\circ}\text{C}$) permafrost in southern Yukon, and 20-60 m thick in colder permafrost near Beaver Creek and Dawson (Burn, 2004). Temperatures lower in the profile will not be the same as those at the surface, and that they will respond at different rates to changing surface conditions.

Other significant limitations of the data are related to sub-optimal instrumentation performance that has resulted in significant outliers and gaps in the data record. Battery failures, instrumentation errors (possibly due to condensation, extreme cold temperatures and/or wear) and damage by animals or vandalism have been ongoing issues affecting all stations to some degree. Very careful and time-consuming quality control measures are required to filter outlier data and fill gaps by modeling or interpolation where reasonable (based on repeating trends from other years). For cases where this is not possible, incomplete data are omitted resulting in a discontinuous record.

In addition, the accuracy of the HOBO instrumentation is reported in the Onset proprietary specifications as $\pm 0.25^{\circ}\text{C}$ and the resolution is 0.03°C (for TMCx-HD series thermistor probes with HOBO U12 data loggers). For most sites this amount of error is tolerable for characterizing permafrost temperatures below -0.5°C . However, for very warm permafrost sites (e.g., Whitehorse and Watson Lake), where measured mean ground temperatures are as warm as -0.1°C or -0.2°C , the error becomes more significant in distinguishing frozen and unfrozen ground.

DISCUSSION

Permafrost thaw occurs when permafrost temperatures are warmer than -0.5°C (Osterkamp and Romanovsky, 1999). At the Whitehorse, Watson Lake, Dawson School and Ross River School monitoring stations, thawing permafrost is suggested by very warm ($>-0.5^{\circ}\text{C}$) ground temperatures and the occurrence of relatively isothermal mean temperature profiles. Drunken forests surrounding the Whitehorse and Watson Lake monitoring stations are additional visual indicators of thawing or degrading permafrost. The Faro site is also very close to thawing, with a MAGT of -0.6°C .

The colder permafrost conditions observed at the Dawson dump forest (-2.0°C at 2 m depth) and Beaver Creek (-3.0°C at 3 m depth) monitoring stations are likely a product of their higher latitudes, more continental locations and older landscapes where ancient permafrost was cold enough to survive past interglacial periods (Brown, 1970; French, 2007; Froese *et al.*, 2008).

Permafrost is considered “warm” when it is above -2°C because of increasing amounts of unfrozen water present as its temperature approaches 0°C . The thermal regime of warm ice-rich permafrost is dominated by latent heat effects (Romanovsky *et al.*, 2010) which result from the large amounts of energy either consumed to thaw ice or released as water freezes within the ground. This effectively dampens ground temperature variations (Romanovsky and Osterkamp, 2000) and contributes to more isothermal temperature profiles. It also allows permafrost to persist at depth for long periods once thaw has begun (Smith *et al.*, 2010; Osterkamp and Romanovsky, 1999; Froese *et al.*, 2008). Modeling suggests that centuries to millennia are required to completely thaw relatively thin (>15 m) permafrost in the discontinuous zone following natural disturbance and/or under current rates of climate warming (Osterkamp and Romanovsky, 1999; Burn, 1998 and 2004). Ground surface instability resulting from near-surface permafrost thaw or active-layer thickening, may however occur much more rapidly, *i.e.* in less than a decade (Burn, 1998, 2004).

Although the total duration of permafrost monitoring to date has been short (*i.e.*, between 3 and 6 years) for each community, some interesting short-term trends are evident in the mean annual temperature time series graphs (Fig. 3) between 2008 and 2013. Changes in warm ice-rich permafrost temperatures are generally insignificant or smaller in magnitude due to the dampening by latent heat effects (Smith *et al.*, 2005), while colder permafrost tends to warm more rapidly (Romanovsky *et al.*, 2010). In Whitehorse and Dawson, permafrost temperatures have remained relatively stable. Permafrost warmed at rates on the order of $2^{\circ}\text{C}/\text{decade}$ in Beaver Creek, and $0.4\text{--}0.5^{\circ}\text{C}/\text{decade}$ in Faro. In contrast, the permafrost at Ross River School has cooled at a rate of $-0.5^{\circ}\text{C}/\text{decade}$. Caution should be exercised in interpreting these rates of change over such a short monitoring period, and at least 10 years of data are recommended before significant long term changes can be reported. The fact that the 2010 MAATs

appear to have been anomalously warm at all stations may have particularly skewed the short term trends presented.

Long term permafrost warming or cooling is generally driven by changes in snow cover and air temperature. In Alaska, permafrost warming has been attributed primarily to increased snow depths (Osterkamp and Romanovsky, 1999). While snow cover data are collected by Environment Canada near some monitoring stations, they are incomplete or lacking at others. It is therefore recommended that the monitoring stations be equipped with snow cover data loggers (as described in Lewkowicz *et al.*, 2012) so that these relationships can be further explored in future years.

A major limitation of our data is that they only represent very site specific near-surface conditions. It is recommended that YGS examine opportunities to expand its monitoring network to include a wider variety of site conditions, ideally with some deeper boreholes that extend either to the base of permafrost or at least a few metres below the depth of zero annual amplitude. Future stations should also, where practical, be strategically located in areas representative of large regions. In addition, there are many permafrost monitoring stations within Yukon that have been, or are currently maintained by other parties, and access to these data would provide a much more complete picture of permafrost thermal conditions in the territory. A further recommendation is therefore that YGS explore partnering opportunities to access and/or collect these external data in a central repository, and that the collective territory-wide monitoring results be reported at regular intervals.

SUMMARY

While some challenges with network maintenance and instrumentation errors have resulted in significant gaps in the data record, up to 6 years of data have now been collected from Yukon Geological Survey's permafrost monitoring network between 2008 and 2013. These data are valuable for characterizing the local near-surface ground thermal regime at each monitoring station, and have allowed some preliminary short-term changes to be detected, as outlined below.

Results for the 2008-2013 period show that very warm permafrost conditions ($>0.5^{\circ}\text{C}$) exist at the Whitehorse, Watson Lake, Ross River School and Dawson School monitoring stations, and permafrost temperatures in Faro

are marginally below this at -0.6°C , with a slight short-term warming trend apparent. Ground temperatures have not changed significantly at the remaining two sites, with the exception of the Ross River School, where slight cooling is apparent. Because permafrost thaw begins around -0.5°C , latent heat effects dominate the thermal regime in warm permafrost, dampening temperature changes at depth. While near-surface warm permafrost is vulnerable to rapid thaw as a result of surface disturbance and/or climate change, warm permafrost at depth may persist for much longer periods where high thermal offsets are present.

Much colder permafrost conditions were measured at the Dawson dump forest and Beaver Creek monitoring stations, where mean annual ground temperatures are -2.0°C (at 2 m depth) and -2.9°C (at 5 m depth), respectively. These colder temperatures are likely a product of more continental locations, and older permafrost which was cold enough to survive past interglacial periods. While no significant rate of change was observed at the Dawson dump forest site, rapid warming at a rate of $2.1^{\circ}\text{C}/\text{decade}$ occurred over the monitoring period at Beaver Creek (at 3 m depth).

YGS intends to maintain and upgrade the monitoring network as required in order to continue gathering baseline data for the long term. Because these data only represent very site specific conditions, opportunities to expand the network and collaborate with external parties operating similar monitoring stations should be further explored. This would facilitate more complete and more regular reporting on the thermal state of permafrost in Yukon.

ACKNOWLEDGMENTS

Sincere thanks are extended to the many people who have assisted with station maintenance and data collection over the years: Kenji Yoshikawa (University of Alaska Fairbanks); Sarah Laxton and Jeff Bond (Yukon Geological Survey); Lorraine Millar, Steve Colp, Neale Wortley, Brett Isbister and Neal Allison (Compliance Monitoring and Inspections, Yukon Energy Mines and Resources); Steve Caram; Jim Coates (Kryotek Arctic Innovation); Richard Trimble and Justin Pigage (Tetra Tech EBA); and Fabrice Calmels (Northern Climate ExChange, Yukon College). Many improvements were made to this paper based on helpful reviews and suggestions by Jeff Bond and Fabrice Calmels.

REFERENCES

- Bonnaventure, P.P., Lewkowicz, A.G., Kremer, M. and Sawada, M.C., 2012. A permafrost probability model for the southern Yukon and northern British Columbia, Canada. *Permafrost and Periglacial Processes*, vol. 23, p. 52–68.
- Brown, R.J.E., 1970. *Permafrost in Canada – its influence on northern development*. University of Toronto Press, Toronto.
- Burn, C.R., 1998. The response (1958 to 1997) of permafrost and near-surface ground temperatures to forest fire, Takhini River valley, southern Yukon Territory. *Canadian Journal of Earth Sciences*, vol. 35, p. 184–199.
- Burn, C.R., 2004. Permafrost. *In: Ecoregions of the Yukon Territory: biophysical properties of Yukon landscapes*, C.A.S. Smith, J.C. Meikle and C.F. Roots (eds.), Agriculture and Agri-Food Canada, PARC Technical Bulletin No. 04-01, Summerland, British Columbia, p. 32-35.
- Burn, C.R. and Smith, C.A.S., 1988. Observations of the “thermal offset” in near-surface mean annual ground temperatures at several sites near Mayo, Yukon Territory, Canada. *Arctic*, vol. 41, p. 99-104.
- French, H.M., 2007. *The Periglacial Environment*, Third Edition. John Wiley and Sons, Chichester, 478 p.
- Froese, D.G., Westgate, J.A., Reyes, A.V., Enkin, R.J. and Preece, S.J., 2008. Ancient permafrost and a future warmer Arctic. *Science*, vol. 321, p. 1648.
- Heginbottom, J.A., Dubreuil, M.A. and Harker, P.T., 1995. Canada – Permafrost, National Atlas of Canada (5th edition). Natural Resources Canada, Ottawa. Plate/Map 2.1 (MCR 4177), 1:7 500 000 scale.
- Karunaratne, K.C. and Burn, C.R. 2004. Relations between air and surface temperatures in discontinuous permafrost terrain near Mayo, Yukon Territory. *Canadian Journal of Earth Sciences*, vol. 41, p. 1437–1451.
- Lewkowicz, A.G., Bonnaventure, P.P., Smith, S.L. and Kuntz, Z., 2012. Spatial and thermal characteristics of mountain permafrost, northwest Canada. *Geografiska Annaler: Series A, Physical Geography*, vol. 94, p. 195–213.
- Lipovsky, P.S. and Yoshikawa, K., 2009. Initial results from the first year of the Permafrost Outreach Program, Yukon, Canada. *In: Yukon Exploration and Geology 2008*, L.H. Weston, L.R. Blackburn and L.L. Lewis (eds.), Yukon Geological Survey, p. 161-172.
- Osterkamp, T.E. and Romanovsky, V.E., 1999. Evidence for warming and thawing of discontinuous permafrost in Alaska. *Permafrost and Periglacial Processes*, vol. 10, p. 17-37.
- Romanovsky, V.E., and Osterkamp, T.E. 1995. Interannual variations of the thermal regime of the active layer and near-surface permafrost in northern Alaska. *Permafrost and Periglacial Processes*, vol. 6, p. 313–335.
- Romanovsky, V.E. and Osterkamp, T.E., 2000. Effects of unfrozen water on heat and mass transport processes in the active layer and permafrost. *Permafrost and Periglacial Processes*, vol. 11, p. 219-239.
- Romanovsky, V.E., Smith, S.L. and Christiansen, H.H., 2010. Permafrost thermal state in the polar Northern Hemisphere during the International Polar Year 2007–2009: a synthesis. *Permafrost and Periglacial Processes*, vol. 21, p. 106–116.
- Smith, S.L., Burgess, M.M., Riseborough, D.W. and Nixon, F.M., 2005. Recent trends from Canadian permafrost thermal monitoring network sites. *Permafrost and Periglacial Processes*, vol. 16, p. 19–30.
- Smith, M.W. and Riseborough, D.W., 2002. Climate and the limits of permafrost: a zonal analysis. *Permafrost and Periglacial Processes*, vol. 13, p. 1–15.
- Smith, S.L., Romanovsky, V.E., Lewkowicz, A.G., Burn, C.R., Allard, M., Clow, G.D., Yoshikawa, K. and Throop, J., 2010. Thermal State of Permafrost in North America – A contribution to the International Polar Year. *Permafrost and Periglacial Processes*, vol. 21, p. 117–135.
- Throop, J., Lewkowicz, A.G. and Smith, S.L., 2012. Climate and ground temperature relations at sites across the continuous and discontinuous permafrost zones, northern Canada. *Canadian Journal of Earth Sciences*, vol. 49, p. 865-876.

Preliminary detrital zircon geochronology of the Neruokpuk Formation in the Barn Mountains, Yukon

W.C. McClelland¹

Department of Earth and Environmental Sciences, University of Iowa

M. Colpron

Yukon Geological Survey

K. Piepjohn

Bundesanstalt für Geowissenschaften und Rohstoffe (BGR), Geologie der Energierohstoffe, Polargeologie

W. von Gosen

Geozentrum Nordbayern, Krustendynamik, Friedrich-Alexander-Universität Erlangen-Nürnberg,

W. Ward

Department of Earth and Environmental Sciences, University of Iowa

J.V. Strauss

Department of Earth and Planetary Sciences, Harvard University

McClelland, W.C., Colpron, M., Piepjohn, K., von Gosen, W., Ward, W. and Strauss, J.V., 2015. Preliminary Detrital Zircon Geochronology of the Neruokpuk Formation in the Barn Mountains, Yukon. *In: Yukon Exploration and Geology*, K.E. MacFarlane, M.G. Nordling and P.J. Sack (eds.), Yukon Geological Survey, p. 123-143.

ABSTRACT

Neoproterozoic to Cambrian siliciclastic rocks in the Barn Mountains, Yukon are stratigraphically similar to coeval strata on the northwest Laurentian margin and the North Slope subterrane of the Arctic Alaska terrane. Sandstone samples collected for detrital zircon U/Pb geochronology from *Oldhamia*-bearing sections in the Barn Mountains yield age spectra with major Paleoproterozoic and subordinate Mesoproterozoic and Archean peaks that are compatible with a Laurentian cratonal provenance. Comparison of data from the Barn Mountains with available data from the Laurentian margin is permissive of derivation from either the northwestern or the north to northeastern margin of Laurentia.

¹bill-mcclelland@uiowa.edu

INTRODUCTION

Tectonic models for the evolution of northern Yukon, Arctic Alaska, and the adjacent Canada Basin are strongly influenced by the interpreted location and nature of the boundary separating the autochthonous Laurentian margin from displaced terranes. While many of the pre-Carboniferous strata of the Arctic Alaska terrane are characterized by Siberian and/or Baltican faunal and provenance affinities (Patrick and McClelland, 1995; Dumoulin *et al.*, 2002, 2014; Amato *et al.*, 2009; Miller *et al.*, 2011; Till *et al.*, 2014), coeval strata in the North Slope subterrane of the northeast Brooks Range and adjacent Yukon do not appear to be as exotic (Strauss *et al.*, 2013). Long-standing stratigraphic arguments support correlation of Neoproterozoic and Cambrian shelf and basal strata of the Yukon block and Richardson trough with coeval

strata in the British and Barn Mountains in Yukon and the northeastern Brooks Range in Alaska (Fig. 1; e.g., Norris, 1997; Lane, 1991). This correlation is consistent with the requirements of rotational (Grantz *et al.*, 2011) and non-rotational (Lane, 1997) models for Cretaceous opening of the Canada Basin. In contrast, Strauss *et al.* (2013) recently concluded that the North Slope subterrane, differentiated from the rest of the Arctic Alaska terrane by its peri-Laurentian faunal affinity, was allochthonous relative to the Yukon Block (Fig. 1). In particular, Neoproterozoic-Cambrian strata in the Sadlerochit, Shublik and British Mountains more closely resemble the stratigraphy along the northeastern rather than the northwestern Laurentian continental margin. The later model requires a tectonic boundary between the British Mountains and the Yukon Block.

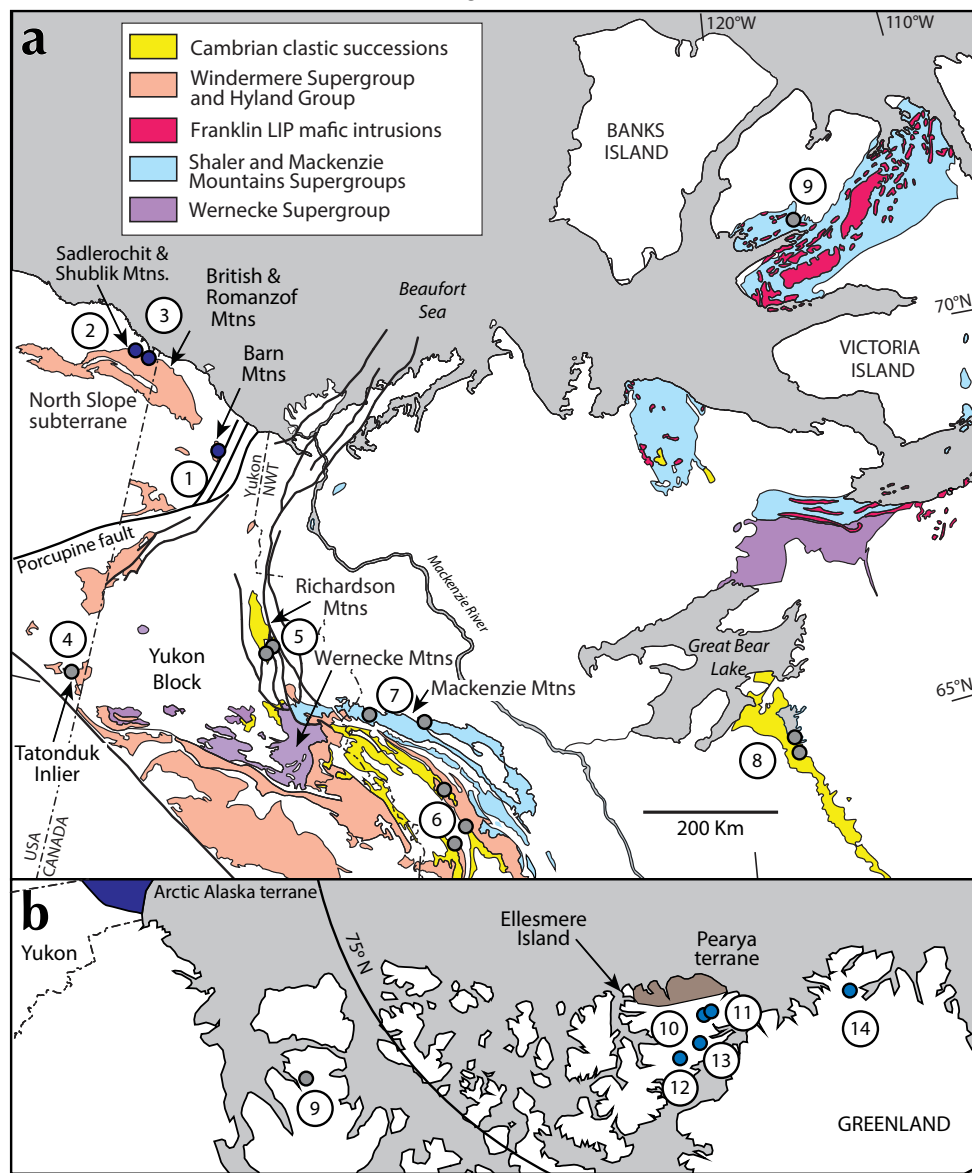


Figure 1. Generalized maps showing (a) the distribution of Precambrian and Cambrian strata and detrital zircon sample locations in northwestern Canada and northeastern Alaska (modified after Lane and Gehrels, 2014) and (b) detrital zircon sample locations on Ellesmere Island and Greenland. Numbered locations are keyed to detrital zircon data plotted in Figures 7 and 8, and coloured according to North Slope subterrane (blue), northwestern Laurentia (grey), and north to northeastern Laurentia (light blue).

One potential boundary separating allochthonous terranes and autochthonous North America is the Porcupine fault (Porcupine megashear of Churkin *et al.*, 1980; also formerly considered an extension of the Kaltag fault from Alaska by Norris and Yorath, 1981 and Norris, 1997) located between the Barn Mountains at the eastern end of the North Slope subterrane and the Yukon Block and Richardson trough (Fig. 1). Displacement on the Porcupine fault system has been proposed to be zero (Lane, 1992, 1998) to hundreds or thousands of kilometres (Norris and Yorath, 1981; Hubbard *et al.*, 1987; Oldow *et al.*, 1987). Zero-displacement models are consistent with the inferred stratigraphic continuity from the Yukon Block to the British Mountains. Alternatively, large-displacement models are consistent with translation models for the opening of the Canada Basin (e.g., Dutro, 1981) as well as models invoking translation of terranes along the Canadian Arctic margin in the Paleozoic (e.g., Lawver *et al.*, 2002; Colpron and Nelson, 2009).

Correlation of Neoproterozoic and Cambrian stratigraphy across the Porcupine fault zone can be evaluated by comparison of detrital zircon signatures from coeval strata on either side of the structure. We present new U/Pb detrital zircon data from three samples in the Barn Mountains and compare the signature with that of the northwestern (Leslie, 2009; Hadlari *et al.*, 2012; Lane and Gehrels, 2014) and northeastern Laurentian margin (Kirkland *et al.*, 2009; Anfinson *et al.*, 2012; Beranek *et al.*, 2013; Hadlari *et al.*, 2014) as well as the signature of coeval strata in the North Slope subterrane defined by Strauss *et al.* (2013).

GEOLOGY OF THE BARN MOUNTAINS AND SAMPLE DESCRIPTIONS

The Barn Mountains are largely underlain by imbricated thrust panels that repeat a stratigraphic succession consisting of a lower siliciclastic section of Neoproterozoic(?)–Cambrian sandstone, siltstone, argillite, and local limestone, overlain by Ordovician–Silurian shale, limestone, and chert section (Figs. 2 and 3; Cecile, 1988; Cecile and Lane, 1991). Age control for the Barn Mountains succession is provided by the presence of the Early to Middle Cambrian trace fossil *Oldhamia* in siltstone interbedded with maroon and green shale of the lower siliciclastic section (Fig. 4; Hofmann *et al.*, 1994; Herbosch and Verniers, 2011) and Ordovician and Silurian graptolites in the overlying shale–chert-dominated section (Lenz and Perry, 1972). The lower siliciclastic

section has been assigned to the Neruokpuk Formation and is considered equivalent to lithologically similar rocks in the British Mountains (Cecile and Lane, 1991; Lane, 1991). The Ordovician–Silurian shale and chert section has traditionally been correlated with the Road River Group of the Richardson trough and Selwyn basin based on lithologic and faunal (graptolites) similarities (Cecile, 1988; Lane, 1991, 2007; Lane *et al.*, 1995; Norris, 1997). Correlative strata are also known from the British Mountains where they are overlain by Upper Silurian–Lower Devonian(?) turbiditic sandstone, shale, and local polymictic conglomerate (Lane, 2007); rocks that are unlike correlatives in Selwyn basin to the south. Based on correlation of the shale–chert sequence with the Road River Group and the occurrence of *Oldhamia* in the lower siliciclastic section, Lane (1991; Lane *et al.*, 1995) proposed correlation between the Neruokpuk Formation and *Oldhamia*-bearing strata of the Hyland Group in Selwyn basin. Neoproterozoic–lower Paleozoic rocks on the eastern flank of the Barn Mountains are overlain by black shale of the Upper Devonian Imperial Formation and intruded by Late Devonian granites of the Old Crow suite. Elsewhere, the imbricate stack in the Barn Mountains is unconformably overlain by the Carboniferous Kekiktuk and Kayak formations (Fig. 2).

Three samples of sandstone from the Barn Mountains were collected for detrital zircon U/Pb geochronology. Sample 13-07 was taken from a 2 m-thick coarse-grained sandstone layer bound above and below by argillite (Fig. 5a). Sample 13-16 is a very coarse-grained sandstone collected from a 10-m-thick sandstone layer (Fig. 5b). Sample 13-18 was collected from a series of 5 to 10-cm-thick sandstone beds interbedded with *Oldhamia*-bearing siltstone (Figs. 4 and 5c). Since age control for the section is limited to the presence of *Oldhamia*, all of the samples are inferred to be roughly coeval and Early to Middle Cambrian in age, perhaps as old as Ediacaran locally.

ANALYTICAL METHODS

Zircons were separated from the sandstone samples by standard gravimetric and magnetic techniques. An aliquot was randomly removed from the heavy mineral separate and non-zircon grains were removed from the aliquot. The remaining zircon grains were mounted with natural zircon standards in 2.5 cm epoxy mounts and polished to expose the grain interiors. Cathodoluminescence images were collected prior to analysis. The zircons were analyzed for U/Pb by laser ablation multicollector

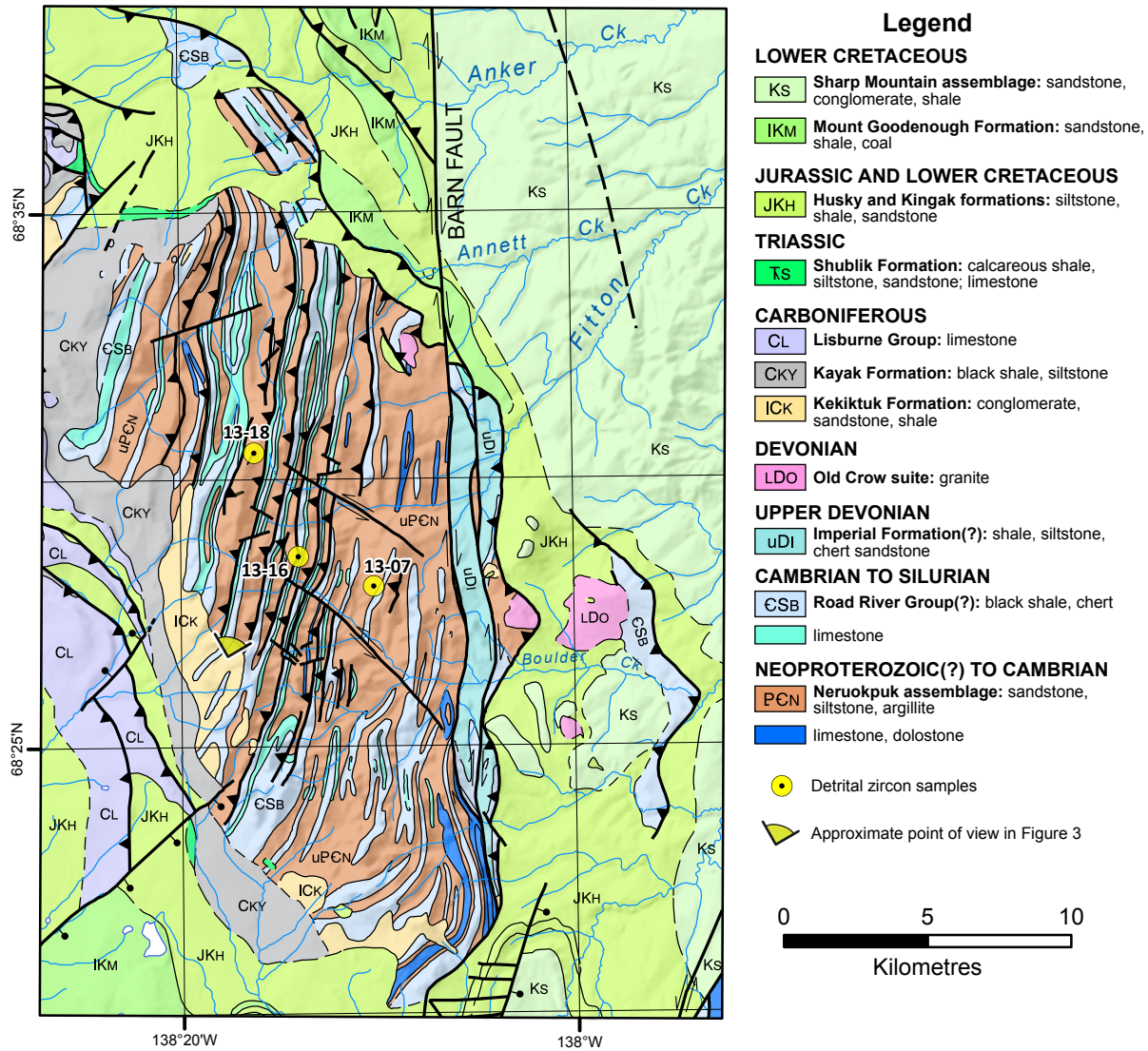


Figure 2. Geological map of the Barn Mountains showing locations of detrital zircon samples presented in this paper. Modified after Cecile and Lane (1991), Dyke (1997), Norris (1981) and our unpublished mapping.



Figure 3. View to the north at the western Barn Mountains displaying the repeated Neoproterozoic(?)–lower Paleozoic succession of sandstone-siltstone (brown), limestone (white) and shale-chert (black). Approximate locations for two of the detrital zircon samples discussed in this paper are shown. Distance between the two sample sites is ~4 km; apparent distance in field of view is ~2.8 km.



inductively coupled plasma mass spectrometry (LA-MC-ICPMS) at the Arizona LaserChron Center (Gehrels *et al.*, 2006, 2008) using a Photon Machines Analyte G2 excimer laser coupled with a Nu HR ICPMS. The sample protocol followed Gehrels *et al.* (2008) using a spot diameter of 30 microns. Common Pb corrections were made using ^{204}Hg -corrected ^{204}Pb measurements for each analysis and initial Pb compositions of Stacey and Kramers (1975). U and Th concentrations and Pb/U fractionation were calibrated

Figure 4. Early to Middle Cambrian trace fossil *Oldhamia* in siltstone of the Neruokpuk Formation, Barn Mountains, at sample site 13-18. Lens cap for scale; letters ~3 mm-wide.

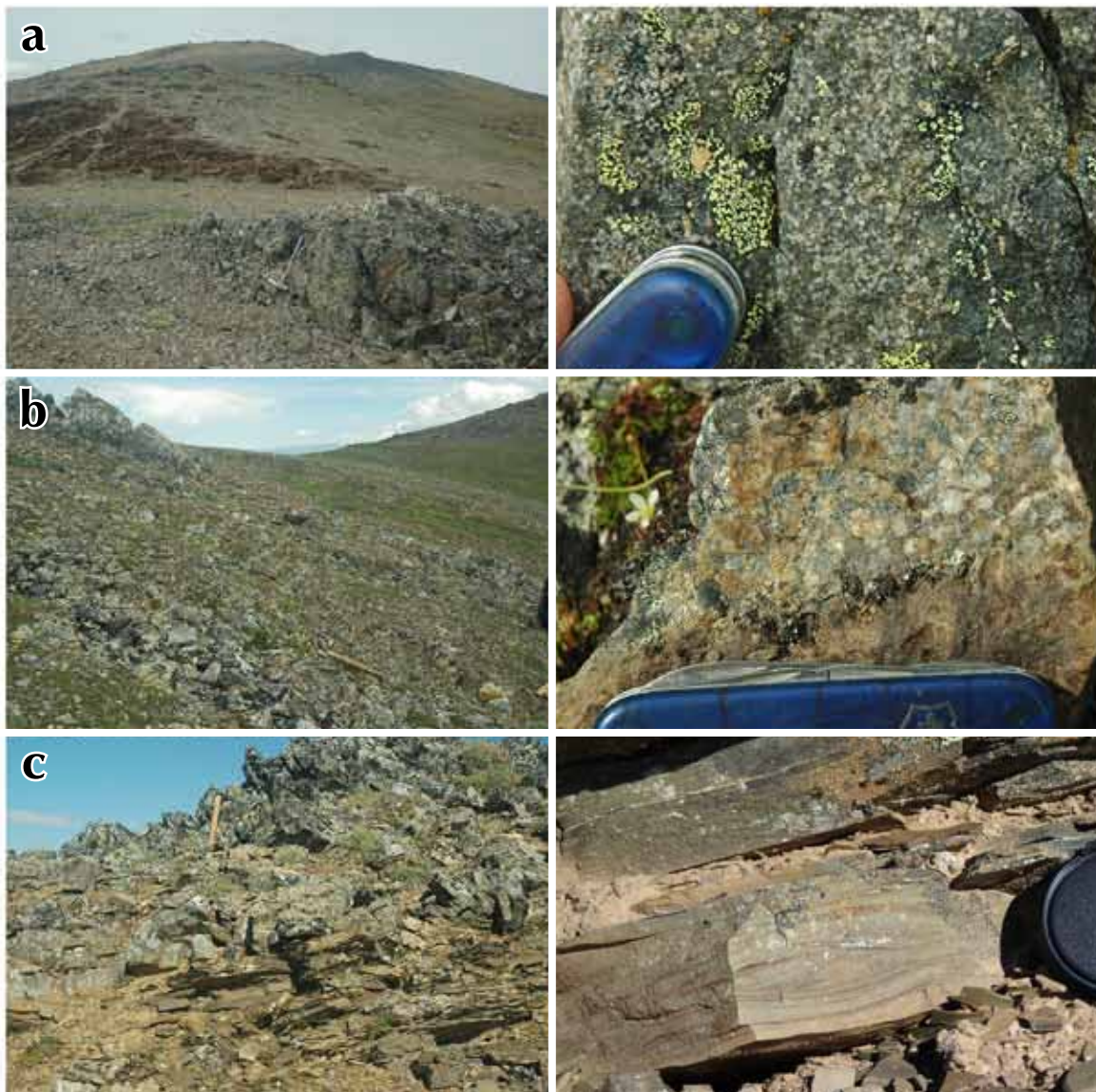


Figure 5. Photographs of outcrops (left) and hand samples (right) for sample sites (a) 13-07, (b) 13-16 (pocket-knife for scale) and (c) 13-18 (lens cap for scale).

against the Arizona Laserchron Center Sri Lanka (SL) zircon standard (563.5 ± 3.2 Ma; ~ 518 ppm U and 68 ppm Th; Gehrels *et al.*, 2008). U/Pb analytical data are reported in Table 1 (located at end of this paper) and plotted in Fig. 6. Analyses that are $>10\%$ discordant, $>5\%$ reversely discordant or have large uncertainties ($>10\%$ at the 2σ level) are not considered in the following discussion. $^{206}\text{Pb}/^{238}\text{U}$ ages are preferred for apparent ages less than 1000 Ma whereas $^{207}\text{Pb}/^{206}\text{Pb}$ ages are used for analyses older than 1000 Ma. In cases where the $^{206}\text{Pb}/^{238}\text{U}$ and $^{207}\text{Pb}/^{206}\text{Pb}$ ages straddle 1000 Ma, the age with lower uncertainty is used. The probability density plots were made with the program by Ludwig (2008). The relative age probability distributions and cumulative probability plots were made using macros provided by G.E. Gehrels at the Arizona Laserchron facility.

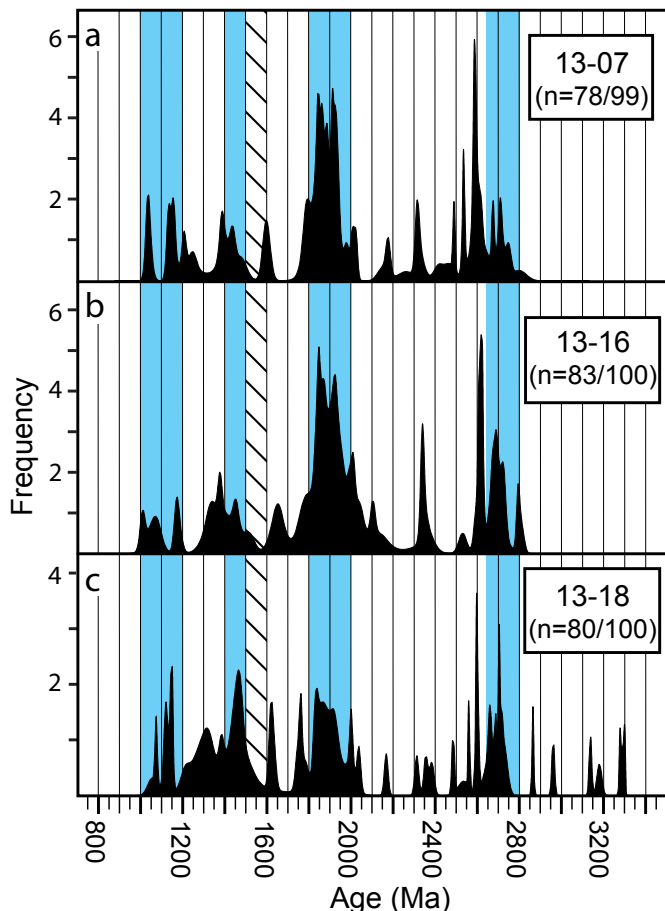


Figure 6. Probability density plots of detrital zircon data from Neoproterozoic(?)–Cambrian strata in the Barn Mountains. Ratio of analyses plotted versus total zircon analyzed is shown in upper right; see Table 1 for details. The coloured bars delineate ages of Laurentian basement as shown by Strauss *et al.* (2013) including the Laurentian magmatic gap (diagonal bars) of Van Schmus *et al.* (1993).

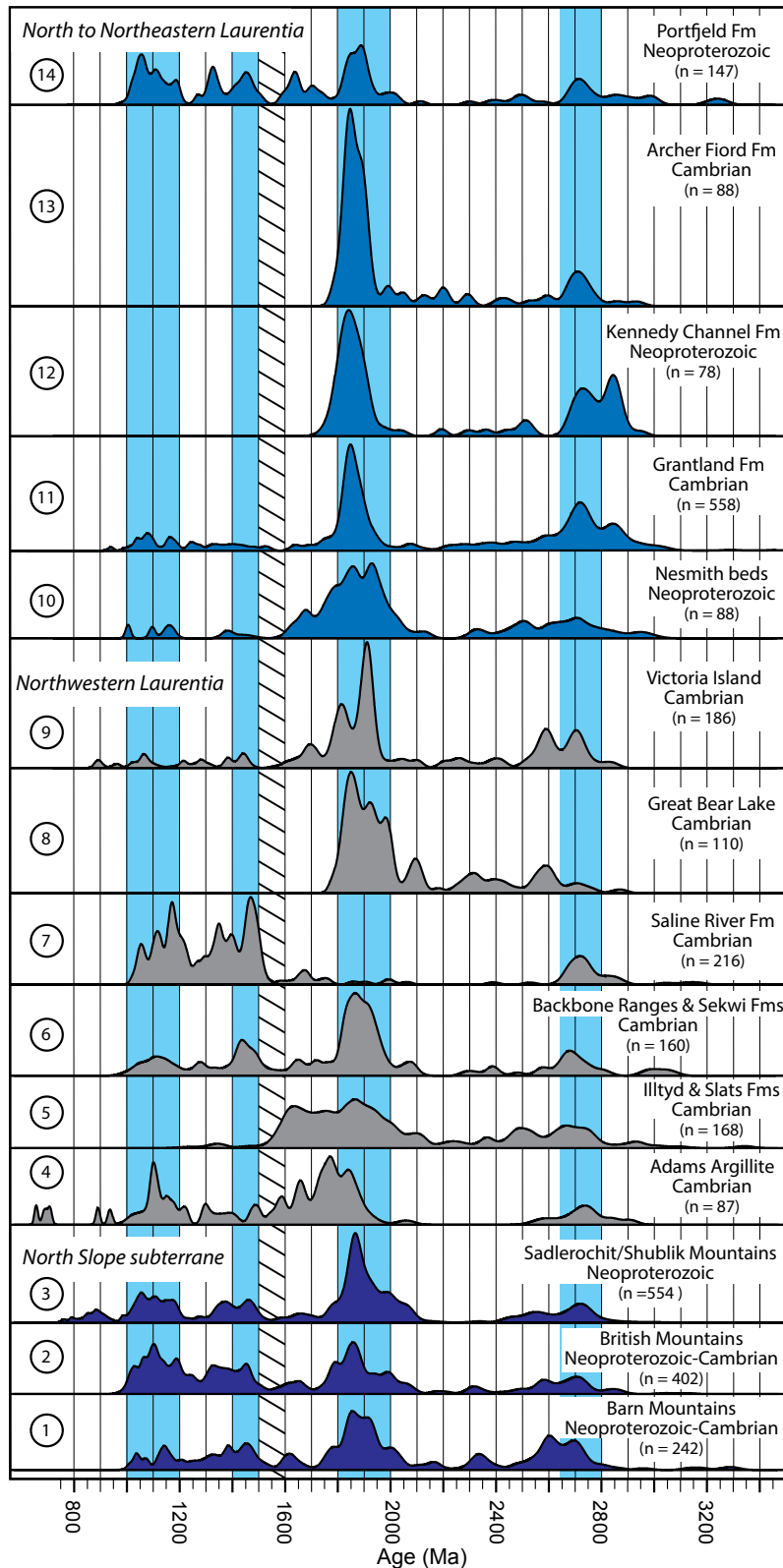
RESULTS

All three samples yielded populations of well-rounded spherical to elongate zircon. Sample 13-07 contains subordinate euhedral grains. Most of the grains have well-developed oscillatory zoning, but some lack zoning or have rims with different CL properties. Samples 13-07 and 13-16 show similar age distributions with prominent peaks at 1850 Ma, 1925 Ma, 2580–2625 Ma, and 2650–2725 Ma (Fig. 6a,b). Subordinate peaks in both samples are between 1000–1250 Ma, 1350–1450 Ma, 1550–1650 Ma, 2000–2100 Ma, 2300–2350 Ma, and 2790–2800 Ma. Sample 13-18 contains the same age components of the other samples, but includes much stronger signals from the 1000–1250 Ma and 1350–1450 Ma populations and contains several Archean grains >2.8 Ga (Fig. 6c). Differences in the age spectra for each sample are not considered to be significant since the variation is largely a function of abundance rather than age. Sample 13-18, the finer-grained sandstone that is interlayered with Oldhamia-bearing siltstone, records the addition of Mesoproterozoic and Archean grains to the Paleoproterozoic signature that dominates samples 13-07 and 13-16.

DISCUSSION

Strata of the Barn Mountains have been correlated with similar rocks in the British Mountains and the northeastern Brooks Range (Lane, 1991) and thus appear to be the easternmost extent of the North Slope subterrane of Arctic Alaska. Detrital zircon ages from Neoproterozoic–Cambrian units in the British Mountains define 1000–1200 Ma, 1300–1500 Ma, 1800–2000 Ma, and 2600–2800 Ma populations, all of which are consistent with derivation from the Laurentian craton (Strauss *et al.*, 2013). The age distribution is similar to that seen in the Neruokpuk samples of the Barn Mountains, but the abundances differ (Fig. 7). This variation in abundance is portrayed by the divergence of the composite samples from the British and Barn Mountains in a cumulative probability plot (Fig. 8).

Siliciclastic strata of definite Laurentian origin are exposed on Victoria Island, the Mackenzie Mountains and Selwyn basin and sequences exposed in a series of uplifts or inliers that define the Yukon Block. Studies attempting to characterize the detrital zircon signature of northwestern Laurentia conclude that the detrital signature of Neoproterozoic to Cambrian strata are dominated by Mesoproterozoic ages derived from primary Laurentian basement sources or secondary sources through recycling



(Lane and Gehrels, 2014; Hadlari *et al.*, 2012). Cambrian strata in particular define three main source regions: (1) recycling of the Wernecke Supergroup which is dominated by 1600-1700 Ma, 1800-2000 Ma, 2300-2500 Ma and 2700 Ma populations; (2) recycling of the Mackenzie Mountains Supergroup which is dominated by 1000-1400 Ma grains thought to be derived ultimately from the Grenville orogen (Rainbird *et al.*, 1992, 1997); and (3) Great Bear Lake strata that exhibit a dominant 1800-2000 Ma peak, reflecting proximity to the Great Bear magmatic arc (Hadlari *et al.*, 2012; Lane and Gehrels, 2014).

The detrital zircon record for Cambrian units flanking the Yukon Block in the Richardson trough is provided by samples of the Slats Creek and Illtyd formations, which are characterized by local recycling of Paleoproterozoic grains from the Wernecke Supergroup (Fig. 7; Lane and Gehrels, 2014). The age profile from the Adams Argillite, an *Oldhamia*-bearing unit deposited on the western margin of the Yukon Block, is markedly different due to the presence of Neoproterozoic grains as young as 660 Ma and abundant 1000-1200 Ma grains (Fig. 7; Gehrels *et al.*, 1999; Lane and Gehrels, 2014).

In comparison, the Barn Mountains samples vary in abundance of Mesoproterozoic grains when compared to the Yukon Block samples, but are similar to the Illtyd and Slats Creek formations in Paleoproterozoic grain distribution (Fig. 8).

Figure 7. Relative age probability distributions of detrital zircon U/Pb ages from the Barn Mountains, North Slope subterrane, northwestern Laurentia, and north to northeastern Laurentia. Data are from (1) this study; (2-3) Strauss *et al.* (2013), Macdonald *et al.* (2009); (4-5) Lane and Gehrels (2014); (6) Leslie (2009); (7-9) Hadlari *et al.* (2012); (10-11) Beranek *et al.* (2013), Hadlari *et al.* (2014); (12-13) Anfinson *et al.* (2012); and (14) Kirkland *et al.* (2009). General locations of sampling sites are shown in Figure 1. The coloured bars are the same as in Figure 6.

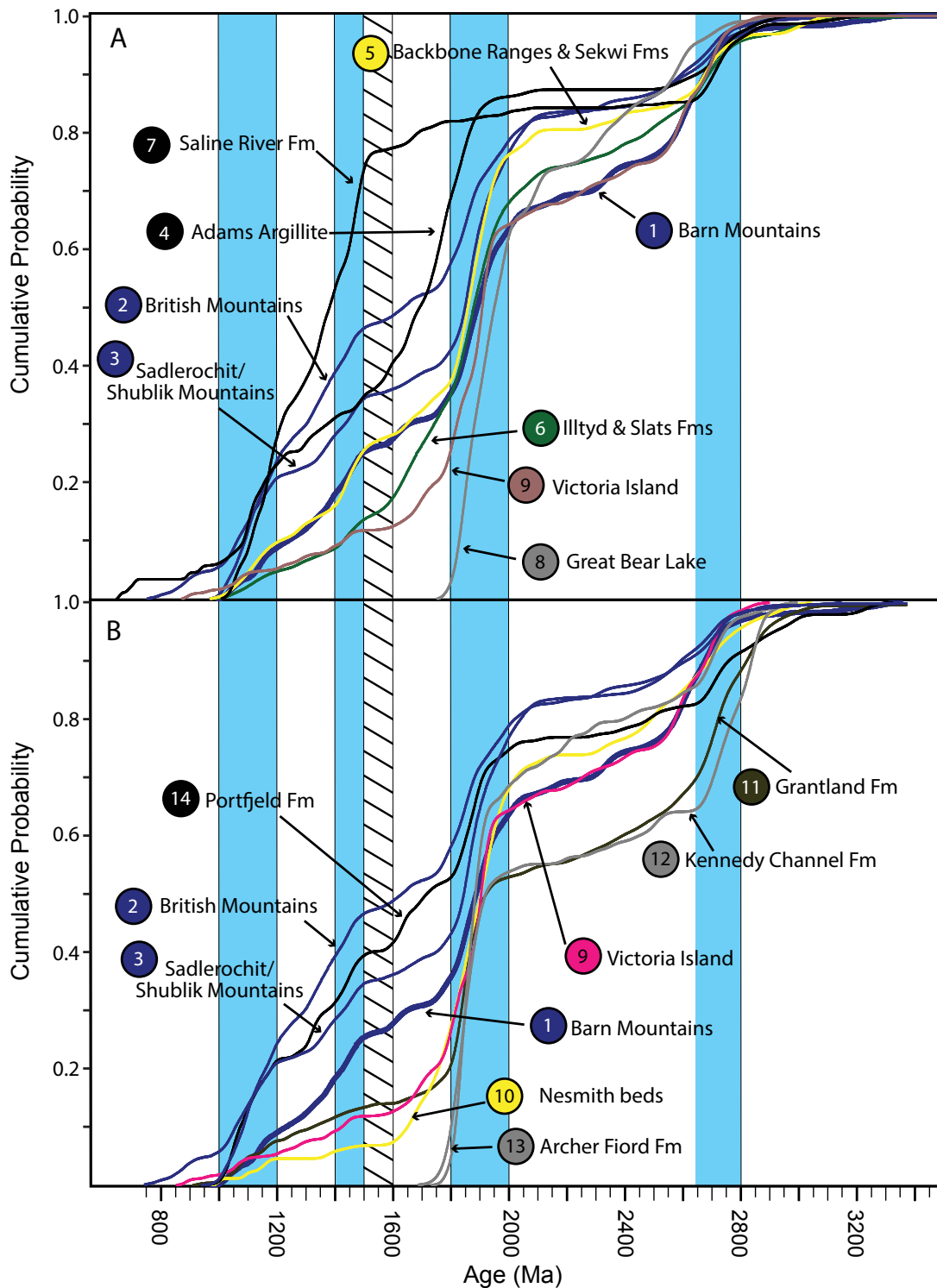


Figure 8. Cumulative probability plots of detrital zircon U/Pb ages from the Barn Mountains, North Slope subterrane, northwestern Laurentia, and north to northeastern Laurentia. Data are from (1) this study; (2-3) Strauss et al. (2013), Macdonald et al. (2009); (4-5) Lane and Gehrels (2014); (6) Leslie (2009); (7-9) Hadlari et al. (2012); (10-11) Beranek et al. (2013), Hadlari et al. (2014); (12-13) Anfinson et al. (2012); and (14) Kirkland et al. (2009). General locations of sampling sites are shown in Figure 1. The coloured bars are the same as in Figure 6.

The Cambrian signature from the Laurentian margin inboard of the Yukon Block is defined by data from the Mackenzie Mountains, Great Bear Lake region, and Victoria Island (Fig. 1; Leslie, 2009; Hadlari *et al.*, 2012). The Mount Cap and Saline River formations in the Mackenzie Mountains are dominated by Mesoproterozoic grains interpreted to have been recycled from the underlying Mackenzie Mountains and Shaler supergroups (Fig. 7; Hadlari *et al.*, 2012). Cambrian samples taken farther south from the Backbone Ranges and Sekwi formations show a Mesoproterozoic signature, but also contain a strong 1800-1900 Ma signature (Fig. 7; Leslie, 2009). The Barn Mountains units are very similar to the Backbone Ranges and Sekwi formations in their Mesoproterozoic signature (Fig. 8). The cratonic signature of the Great Bear magmatic arc is exemplified by the samples from Cambrian units in the Great Bear Lake area that show a prominent 1800-2000 Ma population, subordinate Paleoproterozoic peaks, and a lack of Mesoproterozoic grains (Fig. 7; Hadlari *et al.*, 2012). The lack of Mesoproterozoic grains is in marked contrast to the Barn Mountains detrital signature (Fig. 8).

Cambrian strata on Victoria Island define the detrital record of the western Franklinian margin of northern Laurentia (see Lane and Gehrels, 2014). The signature of three samples is interpreted to record varying mixtures of detrital zircon derived from the craton and recycled from the Shaler Supergroup (Hadlari *et al.*, 2012), corresponding with one of the hybrid signatures of Lane and Gehrels (2014). Apart from a lesser abundance of Mesoproterozoic grains, the detrital signatures from the Barn Mountains and Victoria Island are similar (Figs. 7 and 8). This similarity allows for origin of the Barn Mountains sequence along the Franklinian margin and justifies comparison with coeval strata deposited on the northeastern Laurentian margin. Detrital zircon data from the Franklinian margin on Ellesmere Island is available from the Neoproterozoic Nesmith beds and overlying *Oldhamia*-bearing Cambrian strata of the Grantland Formation (Beranek *et al.*, 2013; Hadlari *et al.*, 2014) and the Kennedy Channel and Archer Fiord formations (Anfinson *et al.*, 2012). The North Greenland margin is represented by data from the Neoproterozoic Portfjeld Formation (Kirkland *et al.*, 2009). Collectively the Ellesmere Island and North Greenland data are dominated by Paleoproterozoic detrital zircon ages with subordinate Mesoproterozoic and Archean populations (Fig. 7). As is the case for the northwest Laurentian samples, the ages observed in the Barn Mountains samples are consistent with those seen on

the northern and northeastern Laurentian margin, but the abundance of Mesoproterozoic versus Paleoproterozoic and Archean populations are variable (Fig. 8).

The broad similarities between the Neoproterozoic-Cambrian signatures observed between samples from the Barn Mountains and both the northwestern and north to northeastern margins of Laurentia are consistent with earlier studies that conclude the detrital zircon reference signatures from different Laurentian margins are non-unique on the basis of available data (e.g., Beranek *et al.*, 2013; Lane and Gehrels, 2014). Thus detrital zircon data alone cannot confirm or refute a northwestern versus northeastern Laurentian origin for the Barn Mountains.

CONCLUSIONS

The new detrital zircon data from the Barn Mountains Neoproterozoic-Cambrian sandstone samples reflects a mixture of Mesoproterozoic zircons derived from the Laurentian craton and/or recycled from Proterozoic sedimentary sections, and Paleoproterozoic to Archean zircons derived from Laurentian basement. Comparison of the age distribution and abundance observed in these samples is consistent with correlation with age equivalent strata on both the northwestern Laurentian margin and the north to northeastern Laurentian margin.

ACKNOWLEDGEMENTS

Field work during 2013 in the Barn and British Mountains, Yukon (Arctic Canada) was completed as part of the CASE 15-Expedition of the Federal Institute for Geosciences and Natural Resources (BGR, Hannover, Germany) led by M. Colpron (Whitehorse, Canada) and K. Piepjohn (Hannover, Germany) and co-funded by the BGR, Yukon Geological Survey (YGS), and Université Pierre et Marie Curie (Paris, France). Transportation and analytical support for W.C. McClelland was provided by National Science Foundation (NSF) grants EAR-0948359 and EAR-1049368 to McClelland and EAR-1032156 to the Arizona Laserchron Facility. Support for expedition participation by W. von Gosen was provided by the Bavarian Research Alliance (Munich, Germany) and German Research Foundation (DFG, proj. Go 405/11-1). Support for J.V. Strauss was provided by a NSF Graduate Research Fellowship and F. Macdonald (NSF EAR-1049463) at Harvard University. David Moynihan (YGS) reviewed an earlier version of the manuscript.

Table 1. U/Pb Geochronologic Data and Apparent Ages

Grain #	U (ppm)	²⁰⁶ Pb/ ²⁰⁴ Pb	Th/U	²⁰⁶ Pb* / ²⁰⁷ Pb*	± (%)	Isotope ratios				Apparent ages (Ma)				Best age (Ma)	± (Ma)	Conc (%)			
						²⁰⁷ Pb* / ²³⁵ U*	± (%)	²⁰⁶ Pb* / ²³⁸ U	± (%)	error corr.	²⁰⁶ Pb* / ²³⁸ U*	± (Ma)	²⁰⁷ Pb* / ²³⁵ U				± (Ma)	²⁰⁶ Pb* / ²⁰⁷ Pb*	± (Ma)
Sample 13-18																			
N68.50877, W138.27055																			
60	654	56,345	0.05	13.4114	0.7	1.8301	2.3	0.1780	2.2	0.96	1056	21	1056	15	1057	14	1056	21	0
9	220	51,191	0.3	13.3212	1.3	1.8790	1.4	0.1815	0.6	0.41	1075	6	1074	9	1070	25	1075	6	0
38	342	186,280	0.9	13.0320	1.0	2.0074	1.2	0.1897	0.7	0.61	1120	8	1118	8	1114	19	1120	8	-1
92	125	45,597	0.3	12.9462	2.2	2.0487	2.5	0.1924	1.1	0.45	1134	12	1132	17	1127	45	1134	12	-1
96	85	31,829	0.4	12.8719	2.6	2.0301	3.0	0.1895	1.4	0.46	1119	14	1126	20	1139	52	1119	14	2
27	213	95,422	0.4	12.8182	1.0	2.0953	1.2	0.1948	0.6	0.52	1147	7	1147	8	1147	20	1147	7	0
28	371	48,310	0.3	12.6932	0.8	2.1205	0.9	0.1952	0.5	0.52	1150	5	1156	6	1167	15	1150	5	1
84	159	129,516	0.4	12.3948	1.1	2.3819	1.6	0.2141	1.2	0.76	1251	14	1237	12	1214	21	1214	21	-3
88	131	48,681	0.5	12.2656	2.8	2.3798	3.6	0.2117	2.2	0.62	1238	25	1237	26	1234	55	1234	55	0
74	112	72,747	0.3	12.0758	1.4	2.5476	1.8	0.2231	1.1	0.61	1298	13	1286	13	1265	28	1265	28	-3
30	178	72,142	0.4	11.9520	1.4	2.5342	1.8	0.2197	1.2	0.66	1280	14	1282	13	1285	27	1285	27	0
12	159	57,695	0.5	11.9021	2.9	2.6927	3.0	0.2324	0.8	0.26	1347	10	1326	22	1293	56	1293	56	-4
53	165	82,686	0.4	11.7484	1.2	2.7149	1.5	0.2313	0.8	0.52	1341	9	1333	11	1318	24	1318	24	-2
97	195	61,713	0.4	11.7462	1.3	2.6412	1.6	0.2250	1.0	0.62	1308	12	1312	12	1319	24	1319	24	1
86	59	29,101	0.4	11.6942	2.7	2.7092	3.1	0.2298	1.6	0.52	1333	20	1331	23	1327	52	1327	52	0
95	217	56,098	0.5	11.6339	1.3	2.5826	1.8	0.2179	1.2	0.66	1271	14	1296	13	1337	26	1337	26	5
25	447	3,871	0.1	11.3476	0.6	2.8805	0.9	0.2371	0.6	0.70	1371	7	1377	7	1385	12	1385	12	1
3	73	30,713	0.6	11.1926	2.1	3.1377	2.5	0.2547	1.3	0.53	1463	17	1442	19	1412	40	1412	40	-4
7	92	14,698	0.5	11.1893	2.4	2.8520	2.7	0.2314	1.4	0.50	1342	17	1369	21	1412	45	1412	45	5
44	187	91,495	0.5	11.0097	1.5	3.1611	2.6	0.2524	2.1	0.81	1451	28	1448	20	1443	29	1443	29	-1
90	88	65,065	0.5	10.9931	1.8	3.1679	2.3	0.2526	1.4	0.61	1452	19	1449	18	1446	35	1446	35	0
19	216	179,187	0.3	10.9637	0.9	3.3446	1.0	0.2659	0.5	0.49	1520	6	1492	8	1451	16	1451	16	-5
31	168	44,667	0.7	10.9424	1.3	3.2018	1.7	0.2541	1.2	0.67	1460	15	1458	13	1455	24	1455	24	0
26	230	80,053	0.6	10.8408	0.7	3.2431	0.9	0.2550	0.5	0.62	1464	7	1468	7	1472	13	1472	13	1
23	170	76,295	0.3	10.8333	0.9	3.2584	1.1	0.2560	0.7	0.62	1469	9	1471	9	1474	17	1474	17	0
15	44	24,645	1.2	10.7254	2.2	3.4067	2.9	0.2650	1.8	0.63	1515	25	1506	23	1493	42	1493	42	-2
81	41	24,024	0.3	10.7023	3.7	3.3162	4.2	0.2574	1.8	0.44	1477	24	1485	33	1497	71	1497	71	1
89	129	74,578	0.5	10.6939	1.9	3.3496	2.2	0.2598	1.2	0.54	1489	16	1493	17	1498	35	1498	35	1
63	76	53,083	0.3	10.6485	2.4	3.4015	2.4	0.2627	0.5	0.22	1504	7	1505	19	1506	45	1506	45	0
57	298	34,146	0.9	10.0262	0.5	3.7914	0.9	0.2757	0.8	0.87	1570	11	1591	7	1619	8	1619	8	3
43	222	97,828	0.6	10.0062	0.7	3.6487	1.4	0.2648	1.2	0.88	1514	17	1560	11	1623	13	1623	13	7
46	207	118,173	0.4	9.9499	0.6	4.0278	1.0	0.2907	0.8	0.77	1645	11	1640	8	1633	11	1633	11	-1

Table 1. (continued)

Grain #	U (ppm)	²⁰⁶ Pb	²⁰⁴ Pb	Th/U	²⁰⁶ Pb* / ²⁰⁷ Pb*	± (%)	²⁰⁷ Pb* / ²³⁵ U*	± (%)	²⁰⁶ Pb* / ²³⁸ U	± (%)	error corr.	²⁰⁶ Pb* / ²³⁸ U*	± (Ma)	²⁰⁷ Pb* / ²³⁵ U	± (Ma)	²⁰⁶ Pb* / ²⁰⁷ Pb*	± (Ma)	²⁰⁶ Pb* / ²⁰⁷ Pb*	± (Ma)	Best age (Ma)	± (Ma)	Conc (%)		
82	215	123,710		0.2	9.3508	0.6	4.6295	1.2	0.3140	1.0	0.87	1760	16	1755	10	1748	10	1748	10	1748	10	1748	10	-1
91	409	242,780		0.2	9.2784	0.3	4.6922	0.8	0.3158	0.8	0.92	1769	12	1766	7	1762	6	1762	6	1762	6	1762	6	0
32	100	63,742		0.6	9.2411	1.3	4.5936	1.6	0.3079	0.9	0.53	1730	13	1748	13	1770	25	1770	25	1770	25	1770	25	2
13	182	173,723		0.4	9.1767	1.0	4.8076	1.2	0.3200	0.7	0.60	1790	11	1786	10	1782	18	1782	18	1782	18	1782	18	0
5	201	141,178		0.4	8.9333	0.6	4.9916	1.0	0.3234	0.8	0.79	1806	12	1818	8	1831	11	1831	11	1831	11	1831	11	1
24	268	231,660		0.2	8.9170	0.6	5.0839	0.9	0.3288	0.6	0.70	1832	10	1833	8	1834	11	1834	11	1834	11	1834	11	0
58	94	43,539		0.4	8.8462	1.0	5.2796	1.7	0.3387	1.3	0.79	1881	21	1866	14	1849	19	1849	19	1849	19	1849	19	-2
59	145	110,411		0.7	8.7949	1.3	5.2617	1.6	0.3356	0.9	0.57	1866	15	1863	14	1859	24	1859	24	1859	24	1859	24	0
80	204	152,169		0.2	8.7879	0.9	5.2459	1.7	0.3344	1.5	0.85	1859	23	1860	15	1861	17	1861	17	1861	17	1861	17	0
21	115	69,433		0.3	8.6968	1.5	5.4450	1.7	0.3434	0.9	0.52	1903	15	1892	15	1880	26	1880	26	1880	26	1880	26	-1
2	100	115,787		0.7	8.6847	1.9	5.4935	2.0	0.3460	0.8	0.39	1916	13	1900	18	1882	34	1882	34	1882	34	1882	34	-2
87	133	42,295		0.6	8.6482	1.1	5.6065	1.8	0.3517	1.5	0.81	1943	25	1917	16	1890	19	1890	19	1890	19	1890	19	-3
1	77	68,240		1.0	8.6132	1.7	5.6799	2.0	0.3548	1.1	0.53	1958	18	1928	17	1897	31	1897	31	1897	31	1897	31	-3
69	54	47,349		1.6	8.4959	1.7	5.6894	2.3	0.3506	1.5	0.64	1937	24	1930	20	1922	31	1922	31	1922	31	1922	31	-1
11	134	131,373		0.8	8.4905	0.9	5.6820	1.3	0.3499	1.0	0.77	1934	17	1929	11	1923	15	1923	15	1923	15	1923	15	-1
10	58	35,562		1.1	8.4749	1.3	5.7122	1.6	0.3511	0.8	0.54	1940	14	1933	13	1926	23	1926	23	1926	23	1926	23	-1
34	164	146,894		0.3	8.2825	3.0	5.6637	6.9	0.3402	6.2	0.90	1888	102	1926	60	1967	54	1967	54	1967	54	1967	54	4
51	63	46,309		0.5	8.2779	1.8	6.0684	2.0	0.3643	1.0	0.49	2003	17	1986	17	1968	31	1968	31	1968	31	1968	31	-2
68	304	182,717		0.5	8.1255	0.4	6.3099	0.8	0.3719	0.7	0.88	2038	13	2020	7	2001	7	2001	7	2001	7	2001	7	-2
29	83	137,858		1.3	8.1236	1.1	6.3363	1.2	0.3733	0.5	0.40	2045	8	2023	10	2002	19	2002	19	2002	19	2002	19	-2
100	217	115,803		0.3	7.9560	0.5	6.5049	1.5	0.3753	1.4	0.94	2055	24	2047	13	2039	9	2039	9	2039	9	2039	9	-1
6	215	53,047		0.5	7.3910	0.5	7.4294	2.9	0.3982	2.9	0.98	2161	53	2165	26	2168	9	2168	9	2168	9	2168	9	0
48	242	280,736		0.5	6.7966	0.5	8.6456	2.0	0.4262	1.9	0.96	2288	37	2301	18	2313	9	2313	9	2313	9	2313	9	1
8	150	128,026		0.5	6.6287	0.6	9.3689	0.8	0.4504	0.6	0.72	2397	12	2375	7	2356	10	2356	10	2356	10	2356	10	-2
40	120	124,541		0.4	6.5179	0.7	9.4143	1.4	0.4450	1.3	0.88	2373	25	2379	13	2384	11	2384	11	2384	11	2384	11	0
85	205	179,943		0.4	6.1401	0.4	10.6516	1.1	0.4743	1.1	0.95	2503	22	2493	11	2486	6	2486	6	2486	6	2486	6	-1
35	51	65,536		0.6	5.9611	1.5	11.2718	1.9	0.4873	1.2	0.60	2559	24	2546	18	2535	26	2535	26	2535	26	2535	26	-1
71	258	160,943		0.4	5.8705	0.2	11.6246	1.6	0.4949	1.6	0.99	2592	34	2575	15	2561	4	2561	4	2561	4	2561	4	-1
83	94	93,021		0.5	5.7534	0.4	11.7603	0.8	0.4907	0.7	0.88	2574	15	2586	8	2595	7	2595	7	2595	7	2595	7	1
76	301	26,612		0.4	5.7433	0.2	11.6250	3.4	0.4842	3.4	1.00	2546	71	2575	32	2598	3	2598	3	2598	3	2598	3	2
17	236	281,965		0.6	5.7180	0.3	12.0269	0.4	0.4988	0.2	0.63	2609	5	2607	3	2605	5	2605	5	2605	5	2605	5	0
45	53	37,607		0.8	5.5994	1.2	12.5362	2.3	0.5091	1.9	0.84	2653	41	2645	21	2640	21	2640	21	2640	21	2640	21	0
64	98	70,216		1.3	5.5321	0.4	13.0231	1.2	0.5225	1.2	0.93	2710	25	2681	12	2660	7	2660	7	2660	7	2660	7	-2
41	55	45,857		0.9	5.5309	1.0	13.3209	1.6	0.4942	1.3	0.79	2589	27	2629	15	2660	17	2660	17	2660	17	2660	17	3
62	60	64,548		0.8	5.4542	0.9	13.0954	1.2	0.5180	0.8	0.67	2691	18	2687	11	2683	15	2683	15	2683	15	2683	15	0
98	105	92,134		0.5	5.4321	0.4	13.1936	1.1	0.5198	1.0	0.92	2698	22	2694	10	2690	7	2690	7	2690	7	2690	7	0
14	218	117,240		1.2	5.3838	0.2	13.2455	0.4	0.5172	0.4	0.91	2687	9	2697	4	2705	3	2705	3	2705	3	2705	3	1

Table 1. (continued)

Grain #	U (ppm)	²⁰⁶ Pb	²⁰⁴ Pb	Th/U	²⁰⁶ Pb* / ²⁰⁷ Pb*	± (%)	²⁰⁷ Pb* / ²³⁵ U*	± (%)	²⁰⁶ Pb* / ²³⁸ U	± (%)	error corr.	²⁰⁶ Pb* / ²³⁸ U*	± (Ma)	²⁰⁷ Pb* / ²³⁵ U	± (Ma)	²⁰⁶ Pb* / ²⁰⁷ Pb*	± (Ma)	Best age (Ma)	± (Ma)	Conc (%)
37	112	96,786	0.8	5.3539	0.4	13.5541	0.9	0.5263	0.8	0.89	2726	18	2719	9	2714	7	2714	7	0	
16	90	107,496	0.9	5.3182	0.8	13.7050	1.0	0.5286	0.6	0.59	2736	13	2730	10	2725	13	2725	13	0	
66	38	56,596	0.7	5.2889	1.0	13.9267	1.8	0.5342	1.5	0.84	2759	33	2745	17	2734	16	2734	16	-1	
65	249	135,895	0.6	4.8847	0.3	15.4446	1.3	0.5472	1.3	0.98	2813	30	2843	13	2864	4	2864	4	2	
56	81	249,279	0.9	4.6019	0.4	17.2657	0.9	0.5763	0.8	0.88	2933	18	2950	8	2961	7	2961	7	1	
22	96	99,351	0.4	4.1198	0.4	21.0285	0.7	0.6283	0.6	0.84	3143	15	3140	7	3138	6	3138	6	0	
36	156	218,243	0.6	4.0121	0.8	21.1235	1.2	0.6147	0.9	0.78	3089	23	3144	12	3180	12	3180	12	3	
70	84	251,383	0.7	3.7645	0.3	24.7659	0.9	0.6762	0.8	0.94	3330	22	3299	9	3280	5	3280	5	-2	
77	157	213,460	0.8	3.7240	0.3	25.3236	1.2	0.6840	1.1	0.98	3360	30	3321	11	3297	4	3297	4	-2	
Rejected analyses (>10% discordant; >5% reverse discordance; >10% 2-sigma uncertainty)																				
52	553	18,682	0.2	13.3677	0.9	1.5615	2.5	0.1514	2.3	0.94	909	20	955	15	1063	18		18	15	
42	255	12,804	0.9	8.4137	0.4	4.9561	2.1	0.3024	2.1	0.98	1703	31	1812	18	1939	7		7	12	
75	167	11,339	0.6	13.2386	2.1	1.6841	2.8	0.1617	1.9	0.66	966	17	1003	18	1083	42		42	11	
94	61	39,700	0.4	12.0250	4.3	2.2640	5.0	0.1975	2.5	0.50	1162	26	1201	35	1273	84		84	9	
39	52	12,762	0.5	12.3591	4.3	2.1746	4.6	0.1949	1.7	0.36	1148	17	1173	32	1219	85		85	6	
99	59	20,422	0.4	12.6998	3.6	2.1026	4.2	0.1937	2.1	0.51	1141	22	1150	29	1166	71		71	2	
93	36	8,738	0.7	10.6762	6.6	3.3211	7.4	0.2572	3.4	0.46	1475	45	1486	58	1501	125		125	2	
50	24	8,511	0.4	11.6375	5.7	2.7280	6.3	0.2302	2.6	0.41	1336	31	1336	47	1337	111		111	0	
73	83	2,247	0.8	9.8401	4.8	4.1530	5.4	0.2964	2.5	0.47	1673	37	1665	44	1654	88		88	-1	
55	49	55,148	0.4	12.9642	6.2	2.1047	6.5	0.1979	2.1	0.32	1164	22	1150	45	1125	123		123	-3	
49	37	38,555	1.5	10.3257	5.0	3.8716	5.3	0.2899	1.9	0.36	1641	28	1608	43	1564	93		93	-5	
18	119	156,082	1.0	5.6950	0.4	12.9186	0.7	0.5336	0.5	0.80	2757	12	2674	6	2612	7		7	-6	
20	489	6,019	0.6	10.8743	0.8	1.7563	3.3	0.1385	3.2	0.97	836	25	1029	21	1467	15		15	43	
33	158	7,552	1.3	5.3783	0.9	9.3940	6.1	0.3664	6.0	0.99	2013	104	2377	56	2706	14		14	26	
47	64	21,497	0.5	11.5013	2.6	3.0637	2.7	0.2556	0.9	0.33	1467	12	1424	21	1359	50		50	-8	
54	161	11,348	1.2	10.7460	3.9	2.6567	5.1	0.2071	3.2	0.63	1213	36	1316	38	1489	75		75	19	
61	13	11,510	1.7	9.5847	7.6	4.7695	8.0	0.3316	2.6	0.32	1846	42	1780	68	1703	140		140	-8	
67	88	19,049	0.5	16.3045	6.9	0.9583	7.1	0.1133	1.8	0.25	692	12	682	35	651	149		149	-6	
72	31	31,359	1.1	8.9445	3.2	5.3757	3.6	0.3487	1.7	0.47	1929	28	1881	31	1829	57		57	-5	
78	84	26,893	0.3	13.9251	3.9	1.7165	4.5	0.1734	2.2	0.49	1031	21	1015	29	981	80		80	-5	
79	57	42,946	0.3	9.9165	4.6	3.8079	4.8	0.2739	1.2	0.24	1560	16	1594	38	1640	86		86	5	

Table 1. (continued)

Grain #	U (ppm)	²⁰⁶ Pb	Th/U	²⁰⁶ Pb* / ²⁰⁷ Pb*	²⁰⁷ Pb* / ²³⁵ U* (%)	²⁰⁷ Pb* ± (%)	²⁰⁶ Pb* / ²³⁸ U* (%)	²⁰⁶ Pb* ± (%)	error corr.	²⁰⁶ Pb* / ²³⁸ U* (Ma)	²⁰⁷ Pb* / ²³⁵ U (Ma)	²⁰⁶ Pb* ± (Ma)	²⁰⁷ Pb* ± (Ma)	²⁰⁶ Pb* / ²⁰⁷ Pb* (Ma)	Best age (Ma)	± (Ma)	Conc (%)	
Sample 13-07																		
N68.46701, W138.1698																		
95	186	39,457	0.6	13.4295	2.7	1.8046	3.1	0.1758	1.5	0.49	1044	15	1047	20	1054	55	1044	1
31	136	130,478	0.4	13.3984	2.2	1.7932	2.4	0.1743	1.0	0.42	1036	9	1043	15	1059	44	1036	2
74	200	125,504	0.4	13.3480	2.5	1.8009	2.8	0.1743	1.3	0.46	1036	12	1046	18	1066	50	1036	3
78	250	51,500	0.2	12.9372	2.0	2.0662	2.2	0.1939	1.1	0.49	1142	12	1138	15	1129	39	1142	-1
72	229	75,688	0.3	12.7735	1.8	2.1175	2.6	0.1962	1.8	0.71	1155	19	1155	18	1154	36	1155	0
23	146	156,161	0.3	12.7683	2.7	2.0731	2.8	0.1920	0.9	0.30	1132	9	1140	19	1155	54	1132	2
21	292	72,810	0.3	12.7023	1.0	2.1369	1.2	0.1969	0.7	0.61	1158	8	1161	8	1165	19	1158	1
18	123	43,812	0.4	12.4670	1.8	2.1708	2.8	0.1963	2.2	0.76	1155	23	1172	20	1202	36	1202	4
54	392	128,957	0.5	12.4329	0.5	2.3031	0.9	0.2077	0.7	0.82	1216	8	1213	6	1208	10	1208	-1
67	277	184,348	0.1	12.1740	0.9	2.5191	1.5	0.2224	1.2	0.80	1295	14	1278	11	1249	18	1249	-4
29	72	32,973	0.6	11.9344	2.4	2.5156	3.1	0.2177	2.0	0.64	1270	23	1277	23	1288	47	1288	1
59	167	133,408	0.4	11.3357	0.5	2.9159	1.3	0.2397	1.2	0.91	1385	15	1386	10	1387	10	1387	0
30	132	70,491	0.3	11.3051	1.8	2.9278	2.0	0.2401	1.0	0.48	1387	12	1389	15	1392	34	1392	0
35	149	383,795	0.3	11.2515	1.1	3.0537	1.8	0.2492	1.4	0.78	1434	18	1421	14	1401	22	1401	-2
24	119	55,287	0.5	11.1294	2.1	2.9833	2.4	0.2408	1.2	0.49	1391	15	1403	19	1422	41	1422	2
80	331	148,265	0.4	11.0340	0.6	3.2919	1.6	0.2634	1.5	0.92	1507	20	1479	13	1439	12	1439	-5
19	81	34,883	0.6	11.0311	2.7	3.1894	3.0	0.2552	1.3	0.42	1465	16	1455	23	1439	51	1439	-2
32	148	126,840	0.5	10.7821	1.3	3.3073	1.5	0.2586	0.9	0.58	1483	12	1483	12	1483	24	1483	0
73	203	227,337	0.6	10.1772	0.8	3.8198	1.2	0.2819	0.9	0.72	1601	12	1597	10	1591	16	1591	-1
92	292	260,328	0.7	10.1303	0.9	3.8144	1.9	0.2803	1.7	0.89	1593	24	1596	15	1600	16	1600	0
62	161	64,249	0.4	10.0972	0.9	3.9589	1.7	0.2899	1.4	0.84	1641	21	1626	14	1606	17	1606	-2
60	114	74,693	1.1	9.1861	1.1	4.8929	1.5	0.3260	1.0	0.65	1819	15	1801	12	1780	20	1780	-2
82	195	134,745	1.0	9.1631	0.7	4.8924	1.2	0.3251	0.9	0.80	1815	15	1801	10	1785	13	1785	-2
7	70	37,348	0.7	9.0731	0.8	4.8926	2.3	0.3220	2.2	0.94	1799	34	1801	19	1803	14	1803	0
28	70	46,975	0.7	8.9814	1.9	5.0484	2.3	0.3288	1.4	0.58	1833	22	1827	20	1821	34	1821	-1
8	39	27,571	0.7	8.9599	2.1	5.0580	2.7	0.3287	1.6	0.60	1832	25	1829	23	1826	39	1826	0
69	131	63,657	0.8	8.9099	0.7	5.1231	1.1	0.3311	0.8	0.74	1844	13	1840	9	1836	13	1836	0
5	209	201,858	0.4	8.8854	1.2	5.0954	1.4	0.3284	0.8	0.55	1830	12	1835	12	1841	21	1841	1
33	252	310,507	0.6	8.8708	0.3	5.2182	1.5	0.3357	1.5	0.97	1866	24	1856	13	1844	6	1844	-1
50	43	1,691	0.8	8.8638	2.8	5.2388	3.4	0.3368	1.9	0.56	1871	30	1859	29	1845	50	1845	-1
63	58	51,755	0.8	8.8607	1.6	5.2348	2.0	0.3364	1.2	0.60	1869	19	1858	17	1846	29	1846	-1
84	165	110,395	0.4	8.8514	0.9	5.1307	1.1	0.3294	0.6	0.56	1835	10	1841	9	1848	16	1848	1
52	105	100,484	1.2	8.8021	1.0	5.3358	1.8	0.3406	1.6	0.85	1890	25	1875	16	1858	17	1858	-2
58	28	6,756	1.4	8.7988	4.1	5.1010	4.4	0.3255	1.5	0.35	1817	24	1836	37	1859	74	1859	2
10	228	124,227	0.3	8.7761	0.4	5.4072	2.5	0.3442	2.5	0.99	1907	41	1886	22	1863	7	1863	-2

Table 1. (continued)

Grain #	U (ppm)	²⁰⁶ Pb / ²⁰⁴ Pb	Th/U	²⁰⁶ Pb* / ²⁰⁷ Pb*	± (%)	²⁰⁷ Pb* / ²³⁵ U* (%)	± (%)	²⁰⁶ Pb* / ²³⁸ U (%)	± (%)	error corr.	²⁰⁶ Pb* / ²³⁸ U* (Ma)	± (Ma)	²⁰⁷ Pb* / ²³⁵ U (Ma)	± (Ma)	²⁰⁶ Pb* / ²⁰⁷ Pb* (Ma)	± (Ma)	Best age (Ma)	± (Ma)	Conc (%)
87	103	77,402	0.7	8.7700	1.1	5.3787	1.9	0.3421	1.5	0.81	1897	25	1881	16	1865	20	1865	20	-2
3	120	97,836	0.3	8.7039	1.1	5.3481	1.8	0.3376	1.5	0.81	1875	24	1877	16	1878	19	1878	19	0
96	407	182,163	0.2	8.6647	0.4	5.1605	2.0	0.3243	2.0	0.98	1811	31	1846	17	1886	8	1886	8	4
25	177	121,275	0.7	8.6558	0.8	5.3912	1.2	0.3384	0.8	0.69	1879	13	1883	10	1888	15	1888	15	0
34	113	54,621	0.4	8.6158	1.4	5.3813	2.1	0.3363	1.6	0.74	1869	26	1882	18	1896	26	1896	26	1
68	106	56,633	0.6	8.5964	0.9	5.3556	1.5	0.3339	1.1	0.77	1857	18	1878	13	1901	17	1901	17	2
38	221	105,335	0.0	8.5461	0.3	5.6334	1.1	0.3492	1.0	0.96	1931	17	1921	9	1911	6	1911	6	-1
55	253	199,972	0.3	8.5213	0.6	5.4417	1.4	0.3363	1.3	0.89	1869	21	1891	12	1916	12	1916	12	2
49	160	141,937	0.6	8.4817	0.7	5.7308	1.3	0.3525	1.1	0.85	1947	19	1936	11	1925	12	1925	12	-1
1	49	32,716	0.6	8.4744	2.2	5.4598	2.8	0.3356	1.7	0.62	1865	28	1894	24	1926	40	1926	40	3
88	134	176,115	0.9	8.4673	0.5	5.6623	1.1	0.3477	0.9	0.88	1924	15	1926	9	1928	9	1928	9	0
11	118	137,677	0.5	8.4463	0.8	5.6823	1.4	0.3481	1.2	0.83	1925	19	1929	12	1932	14	1932	14	0
42	197	108,989	0.4	8.4219	0.6	5.6587	0.9	0.3456	0.7	0.76	1914	11	1925	8	1937	10	1937	10	1
36	57	46,967	1.2	8.4023	1.4	5.7534	2.6	0.3506	2.2	0.85	1938	37	1939	22	1941	25	1941	25	0
76	189	128,160	0.5	8.2187	0.7	6.0578	1.3	0.3611	1.0	0.83	1987	18	1984	11	1981	12	1981	12	0
97	261	128,446	0.5	8.0969	0.5	6.2849	1.1	0.3691	1.0	0.90	2025	17	2016	9	2007	8	2007	8	-1
15	287	206,398	0.5	8.0214	0.4	6.3204	1.3	0.3677	1.2	0.94	2019	21	2021	11	2024	8	2024	8	0
94	71	31,284	0.8	7.4514	1.5	7.4184	2.3	0.4009	1.7	0.77	2173	32	2163	20	2154	26	2154	26	-1
56	134	117,525	0.5	7.3528	0.6	7.7554	0.8	0.4136	0.5	0.66	2231	10	2203	7	2177	11	2177	11	-2
39	65	2,322	0.7	7.0017	2.2	8.4253	3.2	0.4278	2.3	0.72	2296	45	2278	29	2262	38	2262	38	-2
51	185	108,358	0.7	6.7962	0.5	8.8327	1.1	0.4354	1.0	0.88	2330	19	2321	10	2313	9	2313	9	-1
99	129	132,078	0.6	6.7703	0.7	8.7554	1.5	0.4299	1.4	0.90	2305	27	2313	14	2319	11	2319	11	1
41	86	71,288	1.4	6.7053	1.1	7.9920	2.7	0.3887	2.4	0.91	2117	44	2230	24	2336	19	2336	19	9
12	62	91,513	1.0	6.3974	1.4	9.8023	2.1	0.4548	1.6	0.75	2417	32	2416	19	2416	23	2416	23	0
40	42	89,929	1.3	6.2040	1.4	10.3952	2.4	0.4677	2.0	0.82	2474	41	2471	22	2468	23	2468	23	0
4	188	136,508	0.4	6.1247	0.3	10.4436	0.6	0.4639	0.5	0.83	2457	9	2475	5	2490	5	2490	5	1
53	92	105,415	1.0	5.9618	0.5	11.1480	1.0	0.4820	0.9	0.87	2536	19	2536	9	2535	8	2535	8	0
100	161	168,388	0.6	5.9617	0.3	11.1338	1.1	0.4814	1.1	0.97	2533	23	2534	10	2535	4	2535	4	0
48	88	113,766	0.4	5.8154	0.8	11.7300	1.3	0.4947	1.0	0.77	2591	21	2583	12	2577	14	2577	14	-1
71	148	179,062	0.7	5.7845	0.3	11.8359	1.8	0.4966	1.8	0.98	2599	38	2592	17	2586	5	2586	5	-1
16	36	48,349	1.0	5.7794	2.2	11.8078	2.6	0.4949	1.5	0.56	2592	31	2589	24	2587	36	2587	36	0
27	184	184,880	0.4	5.7784	0.4	11.7342	1.3	0.4918	1.3	0.95	2578	27	2583	13	2587	7	2587	7	0
2	155	113,601	0.6	5.7690	0.4	11.7799	1.3	0.4929	1.2	0.94	2583	26	2587	12	2590	7	2590	7	0
75	10	11,299	0.2	5.7527	3.8	12.1725	7.3	0.5079	6.2	0.86	2648	135	2618	68	2595	63	2595	63	-2
6	63	68,689	1.4	5.7524	0.8	11.1319	1.2	0.4644	1.0	0.79	2459	20	2534	12	2595	13	2595	13	5
79	100	84,180	0.6	5.7448	0.6	12.3377	1.3	0.5141	1.1	0.87	2674	25	2630	12	2597	11	2597	11	-3
46	57	112,510	0.6	5.6804	1.3	12.1292	2.2	0.4997	1.8	0.81	2613	38	2614	20	2616	21	2616	21	0

Table 1. (continued)

Grain #	U (ppm)	²⁰⁶ Pb	Th/U	²⁰⁶ Pb* / ²⁰⁷ Pb*	± (%)	²⁰⁷ Pb* / ²³⁵ U*	± (%)	²⁰⁶ Pb* / ²³⁸ U*	± (%)	error corr.	²⁰⁶ Pb* / ²³⁸ U*	± (Ma)	²⁰⁷ Pb* / ²³⁵ U	± (Ma)	²⁰⁶ Pb* / ²⁰⁷ Pb*	± (Ma)	Best age (Ma)	± (Ma)	Conc (%)
47	79	89,712	0.9	5.6764	0.5	12.2236	1.2	0.5032	1.1	0.89	2628	23	2622	11	2617	9	2617	9	0
61	50	78,940	1.4	5.5615	1.3	12.6394	1.9	0.5098	1.4	0.72	2656	30	2653	18	2651	22	2651	22	0
70	161	129,028	1.0	5.4833	0.3	12.9042	1.1	0.5132	1.0	0.95	2670	23	2673	10	2675	6	2675	6	0
17	61	68,512	1.0	5.4068	0.9	13.8369	6.3	0.5426	6.2	0.99	2794	141	2739	60	2698	15	2698	15	-4
26	194	17,773	0.2	5.3669	0.5	13.2399	1.2	0.5154	1.1	0.92	2679	24	2697	11	2710	8	2710	8	1
13	57	73,203	0.5	5.3294	0.9	13.7965	1.2	0.5333	0.8	0.68	2755	18	2736	11	2722	15	2722	15	-1
22	39	53,391	0.8	5.2395	0.7	13.9481	1.9	0.5300	1.8	0.93	2742	40	2746	18	2750	12	2750	12	0
20	29	22,661	0.3	5.0836	2.1	14.5154	3.4	0.5352	2.7	0.79	2763	61	2784	32	2799	34	2799	34	1
Rejected analyses (>10% discordant; >5% reverse discordance; >10% 2-sigma uncertainty)																			
83	158	20,450	0.5	5.8036	0.5	9.2696	3.0	0.3902	2.9	0.98	2124	53	2365	27	2580	9	2580	9	18
93	317	27,778	0.7	8.6923	0.5	4.3214	3.2	0.2724	3.2	0.99	1553	44	1697	27	1881	9	1881	9	17
14	249	28,971	0.5	5.7333	0.4	10.2181	3.8	0.4249	3.8	1.00	2283	74	2455	36	2600	6	2600	6	12
45	83	50,722	0.3	12.8913	4.2	2.0998	6.1	0.1963	4.5	0.73	1156	47	1149	42	1136	84	1136	84	-2
89	36	10,141	0.4	13.0233	5.0	2.0790	5.7	0.1964	2.7	0.48	1156	29	1142	39	1116	99	1116	99	-4
85	83	12,758	0.6	12.5027	4.2	2.3519	7.7	0.2133	6.5	0.84	1246	74	1228	55	1197	83	1197	83	-4
9	476	11,536	0.6	6.0771	1.3	10.1335	15.8	0.4466	15.7	1.00	2380	314	2447	147	2503	21	2503	21	5
37	57	24,028	3.7	13.9708	2.7	1.7172	4.6	0.1740	3.8	0.81	1034	36	1015	30	974	55	974	55	-6
43	217	9,568	0.7	5.6914	0.4	5.9889	12.6	0.2472	12.6	1.00	1424	161	1974	110	2613	6	2613	6	45
44	3	2,476	0.3	5.1936	161.0	8.5988	162.1	0.3239	18.2	0.11	1809	287	2296	-	2764	517	2764	517	35
57	391	10,280	0.7	5.8002	2.6	7.1413	8.0	0.3004	7.6	0.95	1693	113	2129	72	2581	43	2581	43	34
64	21	11,735	0.4	14.6400	22.9	1.8407	25.2	0.1954	10.6	0.42	1151	112	1060	167	878	479	878	479	-31
65	588	127,994	1.2	6.2595	1.0	2.5997	10.8	0.1180	10.7	1.00	719	73	1301	79	2453	17	2453	17	71
77	47	22,907	0.5	13.0644	8.0	2.3257	8.1	0.2204	1.1	0.13	1284	13	1220	57	1109	160	1109	160	-16
81	44	16,213	0.4	15.1153	9.1	1.5997	9.5	0.1754	2.8	0.30	1042	27	970	59	811	190	811	190	-28
86	718	63,926	0.3	8.7126	0.3	6.5631	2.7	0.4147	2.7	1.00	2236	51	2054	24	1876	5	1876	5	-19
90	151	32,319	0.5	5.5269	1.0	8.8143	11.8	0.3533	11.7	1.00	1950	197	2319	108	2661	17	2661	17	27
91	647	11,282	0.6	7.1592	1.8	3.4249	9.3	0.1778	9.2	0.98	1055	89	1510	74	2223	31	2223	31	53
98	239	23,819	0.4	8.9693	0.8	3.9038	4.0	0.2539	3.9	0.98	1459	51	1614	32	1824	15	1824	15	20
66	375	86,195	0.2	17.0515	2.7	0.7311	3.7	0.0904	2.6	0.69	558	14	557	16	554	58	554	58	-1
Sample 13-16																			
98	117	167,452	1.0	13.8208	2.9	1.6927	3.2	0.1697	1.2	0.39	1010	12	1006	20	996	59	1010	12	-1
15	65	19,788	0.4	13.1692	5.7	1.8506	6.7	0.1768	3.4	0.51	1049	33	1064	44	1093	115	1049	33	4
40	35	10,758	0.5	12.6872	9.1	1.9772	9.3	0.1819	2.2	0.24	1078	22	1108	63	1168	180	1078	22	8
91	154	46,967	1.2	13.1653	1.7	1.8784	4.0	0.1794	3.6	0.90	1063	36	1074	27	1094	35	1063	35	3

Sample 13-16 N68.47654, W138.2338

Table 1. (continued)

Grain #	U (ppm)	²⁰⁶ Pb/ ²⁰⁴ Pb	Th/U	²⁰⁶ Pb* ²⁰⁷ Pb*	± (%)	²⁰⁷ Pb* ²³⁵ U*	± (%)	²⁰⁶ Pb* ²³⁸ U	± (%)	error corr.	²⁰⁶ Pb* ²³⁸ U*	± (Ma)	²⁰⁷ Pb* ²³⁵ U	± (Ma)	²⁰⁶ Pb* ²⁰⁷ Pb*	± (Ma)	Best age (Ma)	± (Ma)	Conc (%)
73	114	63,311	0.5	12,8919	2.4	2,1515	2.9	0.2012	1.5	0.51	1182	16	1166	20	1136	49	1182	16	-4
39	466	261,527	0.3	12,7106	0.9	2,1616	1.3	0.1993	1.0	0.76	1171	11	1169	9	1164	17	1171	11	-1
2	117	57,275	0.2	11,7486	2.1	2,7953	2.5	0.2382	1.4	0.54	1377	17	1354	19	1318	41	1318	41	-4
1	116	55,347	0.3	11,6847	1.5	2,7346	1.9	0.2317	1.2	0.61	1344	14	1338	14	1329	29	1329	29	-1
76	311	319,164	0.2	11,6348	1.1	2,7639	1.6	0.2332	1.2	0.73	1351	14	1346	12	1337	21	1337	21	-1
93	106	61,460	0.3	11,3949	1.6	2,8789	1.9	0.2379	0.9	0.46	1376	11	1375	14	1377	32	1377	32	0
89	341	154,584	0.2	11,3888	0.5	2,8727	1.0	0.2373	0.9	0.86	1373	11	1375	7	1378	10	1378	10	0
90	171	117,914	0.2	11,2333	1.4	2,9680	1.6	0.2418	0.8	0.47	1396	10	1399	12	1405	28	1405	28	1
68	51	24,083	0.7	11,2175	3.5	2,9433	3.9	0.2395	1.8	0.45	1384	22	1393	30	1407	67	1407	67	2
52	148	112,265	0.6	11,1815	2.3	3,1049	2.5	0.2518	1.1	0.42	1448	14	1434	20	1413	44	1413	44	-2
25	534	20,546	0.8	10,9501	0.7	3,2720	7.9	0.2599	7.9	1.00	1489	105	1474	62	1453	14	1453	14	-2
36	108	56,542	0.5	10,8853	1.7	3,3617	2.0	0.2654	1.1	0.54	1517	15	1496	16	1465	33	1465	33	-4
66	88	51,058	0.5	10,5710	1.3	3,4085	1.7	0.2613	1.1	0.66	1497	15	1506	14	1520	24	1520	24	2
38	74	36,568	1.5	9,9900	1.5	4,0287	2.3	0.2919	1.7	0.75	1651	25	1640	19	1626	28	1626	28	-2
9	127	43,438	1.0	9,8716	1.2	3,9949	1.6	0.2860	1.0	0.64	1622	15	1633	13	1648	23	1648	23	2
71	182	155,851	0.9	9,8165	1.2	4,0351	1.5	0.2873	0.9	0.60	1628	13	1641	12	1658	21	1658	21	2
59	53	24,345	0.5	9,6646	1.7	4,3446	2.9	0.3045	2.4	0.81	1714	36	1702	24	1687	31	1687	31	-2
61	88	305,974	0.3	9,2648	1.2	4,7030	2.0	0.3160	1.5	0.78	1770	24	1768	16	1765	23	1765	23	0
75	73	67,280	0.4	9,2348	2.0	4,8078	2.5	0.3220	1.4	0.56	1800	22	1786	21	1771	37	1771	37	-2
7	100	39,448	0.8	9,1048	1.3	5,0490	2.3	0.3334	1.9	0.83	1855	31	1828	20	1797	23	1797	23	-3
87	99	54,424	0.7	9,0951	1.8	4,9676	2.7	0.3277	2.1	0.77	1827	34	1814	23	1799	32	1799	32	-2
13	99	120,658	1.8	8,9583	1.8	5,0965	2.5	0.3311	1.8	0.70	1844	28	1836	21	1826	33	1826	33	-1
72	210	165,018	0.8	8,8931	0.6	5,1384	0.9	0.3314	0.6	0.69	1845	10	1842	7	1839	11	1839	11	0
62	121	95,619	0.9	8,8856	0.8	5,2060	1.5	0.3355	1.3	0.85	1865	20	1854	13	1841	14	1841	14	-1
12	168	85,415	0.5	8,8517	0.4	5,2644	1.3	0.3380	1.2	0.96	1877	20	1863	11	1848	7	1848	7	-2
79	115	62,418	0.7	8,8225	1.0	5,1673	1.9	0.3306	1.6	0.86	1841	26	1847	16	1854	17	1854	17	1
24	42	34,619	0.6	8,8071	1.7	5,3530	2.7	0.3419	2.1	0.79	1896	35	1877	23	1857	30	1857	30	-2
4	80	56,806	0.4	8,7971	1.3	5,2739	1.4	0.3365	0.5	0.38	1870	9	1865	12	1859	24	1859	24	-1
26	42	35,305	1.3	8,7809	3.3	5,2398	3.6	0.3337	1.4	0.40	1856	23	1859	31	1862	60	1862	60	0
99	63	83,263	0.7	8,7737	2.0	5,1955	2.2	0.3306	1.0	0.43	1841	16	1852	19	1864	37	1864	37	1
58	182	179,524	0.3	8,7544	0.6	5,3578	1.3	0.3402	1.1	0.88	1888	18	1878	11	1868	11	1868	11	-1
67	124	166,634	0.9	8,7279	0.6	5,3605	1.7	0.3393	1.6	0.93	1883	26	1879	15	1873	11	1873	11	-1
33	101	53,528	0.4	8,6445	1.1	5,5641	1.3	0.3488	0.6	0.51	1929	11	1911	11	1890	20	1890	20	-2
69	67	48,100	0.4	8,6222	1.3	5,4487	1.9	0.3407	1.4	0.71	1890	22	1893	16	1895	24	1895	24	0
70	123	100,486	0.4	8,5861	0.8	5,7277	2.4	0.3567	2.3	0.94	1966	38	1936	21	1903	14	1903	14	-3
28	86	48,183	1.0	8,5258	1.4	5,7802	1.6	0.3574	0.9	0.55	1970	15	1943	14	1915	24	1915	24	-3
92	83	44,712	0.6	8,5140	1.6	5,5926	1.8	0.3453	0.7	0.40	1912	12	1915	15	1918	29	1918	29	0

Table 1. (continued)

Grain #	U (ppm)	²⁰⁶ Pb/ ²⁰⁴ Pb	Th/U	²⁰⁶ Pb*/ ²⁰⁷ Pb*	± (%)	²⁰⁷ Pb*/ ²³⁵ U*	± (%)	²⁰⁶ Pb*/ ²³⁸ U	± (%)	error corr.	²⁰⁶ Pb*/ ²³⁸ U*	± (Ma)	²⁰⁷ Pb*/ ²³⁵ U	± (Ma)	²⁰⁶ Pb*/ ²⁰⁷ Pb*	± (Ma)	Best age (Ma)	± (Ma)	Conc (%)
83	109	83,551	3.0	8.4962	1.2	5.7266	1.5	0.3529	1.0	0.62	1948	16	1935	13	1922	22	1922	22	-1
97	159	107,660	0.4	8.4782	0.5	5.7001	0.9	0.3505	0.7	0.78	1937	11	1931	7	1925	10	1925	10	-1
80	79	73,800	1.0	8.4581	1.3	5.6468	1.4	0.3464	0.6	0.44	1917	10	1923	12	1930	23	1930	23	1
47	33	20,018	1.5	8.3794	3.2	6.1196	4.1	0.3719	2.5	0.62	2038	44	1993	36	1946	57	1946	57	-5
78	132	144,808	0.7	8.3714	1.3	5.6755	1.5	0.3446	0.8	0.54	1909	13	1928	13	1948	23	1948	23	2
3	70	46,529	1.0	8.3709	1.3	5.9069	2.1	0.3586	1.7	0.78	1976	29	1962	19	1948	24	1948	24	-1
6	28	22,450	0.7	8.3463	3.3	5.7612	3.7	0.3487	1.7	0.46	1929	29	1941	32	1953	59	1953	59	1
51	36	68,788	1.7	8.3435	2.6	5.7040	2.8	0.3452	1.1	0.39	1911	18	1932	24	1954	47	1954	47	2
56	70	63,993	0.9	8.3151	1.3	6.0770	1.9	0.3665	1.4	0.75	2013	25	1987	17	1960	22	1960	22	-3
95	44	33,048	0.9	8.1908	3.0	6.1248	3.1	0.3638	1.0	0.32	2000	17	1994	27	1987	53	1987	53	-1
63	148	90,593	0.4	8.1558	0.6	6.2626	1.4	0.3704	1.2	0.89	2031	22	2013	12	1995	11	1995	11	-2
55	126	169,555	0.8	8.0775	0.5	6.3244	1.2	0.3705	1.1	0.91	2032	19	2022	10	2012	9	2012	9	-1
100	32	35,516	0.8	8.0186	1.9	5.8410	2.1	0.3397	0.9	0.46	1885	15	1953	18	2025	33	2025	33	7
19	150	137,568	0.6	7.9520	1.1	6.5372	1.8	0.3770	1.5	0.81	2062	26	2051	16	2039	19	2039	19	-1
14	28	10,817	1.5	7.8791	2.2	6.6645	3.4	0.3808	2.6	0.77	2080	47	2068	30	2056	39	2056	39	-1
41	151	85,564	0.4	7.6651	0.6	6.4493	4.3	0.3585	4.3	0.99	1975	73	2039	38	2104	11	2104	11	6
27	47	40,559	0.5	7.5363	1.8	7.0560	4.3	0.3857	3.9	0.91	2103	71	2119	39	2134	32	2134	32	1
46	25	25,605	0.6	7.4210	3.0	7.1491	3.5	0.3848	1.8	0.51	2099	32	2130	31	2161	53	2161	53	3
60	10	9,164	0.1	6.7252	3.2	8.8638	8.3	0.4323	7.6	0.92	2316	148	2324	75	2331	54	2331	54	1
5	177	318,771	0.6	6.6924	0.5	8.9524	1.5	0.4345	1.4	0.95	2326	27	2333	13	2339	8	2339	8	1
94	135	135,534	1.0	6.6911	0.5	8.9063	0.9	0.4322	0.7	0.81	2316	14	2328	8	2340	9	2340	9	1
18	45	51,872	1.0	6.6578	0.9	9.3229	1.3	0.4502	1.0	0.72	2396	19	2370	12	2348	16	2348	16	-2
20	44	30,024	1.3	6.5788	1.6	9.0183	3.9	0.4303	3.6	0.91	2307	69	2340	36	2369	27	2369	27	3
34	68	131,884	0.5	5.9768	1.1	11.1678	1.6	0.4841	1.1	0.69	2545	23	2537	15	2531	19	2531	19	-1
84	73	59,106	0.4	5.7577	0.7	11.8092	1.2	0.4931	1.0	0.83	2584	22	2589	11	2593	11	2593	11	0
88	234	319,229	0.3	5.7068	0.3	12.1209	0.7	0.5017	0.7	0.92	2621	14	2614	7	2608	5	2608	5	0
64	62	97,101	1.1	5.6920	0.7	12.3593	2.8	0.5102	2.7	0.97	2658	59	2632	26	2613	11	2613	11	-2
49	101	122,196	1.1	5.6842	0.5	12.5299	1.1	0.5166	1.0	0.91	2685	23	2645	11	2615	8	2615	8	-3
85	67	67,872	0.9	5.6689	0.7	12.1770	0.9	0.5007	0.6	0.64	2617	13	2618	9	2619	12	2619	12	0
53	107	89,439	0.8	5.6595	0.3	12.1970	1.1	0.5006	1.1	0.98	2617	24	2620	11	2622	4	2622	4	0
32	109	102,931	0.8	5.6495	0.4	12.5678	1.5	0.5150	1.5	0.96	2678	32	2648	14	2625	7	2625	7	-2
35	204	868,515	0.3	5.5377	0.8	12.9220	1.0	0.5190	0.6	0.63	2695	14	2674	10	2658	13	2658	13	-1
23	71	72,332	0.4	5.4859	0.5	13.1520	0.9	0.5233	0.8	0.84	2713	18	2691	9	2674	8	2674	8	-1
86	77	61,629	0.8	5.4312	0.5	13.3135	1.8	0.5244	1.8	0.96	2718	39	2702	17	2690	8	2690	8	-1
50	46	32,438	0.8	5.4255	1.2	13.4314	1.8	0.5285	1.4	0.77	2735	32	2710	17	2692	19	2692	19	-2
74	41	61,369	1.6	5.4036	1.1	13.6025	1.5	0.5331	1.0	0.68	2754	23	2722	15	2699	19	2699	19	-2
17	29	26,369	1.0	5.3956	1.7	13.2041	5.2	0.5167	4.9	0.95	2685	107	2694	49	2701	28	2701	28	1

Table 1. (continued)

Grain #	U (ppm)	²⁰⁶ Pb/ ²⁰⁴ Pb	Th/U	²⁰⁶ Pb*/ ²⁰⁷ Pb*	± (%)	²⁰⁷ Pb*/ ²³⁵ U*	± (%)	²⁰⁶ Pb*/ ²³⁸ U	± (%)	error corr.	²⁰⁶ Pb*/ ²³⁸ U*	± (Ma)	²⁰⁷ Pb*/ ²³⁵ U	± (Ma)	²⁰⁶ Pb*/ ²⁰⁷ Pb*	± (Ma)	Best age (Ma)	± (Ma)	Conc (%)
81	14	12,994	0.4	5.3515	2.8	13.2954	3.5	0.5160	2.1	0.61	2682	46	2701	33	2715	45	2715	45	1
45	76	89,500	0.8	5.3499	1.0	13.8482	1.3	0.5373	0.9	0.64	2772	19	2739	13	2715	17	2715	17	-2
54	147	117,807	0.9	5.3140	0.6	12.0544	4.0	0.4646	3.9	0.99	2460	81	2609	37	2726	10	2726	10	10
82	63	213,309	0.8	5.1004	0.5	14.4629	1.0	0.5350	0.8	0.88	2763	19	2781	9	2794	7	2794	7	1
21	107	242,593	0.6	5.0546	0.8	13.5523	1.8	0.4968	1.6	0.90	2600	35	2719	17	2808	13	2808	13	7
Rejected analyses (>10% discordant; >5% reverse discordance; >10% 2-sigma uncertainty)																			
29	60	1,938	0.4	8.2443	2.1	4.7609	2.7	0.2847	1.7	0.63	1615	24	1778	23	1975	38			18
31	268	51,839	0.4	7.6855	0.4	5.4987	0.9	0.3065	0.8	0.88	1723	12	1900	8	2099	8			18
10	277	33,966	0.4	8.4591	0.5	4.9251	3.5	0.3022	3.4	0.99	1702	51	1807	29	1929	10			12
96	36	10,000	0.4	12.1504	7.1	2.1495	7.7	0.1894	2.9	0.37	1118	29	1165	53	1253	139			11
77	45	31,777	0.5	10.6298	5.1	3.2795	5.3	0.2528	1.4	0.27	1453	19	1476	42	1510	97			4
8	2	2,307	0.4	7.4629	44.5	6.2061	52.7	0.3359	28.3	0.54	1867	460	2005	497	2151	823			13
11	167	46,877	0.4	6.9030	3.1	5.6477	10.2	0.2828	9.8	0.95	1605	139	1923	89	2286	54			30
16	39	26,706	2.6	9.2235	2.7	5.1020	3.8	0.3413	2.8	0.72	1893	46	1836	33	1773	48			-7
22	41	45,644	0.8	8.8124	2.2	5.6778	3.2	0.3629	2.3	0.73	1996	40	1928	28	1856	40			-8
30	66	24,681	0.4	11.6796	3.1	2.8991	4.0	0.2456	2.5	0.64	1416	32	1382	30	1330	59			-6
37	33	22,667	0.4	14.2765	6.1	1.7502	7.2	0.1812	3.9	0.54	1074	38	1027	47	930	125			-15
42	44	52,873	0.9	10.2680	2.3	3.9530	3.0	0.2944	2.0	0.65	1663	29	1625	25	1575	43			-6
43	53	17,359	0.7	14.0084	5.8	1.8362	5.9	0.1866	1.1	0.19	1103	11	1058	39	968	119			-14
44	208	11,303	0.5	8.1635	0.8	4.0941	4.9	0.2424	4.8	0.99	1399	60	1653	40	1993	14			30
48	141	12,651	0.6	9.0775	1.5	2.1248	23.5	0.1399	23.5	1.00	844	186	1157	164	1802	27			53
57	237	3,204	1.1	5.8188	1.2	9.6246	4.0	0.4062	3.8	0.95	2197	70	2400	37	2576	20			15
65	98	1,016	1.0	8.7507	3.5	3.4270	4.5	0.2175	2.8	0.63	1269	33	1511	35	1868	63			32

Notes:

1. Best age is determined from ²⁰⁷Pb/²⁰⁶Pb age for analyses with ²⁰⁶Pb/²³⁸U age > 1000 Ma.
2. Concordance is based on (²⁰⁶Pb/²³⁸U age)/(²⁰⁶Pb/²⁰⁷Pb age).
3. Analyses with >10% discordance, >5% reverse discordance, or >10% uncertainty (2-sigma) in Best Age are not included in discussion.
4. All uncertainties are reported at the 1-sigma level, and include only measurement errors.
5. Systematic errors are as follows (at 2-sigma level): 1.1% (²⁰⁶Pb/²³⁸U) & 1.1% (²⁰⁷Pb/²⁰⁶Pb).
6. Analyses conducted by LA-MC-ICPMS, as described by Gehrels et al. (2008).
7. U concentration and U/Th are calibrated relative to Sri Lanka zircon standard and are accurate to ~20%.
8. Common Pb correction is from measured ²⁰⁴Pb with common Pb composition interpreted from Stacey and Kramers (1975).
9. Common Pb composition assigned uncertainties of 1.5 for ²⁰⁶Pb/²⁰⁴Pb, 0.3 for ²⁰⁷Pb/²⁰⁴Pb, and 2.0 for ²⁰⁸Pb/²⁰⁴Pb.
10. U/Pb and ²⁰⁷Pb/²⁰⁶Pb fractionation is calibrated relative to fragments of a large Sri Lanka zircon of 563.5 ± 3.2 Ma (2-sigma).
11. U decay constants and composition as follows: ²³⁸U = 9.8485 x 10⁻¹⁰, ²³⁵U = 1.55125 x 10⁻¹⁰, ²³⁸U/²³⁵U = 137.88.

REFERENCES

- Amato, J.M., Toro, J., Miller, E.L., Gehrels, G.E., Farmer, G.L., Gottlieb, E.S. and Till, A.B., 2009. Late Proterozoic-Paleozoic evolution of the Arctic Alaska-Chukotka terrane based on U-Pb igneous and detrital zircon ages: Implications for Neoproterozoic paleogeographic reconstructions. *Geological Society of America Bulletin*, vol. 121, p. 1219-1235.
- Anfinson, O.A., Leier, A., Embry, A.F. and Dewing, K., 2012. Detrital zircon geochronology and provenance of the Neoproterozoic to Late Devonian Franklinian basin, Canadian Arctic Islands. *Geological Society of America Bulletin*, vol. 124, p. 415-430.
- Beranek, L.P., Pease, V., Scott, R.A. and Thomsen, T.B., 2013. Detrital zircon geochronology of Ediacaran to Cambrian deep-water strata of the Franklinian basin, northern Ellesmere Island, Nunavut: implications for regional stratigraphic correlations. *Canadian Journal of Earth Sciences*, vol. 50, p. 1007-1018.
- Cecile, M.P., 1988. Corridor traverse through Barn Mountains, northernmost Yukon. *Geological Survey of Canada, Paper 88-1D*, p. 99-103.
- Cecile, M.P. and Lane, L.S., 1991. Geology of the Barn uplift, northern Yukon. *Geological Survey of Canada, Open File Map 2342*, scale 1:50 000.
- Churkin, M., Carter, C. and Trexler, J.H., 1980. Collision-deformed Paleozoic continental margin of Alaska - Foundation for microplate accretion. *Geological Society of America Bulletin*, vol. 91, p. 648-654.
- Colpron, M. and Nelson, J., 2009. A Paleozoic Northwest Passage: incursion of Caledonian, Baltican and Siberian terranes into eastern Panthalassa, and the early evolution of the North American Cordillera. *In: Earth Accretionary Systems in Space and Time*, P.A. Cawood and A. Kroner (eds.), *Geological Society of London Special Publication*, vol. 318, p. 273-307.
- Dumoulin, J.A., Harris, A.G. and Repetski, J.E., 2014. Carbonate rocks of the Seward Peninsula, Alaska: Their correlation and paleogeographic significance. *In: Reconstruction of a Late Proterozoic to Devonian continental margin sequence, northern Alaska, its paleogeographic significance, and contained base-metal sulfide deposits*, J.A. Dumoulin and A.B. Till (eds.), *Geological Society of America, Special Paper 506*, p. 59-110.
- Dumoulin, J.A., Harris, A.G., Gagiev, M., Bradley, D.C. and Repetski, J.E., 2002. Lithostratigraphic, conodont, and other faunal links between lower Paleozoic strata in northern and central Alaska and northeastern Russia. *In: Tectonic Evolution of the Bering Shelf - Chukchi Sea - Arctic Margin and Adjacent Land Masses*, E.L. Miller, A. Grantz, and S. Klemperer (eds.), *Geological Society of America, Special Paper 360*, p. 291-312.
- Dutro, J.T., Jr., 1981. Geology of Alaska bordering the Arctic Ocean. *In: The Arctic Ocean*, in A.E.M. Nairn, A.E.M., M. Churkin Jr., and F.G. Stehli (eds.), *The ocean basins and margins*, New York, Plenum, vol. 5, p. 21-36.
- Dyke, L.D., 1997. White, Barn and Campbell uplifts. *In: The geology, mineral and hydrocarbon potential of the northern Yukon Territory and northwestern District of Mackenzie*, D.K. Norris, D.K. (ed.), *Geological Survey of Canada Bulletin*, vol. 422, p. 333-358.
- Gehrels, G.E., Johnsson, M.J. and Howell, D.G., 1999. Detrital zircon geochronology of the Adams Argillite and Nation River Formation, east-central Alaska, U.S.A. *Journal of Sedimentary Research*, vol. 69, p. 135-144.
- Gehrels, G.E., Valencia, V. and Pullen, A., 2006. Detrital zircon geochronology by Laser-Ablation Multicollector ICPMS at the Arizona LaserChron Center. *In: Geochronology: Emerging Opportunities*, T. Loszewski, and W. Huff (eds.), *Paleontology Society Short Course: Paleontology Society Papers*, vol. 11, 10 p.
- Gehrels, G.E., Valencia, V. and Ruiz, J., 2008. Enhanced precision, accuracy, efficiency, and spatial resolution of U-Pb ages by laser ablation-multicollector-inductively coupled plasma-mass spectrometry. *Geochemistry, Geophysics, Geosystems*, vol. 9, Q03017.
- Grantz, A., Hart, P.E. and Childers, V.A., 2011. Geology and tectonic development of the Amerasia and Canada Basins, Arctic Ocean. *In: Arctic Petroleum Geology*, A.M. Spencer, A.F. Embry, D.L. Gautier, A.V. Stoupakova, and K. Sørensen (eds.), *Geological Society of London Memoir*, vol. 35, p. 771-799.
- Hadlari, T., Davis, W.J. and Dewing, K., 2014. A pericratonic model for the Pearya terrane as an extension of the Franklinian margin of Laurentia, Canadian Arctic. *Geological Society of America Bulletin*, vol. 126, p. 182-200.

- Hadlari, T., Davis, W.J., Dewing, K., Heaman, L. M., Lemieux, Y., Ootes, L., Pratt, B. R. and Pyle, L.J., 2012. Two detrital zircon signatures for the Cambrian passive margin of northern Laurentia highlighted by new U-Pb results from northern Canada. *Geological Society of America Bulletin*, vol. 124, p. 1155-1168.
- Herbosch, A. and Verniers, J., 2011. What is the biostratigraphic value of the ichnofossil *Oldhamia* for the Cambrian: a review. *Geologica Belgica*, vol. 14, p. 229-248.
- Hofmann, H.J., Cecile, M.P. and Lane, L.S., 1994. New occurrences of *Oldhamia* and other trace fossils from Arctic North America. *Canadian Journal of Earth Sciences*, vol. 31, p. 767-782.
- Hubbard, R.J., Edrich, S.P. and Rattey, R.P., 1987. Geologic evolution and hydrocarbon habitat of the Arctic Alaska microplate. *Marine and Petroleum Geology*, vol. 4, p. 2-34.
- Kirkland, C.L., Pease, V., Whitehouse, M.J. and Ineson, J.R., 2009. Provenance record from Mesoproterozoic-Cambrian sediments of Peary Land, North Greenland: Implications for the ice-covered Greenland Shield and Laurentian paleogeography. *Precambrian Research*, vol. 170, p. 43-60.
- Lane, L.S., 1991. The pre-Mississippian "Neruokpuk Formation," northeastern Alaska and northwestern Yukon: Review and new regional correlation. *Canadian Journal of Earth Sciences*, vol. 28, p. 1521-1533.
- Lane, L.S., 1992. Kaltag Fault, northern Yukon, Canada: constraints on evolution of Arctic Alaska. *Geology*, vol. 20, p. 653-656.
- Lane, L.S., 1997. Canada Basin, Arctic Ocean: Evidence against a rotational model. *Tectonics*, vol. 16, p. 363-387.
- Lane, L.S., 1998. Latest Cretaceous - Tertiary tectonic evolution of northern Yukon and adjacent Arctic Alaska. *American Association of Petroleum Geology Bulletin*, vol. 82, p. 1353-1371.
- Lane, L.S., 2007. Devonian-Carboniferous paleogeography and orogenesis, northern Yukon and adjacent Arctic Alaska. *Canadian Journal of Earth Sciences*, vol. 44, p. 679-694.
- Lane, L.S. and Gehrels, G.E., 2014. Detrital zircon lineages of late Neoproterozoic and Cambrian strata, NW Laurentia. *Geological Society of America Bulletin*, vol. 126, p. 398-414.
- Lane, L.S., Kelley, J.S. and Wrucke, C.T., 1995. Stratigraphy and structure of the Clarence River area, Yukon-Alaska north slope: a USGS-GSC co-operative project. *In: Current Research 1995-E, Geological Survey of Canada*, p. 1-9.
- Lawver, L.A., Grantz, A. and Gahagan, L.M., 2002. Plate kinematic evolution of the present Arctic region since the Ordovician. *In: Tectonic Evolution of the Bearing Shelf - Chukchi Sea- Arctic Margin and Adjacent Landmasses*, E.L. Miller, A. Grantz, and S.L. Klemperer (eds.), Geological Society of America Special Paper 360, p. 333-358.
- Lenz, A.C. and Perry, D.G., 1972. The Neruokpuk Formation of the Barn Mountains and Driftwood Hills, northern Yukon; its age and graptolite fauna. *Canadian Journal of Earth Sciences*, vol. 9, p. 1129-1138.
- Leslie, C.D., 2009. Detrital zircon geochronology and rift-related magmatism: Central Mackenzie Mountains, Northwest Territories. MSc Thesis, Vancouver, British Columbia, University of British Columbia, 224 p.
- Ludwig, K.R., 2008. Isoplot 3.60. Berkeley Geochronology Center, Special Publication No. 4, 77 p.
- Macdonald, F.A., McClelland, W.C., Schrag, D.P. and Macdonald, W.P., 2009. Neoproterozoic glaciation on a carbonate platform margin in Arctic Alaska and the origin of the North Slope subterranean. *Geological Society of America Bulletin*, vol. 121, p. 448-473.
- Miller, E.L., Kuznetsov, N., Soboleva, A., Udoratina, O., Grove, M.J. and Gehrels, G.E., 2011. Baltica in the Cordillera? *Geology*, vol. 39, p. 791-794.
- Norris, D.K., 1981. Geology, Blow River and Davidson Mountains, Yukon Territory - District of Mackenzie. Geological Survey of Canada, Map 1516A, scale 1:250 000.
- Norris, D.K., 1997. The Geology, Mineral, and Hydrocarbon Potential of Northern Yukon Territory and Northwest District of Mackenzie. Geological Survey of Canada Bulletin 422, 401 p.

- Norris, D.K. and Yorath, C.J., 1981. The North American plate from the Arctic Archipelago to the Romanzof Mountains. *The Ocean Basins and Margins – The Arctic Ocean*, vol. 5, Plenum, New York, p. 37-103.
- Oldow, J.S., Avé Lallemant, H.G., Julian, F.E. and Seidensticker, C.M., 1987. Ellesmerian(?) and Brookian deformation in the Franklin Mountains, northeastern Brooks Range, Alaska, and its bearing on the origin of the Canada Basin. *Geology*, vol. 15, p. 37-41.
- Patrick, B.E. and McClelland, W.C., 1995. Late Proterozoic granitic magmatism on Seward Peninsula and a Barentian origin for Arctic Alaska-Chukotka. *Geology*, vol. 23, p. 81-84.
- Rainbird, R.H., Heaman, L. and Young, G.M., 1992. Sampling Laurentia: detrital zircon geochronology offers evidence for an extensive Neoproterozoic river system originating from the Grenville orogen. *Geology*, vol. 20, p. 351-354.
- Rainbird, R.H., McNicoll, V. and Theriault, R., 1997. Pancontinental river system draining Grenville orogen recorded by U–Pb and Sm–Nd geochronology of Neoproterozoic quartzarenites and mudrocks northwestern Canada. *Journal of Geology*, vol. 105, p. 1-17.
- Stacey, J.S. and Kramers, J.D., 1975. Approximation of terrestrial lead isotope evolution by a two stage model. *Earth and Planetary Science Letters*, vol. 26, p. 207-221.
- Strauss, J.V., Macdonald, F.A., Taylor, J.F., Repetski, J.E. and McClelland, W.C., 2013. Laurentian origin for the North Slope of Alaska: Implications for the tectonic evolution of the Arctic. *Lithosphere*, vol. 5, p. 477-482.
- Till, A.B., Amato, J.M., Aleinikoff, J.N. and Bleick, H.A., 2014. U-Pb detrital zircon geochronology as evidence for the origin of the Nome Complex, northern Alaska, and implications for regional and trans-Arctic correlations. *In: Reconstruction of a Late Proterozoic to Devonian continental margin sequence, northern Alaska, its paleogeographic significance, and contained base-metal sulfide deposits*, J.A. Dumoulin and A.B. Till (eds.), Geological Society of America, Special Paper 506, p. 111-131.
- Van Schmus, W.R., Bickford, M.E., Anderson, J.L., Bender, E.E., Anderson, R.R., Bauer, P.W., Robertson, J.M., Bowring, S.A., Condie, K.C., Denison, R.E., Gilbert, M.C., Grambling, J.A., Mawer, C.K., Shearer, C.K., Hinje, W.J., Karlstrom, K.E., Kisvarsanyi, E.B., Lidiak, E.G., Reed, J.C., Jr., Sims, P.K., Tweto, O., Silver, L.T., Treves, S.B., Williams, M.L. and Wooden, J.L., 1993. Transcontinental Proterozoic provinces. *In: Precambrian Conterminous U.S.*, J.C. Reed, Jr., M.E. Bickford, R.S. Houston, P.K. Link, D.W. Rankin, P.K. Sims, and W.R. Van Schmus, (eds.) Geological Society of America, *Geology of North America*, vol. C-2, p. 171–334.

Soft sediment textures in clasts in Wernecke Breccia: Reconstruction of an eroded late Paleoproterozoic succession in northern Yukon

J. Verbaas¹, D.J. Thorkelson, H.D. Gibson, D.D. Marshall and D. Milidragovic
Simon Fraser University, Department of Earth Sciences

Verbaas, J., Thorkelson, D.J., Gibson, H.D., Marshall, D.D. and Milidragovic, D., 2015. Soft sediment textures in clasts in Wernecke Breccia: Reconstruction of an eroded late Paleoproterozoic succession in northern Yukon. *In: Yukon Exploration and Geology 2014*, K.E. MacFarlane, M.G. Nordling and P.J. Sack (eds.), Yukon Geological Survey, p. 145-156.

ABSTRACT

The 1.60 Ga hydrothermal Wernecke Breccia are hosted within metasedimentary rocks of the Wernecke Supergroup and exposed in the Wernecke, Ogilvie and southern Richardson Mountains of northern Yukon. Breccia clasts with soft sediment deformation textures were previously identified and interpreted as fragments of the Wernecke Supergroup that were torn off and carried upward during mud volcanism. This model was subsequently discounted because field relations and geochronology indicated that the Wernecke Supergroup was lithified and metamorphosed prior to brecciation. Our recent work confirms the presence of soft sediment within zones of Wernecke Breccia and demonstrates the need for an unlithified sediment source. Two types of soft sediment materials have been identified: red mudstone to sandstone, and green mudstone. These unlithified sediments were likely derived from late Paleoproterozoic water-saturated sediments. During breccia formation, the surface was breached and fragments of the unlithified sediments foundered into the breccia zones, mixing with clasts of lithified wallrock. The sediments descended to depths of at least 4 km where they were lithified and encased by hydrothermal cement. Subsequent erosion removed the source beds and exposed the breccia zones.

¹jacobverbaas@gmail.com

INTRODUCTION

Wernecke Breccia is a collective term for a set of hydrothermal breccia zones that are distributed over more than 48 000 km² in the Wernecke, Ogilvie, and southern Richardson mountains in northern Yukon (Fig. 1; Thorkelson *et al.*, 2001a). Individual breccia zones range in size from several metres to several kilometres across. They are hydrothermal in origin and were dated at 1599 Ma by U-Pb metasomatic titanite (Furlanetto *et al.*, 2013). Iron oxide copper gold (IOCG) occurrences in and near the breccia zones have attracted significant exploration interest (Hunt *et al.*, 2011).

The Wernecke Breccia is hosted by the Wernecke Supergroup, a >13 km thick succession of clastic and carbonate rocks deposited on the western margin of ancestral North America (Delaney, 1981; Furlanetto *et al.*, 2013). The Wernecke Supergroup was deformed and metamorphosed to greenschist facies during the ca. 1.6 Ga Racklan Orogeny prior to the hydrothermal brecciation. Strata of the Fifteenmile group and the Pinguicula Group (Thompson *et al.*, 1992; Medig *et al.*, 2010) unconformably overlie the Wernecke Supergroup and Wernecke Breccia. The Wernecke Supergroup is presumed to have been deposited on either crystalline basement or an intervening sedimentary succession (Thorkelson *et al.*, 2005). Detrital zircon analysis constrains the Wernecke Supergroup to ≤ 1.66 Ga (Furlanetto *et al.*, 2013, 2014).

The majority of clasts in Wernecke Breccia consist of siltstone, shale, sandstone, carbonate and minor phyllite and fine-grained schist that were sourced from the Wernecke Supergroup (Thorkelson *et al.*, 2001a). Previously, Lane (1990) showed that a small proportion of the clasts displayed soft sediment textures indicating they were incorporated into Wernecke Breccia prior to lithification. He also suggested that these clasts were derived from the Wernecke Supergroup. However, this interpretation is incompatible with the current understanding that the Wernecke Supergroup was entirely lithified and metamorphosed before breccia formation (Mercier, 1989; Thorkelson, 2001a). In this paper, we address the issue of soft sediment textures in clasts of the Wernecke Breccia. We suggest an alternative source for the soft sediments, explore the crustal conditions at the time of brecciation, and speculate on the geological processes that led to mixing of soft sediment and lithified materials.

LOCATION AND ACCESS

Sedimentary lithologies with soft sediment textures occur in two areas in the Ogilvie Mountains. The first area is near the headwaters of the Fifteenmile River (Fig. 2a). This area is rugged and mountainous, and best accessed by helicopter. The second is located near the Dempster highway on both sides of the Blackstone River (Fig. 2b).

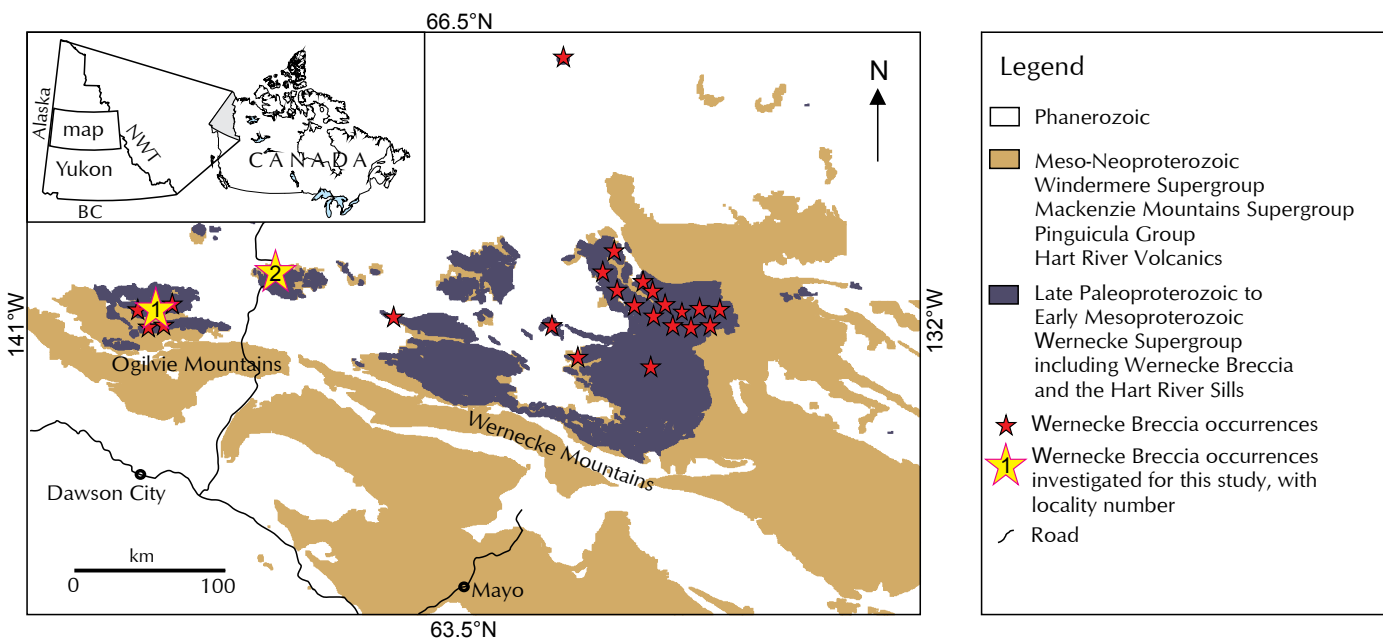


Figure 1. Proterozoic inliers in Yukon showing locations of Wernecke Breccia zones and study areas.

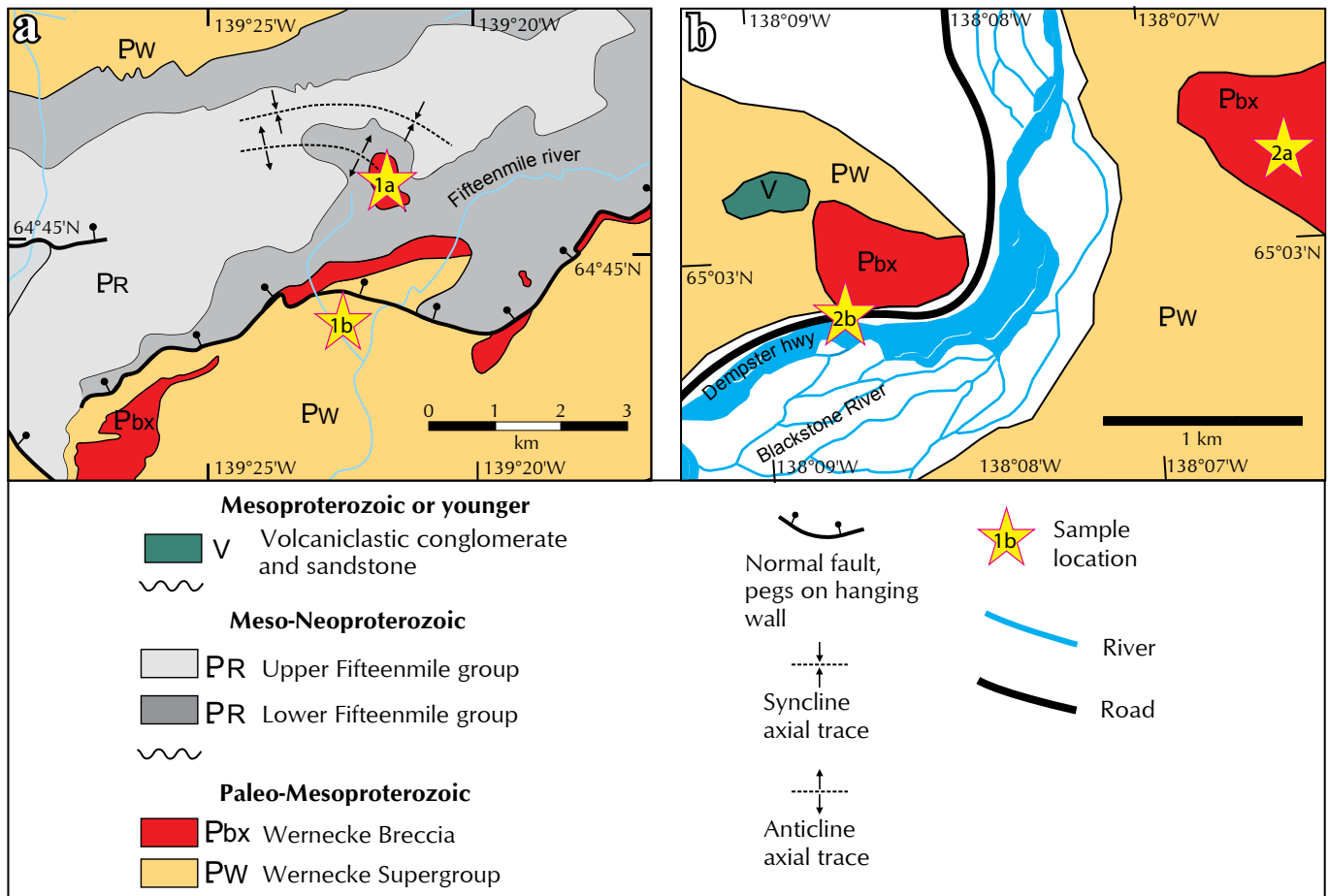


Figure 2. Locations where Wernecke Breccia clasts with soft sediment textures are present in outcrop and float.

The exposures and related coarse rip-rap on the west side of the river are adjacent to the highway. The exposures to the east of the Blackstone River occur in the bed of “Spectacular creek” (Yukon MINFILE 116G082) and are accessible by a combination of light watercraft and foot traverse.

GEOLOGICAL FRAMEWORK

EXOTIC CLASTS IN WERNECKE BRECCIA AND THE BONNETIA MODEL

Locally abundant igneous clasts occur within the breccia zones. The Wernecke Supergroup does not contain any igneous rocks and these clasts were therefore derived from a different source. Three main types of igneous clasts have been identified: 1) the Bonnet Plume River intrusions (Thorkelson *et al.*, 2001b; Nielsen *et al.*, 2013); 2) the Slab volcanics (Thorkelson and Wallace, 1998; Laughton *et al.*, 2005); and 3) the Devil volcanics (Nielsen

et al., 2011, 2013). The largest known igneous clast is a block of diorite 900 m long, 300 m wide and a minimum of 30 m thick (Thorkelson and Wallace, 1998; Nielsen *et al.*, 2013). Clasts of the Slab volcanics are known in at least three localities in the Wernecke Mountains, with the largest clast consisting of a 160-m-thick succession of 31 mafic lava flows intercalated with minor volcanic breccia and sandstone (Laughton *et al.*, 2005; Fig. 3). Sedimentary megaclasts from the Wernecke Supergroup are also locally present and range up to hundreds of metres across (Hunt *et al.*, 2002).

The Bonnet Plume River intrusions have been dated at 1.71 Ga by U-Pb zircon (Thorkelson *et al.*, 2001b). As demonstrated by Furlanetto *et al.* (2014), the age of the Wernecke Supergroup is <1.66 Ga, which is at least 50 m.y. younger than the dated igneous clasts (Thorkelson *et al.*, 2005; Nielsen *et al.*, 2013). Furlanetto *et al.* (2013) postulated that the source of the igneous clasts was an obducted terrane, which they named Bonnetia. Clasts of Bonnetia foundered into the breccia zones during



Figure 3. Igneous megaclasts in the Wernecke Breccia zone at Slab Mountain as described by Hunt *et al.* (2002), and Laughton *et al.*, (2005).

brecciation and became juxtaposed with the underlying Wernecke Supergroup. Bonnetia was completely eroded after the brecciation, and igneous clasts that are now exposed within zones of Wernecke Breccia are the only record of its existence (Furlanetto *et al.*, 2013; Nielsen *et al.*, 2013). If the Bonnetia model is correct, it opens the possibility that not only the igneous clasts were derived from above the Wernecke Supergroup, but perhaps some of the sedimentary clasts were as well.

SOFT SEDIMENT DEFORMATION

Lane (1990) described soft sediment “plastic” deformation in a minority of clasts within the Wernecke Breccia. These clasts were interpreted to have been derived from the Fairchild Lake Group, the lowest member of the Wernecke Supergroup. The brecciating mechanism that

Lane (1990) invoked was hydraulic over-pressurization and mud diapirism originating in the Fairchild Lake Group. Similarly, a model involving evaporate diapirism, dissolution and collapse (Bell, 1986) may explain the plastic deformation noted by Lane (1990). However, the Wernecke Supergroup was deformed and metamorphosed to greenschist grade during the Racklan orogeny, prior to the formation of the Wernecke Breccia (Furlanetto *et al.*, 2013; Thorkelson *et al.*, 2001a), and was entirely lithified at the time of breccia formation. Neither mud diapirism nor evaporate diapirism are plausible in rocks that have undergone contractional deformation and greenschist-grade metamorphism. Furthermore, the majority of researchers agree that brecciation and related metasomatism were driven by hydrothermal activity (Laznicka and Edwards, 1979; Laznicka and Gaboury,

1988; Lane, 1990; Hitzman *et al.*, 1992; Laughton *et al.*, 2005). Hunt *et al.* (2011) calculated the temperature of the brecciating fluids to have been 185-350°C at approximate depths of 6-11 km. The presence of plastically deformed sediment in hot hydrothermal breccia zones hosted by metamorphosed rock is a conundrum that requires explanation.

SOFT SEDIMENT LITHOLOGIES

LITHOLOGIES AND LOCATIONS

Lithologies with soft sediment deformation features were examined near the headwaters of the Fifteenmile River (locality 1) and along the Dempster highway (locality 2, Fig. 2). We group the rocks that display soft sediment textures into two lithotypes: 1) red soft sediment lithotype (SSL) and 2) green mudstone. The red SSL occurs in localities 1, 2a and 2b. Numerous examples are visible, particularly in rip-rap derived from locality 2a and deposited along the bank of the Blackstone River. The green mudstone occurs in location 2a and 2b. Additional occurrences of lithologies exhibiting soft sediment deformation were reported by Lane (1990) but were not examined in our field work.

RED SOFT SEDIMENT LITHOTYPE

The term red SSL is herein collectively applied to red to pink sedimentary lithologies in Wernecke Breccia that commonly exhibit soft sediment deformation. Red SSL includes red mudstone, red sandstone and pink sandstone and occurs as two textural end-members and intermediate varieties. One end-member consists of interbedded red mudstone and fine-grained pink sandstone (Fig. 4a). Stratification thickness ranges from 2 mm to 10 cm. Cross-stratification is present locally. The other end-member is a clast-supported granule and pebble-sized breccia also composed of red mudstone to sandstone (Fig. 4b). Some fragments within the second end-member are rounded but many have irregular outlines that fit tightly together in jigsaw-like patterns without intervening matrix (Fig. 4c-h).

The red SSL clast-supported breccia consists of ovoid to irregularly shaped fragments (Fig. 4c-h). There is no Wernecke Breccia matrix present among the clasts. Some clasts of sandstone taper into folded streaks surrounded by an irregular patchwork of mudstone and wacke clasts (Fig. 4c). Many clasts show distorted internal layering (Fig. 4f). The red SSL breccia is interpreted to have

formed from a red sandstone to mudstone succession that was disaggregated into soft and ductile clasts and penecontemporaneously reconstituted into a tightly packed assemblage. None of these textures are prevalent in the Wernecke Supergroup, or in the Wernecke Supergroup clasts that are present in Wernecke Breccia.

A gradational contact (Fig. 5a) exists between the red SSL and typical Wernecke Breccia (Fig. 5b). The gradation is characterized by a mixture of red SSL and other breccia clast types including orange, black and grey weathering mudstone, dolomitic sandstone and minor phyllite that appear to have been derived from the Wernecke Supergroup host-rock (Fig. 5c). Other notable clasts within this gradational contact include fine-grained to aphanitic green mafic igneous rocks of the Devil volcanics (Nielsen *et al.*, 2013; Fig. 5d). Clasts of red SSL have angular to subangular edges and irregular shapes. In localities 2a and b, clasts of red SSL wrap around clasts of previously lithified igneous rock and Wernecke Supergroup. These relations indicate that clasts of the red SSL were unlithified and ductile when they were incorporated into Wernecke Breccia.

This section petrography reveals that the red mudstone is poorly sorted and immature. The red mudstone consists of a submicroscopic assemblage, opaque minerals and minor sand grains (Fig. 6a). Some of the opaque grains are fine-grained hematite that formed metasomatically during breccia formation; others may be detrital. Metasomatic carbonate minerals and scapolite occur as veins and disseminated grains. Clasts of the mudstone have curved edges and internally deformed layering (Fig. 6b). The sandstone component is poorly sorted and contains rounded to subrounded grains of quartz and minor carbonate. Laminations within the sandstone are commonly contorted and attenuated. The red SSL is not strongly compacted or metamorphosed, in contrast with the highly compacted and variably metamorphosed Wernecke Supergroup (Furlanetto *et al.*, 2013, 2009).

Figure 7 is an idealized diagram that shows how the different end-members and intermediate varieties of the red SSL occur within Wernecke Breccia. Large clasts of interbedded sandstone to mudstone are surrounded by a carapace of smaller clasts, forming a tightly packed breccia. The gradational boundary around the red SSL breccia is a mixture of soft sediment fragments and other clasts of Wernecke Breccia. Surrounding this mixture is typical Wernecke Breccia with few, if any, fragments of red SSL.

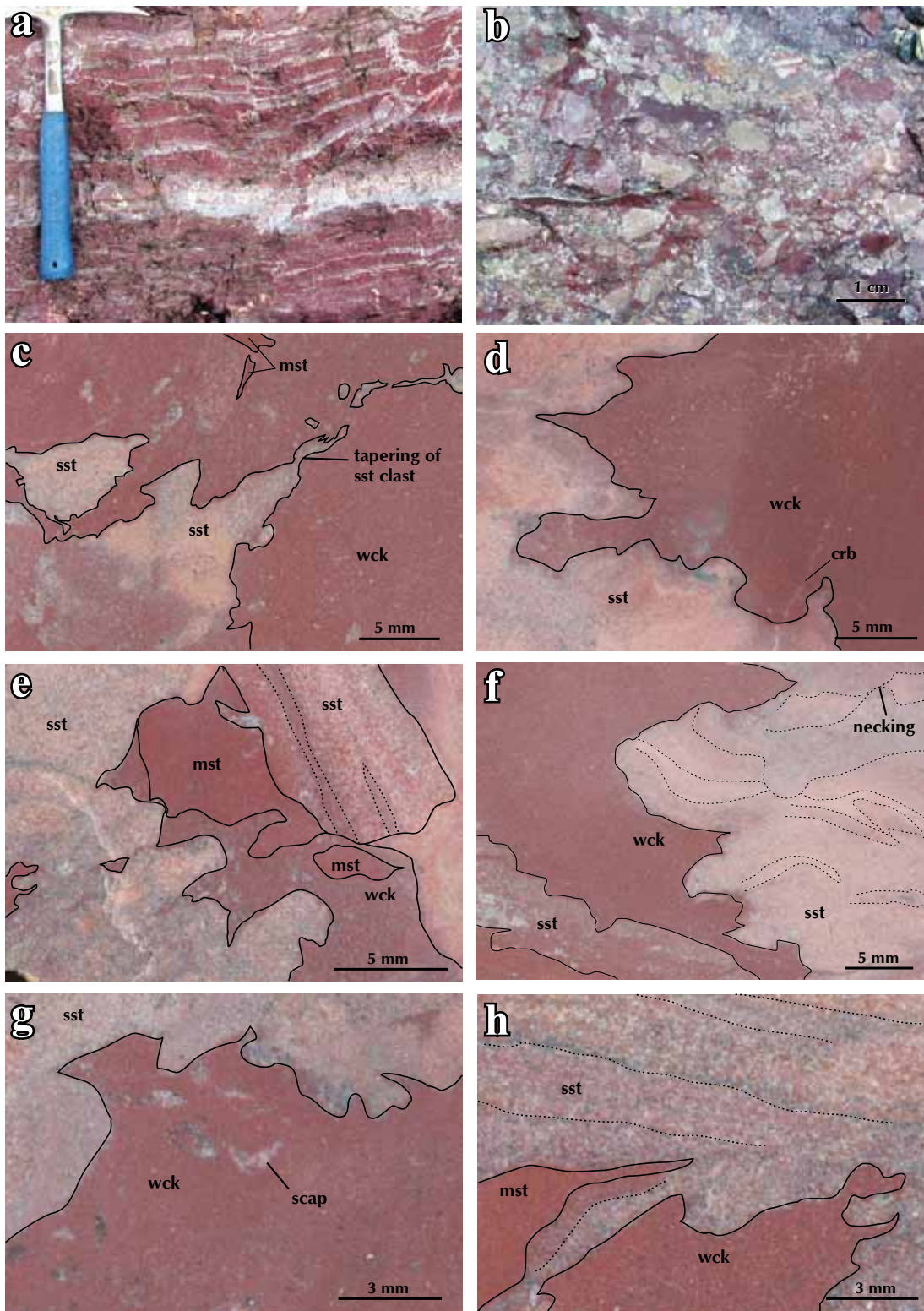


Figure 4. Red sandstone to mudstone end members and field relations. (a) End-member 1: well-bedded red mudstone and pink sandstone lacking soft sediment deformation textures. (b) End-member 2: breccia consisting of tightly packed clasts of sandstone to mudstone with soft sediment deformation textures (textures are clear in Fig 4c-h). (c) Breccia showing a sandstone clast tapering out, a wacke matrix and two distinct mudstone clasts. (d) An irregular boundary between sandstone and wacke. Note also the secondary carbonate veinlet. (e) Mudstone and wacke clasts with slightly more competent sandstone clasts. (f) Sandstone and wacke clasts Note the contorted layering and necking of layers within the sandstone clast. (g) Irregular sandstone clast and wacke. Note secondary scapolite. (h) highly irregular boundaries of mudstone, wacke and sandstone. Note the lack of any metasomatic Wernecke Breccia cement and matrix in between mudstone, sandstone and wacke in c-h.

The presence of soft sediment textures in the red SSL, and its gradational boundary with typical Wernecke Breccia, indicate that this lithotype was only partially consolidated at the time of breccia formation. After its incorporation into the breccia and mixing with other lithologies, the red SSL became lithified.

GREEN MUDSTONE

The second SSL is a light green mudstone. It occurs in outcrop at location 2 and in stream boulders at location 1 (Fig 2). The mudstone occurs interstitially between Wernecke Breccia clasts as curvilinear coatings, streaks and bands up to 5 cm thick (Fig. 8a,b). Where it is thick, the mudstone serves as matrix to Wernecke Breccia clasts, such that smaller (cm-scale) clasts of Wernecke

Breccia are completely encapsulated within the mudstone. The encapsulated fragments include both Wernecke Supergroup clasts (Fig. 8a) and red mudstone clasts (Fig. 8b). We did not identify individual clasts of the green mudstone.

The green mudstone is immature and consists of a submicroscopic assemblage and very fine grained quartz, muscovite and flakes of metasomatic hematite associated with Wernecke Breccia formation. Lamination within the green mudstone is curvilinear, mantling the boundaries of adjacent sandstone clasts (Fig. 8c). Some of the laminated texture may reflect original sedimentary layering, and some may have been generated during flow within the breccia zone. Locally dark green chlorite-hematite coatings rim the margins of the green mudstone (Fig. 8d).

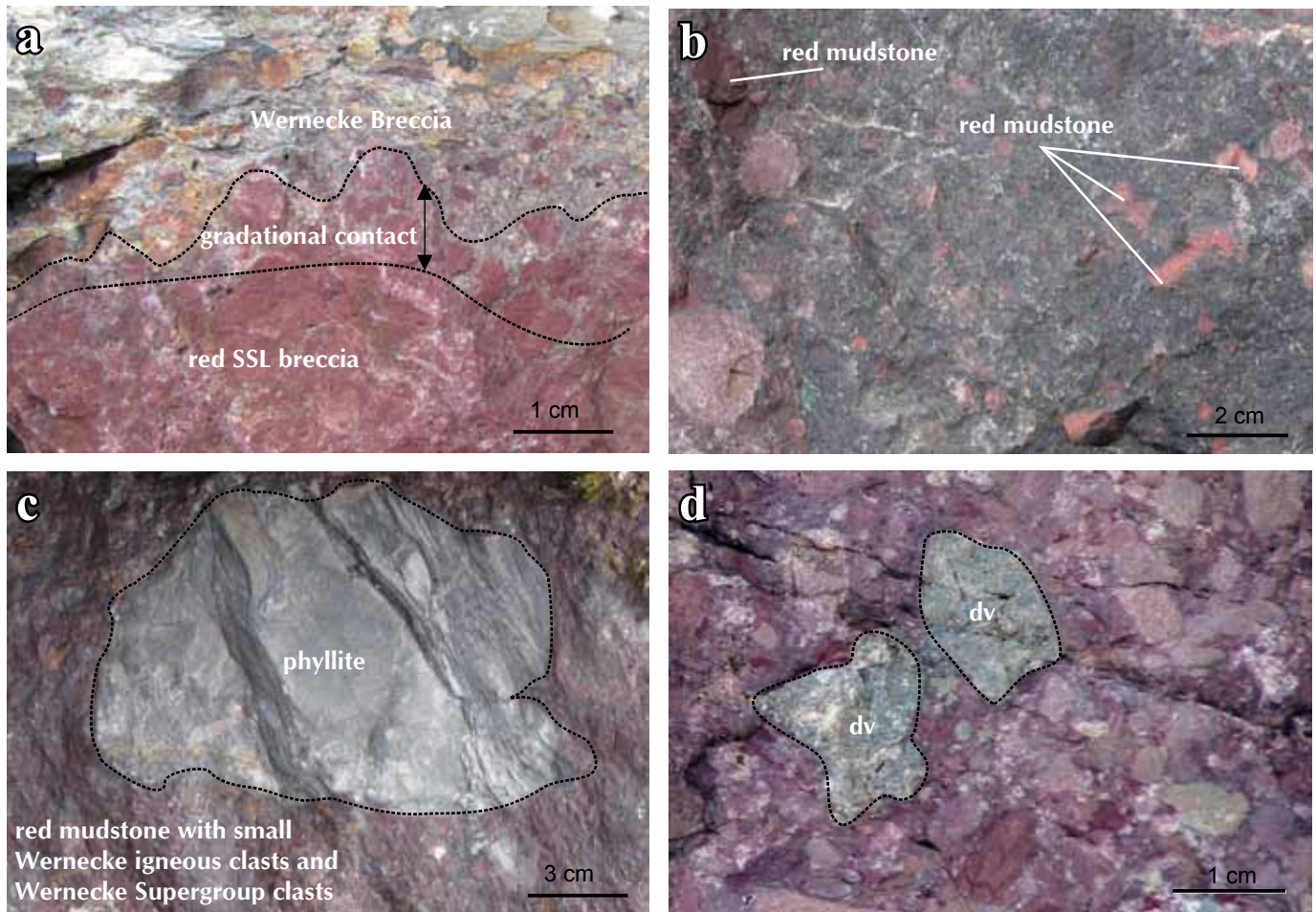


Figure 5. (a) Gradational boundary of the red SSL breccia. Igneous clasts and clasts of Wernecke Supergroup may be present within the gradation. (b) Wernecke Breccia with red mudstone and pink sandstone clasts. (c) Wernecke Supergroup phyllite in gradational boundary of the red SSL. Note there is no Wernecke Breccia metasomatic matrix present in between clasts, the red SSL serves as matrix. (d) Devil volcanic clasts (ig) and Wernecke Supergroup clasts (wsg) embedded within the gradational boundary of the red SSL.

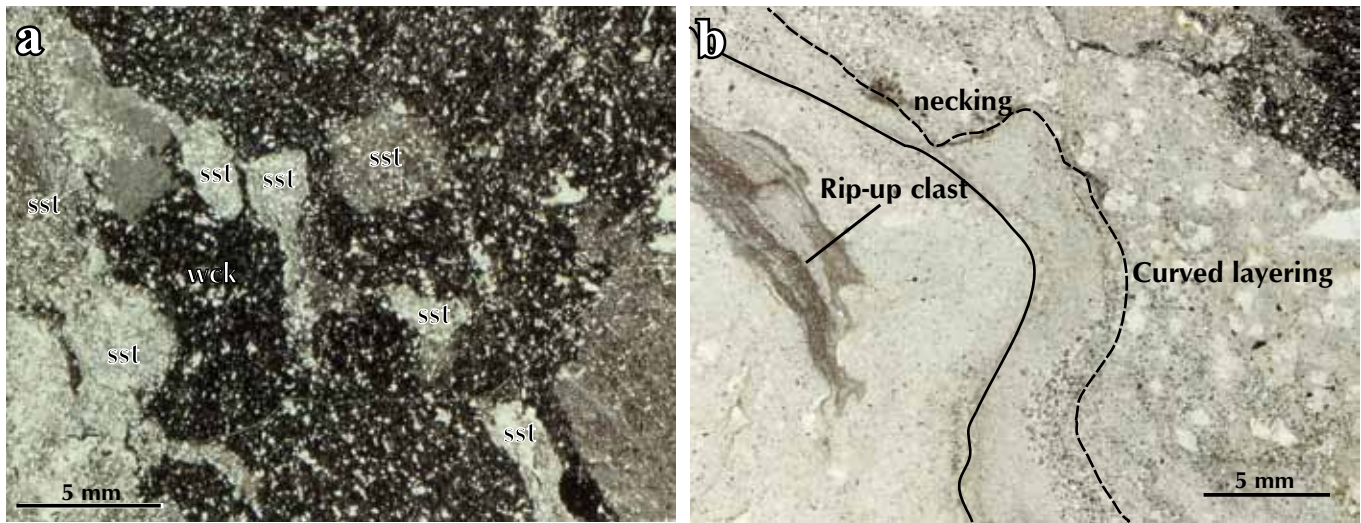


Figure 6. Microstructures of the red SSL breccia. (a) Wacke serves as a matrix to sandstone clasts without intervening Wernecke Breccia metasomatic matrix. (b) Soft sediment textures in the red sandstone to mudstone.

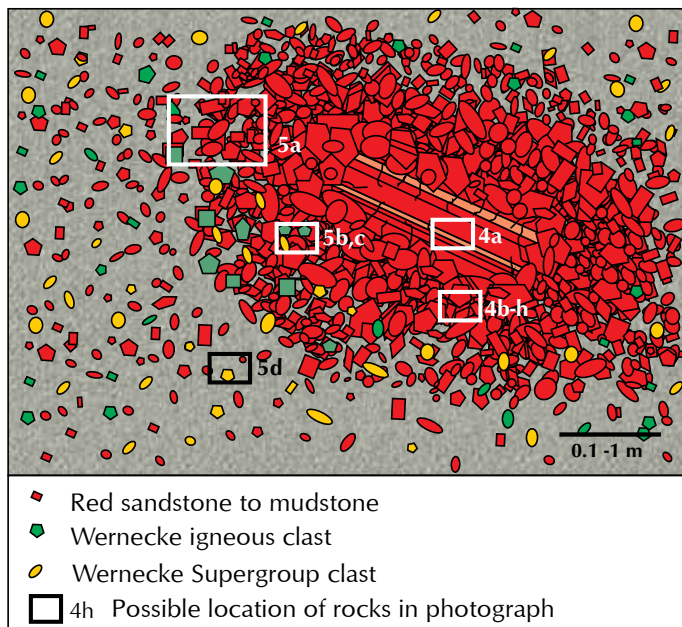


Figure 7. Conceptual diagram of how the different end-members and intermediate varieties of red sandstone to mudstone are present within the Wernecke Breccia. The layered clasts devoid of soft sediment deformation features are surrounded by a carapace of tightly packed clasts. This carapace is surrounded by a gradational boundary with typical Wernecke Breccia in which Wernecke igneous clasts and Wernecke Supergroup clasts occur. The positions of photographs in Fig. 4 are indicated.

The irregular shapes and matrix-forming nature of the green mudstone and its relation to the Wernecke Supergroup clasts suggest that this material was entirely unconsolidated and flowed through the breccia zone as liquid mud at the time of Wernecke Breccia formation. After the mud came to rest, it became lithified within the interstices among breccia clasts and was affected by hydrothermal alteration.

DISCUSSION

THE SIGNIFICANCE OF SOFT SEDIMENT DEFORMATION

The incorporation of soft sediment into zones of Wernecke Breccia poses a complex geological problem. Hunt *et al.*, (2011) addressed the depth at which mineralization in Wernecke Breccia took place. Using a combination of new fluid inclusion data and Delaney's (1981) estimates for stratigraphic thickness, Hunt *et al.* (2011) proposed that the hydrothermal activity within various zones of Wernecke Breccia occurred at pressures of 0.4-2.4 kbar, corresponding to depths of 1.2-7.2 km. However, stratigraphic thickness cannot be used as an estimate of depth because the Wernecke Supergroup was deformed and overthrust by Bonnetia prior to the formation of the Wernecke Breccia (Thorkelson *et al.*, 2001a; Furlanetto *et al.*, 2013). Consequently, two other estimates of depth derived from data in Hunt *et al.* (2011)

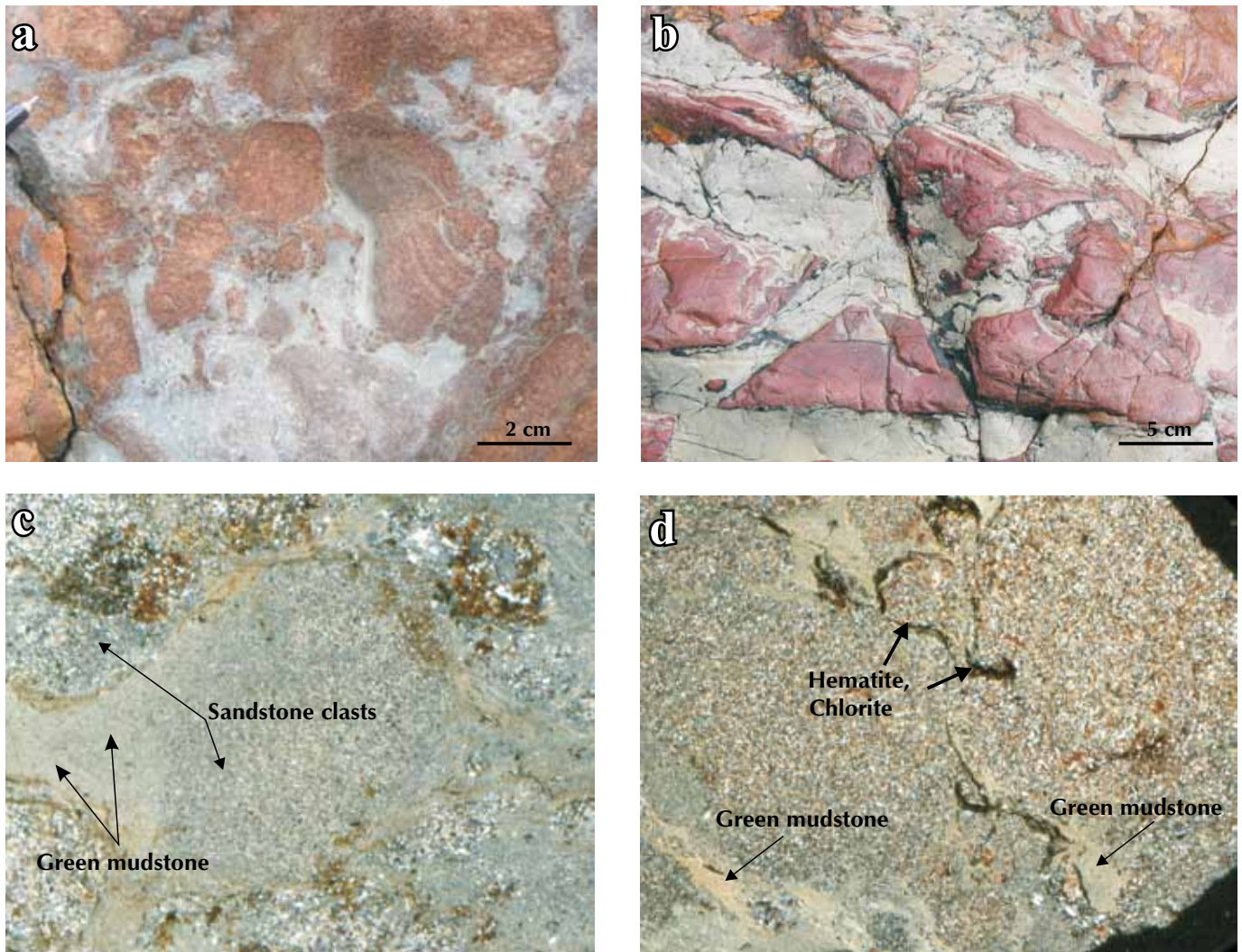


Figure 8. Meso-scale (a,b) and micro-scale (c,d) structures and field relations of the green mudstone. (a) Green mudstone encapsulating clasts of Wernecke Supergroup; (b) green mudstone encapsulating clasts of red mudstone; (c) sandstone clast rimmed by green mudstone; image in crossed polars; (d) green mudstone is locally associated with hematite and chlorite; image in crossed polars.

are herein considered more reliable. One estimate, based on the fluid inclusion studies alone, ranges from 5.7-11.3 km. The other estimate equates equilibration temperatures from stable isotopes to depth based on an assumed geothermal gradient. At equilibration temperatures of (250-295°C) and a geothermal gradient of 25-30°C/km, calculated depths range from 7-9 km. Note that these estimates are for different breccia zones in the Wernecke Mountains whereas the breccia in our study is located in the Ogilvie Mountains and has not been thoroughly evaluated for pressures and temperatures. However, the metasomatic mineral assemblage of the

Wernecke breccia in the Ogilvie Mountains includes chlorite, mica and feldspar and lacks clay or other low metamorphic-grade minerals. Hence the Wernecke Breccia zones that host the soft sediment materials were likely positioned at several km depth.

The only plausible source of the unconsolidated green mudstone is a water-saturated sedimentary deposit on the surface of the Earth. The source of the red soft sediments is likely to have been a partially lithified sedimentary succession that had been buried to shallow depths. Mixing of the Wernecke Supergroup and Bonnetia clasts with the non-lithified materials must have occurred rapidly,

allowing sediment from the surface and near-surface environments to mix and come to rest at depths of several km beneath the surface. The structure of the Proterozoic crust prior to brecciation is depicted in Fig. 9 based on the foregoing descriptions of the sedimentary rocks. If water were present above the green mudstone, in the form of a lake or sea, it probably would have flowed down into the breccia zones along with the unlithified sediments. Phreatic activity may have accompanied breaching of the surface by the Wernecke Breccia.

VERTICAL TRANSPORT

Considerable downward transport of the igneous clasts derived from Bonnetia to within zones of Wernecke Breccia is required (Furlanetto *et al.*, 2013). Nielsen *et al.* (2013) estimated the most likely transport distance of the igneous clasts to be 1-2 km. That estimate was based on the perceived need to minimize the transport distance by deriving the clasts from a short distance above the surface of obduction, and by regarding the current mountain peaks to lie a nominal distance of 1 km below the obduction surface (Nielsen *et al.*, 2013). The existence of lithologies with soft sediment textures within the Wernecke Breccia that were sourced from the surface corroborates the interpretation of overall downward transport of clasts. A surface origin would require that the unconsolidated sediments descended through the entire Bonnetia nappe, which locally may have been up to 9 km thick (Nielsen *et al.*, 2013). These considerations are consistent with foundering of the unlithified sediments for several km (possibly >9 km) into the Earth's crust.

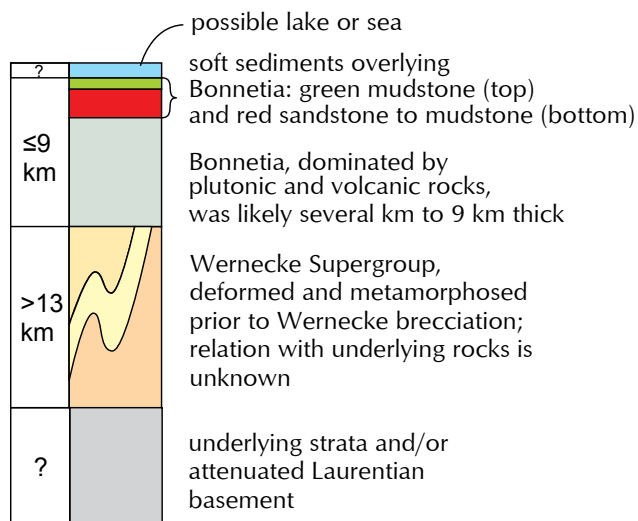


Figure 9. The crustal column of Mesoproterozoic Yukon prior to Wernecke Breccia formation at 1.60 Ga (not to scale).

REFINEMENT OF A GEOLOGICAL MODEL

The foregoing model accords with a depiction of hydrothermal breccia formation offered by Laznicka and Edwards (1979), utilized by Hitzman *et al.* (1992) and developed by Thorkelson *et al.* (2001a), Laughton *et al.*, (2005), Furlanetto *et al.* (2013) and Nielsen *et al.* (2013). In particular, the model involves the ascent of hydrothermal solutions from depth, fragmentation of country rock, breaching of the surface, development of open space by some combination of dilation and expulsion of rock at the surface, and descent of clasts for thousands of metres (Fig. 10). The recognition of surface-derived unconsolidated material within Wernecke Breccia underscores the need for breaching of the surface. As such, the Earth's surface in this region would have been ruptured by numerous large hydrothermal vents, some or all of which may have been under water. The vents are envisaged as large openings that existed long enough for wall-rock and water-saturated surface materials to collapse, founder, mix with hydrothermal solutions and settle to depths of several km.

CONCLUSIONS

Clasts in Wernecke Breccia showing soft sediment deformation were noted by Lane (1990). Our investigation corroborates Lane's findings and has led to the identification of two sedimentary lithologies with soft sediment textures. One is red mudstone to pink sandstone and the other is green mudstone. The soft sediment textures indicate derivation from at or near the Earth's surface. The red lithology appears to have been consolidated but unlithified whereas the green lithology appears to have been unconsolidated. The unlithified sediments flowed downward into zones of Wernecke Breccia in response to breaching of the surface. The soft sediments are estimated to have descended to depths of at least several km.

We regard the most likely source for the soft sediments to have been a weakly to non-lithified succession that was deposited on top of the obducted terrane Bonnetia shortly before the formation of Wernecke Breccia. The soft sediments mixed with other clasts, came to rest at depth and became lithified. The terrane and its overlying succession were entirely eroded in the Mesoproterozoic (Furlanetto *et al.*, 2013).

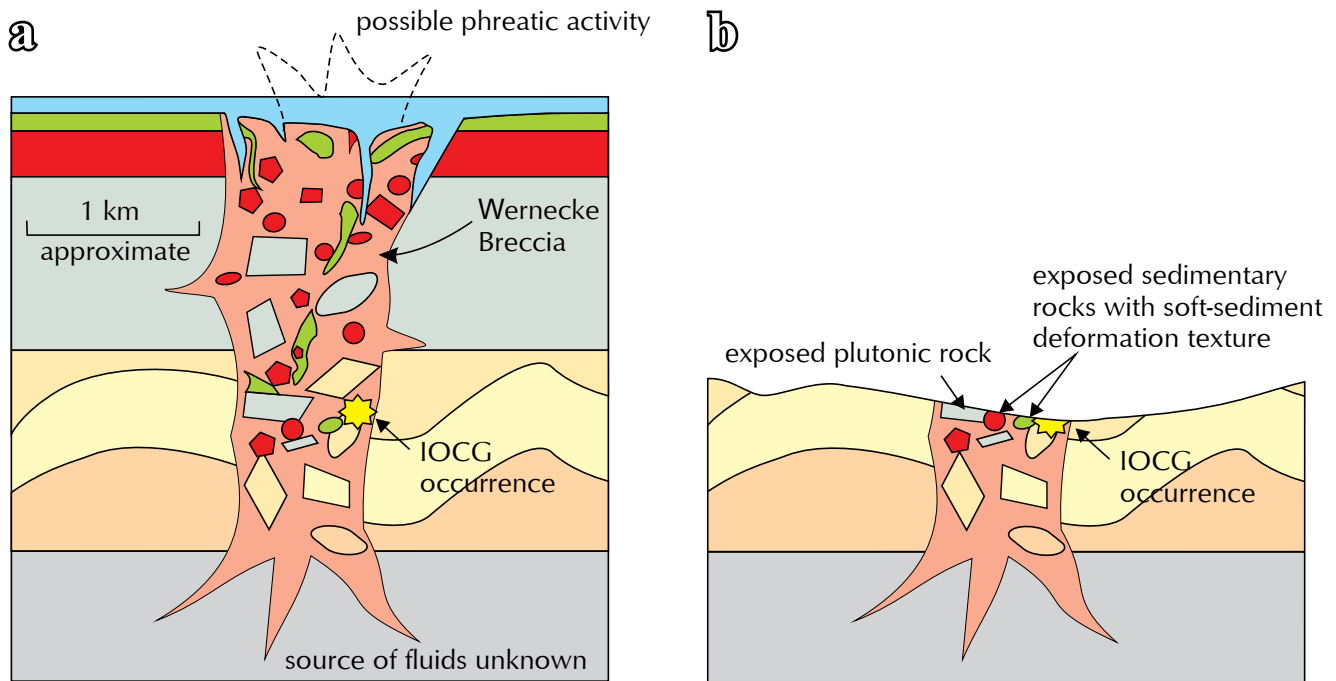


Figure 10. Crustal cross sections at 1.60 Ga (a) and present day (b). During hydrothermal activity clasts and masses of fluidized mud foundered into the breccia zone, mixed with other clasts, and came to rest alongside the Wernecke Supergroup. Water from a lake or sea may also have flowed down into the breccia zone. The hydrothermal event may have been accompanied by phreatic activity. Erosion subsequently removed the sediments, Bonnetia and the upper parts of the Wernecke Supergroup and Wernecke Breccia. IOCG = iron oxide copper gold.

ACKNOWLEDGEMENTS

Funding was provided by NSERC grants to DJT. The Yukon Geological Survey provided logistical support in 2012. Jim Mortensen provided input on an earlier draft. Grant Abbott and Patrick Sack provided input that led to significant improvements.

REFERENCES

- Bell, R.T., 1986. Megabreccias in northeastern Wernecke Mountains, Yukon Territory. *In: Current Research, Part A, Geological Survey of Canada, Paper 1986-1A*, p. 375-384.
- Delaney, G.D., 1981. The Mid-Proterozoic Wernecke Supergroup, Wernecke Mountains, Yukon Territory: Proterozoic basins of Canada. Geological Survey of Canada, Paper 81-10 p. 1-23.
- Furlanetto, F., Thorkelson, D., Davis, W.J., Gibson, H.D., Rainbird, R.H. and Marshall, D.D., 2009. Preliminary results of detrital zircon geochronology, Wernecke Supergroup, Yukon. *In: Yukon Exploration and Geology 2008*, Weston, L.H., Blackburn, L.R., Lewis, L.L. (eds.), Yukon Geological Survey, p. 125-135.
- Furlanetto, F., Thorkelson, D., Gibson, H.D., Marshall, D.D., Rainbird, R.H., Davis, W.J., Crowley, J.L. and Vervoort, J.D., 2013. Late Proterozoic terrane accretion in northwestern Canada and the case for circum-Columbian orogenesis: Precambrian Research, vol. 224, p. 512-528.
- Furlanetto, F., Thorkelson, D., Rainbird, R., Davis, W., Gibson, D. and Marshall, D., 2014. Geological Society of America General Meeting Vancouver, British Columbia, Canada.

- Hitzman, M.W., Oreskes, N. and Einaudi, M.T., 1992. Geological characteristics and tectonic setting of Proterozoic Iron-Oxide (Cu-U-Au-Ree) deposits. *Precambrian Research*, vol. 58, p. 241-287.
- Hunt, J.A., Laughton, J.R., Brideau, M.-A., Thorkelson, D.J., Brookes, M.L. and Baker, T., 2002. New mapping around the Slab iron oxide-copper-gold occurrence, Wernecke Mountains. *In: Yukon Exploration and Geology 2001*, D.S. Emond, L.H. Weston and L.L. Lewis (eds.), Exploration and Geological Services Division, Yukon Region, Indian and Northern Affairs Canada, p. 125-138.
- Hunt, J.A., Baker, T., Cleverley, J., Davidson, G.J., Fallick, A.E., Thorkelson, D.J. and Harris, A., 2011. Fluid inclusion and stable isotope constraints on the origin of Wernecke Breccia and associated iron oxide-copper-gold mineralization, Yukon. *Canadian Journal of Earth Sciences*, vol. 48, p. 1425-1445.
- Lane, R.A., 1990. Geologic setting and Petrology of the Proterozoic Ogilvie Mountain Breccia of the Coal Creek Inlier, Southern Ogilvie Mountains, Northern Yukon. M.Sc. Thesis, University of British Columbia.
- Laughton, J.R., Thorkelson, D.J., Brideau, M.-A., Hunt, J.A. and Marshall, D.D., 2005. Early Proterozoic orogeny and exhumation of Wernecke Supergroup revealed by vent facies of Wernecke Breccia, Yukon, Canada. *Canadian Journal of Earth Sciences*, vol. 42, p. 1033-1044.
- Laznicka, P. and Edwards, R.J., 1979. Dolores Creek, Yukon – A disseminated copper mineralization in sodic metasomatites. *Economic Geology*, vol. 74, p. 1352-1370.
- Laznicka, P. and Gaboury, D., 1988. Wernecke Breccias and Fe, Cu, U mineralization: Quartet Mountain-Igor area (NTS 106E). *Yukon Geology* vol. 2, Exploration and Geological Services Division, Indian and Northern Affairs Canada, p. 44-50.
- Medig, K.P.R., Thorkelson, D.J. and Dunlop, R.L., 2010. The Proterozoic Pinguicula Group: Stratigraphy, contact relationships and possible correlations. *In: Yukon Exploration and Geology 2009*, K.E. MacFarlane, L.H. Weston and L.R. Blackburn (eds.), Yukon Geological Survey, p. 265-278.
- Mercier, E. 1989. Evenements Tectoniques d'origines compressive dans le Proterozoique du nord de la Cordillere canadienne (montagnes Ogilvie, Yukon). *Canadian Journal of Earth Sciences*, vol. 26, p. 199-205.
- Nielsen, A.B., Thorkelson, D.J., Gibson, H.D. and Marshall, D.D., 2013. The Wernecke igneous clasts in Yukon, Canada: Fragments of the Paleoproterozoic volcanic arc terrane Bonnetia. *Precambrian Research*, vol. 238, p. 78-92.
- Thompson, R.I., Roots, C.F. and Mustard, P.S., 1992. Geology of Dawson map area (116B, C) (northeast of Tintina Trench). Geological Survey of Canada, Open File 2849, 13 sheets, scale 1:50 000.
- Thorkelson, D.J., Abbott, J.G., Mortensen, J.K., Creaser, R.A., Villeneuve, M.E., McNicoll, V.J. and Layer, P.W., 2005. Early and Middle Proterozoic evolution of Yukon, Canada. *Canadian Journal of Earth Sciences*, vol. 42, p. 1045-1071.
- Thorkelson, D.J., Mortensen, J.K., Davidson, G.J., Creaser, R.A., Perez, W.A. and Abbott, G.J., 2001a. Early Mesoproterozoic intrusive breccias in Yukon, Canada: The role of hydrothermal systems in reconstructions of North America and Australia. *Precambrian Research*, vol. 111, p. 31-55.
- Thorkelson, D.J., Mortensen, J.K., Creaser, R.A., Davidson, G.J. and Abbott, J.G., 2001b. Early Proterozoic magmatism in Yukon, Canada: constraints on the evolution of northwestern Laurentia. *Canadian Journal of Earth Sciences*, vol. 38, p. 1479-1494.
- Thorkelson, D.J., and Wallace, C.A., 1998. Geological map of 'Dolores Creek' area, Wernecke Mountains, Yukon (106C/14). Indian and Northern Affairs Canada, Exploration and Geological Services Division, Geoscience Map 1998-9, scale 1:50 000.
- Yukon MINFILE 2014 – A database of mineral occurrences. Yukon Geological Survey, <http://www.geology.gov.yk.ca/databases_gis.html>.

Fault tectonics in the Rapid depression of the Yukon North Slope (Canadian Arctic) - Summary of preliminary results

W. von Gosen¹

Geozentrum Nordbayern, Krustendynamik, Friedrich-Alexander-Universität Erlangen-Nürnberg

K. Piepjohn

Bundesanstalt für Geowissenschaften und Rohstoffe (BGR), Geologie der Energierohstoffe, Polargeologie

D.C. Murphy

Yukon Geological Survey

C. Brandes

Institut für Geologie, Leibniz Universität Hannover

W.C. McClelland

Department of Earth and Environmental Sciences, University of Iowa

M. Colpron

Yukon Geological Survey

von Gosen, W., Piepjohn, K., Murphy, D.C., Brandes, C., McClelland, W.C. and Colpron, M., 2015. Fault tectonics in the Rapid depression of the Yukon North Slope (Canadian Arctic) – Summary of preliminary results. *In: Yukon Exploration and Geology 2014*, K.E. MacFarlane, M.G. Nordling and P.J. Sack (eds.), Yukon Geological Survey, p. 157-165.

ABSTRACT

Mesozoic to Tertiary rocks in the Rapid depression on the Yukon North Slope are dissected by a N-NNE striking fault array. Two phases of Tertiary deformation are recorded across the Rapid depression east of the Barn fault: D_1 is characterized by faults with either sinistral or dextral strike-slip displacement and overall ~W-E to NW-SE contraction; D_2 faults developed under a regime of ~W-E-oriented contraction and N-S extension. The southern segment of the Barn fault is interpreted as an oblique dextral fault. The structural style is inconsistent with the propagation of a large-scale strike-slip fault zone such as the Kaltag fault through the Rapid depression, as previously suggested, but rather may indicate reactivation of older structural heterogeneity in the subsurface.

¹werner.von.gosen@fau.de

INTRODUCTION

In northernmost Yukon (Canadian Arctic), south of the Beaufort Sea, there is a wide area known as the Yukon North Slope. The Rapid depression (Fig. 1), in the eastern part of the Yukon North Slope, is a broad trough

predominantly underlain by Mesozoic sedimentary rocks. It is flanked to the west by structural culminations of the Barn and Romanzof uplifts and to the east by the Aklavik arch complex (including Rat, Scho, White and Cache Creek uplifts; Fig. 1; Norris, 1997); Paleozoic and locally older rocks are exposed in both regions. Mesozoic rocks

of the Rapid depression straddle the boundary between the Paleozoic North American continental margin in the east and Arctic Alaska terrane in the west. Mesozoic and locally Tertiary rocks in the depression are cut by a swarm of N~NNE striking faults which occur in a north-south corridor ~60 km wide (Rapid fault array; see Norris and Yorath, 1981; Norris, 1997).

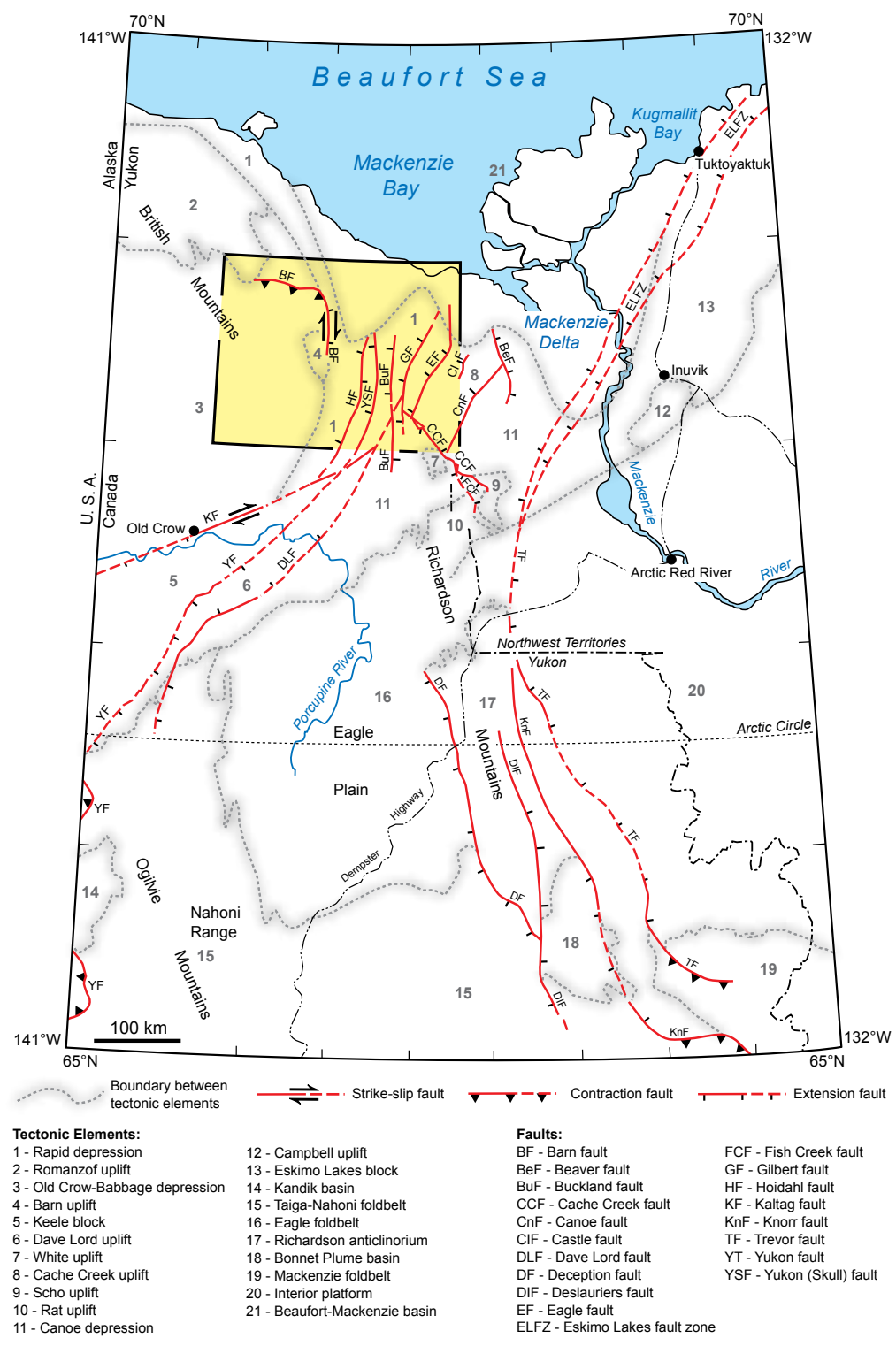


Figure 1. Tectonic elements and main faults in northern Yukon and adjacent Northwest Territories, Canada (map modified from Norris, 1997). Frame with yellow fill shows location of the map of the study area (Fig. 3). Note that the extension of the Tertiary, strike-slip Kaltag fault into Yukon is called into question here and in Lane (1992).

Structural information from the depression is critical to reconstructing the nature of interactions between Arctic Alaska and the northwestern North American margin in late Mesozoic and Tertiary. Furthermore, these data might give insight into the plate tectonic significance of the faults and related structures and answer the question of whether the tectonic development in the Rapid depression can be geometrically and kinematically linked to the Eurekan deformation in the Canadian Arctic Archipelago, North Greenland and Svalbard (compare, for example, Balkwill, 1978; Kerr, 1981; Tessensohn and Piepjohn, 2000).

PREVIOUS WORK

The Rapid depression has been inferred to be the locus of the continuation of the Kaltag fault, a major ENE-WSW dextral strike-slip fault defined in western and central Alaska (cf., Norris, 1976, 1981, 1997; Fig. 1). Although the Kaltag fault has been included in Cenozoic plate tectonic

reconstructions of the Arctic (e.g., Jones, 1980; McWhae, 1986), it appears restricted to the western and central parts of Alaska (e.g., Grantz, 1966; Patton and Hoare, 1968; Patton 1973; Fig. 2). Lane (1992) argued against its along-strike continuation into northern Yukon.

Deformation in the Rapid depression has been characterized as a Paleocene-Eocene fold-and-thrust belt, lacking regionally important strike-slip faults (Lane, 1988). This belt continues northward into major fold structures of the arcuate Beaufort fold-and-thrust belt offshore in the southern Beaufort Sea (e.g., Lane, 1998; Fig. 2). Several interpretations of seismic lines from these offshore areas have shown that the arcuate belt was mainly formed during the Paleocene-Eocene but youngs towards its outboard northern and eastern parts (compare, for example, Dietrich *et al.*, 1989; Lane and Dietrich, 1991; Lane, 1998, 2002; Dixon *et al.*, 2001; Dinkelman *et al.*, 2008; Helwig *et al.*, 2011).

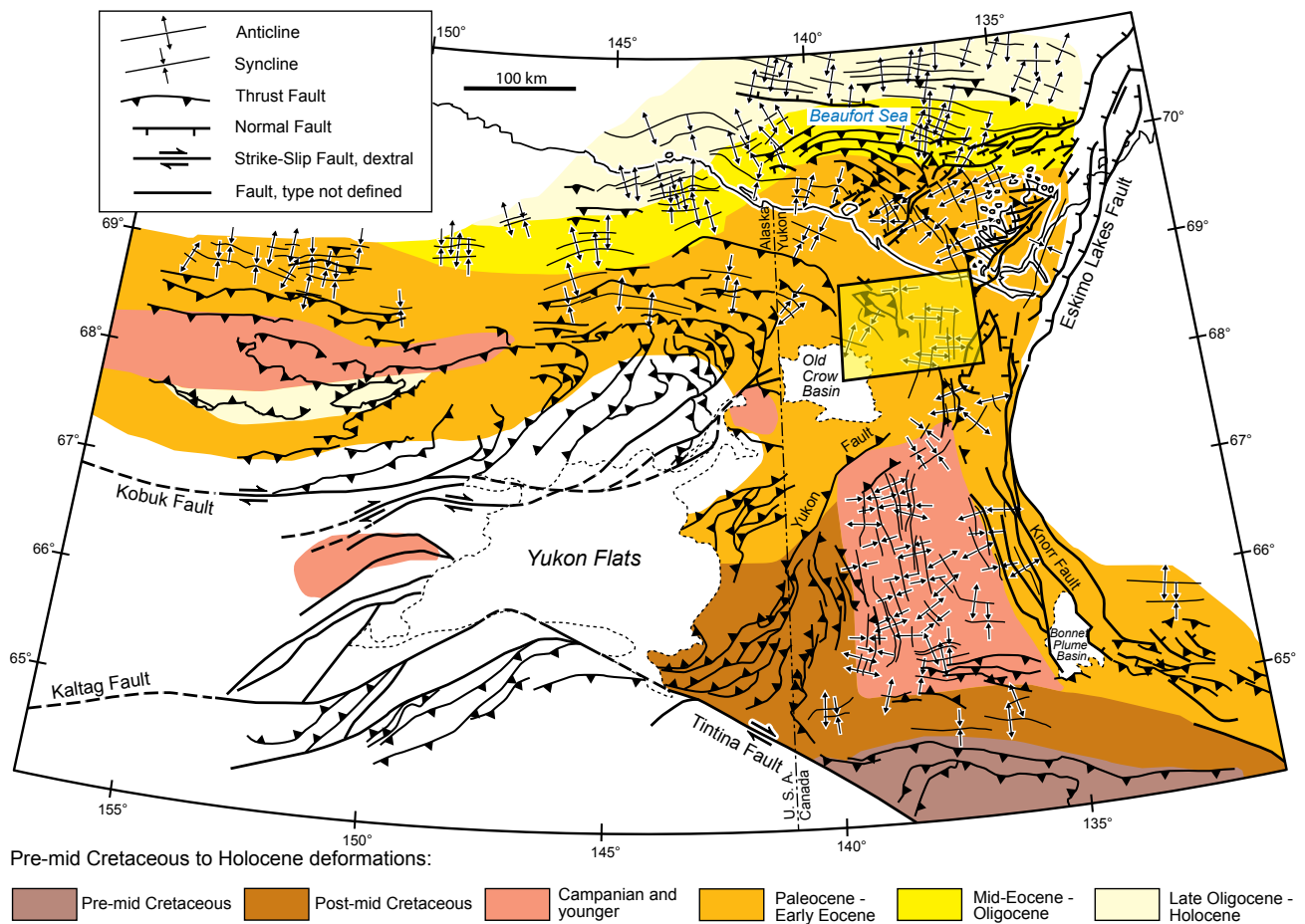


Figure 2. Simplified tectonic map of northeastern Alaska, northern Yukon, and adjacent Northwest Territories (Canada) showing the trends of major Late Cretaceous-Tertiary structures and approximate ages of pre-mid Cretaceous to Holocene deformations (modified from Lane, 1998, 2002). Frame with yellow fill shows location of map in Figure 3.

GEOLOGIC SETTING OF THE RAPID DEPRESSION

The Barn uplift, partly bounding the western edge of the Rapid depression (Figs. 1 and 3), consists of Neoproterozoic to lower Paleozoic (meta-)clastic and carbonate rocks intruded by granitic plutons of Late Devonian age (Lane, 2007), all part of the Arctic Alaska terrane. The pre-Carboniferous succession is folded and dissected by several east-directed thrust faults (Cecile, 1988; Cecile and Lane, 1991; Dyke, 1997). The first phase of deformation in the core of the Barn uplift has been interpreted as post-Late Silurian to pre-Early Carboniferous

(Cecile, 1988) or Middle-Late Devonian (Dyke, 1997); it is inferred to be related either to the Ellesmerian Orogeny or to the Romanzof Orogeny (Lane, 2007). The Barn uplift is bounded on the east by the Barn fault. In the north, west, and south, the rocks in the uplift are unconformably overlain by Carboniferous and younger clastic deposits (Fig. 3).

The Rapid depression and areas surrounding the Barn uplift are underlain by Jurassic to Upper Cretaceous, and locally Tertiary clastic deposits (Fig. 3). The eastern margin of the Rapid depression, in the Richardson Mountains, consists of upper Paleozoic deposits overlain by Mesozoic rocks in the White and Cache Creek uplifts (Figs. 1 and 3).

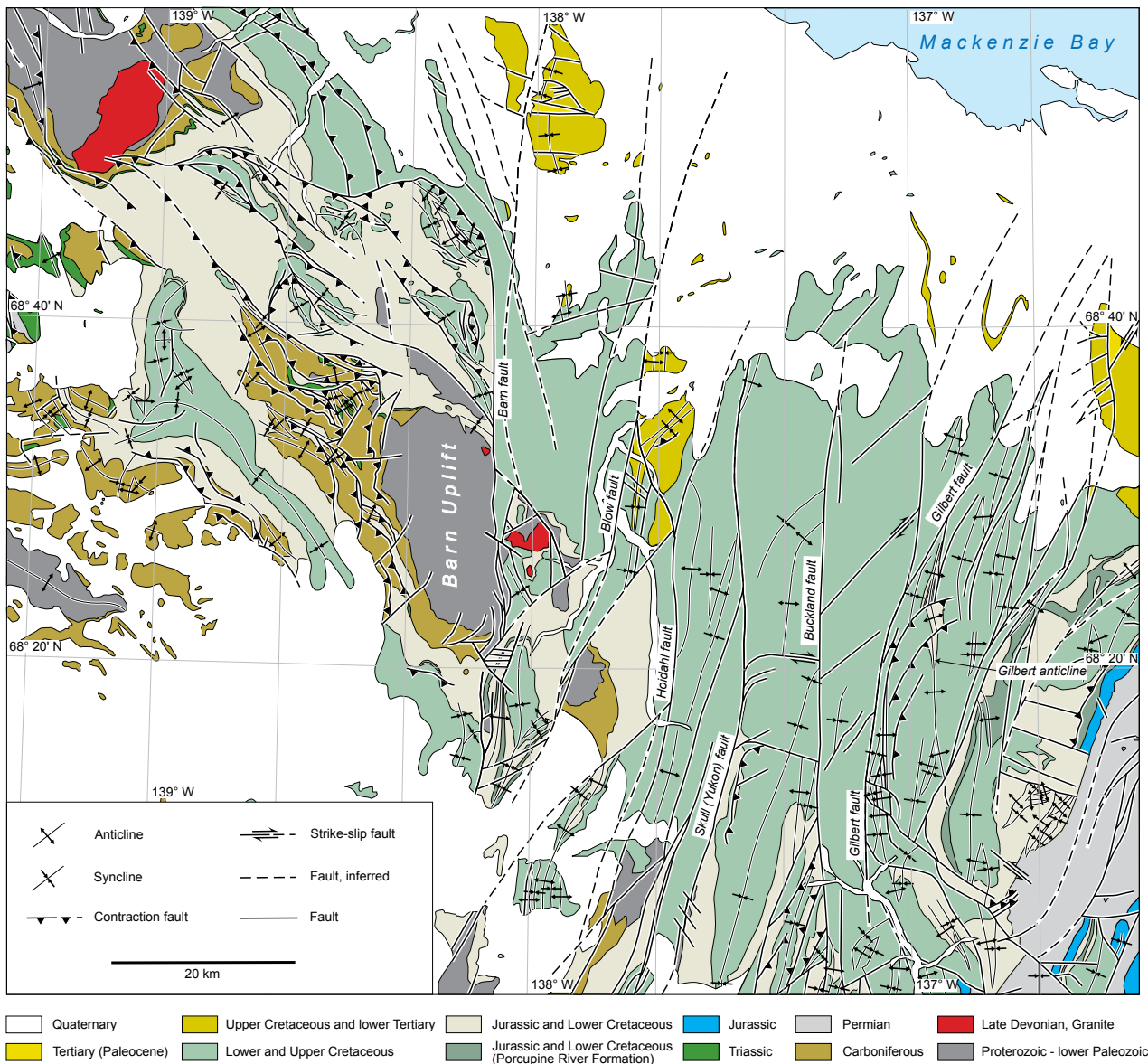


Figure 3. Simplified geological map of the Rapid depression and adjacent areas (north Yukon, Canada) modified from Norris (1981). For location see Figures 1 and 2.

FAULTING IN THE RAPID DEPRESSION

From west to east the major faults in the Rapid depression are as follows (Norris, 1981, 1997; Fig. 3):

(1) The N striking Barn fault separates the Barn uplift to the west from Cretaceous rocks of the Rapid depression to the east. Its northern continuation cuts through Cretaceous rocks and, farther northwards, turns to the northwest and west. To the east of the southern segment of the Barn uplift, two faults, striking NW and NE, separate pre-Mesozoic rocks from Jurassic and Cretaceous deposits.

(2) The NNE striking Blow fault cuts Jurassic to Tertiary rocks and possibly older rock of the Arctic Alaska terrane in the south.

(3) The NNE striking Hoidahl fault (new name, replacing the name 'Kaltag fault' on the map of Norris, 1981) affects Cretaceous rocks in its central and northern segments but displaces lower Paleozoic and/or older rocks of Arctic Alaska terrane in the south. Norris (1981) interpreted this fault as the northeast extension of the Kaltag fault from Alaska; however, following Lane (1992) this correlation appears unlikely and therefore the name Hoidahl fault is proposed here for this structure.

(4) The NNE to N striking Skull (Yukon) fault cuts mostly Cretaceous rocks and in the south also cuts lower Paleozoic rocks of Arctic Alaska terrane. East and southeast of Old Crow, the Yukon fault strikes NE (Fig. 1; Norris, 1981) and also affects Proterozoic, Cambrian to Devonian, and upper Paleozoic rocks of North American affinity. From there, it continues farther south with a NNE strike (Journey *et al.*, 2000).

(5) The N striking Buckland fault cuts Cretaceous rocks in the north and Jurassic rocks in the south.

(6) In the north, the Gilbert fault has a NNE strike and cuts Cretaceous rocks; its strike changes to a N strike in the south. Farther south, it ends directly north of NNE trending folds in Cretaceous rocks (compare Norris, 1981; present Fig. 3). The Gilbert fault is accompanied by several faults and folds to the east.

Most faults in the Rapid depression have a N to NNE strike. The curved Barn fault is an exception (Fig. 3). Additional NW striking reverse faults, affecting Carboniferous but mostly Jurassic and Cretaceous rocks, occur west and north of the Barn uplift (Fig. 3; Norris, 1981). All faults in the region cut Cretaceous rocks and are therefore Cretaceous or younger.

STRUCTURAL OBSERVATIONS RELEVANT TO FAULT KINEMATICS

The major faults and their damage zones are rarely exposed. This study examined exposures as close to the traces of major faults as possible in order to interpret the fault kinematics. Field observations were then combined with major folds and faults mapped by Norris (1981) to synthesize the overall geometries and relations between the sense of fault displacement and adjacent structures. This synthesis led to a reinterpretation of the sense of displacement for some of these faults compared to those inferred by Norris (1981).

Structural measurements related to D_1 deformation supported an interpretation of kinematics at every study location. The shortening orientations near the faults were used to interpret their sense of displacement during first-stage deformation. Shortening orientations during D_1 deformation for each location were determined based individually or collectively on orientations perpendicular to the maxima of B_1 fold axes, δ_1 intersection lineations, and/or girdles through poles of bedding planes.

D_1 DEFORMATION

All Jurassic to Tertiary clastic sedimentary sequences are affected by a D_1 deformation. Open, N to NE trending F_1 folds measure anywhere from a decimetre to more than 100 m and are typically symmetrical, chevron-like structures; however, folds can display either ~E or W vergence. The large Gilbert anticline in the eastern part of the Rapid depression is a good example of an F_1 structure with a N trending axis (Fig. 3). The folds are accompanied by S_1 fracture cleavage with spatially variable intensity. Tertiary sandstones east of the Blow fault display an incipient S_1 fracture cleavage. These rocks are affected by a map-scale, broad, open F_1 syncline with a ~NE trending axis (Fig. 3). Local reverse faults in the Mesozoic succession represent accommodation faults related to F_1 folding. The general picture suggests a ~E to SE contraction direction during the D_1 deformation east of the Barn fault.

In this study's interpretation, the southern, N striking segment of the Barn fault represents an oblique dextral fault with an east-directed reverse component. This segment has been interpreted as a right-lateral fault with 10 km of displacement (Norris, 1997, p. 56) and a minimum vertical separation of approximately 300 m (Dyke, 1997, p. 341). In its northern NW to W striking segment, the Barn fault was interpreted as a thrust fault (Norris, 1981, 1997). This reverse sense is also supported

by the data collected in this study and the NW strike of reverse faults along this segment of the hanging wall.

The Blow fault is interpreted as a sinistral strike-slip fault based on the NW-SE contraction related to development of a F_1 syncline in Tertiary clastic rocks to the east. However, based on the stratigraphic successions preserved on either side of the fault, Young (1974, p. 295) reported that the west side was displaced upward relative to the east side during three main episodes of Early Cretaceous deformation.

For the Hoidahl and Skull (Yukon) faults in the east a sinistral displacement is proposed. On the latter, 5 km of left-lateral separation was reported by Norris (1997, p. 57).

The Gilbert fault, in the eastern side of the Rapid depression, can be interpreted as a dextral strike-slip fault with related F_1 folding to the east (Gilbert anticline). There, the axes of spatially associated folds are obliquely oriented at a small angle with respect to the Gilbert fault and other parallel dextral fault lines (Fig. 3). To the south, the N-S oriented branch of the Gilbert fault is interpreted as a reverse fault, possibly with a dextral component. The southern termination of this fault is within Cretaceous clastic rocks.

It should be emphasized that all faults with lateral displacements during this first stage of deformation are not interpreted as pure strike-slip faults. It is more reasonable to suggest that displacements were accompanied by varying reverse components during fold-and-thrust belt deformation.

The overall shortening, shown by the open F_1 folding and partly continuous trends of folds in the clastic succession, argues for a detachment fault (or faults) in the subsurface. However, the depth, extent, and geometry of such a horizon (or horizons) remain unclear.

D₂ DEFORMATION

In the outcrops studied, the D_1 structural elements are crosscut by sets of younger brittle shear and fault planes. Their senses of shear and displacement are shown by slickensides and steps. The precise time difference to D_1 structures, however, is unclear. For the measured D_2 structural elements, the kinematic P (shortening) and T (extension) axes (Marrett and Allmendinger, 1990) and the fault plane solutions were calculated with the program FaultKin (version 6.5.0) of Allmendinger (2013).

D_2 deformation is best exemplified in the area of the Gilbert anticline and Gilbert fault (Fig. 3). There, the N trending F_1 Gilbert anticline is cross cut and displaced along NE striking and ~NW directed reverse faults which curve into a southern N-S oriented branch of either the Gilbert fault or a parallel fault (Fig. 3). A NW verging F_2 fold structure, which overprints S_1 cleavage planes and is floored by a detachment, was observed in the hanging wall of one of these reverse faults. Faults and shear planes with similar orientations and calculated P axes were also observed in the hinge zone of the Gilbert anticline, suggesting NNW-SSE contraction across this region during D_2 deformation.

Overall, the calculated P axes and fault plane solutions indicate a tectonic regime with ~W-E-oriented contraction and N-S extension during D_2 in the Rapid depression, east of the Barn fault. This sense of contraction caused a reactivation of older (D_1) strike-slip faults with the same or opposite strike-slip motion relative to the previous displacement. An instructive example is the Gilbert fault and areas to the east (Fig. 3). This study's data from the Gilbert fault have shown that after its first dextral stage with related folding (see above), the sense of displacement changed to sinistral strike-slip along the N trending fault segment and northward. In the south, however, the fault ends in folded Cretaceous rocks with ~NE trending fold axes. This observation suggests that displacement, during both D_1 and D_2 , transferred onto another fault, thereby avoiding the sedimentary succession at the south end of the Gilbert fault. This argues for strike-slip faulting in limited segments, probably caused by inherited older and reactivated structures in the subsurface (see below).

All other faults to the west of the Gilbert fault are interpreted as sinistral strike-slip faults, combined with a reverse component, and partly changing into reverse faults along strike during D_2 . The sense of displacement along the Hoidahl fault, however, remains unclear. In the west, the N-S oriented section of the Barn fault seems to have remained active as an oblique, dextral fault.

INTERPRETATIONS AND CONCLUSIONS

The structural geometry and kinematic evolution reported here provide argument against a simple high-level fold-and-thrust belt within the Rapid depression. Fold axes that are oblique with respect to many fault lines, suggest that folding occurred concurrently with strike-slip movements.

The entire picture, however, does not support a large-scale, uniform, strike-slip dominated regime. If it were an overall regime of strike-slip tectonics, a single sense of shear, either dextral or sinistral, would be expected. Instead, this study interprets two stages of fault tectonics with different sense of displacements and a more complex tectonic history during the early Cenozoic. There is no evidence for a through-going and significant Tertiary strike-slip fault, such as the Kaltag fault, that could be interpreted as an intracontinental displacement zone of plate tectonic significance.

The precise age of the clastic Tertiary deposits in the Rapid depression, affected by both stages of deformation, is unclear. It can only be stated that they are Paleocene. It is assumed that the first-stage deformation (D_1) is Paleocene or Eocene in age (see also Lane, 1988, 1998, 2002; compare with Fig. 2) whereas the second stage (D_2) might be Eocene and/or younger. Therefore, both phases of deformation seem to have taken place during the time of Eureka deformation in the Canadian Arctic Archipelago (e.g., Balkwill, 1978; Tessensohn and Piepjohn, 2000; von Gosen *et al.*, 2012; Piepjohn *et al.*, 2013) and postdate the Cretaceous opening of the Amerasia Basin.

It seems reasonable that strike-slip faulting and their present surface expressions were caused by structural heterogeneities in the subsurface. As the area under discussion represents the western marginal part of the North American craton to the east, and has been affected by pre-Mesozoic (Monger and Price, 2002) or younger (O'Leary *et al.*, 1995; Lane, 1998) extension and rifting, older and rift-related (normal) faults could have been reactivated during Tertiary compressional faulting and folding. They might have led to the development of the observed strike-slip faults. Reverse faulting and parallel dextral and sinistral faults in the Rapid depression during D_1 deformation support this interpretation.

The Eskimo Lakes fault zone is a possible candidate for a structure of plate tectonic significance (Figs. 1 and 2). It continues offshore towards the northeast into the Beaufort Sea and possibly defined the former margin of the North American craton. Arcuate bending of the Tertiary structures occurs to the west and northwest of this fault zone. This might suggest that faulting and folding were contemporaneous events and the Eskimo Lakes fault zone accommodated crustal shortening by dextral strike-slip. Bending of the structures in the northeast Alaskan area, however, might have been accommodated by the dextral Kobuk fault to the south (Fig. 2) and not the Kaltag fault.

ACKNOWLEDGEMENTS

Field work in north Yukon (Arctic Canada) was carried out during the CASE 15-Expedition of the Federal Institute for Geosciences and Natural Resources (BGR, Hannover, Germany) led by M. Colpron (Yukon Geological Survey (YGS), Whitehorse, Canada) and K. Piepjohn (BGR, Hannover, Germany). C. Brandes, W. von Gosen, and W. C. McClelland are grateful to this institution for the invitation to participate in this expedition. W. von Gosen gratefully acknowledges financial supports for pre-expedition travel from the Bavarian Research Alliance (Munich, Germany) and for the expedition project from the German Research Foundation (DFG, proj. Go 405/11-1). Support for W.C. McClelland was provided by National Science Foundation (NSF) grants EAR-0948359 and EAR-1049368. Finally, many thanks to David Moynihan (YGS) for critically reviewing an earlier draft of this manuscript.

REFERENCES

- Allmendinger, R.W., 2013. FaultKin (version 6.5.0) for Mac OS X and Windows 7/XP. Department of Geological Sciences, Cornell University, Ithaca, New York.
- Balkwill, H.R., 1978. Evolution of the Sverdrup Basin, Arctic Canada. *American Association of Petroleum Geologists Bulletin*, vol. 62, p. 1004-1028.
- Cecile, M.P., 1988. Corridor traverse through Barn Mountains, northernmost Yukon. *In: Current Research, Part D. Geological Survey of Canada, Paper 88-1D*, p. 99-103.
- Cecile, M.P. and Lane, L.S., 1991. Geology of the Barn Uplift, northern Yukon. Geological Survey of Canada, Open File 2342, 1:50 000 scale.
- Dietrich, J.R., Coffin, K.C., Lane, L.S., Dixon, J. and Cook, F.A., 1989. Interpretation of deep seismic reflection data, Beaufort Sea, Arctic, Canada. Geological Survey of Canada, Open File 2106, p. 1-15.
- Dinkelman, M., Kumar, N., Helwig, J., Emmet, P. and Granath, J., 2008. Highlights of petroleum and crustal framework of the Beaufort-Mackenzie Basin: Key results from BeaufortSPAN East Phases I and II surveys. *Canadian Society of Exploration Geophysicists, Recorder*, vol. 23, p. 22-25.
- Dixon, J., Dietrich, J.R., McNeil, D.H. and Lane, L.S., 2001. Geological framework of the Beaufort-Mackenzie Basin. *Rock the Foundation Convention*, June 18-22, 2001, p. 154-1-154-2.

- Dyke, L.D., 1997. White, Barn and Campbell uplifts. *In: The geology, mineral and hydrocarbon potential of the northern Yukon Territory and northwestern District of Mackenzie*, Norris, D.K. (ed.), Geological Survey of Canada, Bulletin 422, p. 333-358.
- Grantz, A., 1966. Strike-slip faults in Alaska. U.S. Geological Survey, Open File Report 66-53, p. 1-82.
- Helwig, J., Kumar, N., Emmet, P. and Dinkelman, M.G., 2011. Regional seismic interpretation of crustal framework, Canadian Arctic passive margin, Beaufort Sea, with comments on petroleum potential. *In: Arctic Petroleum Geology*, A.M. Spencer, A.F. Embry, D.L. Gautier, A.V. Stoupakova, and K. Sørensen (eds.), Geological Society London, Memoirs 35, p. 527-543.
- Jones, P.B., 1980. Evidence from Canada and Alaska on plate tectonic evolution of the Arctic Ocean Basin. *Nature*, vol. 285, p. 215-217.
- Journeay, J.M., Williams, S.P. and Wheeler, J.O., 2000. Tectonic assemblage map, Peel River, Northwest Territories-Yukon Territory-U.S.A. Geological Survey of Canada, Open File 2948p, 1:1 000 000 scale.
- Kerr, J.W., 1981. Evolution of the Canadian Arctic Islands: a transition between the Atlantic and Arctic Oceans. *In: The Ocean Basins and Margins - The Arctic Ocean*, A.E.M., Nairn, M. Churkin and F.G. Stehli (eds.), vol. 5, p. 105-199.
- Lane, L.S., 1988. The Rapid Fault Array: a foldbelt in Arctic Yukon. *In: Current Research, Part D. Geological Survey of Canada, Paper 88-1D*, p. 95-98.
- Lane, L.S., 1992. Kaltag fault, northern Yukon, Canada: Constraints on evolution of Arctic Alaska. *Geology*, vol. 20, p. 653-656.
- Lane, L.S., 1998. Latest Cretaceous-Tertiary tectonic evolution of northern Yukon and adjacent Arctic Alaska. *American Association of Petroleum Geologists Bulletin*, vol. 82, p. 1353-1371.
- Lane, L.S., 2002. Tectonic evolution of the Canadian Beaufort Sea - Mackenzie Delta region: A brief review. *Canadian Society of Exploration Geophysicists, Recorder*, vol. 17, p. 49-56.
- Lane, L.S., 2007. Devonian-Carboniferous paleogeography and orogenesis, northern Yukon and adjacent Arctic Alaska. *Canadian Journal of Earth Sciences*, vol. 44, p. 679-694.
- Lane, L.S. and Dietrich, J.R., 1991. Preliminary interpretation of the 1989 FGP deep seismic reflection program in the western Beaufort Sea. Geological Survey of Canada, Open File 2396, p. 1-14.
- Marrett, R. and Allmendinger, R.W., 1990. Kinematic analysis of fault-slip data. *Journal of Structural Geology*, vol. 12, p. 973-986.
- McWhae, J.R., 1986. Tectonic history of northern Alaska, Canadian Arctic, and Spitsbergen regions since Early Cretaceous. *American Association of Petroleum Geologists Bulletin*, vol. 70, p. 430-450.
- Monger, J. and Price, R., 2002. The Canadian Cordillera: Geology and tectonic evolution. *Canadian Society of Exploration Geophysicists, Recorder*, vol. 17, p. 17-36.
- Norris, D.K., 1976. Geology, Old Crow, Yukon Territory. Geological Survey of Canada, Map 1518A, 1:250 000 scale.
- Norris, D.K., 1981. Geology, Blow River and Davidson Mountains, Yukon Territory - District of Mackenzie. Geological Survey of Canada, Map 1516A, 1:250 000 scale.
- Norris, D.K., 1997. Geological setting. *In: The geology, mineral and hydrocarbon potential of the northern Yukon Territory and northwestern District of Mackenzie*, Norris, D.K. (ed.), Geological Survey of Canada, Bulletin 422, p. 21-64.
- Norris, D.K. and Yorath, C.J., 1981. The North American plate from the Arctic Archipelago to the Romanzof Mountains. *In: Nairn, A.E.M., Churkin Jr., M., and Stehli, F.G. (eds.), The Ocean Basins and Margins - The Arctic Ocean*, vol. 5. Plenum Press, New York, London, p. 37-103.
- O'Leary, D.M., Ellis, R.M., Stephenson, R.A., Lane, L.S. and Zelt, C.A., 1995. Crustal structure of the northern Yukon and Mackenzie Delta, northwestern Canada. *Journal of Geophysical Research: Solid Earth*, vol. 100, no. B7, p. 9905-9920.
- Patton Jr., W.W., 1973. Reconnaissance geology of the northern Yukon-Koyukuk Province, Alaska. U.S. Geological Survey, Professional Paper 774-A, p. A1-A17.
- Patton Jr., W.W. and Hoare, J.M., 1968. The Kaltag Fault, west-central Alaska. U.S. Geological Survey, Professional Paper 600-D, p. D147-D153.

- Piepjoh, K., von Gosen, W., Läufer, A., McClelland, W.C. and Estrada, S., 2013. Ellesmerian and Eureka fault tectonics at the northern margin of Ellesmere Island (Canadian High Arctic). *Zeitschrift der Deutschen Gesellschaft für Geowissenschaften (German Journal of Geosciences)*, vol. 164, p. 81-105.
- Tessensohn, F. and Piepjoh, K., 2000. Eocene compressive deformation in Arctic Canada, north Greenland and Svalbard and its plate tectonic causes. *Polarforschung*, vol. 68, p. 121-124.
- von Gosen, W., Piepjoh, K. and Reinhardt, L., 2012. Polyphase Eureka deformation along the Vendom Fiord Fault Zone on south Ellesmere Island (Canadian Arctic) and its possible relation to the Wegener Fault. *Zeitschrift der Deutschen Gesellschaft für Geowissenschaften (German Journal of Geosciences)*, vol. 163, p. 261-282.
- Young, F.G., 1974. Cretaceous stratigraphic displacements across Blow Fault Zone, northern Yukon Territory. Geological Survey of Canada, Paper 74-1 (Part B), p. 291-296.

Fault tectonics in the Rapid depression of the Yukon North Slope (Canadian Arctic) - Summary of preliminary results

W. von Gosen¹

Geozentrum Nordbayern, Krustendynamik, Friedrich-Alexander-Universität Erlangen-Nürnberg

K. Piepjohn

Bundesanstalt für Geowissenschaften und Rohstoffe (BGR), Geologie der Energierohstoffe, Polargeologie

D.C. Murphy

Yukon Geological Survey

C. Brandes

Institut für Geologie, Leibniz Universität Hannover

W.C. McClelland

Department of Earth and Environmental Sciences, University of Iowa

M. Colpron

Yukon Geological Survey

von Gosen, W., Piepjohn, K., Murphy, D.C., Brandes, C., McClelland, W.C. and Colpron, M., 2015. Fault tectonics in the Rapid depression of the Yukon North Slope (Canadian Arctic) – Summary of preliminary results. *In: Yukon Exploration and Geology 2014*, K.E. MacFarlane, M.G. Nordling and P.J. Sack (eds.), Yukon Geological Survey, p. 157-165.

ABSTRACT

Mesozoic to Tertiary rocks in the Rapid depression on the Yukon North Slope are dissected by a N-NNE striking fault array. Two phases of Tertiary deformation are recorded from the Barn uplift eastwardly across the Rapid depression. D_1 is characterized by strike-slip faults with either sinistral or dextral displacement in the depression and reverse-dextral oblique displacement on the southern Barn fault, indicating broadly E-W regional contraction. In contrast, D_2 deformation is somewhat more complex with first-order faults in the Rapid depression inferred to be primarily sinistral, while the southern Barn fault maintained its reverse-dextral oblique displacement. The structural style is inconsistent with the propagation of a large-scale strike-slip fault zone such as the Kaltag fault through the Rapid depression, as previously suggested, but rather may indicate reactivation of older structural heterogeneity in the subsurface.

¹werner.von.gosen@fau.de

INTRODUCTION

In northernmost Yukon (Canadian Arctic), south of the Beaufort Sea, there is a wide area known as the Yukon North Slope. The Rapid depression (Fig. 1), in the eastern part of the Yukon North Slope, is a broad trough

predominantly underlain by Mesozoic sedimentary rocks. It is flanked to the west by structural culminations of the Barn and Romanzof uplifts and to the east by the Aklavik arch complex (including Rat, Scho, White and Cache Creek uplifts; Fig. 1; Norris, 1997); Paleozoic and locally older rocks are exposed in both regions. Mesozoic rocks

of the Rapid depression straddle the boundary between the Paleozoic North American continental margin in the east and Arctic Alaska terrane in the west. Mesozoic and locally Tertiary rocks in the depression are cut by a swarm of N~NNE striking faults which occur in a north-south corridor ~60 km wide (Rapid fault array; see Norris and Yorath, 1981; Norris, 1997).

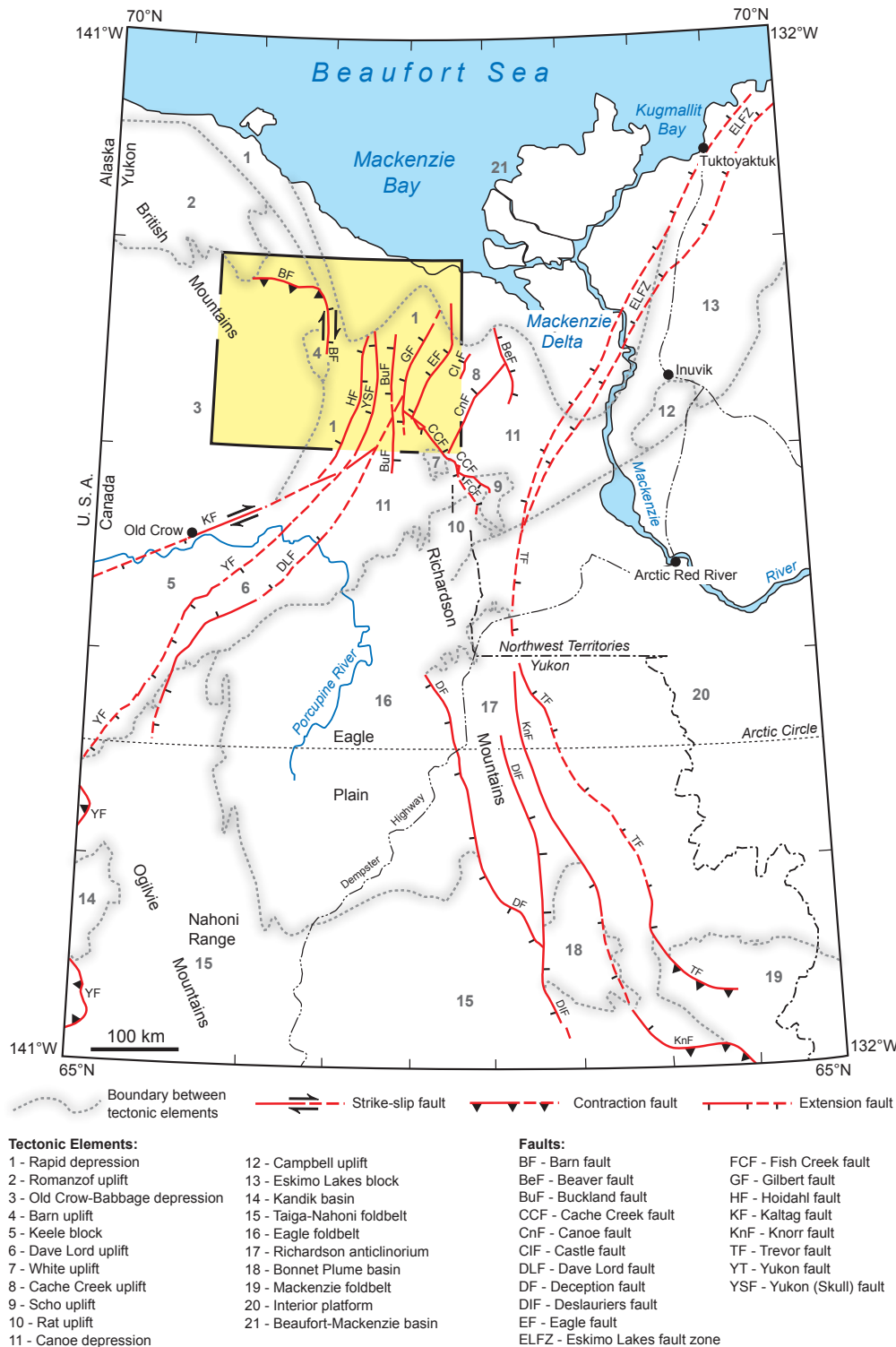


Figure 1. Tectonic elements and main faults in northern Yukon and adjacent Northwest Territories, Canada (map modified from Norris, 1997). Frame with yellow fill shows location of the map of the study area (Fig. 3). Note that the extension of the Tertiary, strike-slip Kaltag fault into Yukon is called into question here and in Lane (1992).

Structural information from the depression is critical to reconstructing the nature of interactions between Arctic Alaska and the northwestern North American margin in late Mesozoic and Tertiary. Furthermore, these data might give insight into the plate tectonic significance of the faults and related structures and answer the question of whether the tectonic development in the Rapid depression can be geometrically and kinematically linked to the Eurekan deformation in the Canadian Arctic Archipelago, North Greenland and Svalbard (compare, for example, Balkwill, 1978; Kerr, 1981; Tessensohn and Piepjohn, 2000).

PREVIOUS WORK

The Rapid depression has been inferred to be the locus of the continuation of the Kaltag fault, a major ENE-WSW dextral strike-slip fault defined in western and central Alaska (cf., Norris, 1976, 1981, 1997; Fig. 1). Although the Kaltag fault has been included in Cenozoic plate tectonic

reconstructions of the Arctic (e.g., Jones, 1980; McWhae, 1986), it appears restricted to the western and central parts of Alaska (e.g., Grantz, 1966; Patton and Hoare, 1968; Patton 1973; Fig. 2). Lane (1992) argued against its along-strike continuation into northern Yukon.

Deformation in the Rapid depression has been characterized as a Paleocene-Eocene fold-and-thrust belt, lacking regionally important strike-slip faults (Lane, 1988). This belt continues northward into major fold structures of the arcuate Beaufort fold-and-thrust belt offshore in the southern Beaufort Sea (e.g., Lane, 1998; Fig. 2). Several interpretations of seismic lines from these offshore areas have shown that the arcuate belt was mainly formed during the Paleocene-Eocene but youngs towards its outboard northern and eastern parts (compare, for example, Dietrich *et al.*, 1989; Lane and Dietrich, 1991; Lane, 1998, 2002; Dixon *et al.*, 2001; Dinkelman *et al.*, 2008; Helwig *et al.*, 2011).

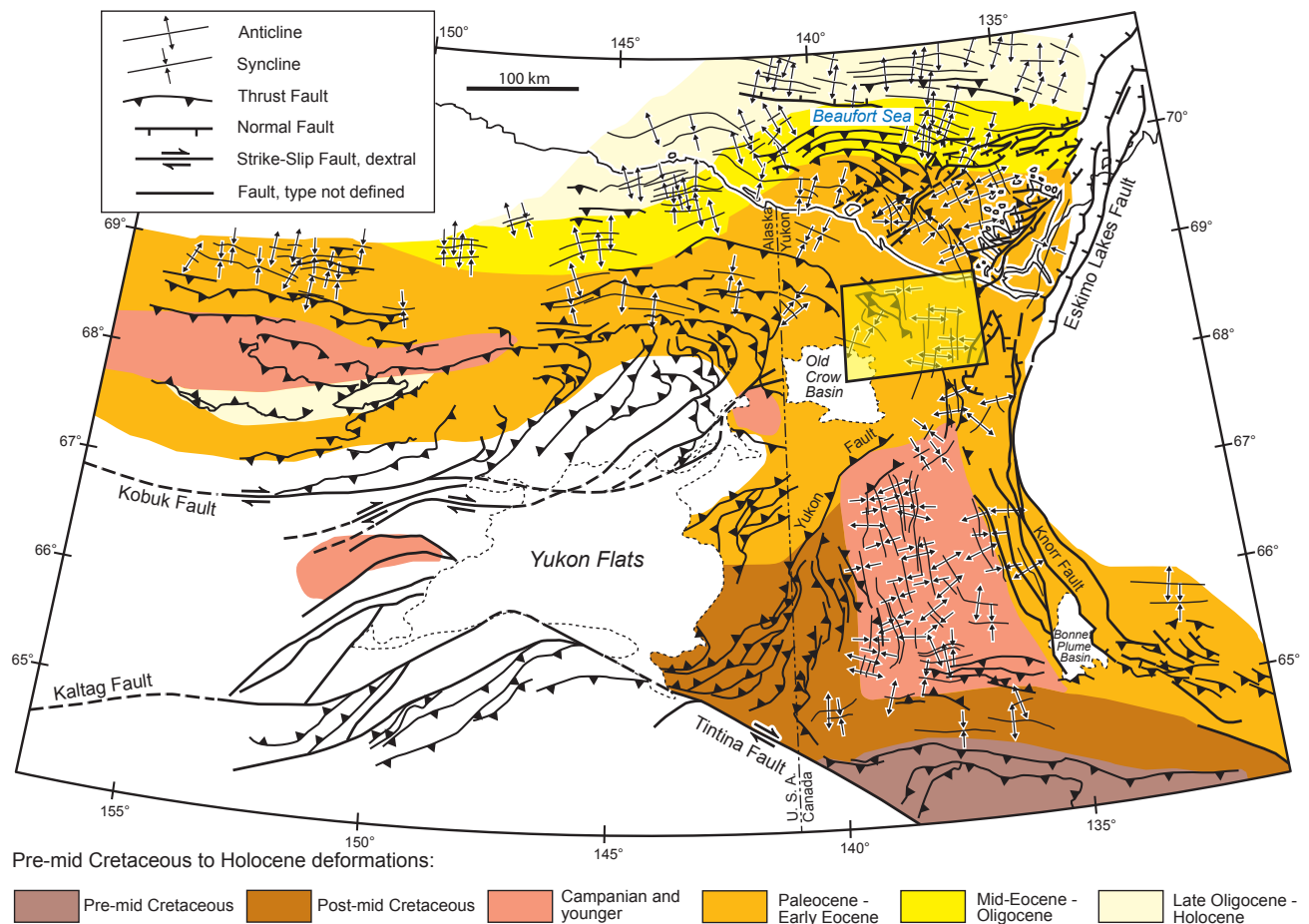


Figure 2. Simplified tectonic map of northeastern Alaska, northern Yukon, and adjacent Northwest Territories (Canada) showing the trends of major Late Cretaceous-Tertiary structures and approximate ages of pre-mid Cretaceous to Holocene deformations (modified from Lane, 1998, 2002). Frame with yellow fill shows location of map in Figure 3.

GEOLOGIC SETTING OF THE RAPID DEPRESSION

The Barn uplift, partly bounding the western edge of the Rapid depression (Figs. 1 and 3), consists of Neoproterozoic to lower Paleozoic (meta-)clastic and carbonate rocks intruded by granitic plutons of Late Devonian age (Lane, 2007), all part of the Arctic Alaska terrane. The pre-Carboniferous succession is folded and dissected by several east-directed thrust faults (Cecile, 1988; Cecile and Lane, 1991; Dyke, 1997). The first phase of deformation in the core of the Barn uplift has been interpreted as post-Late Silurian to pre-Early Carboniferous

(Cecile, 1988) or Middle-Late Devonian (Dyke, 1997); it is inferred to be related either to the Ellesmerian Orogeny or to the Romanzof Orogeny (Lane, 2007). The Barn uplift is bounded on the east by the Barn fault. In the north, west, and south, the rocks in the uplift are unconformably overlain by Carboniferous and younger clastic deposits (Fig. 3).

The Rapid depression and areas surrounding the Barn uplift are underlain by Jurassic to Upper Cretaceous, and locally Tertiary clastic deposits (Fig. 3). The eastern margin of the Rapid depression, in the Richardson Mountains, consists of upper Paleozoic deposits overlain by Mesozoic rocks in the White and Cache Creek uplifts (Figs. 1 and 3).

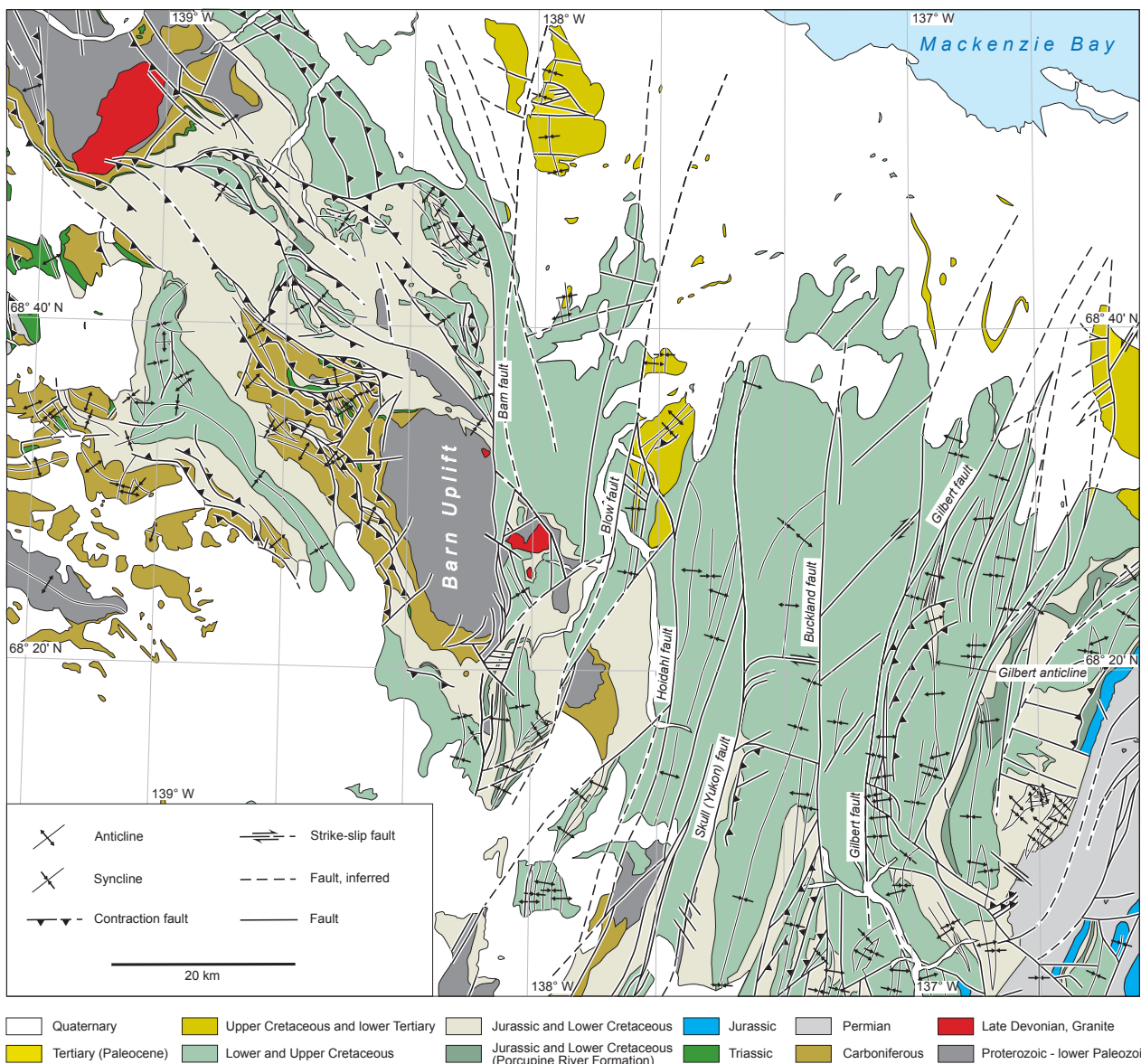


Figure 3. Simplified geological map of the Rapid depression and adjacent areas (north Yukon, Canada) modified from Norris (1981). For location see Figures 1 and 2.

FAULTING IN THE RAPID DEPRESSION

From west to east the major faults in the Rapid depression are as follows (Norris, 1981, 1997; Fig. 3):

(1) The N striking Barn fault separates the Barn uplift to the west from Cretaceous rocks of the Rapid depression to the east. Its northern continuation cuts through Cretaceous rocks and, farther northwards, turns to the northwest and west. To the east of the southern segment of the Barn uplift, two faults, striking NW and NE, separate pre-Mesozoic rocks from Jurassic and Cretaceous deposits.

(2) The NNE striking Blow fault cuts Jurassic to Tertiary rocks and possibly older rock of the Arctic Alaska terrane in the south.

(3) The NNE striking Hoidahl fault (new name, replacing the name 'Kaltag fault' on the map of Norris, 1981) affects Cretaceous rocks in its central and northern segments but displaces lower Paleozoic and/or older rocks of Arctic Alaska terrane in the south. Norris (1981) interpreted this fault as the northeast extension of the Kaltag fault from Alaska; however, following Lane (1992) this correlation appears unlikely and therefore the name Hoidahl fault is proposed here for this structure.

(4) The NNE to N striking Skull (Yukon) fault cuts mostly Cretaceous rocks and in the south also cuts lower Paleozoic rocks of Arctic Alaska terrane. East and southeast of Old Crow, the Yukon fault strikes NE (Fig. 1; Norris, 1981) and also affects Proterozoic, Cambrian to Devonian, and upper Paleozoic rocks of North American affinity. From there, it continues farther south with a NNE strike (Journey *et al.*, 2000).

(5) The N striking Buckland fault cuts Cretaceous rocks in the north and Jurassic rocks in the south.

(6) In the north, the Gilbert fault has a NNE strike and cuts Cretaceous rocks; its strike changes to a N strike in the south. Farther south, it ends directly north of NNE trending folds in Cretaceous rocks (compare Norris, 1981; present Fig. 3). The Gilbert fault is accompanied by several faults and folds to the east.

Most faults in the Rapid depression have a N to NNE strike. The curved Barn fault is an exception (Fig. 3). Additional NW striking reverse faults, affecting Carboniferous but mostly Jurassic and Cretaceous rocks, occur west and north of the Barn uplift (Fig. 3; Norris, 1981). All faults in the region cut Cretaceous rocks and are therefore Cretaceous or younger.

STRUCTURAL OBSERVATIONS RELEVANT TO FAULT KINEMATICS

The major faults and their damage zones are rarely exposed. This study examined exposures as close to the traces of major faults as possible in order to interpret the fault kinematics. Field observations were then combined with major folds and faults mapped by Norris (1981) to synthesize the overall geometries and relations between the sense of fault displacement and adjacent structures. This synthesis led to a reinterpretation of the sense of displacement for some of these faults compared to those inferred by Norris (1981).

Structural measurements related to D_1 deformation supported an interpretation of kinematics at every study location. The shortening orientations near the faults were used to interpret their sense of displacement during first-stage deformation. Shortening orientations during D_1 deformation for each location were determined based individually or collectively on orientations perpendicular to the maxima of B_1 fold axes, δ_1 intersection lineations, and/or girdles through poles of bedding planes.

D_1 DEFORMATION

All Jurassic to Tertiary clastic sedimentary sequences are affected by a D_1 deformation. Open, N to NE trending F_1 folds measure anywhere from a decimetre to more than 100 m and are typically symmetrical, chevron-like structures; however, folds can display either ~E or W vergence. The large Gilbert anticline in the eastern part of the Rapid depression is a good example of an F_1 structure with a N trending axis (Fig. 3). The folds are accompanied by S_1 fracture cleavage with spatially variable intensity. Tertiary sandstones east of the Blow fault display an incipient S_1 fracture cleavage. These rocks are affected by a map-scale, broad, open F_1 syncline with a ~NE trending axis (Fig. 3). Local reverse faults in the Mesozoic succession represent accommodation faults related to F_1 folding. The general picture suggests a ~E to SE contraction direction during the D_1 deformation east of the Barn fault.

In this study's interpretation, the southern, N striking segment of the Barn fault represents an oblique dextral fault with an east-directed reverse component. This segment has been interpreted as a right-lateral fault with 10 km of displacement (Norris, 1997, p. 56) and a minimum vertical separation of approximately 300 m (Dyke, 1997, p. 341). In its northern NW to W striking segment, the Barn fault was interpreted as a thrust fault (Norris, 1981, 1997). This reverse sense is also supported

by the data collected in this study and the NW strike of reverse faults along this segment of the hanging wall.

The Blow fault is interpreted as a sinistral strike-slip fault based on the NW-SE contraction related to development of a F_1 syncline in Tertiary clastic rocks to the east. However, based on the stratigraphic successions preserved on either side of the fault, Young (1974, p. 295) reported that the west side was displaced upward relative to the east side during three main episodes of Early Cretaceous deformation.

For the Hoidahl and Skull (Yukon) faults in the east a sinistral displacement is proposed. On the latter, 5 km of left-lateral separation was reported by Norris (1997, p. 57).

The Gilbert fault, in the eastern side of the Rapid depression, can be interpreted as a dextral strike-slip fault with related F_1 folding to the east (Gilbert anticline). There, the axes of spatially associated folds are obliquely oriented at a small angle with respect to the Gilbert fault and other parallel dextral fault lines (Fig. 3). To the south, the N-S oriented branch of the Gilbert fault is interpreted as a reverse fault, possibly with a dextral component. The southern termination of this fault is within Cretaceous clastic rocks.

It should be emphasized that all faults with lateral displacements during this first stage of deformation are not interpreted as pure strike-slip faults. It is more reasonable to suggest that displacements were accompanied by varying reverse components during fold-and-thrust belt deformation.

The overall shortening, shown by the open F_1 folding and partly continuous trends of folds in the clastic succession, argues for a detachment fault (or faults) in the subsurface. However, the depth, extent, and geometry of such a horizon (or horizons) remain unclear.

D_2 DEFORMATION

In the outcrops studied, the D_1 structural elements are crosscut by sets of younger brittle shear and fault planes. Their senses of shear and displacement are shown by slickensides and steps. The precise time difference to D_1 structures, however, is unclear. For the measured D_2 structural elements, the kinematic P (shortening) and T (extension) axes (Marrett and Allmendinger, 1990) and the fault plane solutions were calculated with the program FaultKin (version 6.5.0) of Allmendinger (2013).

D_2 deformation is best exemplified in the area of the Gilbert anticline and Gilbert fault (Fig. 3). There, the N trending F_1 Gilbert anticline is cross cut and displaced along NE striking and ~NW directed reverse faults which curve into a southern N-S oriented branch of either the Gilbert fault or a parallel fault (Fig. 3). A NW verging F_2 fold structure, which overprints S_1 cleavage planes and is floored by a detachment, was observed in the hanging wall of one of these reverse faults. Faults and shear planes with similar orientations and calculated P axes were also observed in the hinge zone of the Gilbert anticline, suggesting NNW-SSE contraction across this region during D_2 deformation.

Overall, the calculated D_2 P axes and fault plane solutions for structures in the Rapid depression east of the Barn fault range from E-W to NW-SE to N-S. NW-SE axes predominate near first-order faults indicating a sinistral to sinistral-oblique reverse displacement; N-S axes and E-W axes occur at outcrops between first-order faults, the former especially along second-order reverse faults that are kinematically compatible with sinistral offset along first-order faults. The primarily NW-SE sense of contraction caused a reactivation of older (D_1) strike-slip faults with the same or opposite strike-slip motion relative to the previous displacement. An instructive example is the Gilbert fault and areas to the east (Fig. 3). This study's data from the Gilbert fault have shown that after its first dextral stage with related folding (see above), the sense of displacement changed to sinistral strike-slip along the N trending fault segment and northward. In the south, however, the fault ends in folded Cretaceous rocks with ~NE trending fold axes. This observation suggests that displacement, during both D_1 and D_2 , transferred onto another fault, thereby avoiding the sedimentary succession at the south end of the Gilbert fault. This argues for strike-slip faulting in limited segments, probably caused by inherited older and reactivated structures in the subsurface (see below).

All other faults to the west of the Gilbert fault are interpreted as sinistral strike-slip faults, combined with a reverse component, and partly changing into reverse faults along strike during D_2 . The sense of displacement along the Hoidahl fault, however, remains unclear. In the west, the N-S oriented section of the Barn fault seems to have remained active as an oblique, dextral fault.

INTERPRETATIONS AND CONCLUSIONS

The structural geometry and kinematic evolution reported here provide argument against a simple high-level fold-and-thrust belt within the Rapid depression. Fold axes that are oblique with respect to many fault lines, suggest that folding occurred concurrently with strike-slip movements. The entire picture, however, does not support a large-scale, uniform, strike-slip dominated regime. If it were an overall regime of strike-slip tectonics, a single sense of shear, either dextral or sinistral, would be expected. Instead, this study interprets two stages of fault tectonics with different sense of displacements and a more complex tectonic history during the early Cenozoic. There is no evidence for a through-going and significant Tertiary strike-slip fault, such as the Kaltag fault, that could be interpreted as an intracontinental displacement zone of plate tectonic significance.

The precise age of the clastic Tertiary deposits in the Rapid depression, affected by both stages of deformation, is unclear. It can only be stated that they are Paleocene. It is assumed that the first-stage deformation (D_1) is Paleocene or Eocene in age (see also Lane, 1988, 1998, 2002; compare with Fig. 2) whereas the second stage (D_2) might be Eocene and/or younger. Therefore, both phases of deformation seem to have taken place during the time of Eureka deformation in the Canadian Arctic Archipelago (e.g., Balkwill, 1978; Tessensohn and Piepjohn, 2000; von Gosen *et al.*, 2012; Piepjohn *et al.*, 2013) and postdate the Cretaceous opening of the Amerasia Basin.

It seems reasonable that strike-slip faulting and their present surface expressions were caused by structural heterogeneities in the subsurface. As the area under discussion represents the western marginal part of the North American craton to the east, and has been affected by pre-Mesozoic (Monger and Price, 2002) or younger (O'Leary *et al.*, 1995; Lane, 1998) extension and rifting, older and rift-related (normal) faults could have been reactivated during Tertiary compressional faulting and folding. They might have led to the development of the observed strike-slip faults. Reverse faulting and parallel dextral and sinistral faults in the Rapid depression during D_1 deformation support this interpretation.

The Eskimo Lakes fault zone is a possible candidate for a structure of plate tectonic significance (Figs. 1 and 2). It continues offshore towards the northeast into the Beaufort Sea and possibly defined the former margin of the

North American craton. Arcuate bending of the Tertiary structures occurs to the west and northwest of this fault zone. This might suggest that faulting and folding were contemporaneous events and the Eskimo Lakes fault zone accommodated crustal shortening by dextral strike-slip. Bending of the structures in the northeast Alaskan area, however, might have been accommodated by the dextral Kobuk fault to the south (Fig. 2) and not the Kaltag fault.

ACKNOWLEDGEMENTS

Field work in north Yukon (Arctic Canada) was carried out during the CASE 15-Expedition of the Federal Institute for Geosciences and Natural Resources (BGR, Hannover, Germany) led by M. Colpron (Yukon Geological Survey (YGS), Whitehorse, Canada) and K. Piepjohn (BGR, Hannover, Germany). C. Brandes, W. von Gosen, and W. C. McClelland are grateful to this institution for the invitation to participate in this expedition. W. von Gosen gratefully acknowledges financial supports for pre-expedition travel from the Bavarian Research Alliance (Munich, Germany) and for the expedition project from the German Research Foundation (DFG, proj. Go 405/11-1). Support for W.C. McClelland was provided by National Science Foundation (NSF) grants EAR-0948359 and EAR-1049368. Finally, many thanks to David Moynihan (YGS) for critically reviewing an earlier draft of this manuscript.

REFERENCES

- Allmendinger, R.W., 2013. FaultKin (version 6.5.0) for Mac OS X and Windows 7/XP. Department of Geological Sciences, Cornell University, Ithaca, New York.
- Balkwill, H.R., 1978. Evolution of the Sverdrup Basin, Arctic Canada. *American Association of Petroleum Geologists Bulletin*, vol. 62, p. 1004-1028.
- Cecile, M.P., 1988. Corridor traverse through Barn Mountains, northernmost Yukon. *In: Current Research, Part D. Geological Survey of Canada, Paper 88-1D*, p. 99-103.
- Cecile, M.P. and Lane, L.S., 1991. Geology of the Barn Uplift, northern Yukon. Geological Survey of Canada, Open File 2342, 1:50 000 scale.
- Dietrich, J.R., Coflin, K.C., Lane, L.S., Dixon, J. and Cook, F.A., 1989. Interpretation of deep seismic reflection data, Beaufort Sea, Arctic, Canada. Geological Survey of Canada, Open File 2106, p. 1-15.

- Dinkelman, M., Kumar, N., Helwig, J., Emmet, P. and Granath, J., 2008. Highlights of petroleum and crustal framework of the Beaufort-Mackenzie Basin: Key results from BeaufortSPAN East Phases I and II surveys. *Canadian Society of Exploration Geophysicists, Recorder*, vol. 23, p. 22-25.
- Dixon, J., Dietrich, J.R., McNeil, D.H. and Lane, L.S., 2001. Geological framework of the Beaufort-Mackenzie Basin. *Rock the Foundation Convention*, June 18-22, 2001, p. 154-1-154-2.
- Dyke, L.D., 1997. White, Barn and Campbell uplifts. *In: The geology, mineral and hydrocarbon potential of the northern Yukon Territory and northwestern District of Mackenzie*, Norris, D.K. (ed.), Geological Survey of Canada, Bulletin 422, p. 333-358.
- Grantz, A., 1966. Strike-slip faults in Alaska. U.S. Geological Survey, Open File Report 66-53, p. 1-82.
- Helwig, J., Kumar, N., Emmet, P. and Dinkelman, M.G., 2011. Regional seismic interpretation of crustal framework, Canadian Arctic passive margin, Beaufort Sea, with comments on petroleum potential. *In: Arctic Petroleum Geology*, A.M. Spencer, A.F. Embry, D.L. Gautier, A.V. Stoupakova, and K. Sørensen (eds.), Geological Society London, Memoirs 35, p. 527-543.
- Jones, P.B., 1980. Evidence from Canada and Alaska on plate tectonic evolution of the Arctic Ocean Basin. *Nature*, vol. 285, p. 215-217.
- Journey, J.M., Williams, S.P. and Wheeler, J.O., 2000. Tectonic assemblage map, Peel River, Northwest Territories-Yukon Territory-U.S.A. Geological Survey of Canada, Open File 2948p, 1:1 000 000 scale.
- Kerr, J.W., 1981. Evolution of the Canadian Arctic Islands: a transition between the Atlantic and Arctic Oceans. *In: The Ocean Basins and Margins - The Arctic Ocean*, A.E.M., Nairn, M. Churkin and F.G. Stehli (eds.), vol. 5, p. 105-199.
- Lane, L.S., 1988. The Rapid Fault Array: a foldbelt in Arctic Yukon. *In: Current Research, Part D. Geological Survey of Canada, Paper 88-1D*, p. 95-98.
- Lane, L.S., 1992. Kaltag fault, northern Yukon, Canada: Constraints on evolution of Arctic Alaska. *Geology*, vol. 20, p. 653-656.
- Lane, L.S., 1998. Latest Cretaceous-Tertiary tectonic evolution of northern Yukon and adjacent Arctic Alaska. *American Association of Petroleum Geologists Bulletin*, vol. 82, p. 1353-1371.
- Lane, L.S., 2002. Tectonic evolution of the Canadian Beaufort Sea - Mackenzie Delta region: A brief review. *Canadian Society of Exploration Geophysicists, Recorder*, vol. 17, p. 49-56.
- Lane, L.S., 2007. Devonian-Carboniferous paleogeography and orogenesis, northern Yukon and adjacent Arctic Alaska. *Canadian Journal of Earth Sciences*, vol. 44, p. 679-694.
- Lane, L.S. and Dietrich, J.R., 1991. Preliminary interpretation of the 1989 FGP deep seismic reflection program in the western Beaufort Sea. Geological Survey of Canada, Open File 2396, p. 1-14.
- Marrett, R. and Allmendinger, R.W., 1990. Kinematic analysis of fault-slip data. *Journal of Structural Geology*, vol. 12, p. 973-986.
- McWhae, J.R., 1986. Tectonic history of northern Alaska, Canadian Arctic, and Spitsbergen regions since Early Cretaceous. *American Association of Petroleum Geologists Bulletin*, vol. 70, p. 430-450.
- Monger, J. and Price, R., 2002. The Canadian Cordillera: Geology and tectonic evolution. *Canadian Society of Exploration Geophysicists, Recorder*, vol. 17, p. 17-36.
- Norris, D.K., 1976. Geology, Old Crow, Yukon Territory. Geological Survey of Canada, Map 1518A, 1:250 000 scale.
- Norris, D.K., 1981. Geology, Blow River and Davidson Mountains, Yukon Territory - District of Mackenzie. Geological Survey of Canada, Map 1516A, 1:250 000 scale.
- Norris, D.K., 1997. Geological setting. *In: The geology, mineral and hydrocarbon potential of the northern Yukon Territory and northwestern District of Mackenzie*, Norris, D.K. (ed.), Geological Survey of Canada, Bulletin 422, p. 21-64.
- Norris, D.K. and Yorath, C.J., 1981. The North American plate from the Arctic Archipelago to the Romanzof Mountains. *In: Nairn, A.E.M., Churkin Jr., M., and Stehli, F.G. (eds.), The Ocean Basins and Margins - The Arctic Ocean*, vol. 5. Plenum Press, New York, London, p. 37-103.

- O'Leary, D.M., Ellis, R.M., Stephenson, R.A., Lane, L.S. and Zelt, C.A., 1995. Crustal structure of the northern Yukon and Mackenzie Delta, northwestern Canada. *Journal of Geophysical Research: Solid Earth*, vol. 100, no. B7, p. 9905-9920.
- Patton Jr., W.W., 1973. Reconnaissance geology of the northern Yukon-Koyukuk Province, Alaska. U.S. Geological Survey, Professional Paper 774-A, p. A1-A17.
- Patton Jr., W.W. and Hoare, J.M., 1968. The Kaltag Fault, west-central Alaska. U.S. Geological Survey, Professional Paper 600-D, p. D147-D153.
- Piepjohn, K., von Gosen, W., Läufer, A., McClelland, W.C. and Estrada, S., 2013. Ellesmerian and Eureka fault tectonics at the northern margin of Ellesmere Island (Canadian High Arctic). *Zeitschrift der Deutschen Gesellschaft für Geowissenschaften (German Journal of Geosciences)*, vol. 164, p. 81-105.
- Tessensohn, F. and Piepjohn, K., 2000. Eocene compressive deformation in Arctic Canada, north Greenland and Svalbard and its plate tectonic causes. *Polarforschung*, vol. 68, p. 121-124.
- von Gosen, W., Piepjohn, K. and Reinhardt, L., 2012. Polyphase Eureka deformation along the Vendom Fiord Fault Zone on south Ellesmere Island (Canadian Arctic) and its possible relation to the Wegener Fault. *Zeitschrift der Deutschen Gesellschaft für Geowissenschaften (German Journal of Geosciences)*, vol. 163, p. 261-282.
- Young, F.G., 1974. Cretaceous stratigraphic displacements across Blow Fault Zone, northern Yukon Territory. Geological Survey of Canada, Paper 74-1 (Part B), p. 291-296.

YUKON GEOLOGICAL SURVEY

Yukon Geological Survey staff are located in two buildings in Whitehorse: the Elijah Smith Building at 300 Main Street, rooms 102 and 230, and the H.S. Bostock Core Library at Mile 918 on the Alaska Hwy.

BRANCH DIRECTOR

H.S. Bostock Core Library

Relf, Carolyn – Director, (867) 667-8892 carolyn.relf@gov.yk.ca

OPERATIONS

H.S. Bostock Core Library

Roy, Suzanne – Manager, Finance & Operations, (867) 667-8508 suzanne.roy@gov.yk.ca

Kirby, Midori – Administrative Assistant, (867) 455-2800 midori.kirby@gov.yk.ca

REGIONAL GEOLOGY

H.S. Bostock Core Library

Murphy, Don – Head, Regional Geology, (867) 667-8516 don.murphy@gov.yk.ca

Cobbett, Rosie – Project Geologist, (867) 455-2802 rosie.cobbett@gov.yk.ca

Colpron, Maurice – Project Geologist, (867) 667-8235 maurice.colpron@gov.yk.ca

Fraser, Tiffani – Oil & Gas Project Geologist, (867) 667-3228 tiffani.fraser@gov.yk.ca

Hutchison, Matthew – Oil & Gas Project Geologist, (867) 455-2808 matthew.hutchison@gov.yk.ca

Israel, Steve – Project Geologist, (867) 667-5175 steve.israel@gov.yk.ca

Moynihan, David – Project Geologist, (867) 455-2805 david.moynihan@gov.yk.ca

Elijah Smith Building

Roots, Charlie – GSC Research Scientist, (867) 667-8513 charlie.roots@gov.yk.ca

SURFICIAL GEOLOGY AND OUTREACH

Elijah Smith Building

Bond, Jeff – Head, Surficial Geology, (867) 667-8514 jeff.bond@gov.yk.ca

Kennedy, Kristen – Surficial Geologist, (867) 393-7188 kristen.kennedy@gov.yk.ca

Lipovsky, Panya – Surficial Geologist, (867) 667-8520 panya.lipovsky@gov.yk.ca

Van Loon, Sydney – Placer Geologist, sydney.vanloon@gov.yk.ca

H.S. Bostock Core Library

Laxton, Sarah – Outreach Geologist, (867) 393-7187 sarah.laxton@gov.yk.ca

MINERAL SERVICES

Elijah Smith Building

Lewis, Lara – A/Head, Mineral Services, (867) 667-8518 lara.lewis@gov.yk.ca

Deklerk, Robert – MINFILE Geologist, (867) 667-3205 robert.deklerk@gov.yk.ca

Sack, Patrick – Economic Geologist, (867) 667-3203 patrick.sack@gov.yk.ca

Torgerson, Derek – Manager, Yukon Mineral Exploration Program, (867) 456-3828 derek.torgerson@gov.yk.ca

H.S. Bostock Core Library

Slam, Johann – Core Library Technician, (867) 332-7156 johann.slam@gov.yk.ca

EDITORIAL & TECHNICAL SERVICES

Elijah Smith Building

MacFarlane, Karen – Head, Technical Services, (867) 667-8519 karen.macfarlane@gov.yk.ca

Elliot, Brett – Geological Spatial Database Administrator, (867) 667-8481 brett.elliott@gov.yk.ca

Nordling, Monica – Senior Geological Assistant, (867) 667-3201 monica.nordling@gov.yk.ca

Staffen, Bailey – GIS/Cartography Technician, (867) 456-6801 bailey.staffen@gov.yk.ca

H.S. Bostock Core Library

Bruce, Olwyn – Geological Spatial Data Administrator, (867) 393-7186 olwyn.bruce@gov.yk.ca